A47_A11L.UAS.89 – sUAS Mid-Air Collision (MAC) Likelihood: Final Report

February 24, 2023

v 1.1

NOTICE

This document is disseminated under the sponsorship of the U.S. Department of Transportation in the interest of information exchange. The U.S. Government assumes no liability for the contents or use thereof. The U.S. Government does not endorse products or manufacturers. Trade or manufacturers' names appear herein solely because they are considered essential to the objective of this report. The findings and conclusions in this report are those of the author(s) and do not necessarily represent the views of the funding agency. This document does not constitute FAA policy. Consult the FAA sponsoring organization listed on the Technical Documentation page as to its use.

LEGAL DISCLAIMER

The information provided herein may include content supplied by third parties. Although the data and information contained herein has been produced or processed from sources believed to be reliable, the Federal Aviation Administration makes no warranty, expressed or implied, regarding the accuracy, adequacy, completeness, legality, reliability or usefulness of any information, conclusions or recommendations provided herein. Distribution of the information contained herein does not constitute an endorsement or warranty of the data or information provided herein by the Federal Aviation Administration or the U.S. Department of Transportation. Neither the Federal Aviation Administration nor the U.S. Department of Transportation shall be held liable for any improper or incorrect use of the information contained herein and assumes no responsibility for anyone's use of the information. The Federal Aviation Administration and U.S. Department of Transportation shall not be liable for any claim for any loss, harm, or other damages arising from access to or use of data or information, including without limitation any direct, indirect, incidental, exemplary, special or consequential damages, even if advised of the possibility of such damages. The Federal Aviation Administration shall not be liable to anyone for any decision made or action taken, or not taken, in reliance on the information contained herein.

The additional Massachusetts Institute of Technology Lincoln Laboratory's material is based upon work supported by the Federal Aviation Administration under Air Force Contract No. FA8702-15-D-0001. Any opinions, findings, conclusions or recommendations expressed in this material are those of the author(s) and do not necessarily reflect the views of the Federal Aviation Administration.

This document is derived from work done for the FAA (and possibly others), it is not the direct product of work done for the FAA. The information provided herein may include content supplied by third parties. Although the data and information contained herein has been produced or processed from sources believed to be reliable, the Federal Aviation Administration makes no warranty, expressed or implied, regarding the accuracy, adequacy, completeness, legality, reliability or usefulness of any information, conclusions or recommendations provided herein. Distribution of the information contained herein does not constitute an endorsement or warranty of the data or information provided herein by the Federal Aviation Administration or the U.S. Department of Transportation. Neither the Federal Aviation Administration nor the U.S. Department of Transportation shall be held liable for any improper or incorrect use of the information contained herein and assumes no responsibility for anyone's use of the information. The Federal Aviation Administration and U.S. Department of Transportation shall not be liable for any claim for any loss, harm, or other damages arising from access to or use of data or information, including without limitation any direct, indirect, incidental, exemplary, special or consequential damages, even if advised of the possibility of such damages. The Federal Aviation Administration shall not be liable to anyone for any decision made or action taken, or not taken, in reliance on the information contained herein.

TECHNICAL REPORT DOCUMENTATION PAGE

1. Report No. A47_A11L.UAS.87 -002	2. Government Accession No.	3. Recipient's Catalog No.
4. Title and Subtitle sUAS Mid Air Collision Likelihood - Final Report		**5. Report Date** February 24, 2023 **6. Performing Organization Code**
7. Author(s) Armando De Abreu – https://orcid.org/0000-0002-7398-7294 Gerardo Arboleda – https://orcid.org/0000-0002-1953-4673 Gerardo Olivares, PhD – https://orcid.org/0000-0003-0748-3917 Luis Gomez – https://orcid.org/0000-0002-8768-9060 Deepak Singh – https://orcid.org/0000-0001-5142-7520 Timothy Bruner – https://orcid.org/0000-0002-7591-8823 Tom Haritos, PhD. – https://orcid.org/0000-0001-6546-383X Katie Silas – https://orcid.org/0000-0003-0647-4592 Ryan J. Wallace, Ed.D – No ORCID With extensive support from: Andrew Weinert – https://orcid.org/0000-0003-3771-8609		**8. Performing Organization Report No.**
9. Performing Organization Name and Address National Institute for Aviation Research, Wichita State University, 1845 Fairmount St, Wichita, KS, 67260-0193. Kansas State University, Manhattan, KS 66506 Embry-Riddle Aeronautical University, 1 Aerospace Blvd., Daytona Beach, FL 32114 With extensive support from: Massachusetts Institute of Technology Lincoln Laboratory, 244 Wood Street, Lexington, MA 02421-6426		**10. Work Unit No.** **11. Contract or Grant No.** UAS Mid-Air Collision (MAC) Likelihood - A47_A11L.UAS.89
12. Sponsoring Agency Name and Address Federal Aviation Administration FAA PM: Deepak Chauhan, ANG-C33 FAA Sponsor: Adam Hendrickson, AFS-410		**13. Type of Report and Period Covered** Final Report (September 2021 – December 2022) **14. Sponsoring Agency Code** 5401

15. Supplementary Notes

16. Abstract

This research analyzes the risk of a Small UAS (sUAS) Mid-Air Collision (MAC). A complete Mid-Air Collision (MAC) risk assessments require estimates of both collision severity and collision likelihood. The research focuses on sUAS MAC likelihood analysis with commercial transport aircraft, business jet, general aviation aircraft, and rotorcraft. Open-source resources, such as MITLL encounter models, were used to generate and evaluate encounter sets. The probability of a MAC given an NMAC, *P(MAC|NMAC),* was estimated with and without a DAA system.

Four manned aircraft were checked for collisions against six sUAS, and results were tabulated. A severity assessment was performed for the recorded MACs. The assessment leveraged results from previous MAC assessments and adapted them to estimate a wide range of impact conditions. The impact locations were also compared with bird strike locations to determine if any relationship exists.

17. Key Words	18. Distribution Statement
Unmanned Aircraft System, National Airspace System, Beyond Visual Line of Sight, Mid-Air Collision, Well-Clear, DAA, Encounter Models, ACAS sXu	No restrictions.

19. Security Classification (of this report)	20. Security Classification (of this page)	21. No. of Pages	22. Price
Unclassified	Unclassified	233	N/A

Form DOT F 1700.7 (8-72) Reproduction of completed page authorized

ACKNOWLEDGEMENTS

The authors would like to thank all the Federal Aviation Administration (FAA) personnel involved in this research project. In particular, the authors would like to thank Adam Hendrickson, Deepak Chauhan, John Miller, and Kolie Lombard for all their contributions and valuable input throughout the research.

We would like to express our appreciation to Andrew J. Weinert and his team from the Massachusetts Institute of Technology Lincoln Laboratory for their invaluable contribution to this research. Their software tools and support were instrumental in this project's success. We also appreciate their contribution to this report and valuable feedback throughout the research process. We are grateful for their expertise and support.

Lastly, the authors would also like to thank

1) Colonel Stephen P. Luxion, Hannah Thach, and LeighAlison Jones from the FAA's Center of Excellence for Uncrewed Aircraft Systems (ASSURE) for supporting this research.
2) Randal Guendel, Josh Silbermann, Tyler A. Young, Sam Smearcheck, and other members of the RTCA SC-147 committee for their support of our research. Their guidance, expertise, and software tools have been essential to our success.

TABLE OF CONTENTS

TABLE OF FIGURES

TABLE OF TABLES

TABLE OF ACRONYMS

AAP	Airspace Awareness Platform
ACAS	Airborne Collision Avoidance System
ADD	Algorithm Design Description
ADS-B	Automatic Dependent Surveillance-Broadcast
AGL	Above Ground Level
AGT	Absolute Geodetic Track Surveillance
AIAA	American Institute of Aeronautics and Astronautics
AMA	Academy of Model Aeronautics
ASTM	American Society for Testing and Materials
ATC	Air Traffic Control
AUVSI	Association for Unmanned Vehicle Systems International
BVLOS	Beyond Visual Line of Sight
CAMI	Civil Aerospace Medical Institute
CAS	Collision Avoidance System
CFR	Code of Federal Regulations
COC	Clear of Conflict
CPA	Closest Point of Approach
DAA	Detect and Avoid
DEGAS	DAA Evaluation of Guidance, Alerting and Surveillance
DLL	Dynamic Link Library
DOE	Design of Experiments
DOF	Degrees of Freedom
DWF	Dallas-Fort Worth International
FAA	Federal Aviation Administration
FEA	Finite Element Analysis
FWJ	Fixed-Wing Jet
FWME	Fixed-Wing Multiple Engine Aircraft
FWP	Fixed-Wing Prop
FWSE	Fixed-Wing Single Engine Aircraft
GA	General Aviation
GBSS	Ground-Based Surveillance System

GIS	Geographical Information Systems
GLONASS	Russian Global Navigation Satellite System
GNSS	Global Navigation Satellite Systems
GPS	Global Positioning System
HAE	Height Above Ellipsoid
HMD	Horizontal Miss Distance
Hz	Hertz
ICAO	International Civil Aviation Organization
IEEE	Institute of Electrical and Electronics Engineers
INS	Inertial Navigation System
JHU	Johns Hopkins University
LAX	Los Angeles International Airport
LLUEM	Lincoln Lab Uncorrelated Encounter Models
LoWC	Loss of Well-Clear
LoWCR	Loss of Well-Clear Ratio
MAC	Mid-Air-Collision
MEX	Matlab Executable
MIT LL	Massachusetts Institute of Technology Lincoln Laboratory
MOPS	Minimum Operational Performance Standards
MSL	Mean Sea Level
NAS	National Airspace System
NMAC	Near Mid Air Collision
NTIS	National Technical Information Service
OBS	Omni-Bearing Selector
OPSNET	Operations Network
OSN	Open Sky Network
RA	Resolution Advisory
RADES	Radar Evaluation Squadron
RF	Radio Frequency
RMSE	Root Mean Square Error
RR	Risk Ratio
RTCA	Radio Technical Commission for Aeronautics

STM	Surveillance Tracking Module
sUAS	Small Unmanned Aircraft System
TCA	Time of Closest Approach
TCAS	Traffic. Alert and Collision Avoidance System
TRM	Threat Resolution Modules
UAS	Unmanned Aircraft System
UAST	Unmanned Aircraft Safety Team
URSA	Unmanned Robotics Systems Analysis
UTC	Universal Coordinated Time
VFR	Visual Flight Rules
VMD	Vertical Miss Distance
WCV	Well Clear Violation

EXECUTIVE SUMMARY

This document presents the research findings of the *A47 11L.UAS.89 Small UAS (sUAS) Mid-Air Collision (MAC) Likelihood* research, with a focus on sUAS Beyond Visual Line of Sight (BVLOS) operations. Specifically, operations where a Detect and Avoid (DAA) system can be used to waive sections 14 Code of Federal Regulations (CFR) §107.31 and §107.51 or for BVLOS operations entirely outside of Part 107 (such as those under Part 91). This research provides analytical results of encounter set evaluations in terms of the probability of a MAC given a Near Mid-Air Collision (NMAC), *P(MAC|NMAC)*.

This research uses six sUAS models with up to 15 ft. wingspan. Similarly, four different manned aircraft models were identified to perform the collision analysis. Airborne Collision Avoidance System (ACAS) sXu V4R1 was adopted as the DAA logic, along with two surveillance sources for the mitigated encounter evaluation: Automatic Dependent Surveillance-Broadcast (ADS-B) for cooperative intruders and a generic ground-based radar-like for non-cooperative intruders. The DO-396 draft informed the minimum operational performance requirements of each sensor.

The analysis showed that the likelihood of a MAC between an sUAS and a manned aircraft encounter is lower than between two unequipped manned aircraft. Similarly, the size of an sUAS can be considered a passive MAC mitigation factor by up to a factor of 2 for the sUAS models analyzed. On the other hand, the likelihood of a MAC increases for larger aircraft, such as commercial transports, given the same size sUAS. The MAC ratio was less than one in all encounter sets. ACAS sXu also reduced the overall number of collisions with non-cooperative intruders in an encounter set by 95% to 98%. ACAS sXu also showed an overall MAC reduction with cooperative intruders greater than 99.4%. This demonstrates that the benefits of ACAS sXu, with sensor errors modeled according to DO-396, continue beyond reducing NMACs.

A MAC severity assessment of unmitigated and mitigated MAC was completed. The assessment utilized past MAC severity research findings between manned aircraft and sUAS. This report adapted the past findings to fit the broader conditions of the recorded MAC cases. Each manned aircraft model's average unmitigated and mitigated severity was estimated on a 1 to 4 scale. However, the mitigated severity distribution was hindered by the low number of unresolved MACs. The wide confidence intervals evidenced this in the mitigated datasets. Throughout the severity analysis, the lack of severity data was also evident. Previous research only addressed a conservative worst-impact-conditions in manned aircraft locations where head-on collisions were expected. In the future, more impact conditions (aircraft locations, impact orientations, and impact offset conditions) should be evaluated for a comprehensive severity evaluation of all aircraft parts, even if such cases are expected to be low severity. In the same manner, future analyses should include more sUAS architectures. A library of the most widely expected sUAS architecture could be analyzed based on a survey of the ever-changing sUAS landscape. This will enable the creation of robust generalized severity functions that could be extrapolated for future and innovative designs that mix-and-match features of different platforms without requiring a specialized research campaign for each architecture.

This report highlights the process of generating, evaluating, and analyzing an encounter set to determine a DAA system's performance. Several assumptions and limitations were considered in an attempt to generalize the results for multiple sUAS operations. However, the same process can be applied to tailored sUAS operations, including the use of geographic-specific manned aircraft trajectories during the encounter generation, and the existing encounter model trajectories.

1 INTRODUCTION, BACKGROUND, AND MOTIVATION

The *A47 11L.UAS.89 Small UAS (sUAS) Mid-Air Collision (MAC) Likelihood* research will analyze the risk of an sUAS MAC with a manned aircraft. Risk will be estimated for when the sUAS employs or does not employ a detect and avoid (DAA) system, which enables the sUAS comply with applicable operating rules of Title 14 of the Code of Federal Regulations (14 CFR). These rules include Part §91.3, .111, .113(b), .115, .123, and .181(b), which prescribe that aircraft must remain well clear from and prevent a midair collision (MAC) with other aircraft. A complete MAC risk assessment requires estimates of both collision severity and collision likelihood. The research focuses on sUAS MAC likelihood analysis with commercial, rotorcraft and General Aviation (GA) aircraft.

The following research questions should be answered:

- What is the probability of an sUAS without a "Detect and Avoid (DAA) system" colliding with a manned aircraft?
- What is the probability of an sUAS with a DAA system colliding with a manned aircraft?
- What is the overall risk of MAC with and without a detect and avoid system?
- How does sUAS collision risk compare with the risk of a bird strike?

To answer these research questions, the present report addresses the results from Monte Carlo encounter simulations with and without a DAA system. Unmitigated conditional probabilities of an sUAS MAC given a Near Mid-Air Collision (NMAC) are presented in Section 3.3. Similarly, the mitigated conditional probabilities are discussed in Section 4.4. These results are also compared to the conditional probabilities of a MAC between manned aircraft from previous studies. A severity assessment was also performed to understand a MAC's overall risk. The methodology and results of the severity assessment of the recorded MACs are presented in Section 5. Finally, a comparison of the impact locations between sUAS MACs and bird strikes is discussed in Section 6.

1.1 Motivation

The Radio Technical Commission for Aeronautics (RTCA) and the American Society for Testing and Materials (ASTM) are currently developing standards for DAA systems applicable to sUAS (ASTM F3442/F3442M-20, 2020; RTCA, 2021). NMACs are widely used as a safety metric. However, the intended safety goal of DAA systems is to avoid a MAC or an unsafe condition that could lead to a MAC. For manned aircraft, an accepted assumption of the probability of MAC given an NMAC (P(MAC|NMAC)) is 0.1 (RTCA, 2005); although this 0.1 assumption has shown to be conservative for many types of manned vs. manned aircraft encounters (Kochenderfer et al., 2010). A MAC between aircraft is undesirable due to the high fatality risk. sUAS are smaller in size and weight compared to manned aircraft. Therefore, complete risk analyses need to correlate the performance of a DAA system in reducing the probability of MAC and the severity between an sUAS and manned aircraft encounter. The relative smaller size of a sUAS compared to manned aircraft could be a potential strategic mitigation to further reduce the likelihood of a MAC. Ultimately, understanding the relationship between the typical metrics used by RTCA and ASTM (risk ratio and Loss of Well-Clear (LoWC) ratio) and how it translates to the MAC ratio is needed.

For instance, what does a 0.18 risk ratio translate to in terms of overall MAC reduction and MAC ratio?

1.2 Scope

The scope was directly informed by sUAS Beyond Visual Line of Sight (BVLOS) operations. Specifically, operations where a DAA can be used to waive sections 14 Code of Federal Regulations (CFR) §107.31 and §107.51 or for BVLOS operations entirely outside of Part 107 (such as those under Part 91). As such, RTCA SC-147 and ASTM F3442 directly informed the scope of the research. The research will focus on a DAA (Airborne Collision Avoidance System (ACAS) sXu) compliant with ASTM F3442 and the upcoming ACAS sXu Minimum Operational Performance Standards (MOPS). The altitude scope of ASTM F3442 is limited to < 1200 ft. Above Ground Level (AGL) in Class E/G airspace.

The typical sUAS description is 55 lb or less and 25ft or less wingspan. Even though the ASTM does not have a weight limit, previous severity studies conducted by ASSURE universities have used the typical sUAS description. Since the present research will utilize past sUAS severity research, the weight of the sUAS was limited to less than 55 lb. Similarly, the speed of the sUAS is limited to 100 knots.

The type of encounters was limited to unmanned-manned single intruder encounters. Where the unmanned aircraft is an sUAS (as described previously), and the manned aircraft is a conventional aircraft (fixed-wing single or multi-engine and rotorcraft). This study did not consider unconventional aircraft, such as blimps, balloons, and gliders.

ACAS sXu V4R1 was used as the reference DAA system. Surveillance sources compliant with ASTM and RTCA SC-147 (DO-396) were used. Namely, Automatic Dependent Surveillance-Broadcast (ADS-B) for cooperative aircraft and ground radar for non-cooperative aircraft.

1.3 Objectives and Contributions

The primary objective is to determine the correlation between Risk Ratio (RR) and Loss of Well-Clear Ratio (LoWCR) requirements and the actual reduction in realized MAC risk. RR and LoWCR are the typical safety metric used in DAA system requirements. However, the ultimate safety goal is avoidance of a MAC.

Accordingly, the primary contribution is a set of conditional probabilities (i.e., P(MAC|NMAC)) and, by extension, MAC ratios for a select combination of airframes. Additionally, the primary contribution includes an analysis of the severity of the realized MACs for unmitigated and mitigated cases.

A secondary objective is to explore how to use open-source resources, such as the Massachusetts Institute of Technology Lincoln Laboratory (MITLL) encounter models, to evaluate the performance of DAA systems. Standardizing the procedures for assessing a DAA system will allow the Federal Aviation Administration (FAA) and industry to streamline the approval process of BVLOS operations. The secondary contribution is a set of guidelines, suggestions, and methodology to evaluate a DAA system's performance through simulated encounters.

2 METHOD AND APPROACH

This section outlines the method and approach used to create the encounter sets, evaluate them, and the assumptions that were made in the process.

2.1 Prototype Simulation by MIT Lincoln Laboratory

The research effort by ASSURE leverages the lessons learned from preceding analyses by MIT LL in 2020 and 2010. The 2010 study by Kochenderfer et al. (2010) has previously been published but this A47 report is the first public dissemination of the 2020 MIT LL research. All methods and approaches described in this section and leveraged by A47, were first prototyped in the preceding MIT LL efforts. For specific technologies, MIT LL leveraged earlier developmental versions of what was available to A47. Additionally, MIT LL only estimated P(MAC|NMAC) for different encounter conditions and did not evaluate MAC severity, such as described in Section 5. Nor did MIT LL research bird strikes, as in Section 6.

2.2 Monte Carlo Simulation

Monte Carlo simulations allow modeling the probability of an outcome that involves random variables. As such, a DAA system can be exposed to millions of random but realistic encounters so that the researchers can evaluate the system's efficacy in reducing the probability of a MAC. This approach was previously used during the Traffic Alert and Collision Avoidance System (TCAS) Version 7.1 evaluation (Espindle et al., 2009), and it is currently being used by RTCA SC-147 and SC-228 for the development of DAA minimum performance requirements (SC-228, 2021). Espindle et al. (2009) indicate that this type of analysis allows for the simulation of the desired event (MAC in the present research) many times more than has been observed while maintaining a realistic rate of desired events per encounter.

2.3 Manned Aircraft Trajectories

MIT LL has developed several statistical models trained from radars and observations by the OpenSky network (Schäfer et al., 2014) of ADS-B-equipped aircraft. The models are based on Bayesian networks representing the relationship between dynamic variables (i.e., vertical acceleration and turn rates) (Underhill & Weinert, 2021). Figure 1 and Figure 2 highlight the Bayesian networks for the initial and transition distribution, respectively. The initial distribution defines the initial state of the aircraft, while the transition distribution describes how the trajectory changes throughout the encounter.

Version 2.1 of the uncorrelated encounter models have seven variables: Geographic domain; G, Airspace class; A, Altitude layer; L, airspeed; v, acceleration; $\dot{v}$, turn rate; $\dot{\psi}$, and vertical rate; $\dot{h}$ (Weinert et al., 2021). Weinert et al. (2013) provide detailed descriptions of how these variables were extracted from the data. Each variable is dependent on the number of arrows it is connected to in the Bayesian network. For instance, v in Figure 1 is dependent on G, L, and A. Each variable has a set of conditional probability lookup tables from which its value is sampled (Weinert et al., 2013).

From the relationship, the model can construct random aircraft trajectories that are statistically comparable to the data obtained from radars and the OpenSky network. This allows for the generation of manned aircraft trajectories that can be used in Monte Carlo simulations to estimate the likelihood of a MAC. The uncorrelated models are design to represent en-route aircraft that are

assumed to have not received Air Traffic Control (ATC) direction to avoid a collision, including 1200 Mode C / Visual Flight Rules (VFR) conventional aircraft (Weinert et al., 2013).

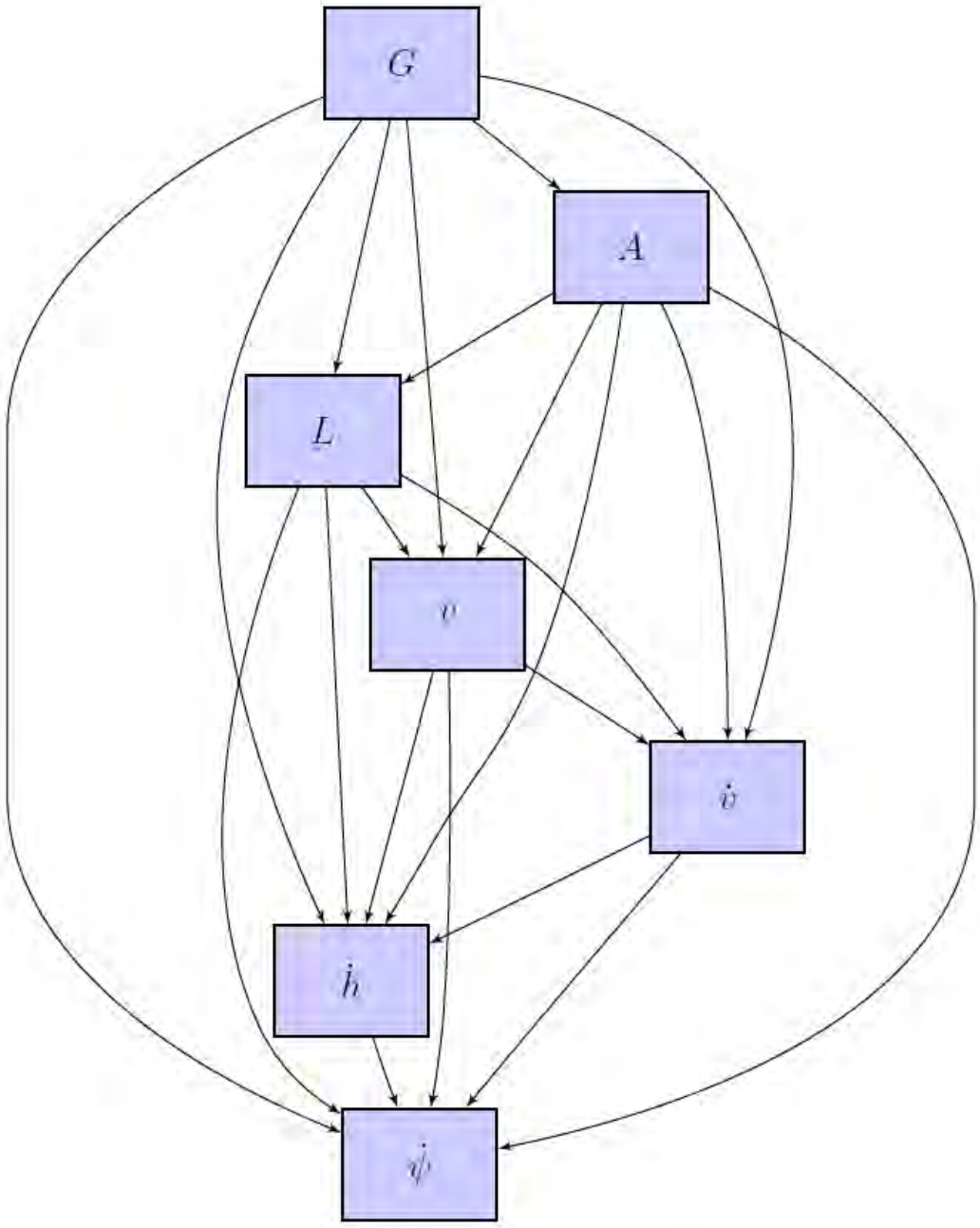

Figure 1. Bayesian network for the initial distribution of the uncorrelated encounter models (Weinert et al., 2013).

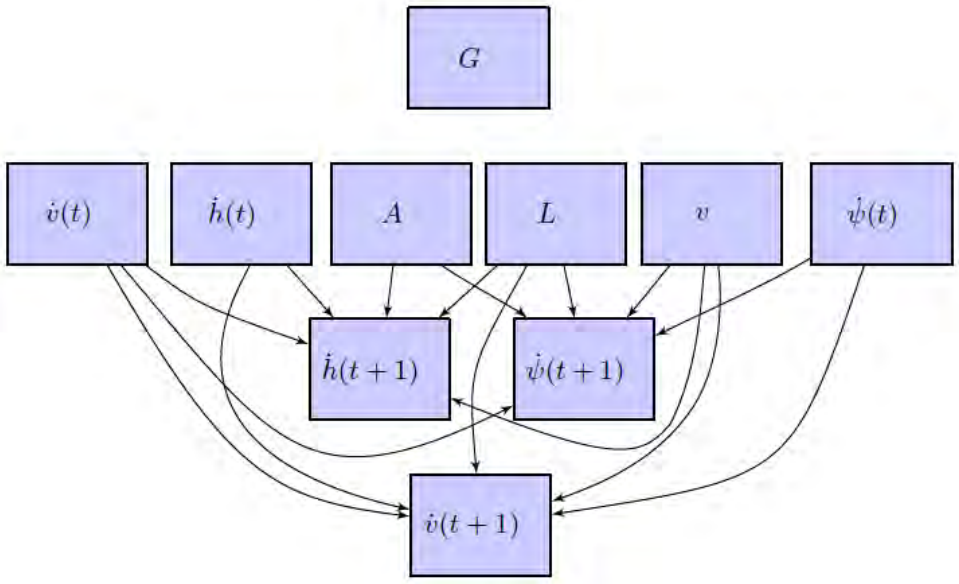

Figure 2. Bayesian network for the transition distribution of the uncorrelated encounter models (Weinert et al., 2013).

2.3.1 *Uncorrelated Encounter Models*

Each encounter model generates statistically representative trajectories according to the data used to train the model. The original uncorrelated model was trained using radar data from the 84th Radar Evaluation Squadron (RADES) network (Kochenderfer et al., 2008). RADES data was filtered using the MODE 3A/C code squawked by the aircraft transponder (Kochenderfer et al., 2008). However, the RADES model cannot differentiate aircraft types and only applies to aircraft trajectories at altitudes above 500 ft (Kochenderfer et al., 2008; Weinert et al., 2013). Due to these limitations, new models trained on observations of ADS-B-equipped aircraft by the OpenSky Network with a lower altitude floor (50 ft AGL) have been developed (Weinert et al., 2019). The new models allowed for the identification of aircraft type (rotorcraft, fixed-wing multi-engine, and single-engine) as well as aircraft squawking 1200-code only and not squawking 1200-code (Underhill & Weinert, 2021). Figure 3 and Figure 4 highlight the distributions of aircraft observed in the 1200-code-only and 1200-code-exclude models, respectively. Underhill & Weinert (2021) and Weinert et al. (2019) provide more details on the development of each of these encounter models. It is important to note that these models are abstract in the sense that they do not provide specific aircraft behavior dependent on density, time of day, or a specific geographic region (Kochenderfer et al., 2008; Underhill & Weinert, 2021; Weinert et al., 2013).

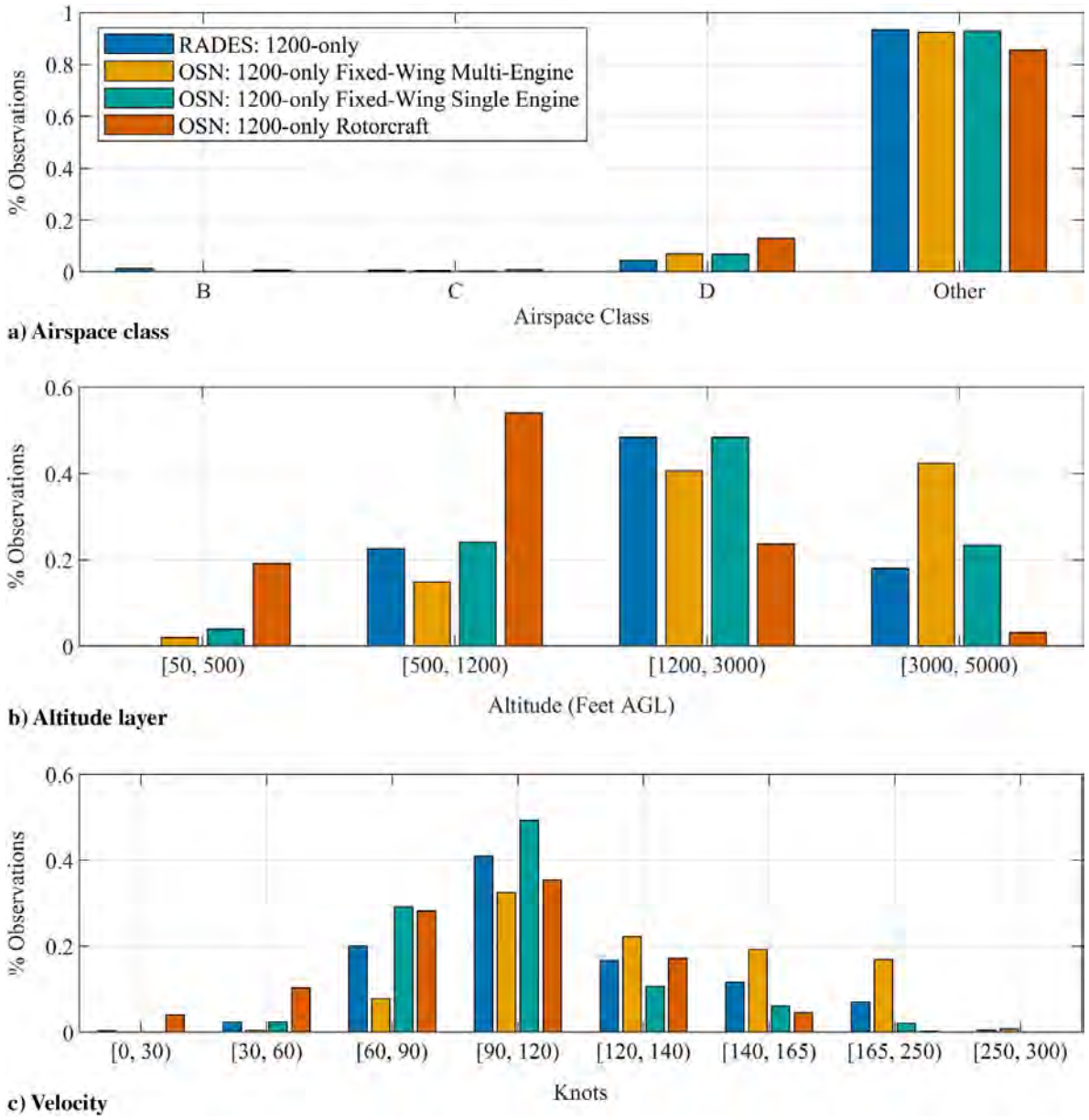

Figure 3. Airspace, altitude, and velocity initial distribution of version 2.1 of 1200-code-only encounter models (Underhill & Weinert, 2021).

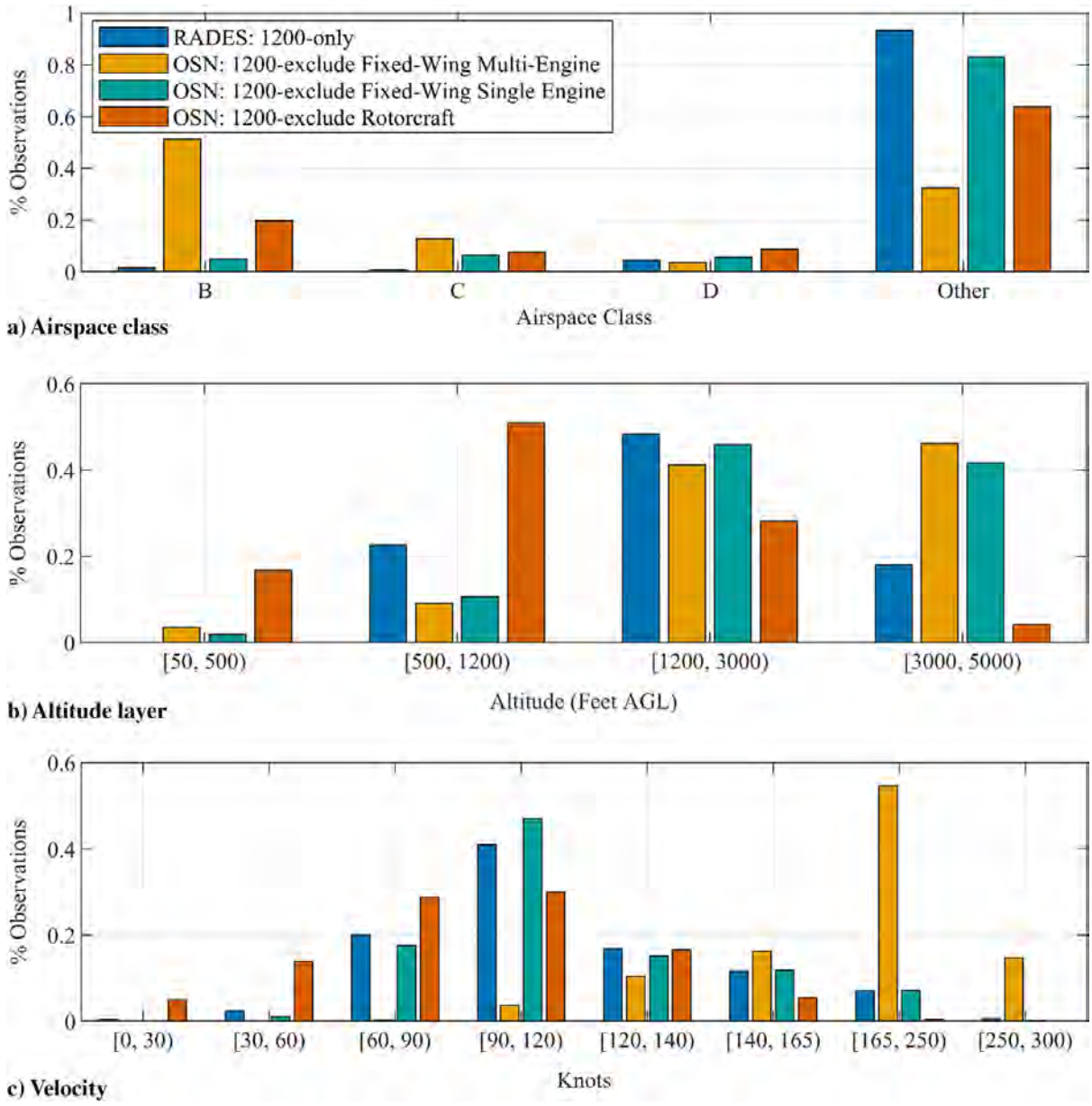

Figure 4. Airspace, altitude, and velocity initial distribution of version 2.1 of 1200-code-exclude encounter models (Underhill & Weinert, 2021).

There is some overlap between the models, as observed in Figure 3. Therefore, some of the generated trajectories in one model could fit the description of another model. However, for safety simulation, such as evaluation related to ASTM F3442, Underhill & Weinert (2021) indicate that all OpenSky Network-based aircraft-specific models should be accordingly leveraged when evaluating the performance of both non-cooperative and cooperative manned aircraft. Underhill & Weinert (2021) also suggest using the 1200-code-only models for low-altitude non-cooperative aircraft (without transponder) cases.

The observations shown in Figure 3 and Figure 4 may not directly correlate with the amount of air traffic in any specific geographic region. This is because air traffic observations vary dramatically

with the sensor coverage area at low altitudes. Sensor coverage at low altitudes falls off with range squared due to earth curvature and obstructions that limit low altitude coverage. Additionally, aircraft density varies significantly in different geographic areas. However, to fully determine the performance of a DAA system, encounters across the expected altitude range (50-1200 ft. in this research) should be evaluated uniformly. This is because the DAA system should properly avoid all low-flying intruders, even if they are not expected frequently. The observations within each altitude layer in the encounter models should be used to determine the intruder flight characteristics in an encounter rather than to justify an air traffic altitude density. Ignoring intruders below an arbitrary altitude threshold could lead to inappropriate avoidance maneuvers when these situations eventually occur. The ultimate decision on whether a DAA is necessary for a low aircraft density region lies with the certifying authority (i.e., FAA). Details on the encounter generation process are further discussed in Section 2.5

2.4 sUAS Trajectories

The lack of readily available sUAS flight data (specifically for BVLOS operations) is a current challenge that has not been addressed. Weinert, Edwards, et al. (2020) proposed and prototyped an approach to generate UAS trajectories from utilitarian assumptions, such as railway lines, waterways, and road inspections (Weinert & Underhill, 2018; Weinert, Edwards, et al., 2020). This is another uncorrelated model under development by MIT LL: the "Geospatial model." The geospatial model is not a Bayesian model, as there is no data available to train the model. Instead, it generates trajectories based on the operational intent of commercial operations from open-source maps of infrastructure, recreational regions, and other common sUAS surveillance targets (Weinert, 2021). This model is not applicable for sUAS recreational and amateur operations governed by 14 CFR Part 101 or 49 U.S.C. 44809.

The trajectories are created as a set of waypoints along features of interest. The features are identified from open-source datasets such as Open Street Maps and the Homeland Infrastructure Foundation-Level Data (Weinert, Edwards, et al., 2020). The features include expected reconnaissance and surveillance targets such as waterways, railways, wind turbines, electric transmission lines, pipelines, farmland, and roads. This approach might not cover all possible BVLOS operations. However, given the lack of actual BVLOS data, Weinert, Edwards, et al. (2020) indicate that this approach is sufficient for current standards developing organizations' activities and has been specifically leveraged by RTCA SC-147. Figure 5 illustrates an example trajectory for an inspection of an electric transmission line.

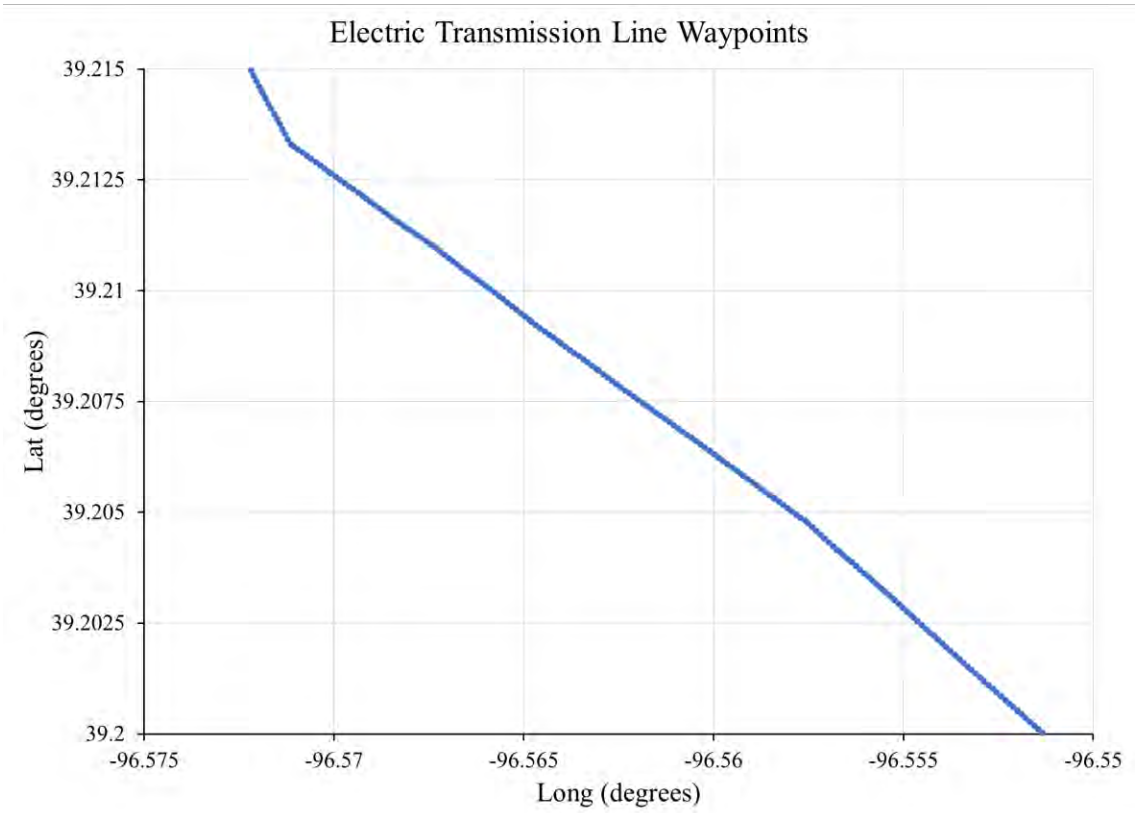

Figure 5. Example trajectory waypoints for electric transmission lines in Kansas.

2.5 **Encounter Set Generation**

Sections 2.3 and 2.4 describe how encounter models can generate individual trajectories. However, individual trajectories have to be paired to create an encounter. For this study, sUAS trajectories generated from the geospatial model are paired with manned trajectories from six Bayesian uncorrelated models. A pairing software developed by MIT was used to pair the trajectories (Weinert, 2021). The software and encounter models used to generate the encounter sets for this study are shown in Table 1. The uncorrelated models listed include surrogates for cooperative (not squawking Mode 3A/C of 1200) and non-cooperative (squawking Mode 3A/C of 1200) aircraft.

Table 1. Software versions used to generate encounter sets.

Software	Version	Description	Reference
em-pairing-geospatial	v2.0.0	Pairing software	(Weinert, 2021)
em-model-geospatial	v1.0	sUAS operational trajectories	(Weinert et al., 2021)
Uncor_1200exclude_fwme	v2.1	Uncorrelated fixed wing multi-engine with ADS-B Out not squawking Mode 3A/C of 1200	(Weinert et al., 2021)
Uncor_1200exclude_fwse	v2.1	Uncorrelated fixed-wing single-engine with ADS-B Out not squawking Mode 3A/C of 1200	(Weinert et al., 2021)
Uncor_1200exclude_rotorcraft	v2.1	Uncorrelated rotorcraft with ADS-B Out not squawking Mode 3A/C of 1200	(Weinert et al., 2021)
Uncor_1200only_fwme	v2.1	Uncorrelated fixed-wing multi-engine with ADS-B Out squawking Mode 3A/C of 1200	(Weinert et al., 2021)
Uncor_1200only_fwse	v2.1	Uncorrelated fixed-wing single-engine with ADS-B Out squawking Mode 3A/C of 1200	(Weinert et al., 2021)
Uncor_1200only_rotorcraft	v2.1	Uncorrelated rotorcraft with ADS-B Out squawking Mode 3A/C of 1200	(Weinert et al., 2021)

To create an encounter, a uniformly spaced grid is created across a region (i.e., a US state), and all possible sUAS trajectories within a range of each grid point (i.e., 1 nm) are identified. Figure 6 shows possible sUAS trajectories in Kansas. The long linear infrastructure features (roads, railways, etc.) are noticeable in the figure.

An uncorrelated manned trajectory is then sampled for each sUAS trajectory within each grid point. The manned trajectory is forced to fly randomly through the center of the grid point and is checked for collision against obstacles and terrain.

The distance between all waypoint combinations between a pair of tracks is filtered to those that meet an encounter threshold criteria. The airspeed and altitude of the sUAS trajectory are sampled, and the tracks are checked against a set of encounter criteria. If the conditions are met, the encounter is created.

The pairing process described above is based on the pairing software description provided by Weinert (2021). The encounter set criteria used for this study are shown in Table 2. The conflict thresholds are not the encounter's horizontal and vertical miss distances. These thresholds are target distances used to filter between waypoints before the airspeed and altitude of the sUAS are sampled. The chosen thresholds were selected to oversample NMAC and achieve numerous MACs so that the performance of the DAA system in reducing MACs could be better analyzed.

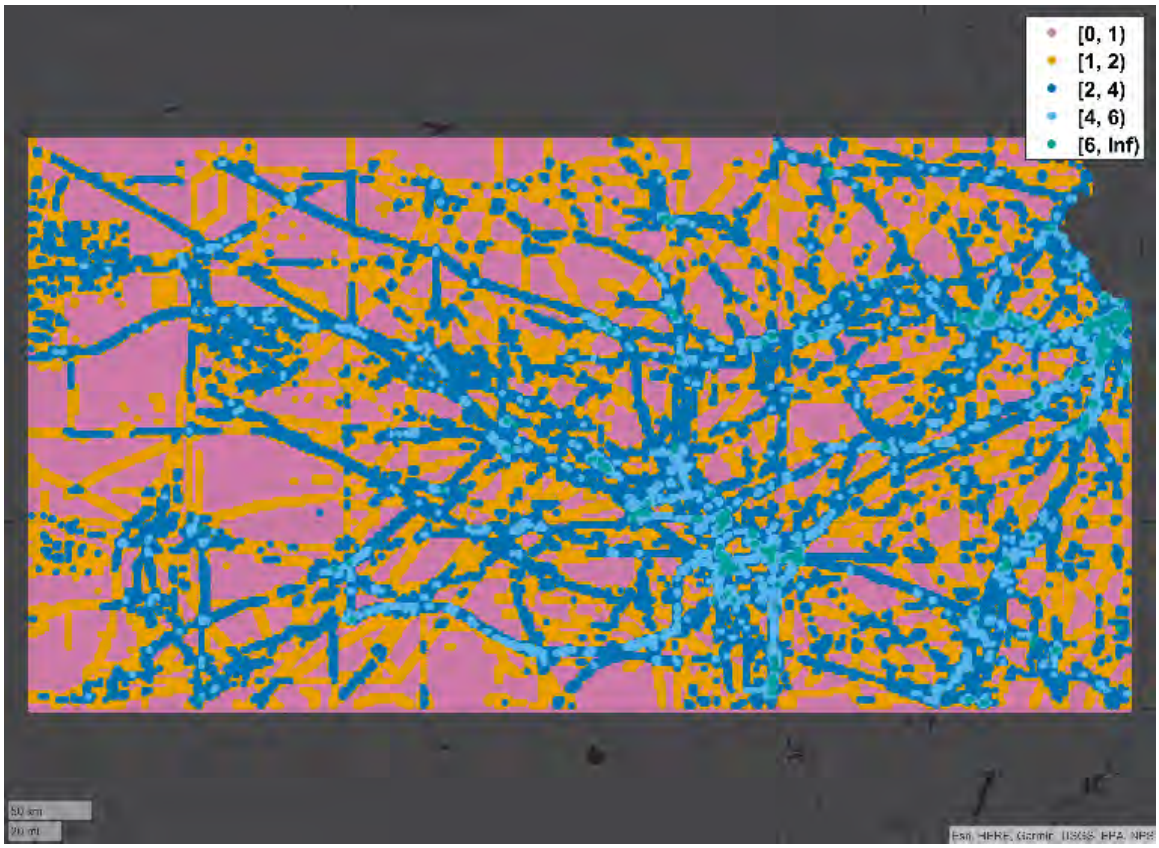

Figure 6. Possible sUAS trajectories within 1 nm range grid points in Kansas. Image generated with the tools from Weinert (2020).

Table 2. Encounter criteria to generate an encounter.

Criteria	Definition
sUAS trajectories (ownship)	em-model-geospatial v1.0
Manned trajectories (intruder)	em-model-bayes v2.1
Ownship altitude	50 – 1200 ft. AGL
Ownship speed	5 – 100 knots
Geospatial region	CO;KS;MS;NC;ND;OK
sUAS operational intent	Roads, waterways, railways, pipelines, electric transmission, wind turbines, and land use.
Conflict Threshold	[100; 500; 2000] ft. Horizontal and [50; 100; 250] ft. Vertical
Conflict time (total encounter time)	90 s (140 s)
Initial horizontal separation	6076 to 97217 ft.
Initial vertical separation	0 to 500ft
FAA regulated airspace class	E and G

The altitude and speed of the sUAS in Table 2 were informed by ASTM F3442/F3442M-20 (2020). Speed and altitude were uniformly sampled with a range of 5-100 knots and 50-1200 ft. AGL respectively. The trajectories were filtered for Class E and G airspace only. Even though ASTM F3442/F3442M-20 (2020) also applies to Classes B, C, and D (below 400 to 500 ft. AGL), encounters in these airspaces were not assessed in this study. The 90 seconds conflict time was chosen to allow slower aircraft to start with an initial separation of at least 6000 ft. A shorter conflict time would result in an encounter with faster aircraft on average.

Geospatial trajectories were sampled from 6 US locations and for all operational intents currently supported by the geospatial model (roads, waterways, railways, pipelines, electric transmission, wind turbines, and land use.). All the available geospatial trajectories were paired with each one of the uncorrelated encounter models listed in Table 1. Approximately 3.1 million encounters were generated. Figure 7 illustrates the resulting Horizontal Miss Distance (HMD) vs. Vertical Miss Distance (VMD) distribution of the encounter sets generated using the encounter criteria in Table 2. The concentration of encounters in the NMAC volume is observed in the yellow region.

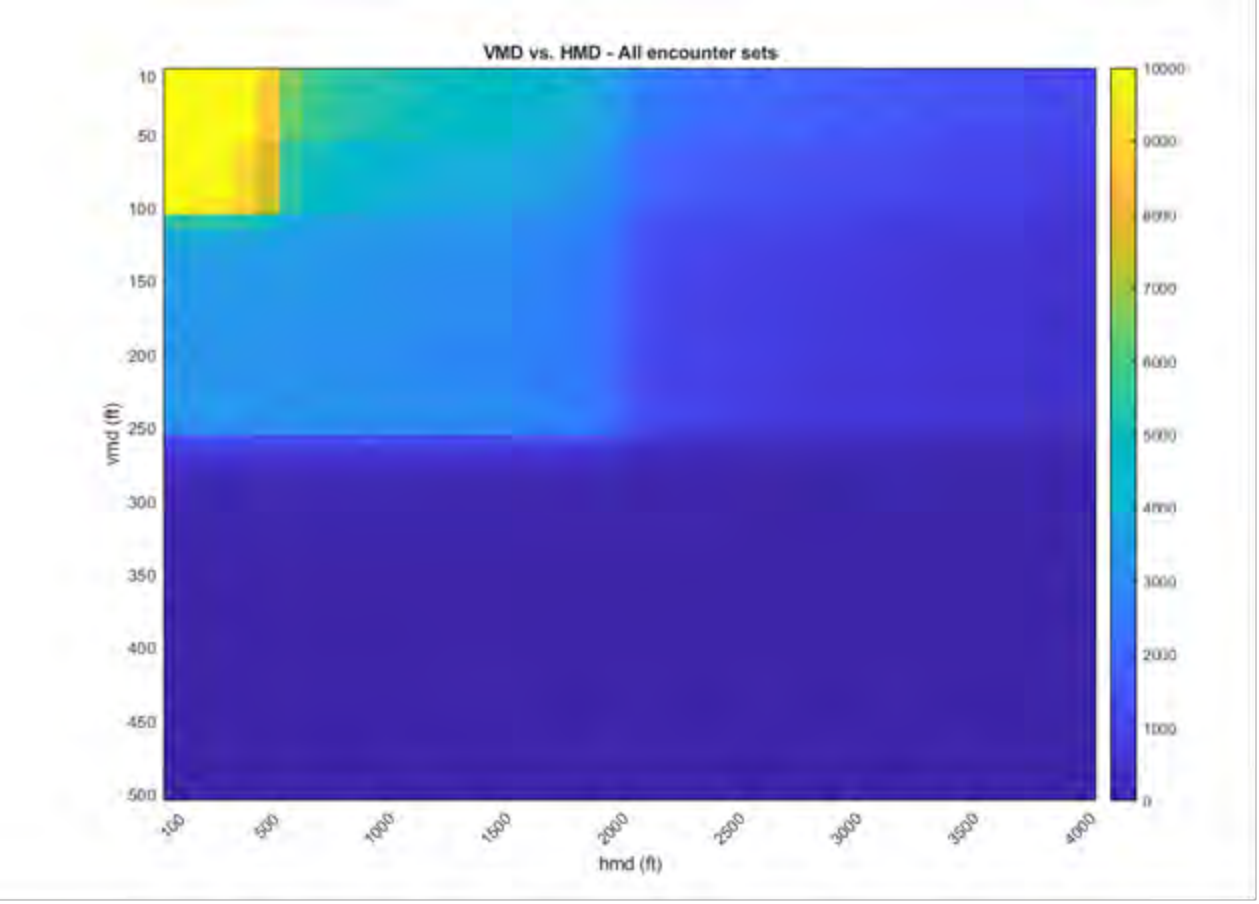

Figure 7. VMD vs. HMD in the encounter sets generated (aggregate) from the geospatial and the uncorrelated encounter model trajectories.

2.6 **Simulation Environment**

This research employs a Monte Carlo simulation analysis to produce metrics with statistical significance for a different set of encounter representations (Section 2.5). This involves the simulation of more than three million *one-to-one* encounters (sUAS vs. conventional manned aircraft) representing situations that could occur in the National Airspace System (NAS).

Previous studies and simulation efforts have demonstrated that the Monte Carlo approach can very well help to evaluate DAA systems by estimating different metrics such as NMAC and LoWC violations (Das, 2021a; Serres et al., 2021; Weinert et al., 2022; Weinert et al., 2018). Simulation environments such as Johns Hopkins University RAVENS, MIT LL CSIM, and MIT LL CASSATT have previously been used as tools for risk assessment studies (Weinert et al., 2022).

The aforementioned simulation environments are not publicly available. However, MIT LL developed an open-sourced version of MIT LL CASSATT, namely DAA Evaluation of Guidance, Alerting and Surveillance (DEGAS) (Serres et al., 2020). DEGAS was developed in Matlab and Simulink allowing the simulation of dynamic time-dependent systems. DEGAS has been adopted as the simulation environment of the present research. Several modifications to integrate ACAS sXu were performed. This contributed to the completion of the unmitigated (Section 3) analysis and enabled the analysis of the mitigated research tasks (Section 4).

DEGAS uses the individual encounters generated in Section 2.5 as input files. The trajectories are reconstructed using a 6 Degrees of Freedom (6-DOF) equation of motion for rigid point masses. Inertial effects and wind were not considered in this analysis. For each encounter evaluated, safety metrics were recorded. These metrics are further explained in Section 2.8. The same encounters are evaluated with a DAA logic (ACAS sXu) and a surveillance source for the mitigated analysis. For the unmitigated analysis, the trajectories of the sUAS (ownship) and manned aircraft (intruder) are not modified during the simulation. For the mitigated analysis, the trajectory of the ownship is modified or altered by commands as a response to any DAA Resolution Advisory (RA) generated during the simulation. A diagram of the DEGAS functionality with a DAA system is illustrated in Figure 8.

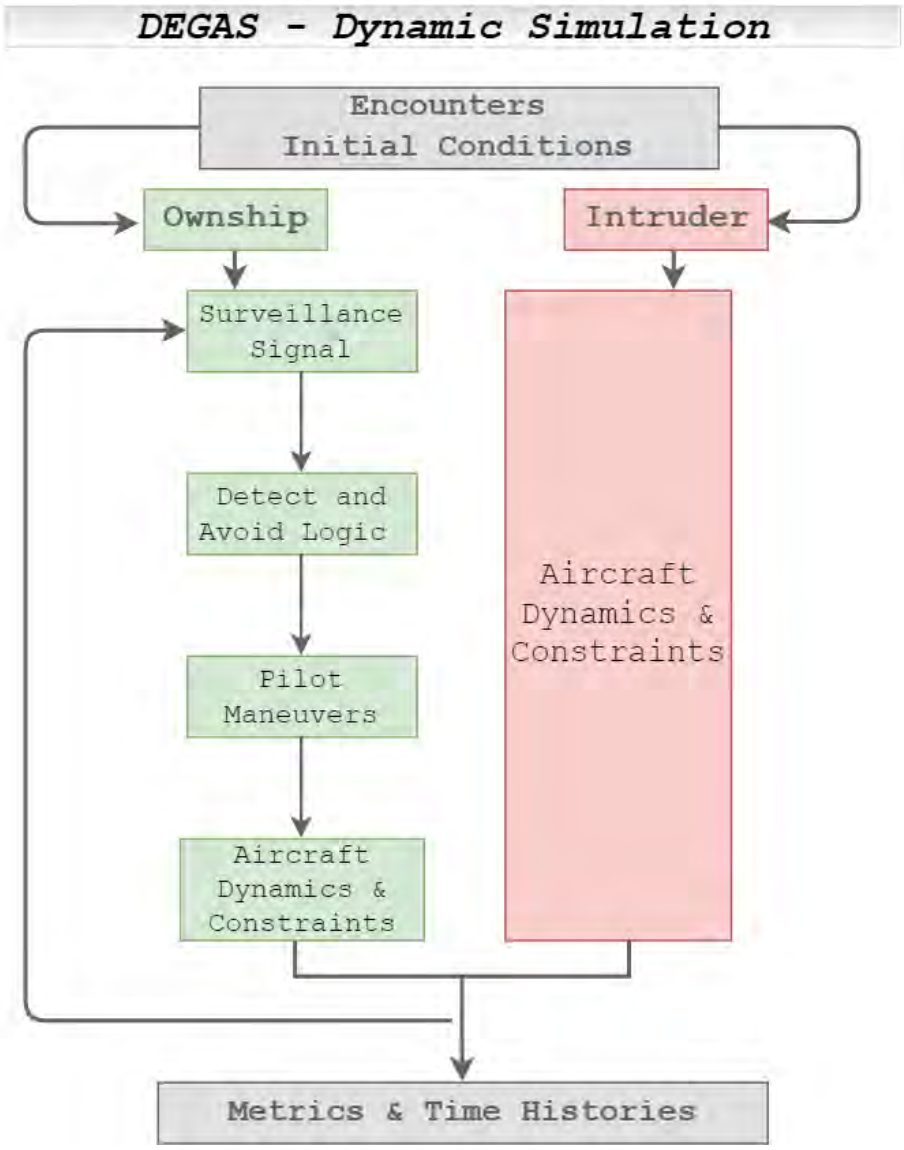

Figure 8. DEGAS functionality (adapted from Serres et al. (2021)).

2.6.1 *DAA Logic*

One of the main objectives of this research was to evaluate the paired trajectories of a small UAS and a manned aircraft (encounter) when the sUAS was equipped with an onboard DAA logic or collision avoidance system. A DAA is a system that enables a remote pilot to "see and avoid" incoming traffic by using sensor and guidance technology (Bender, 2021). This objective was achieved by (1) the identification of a DAA logic that provides a solution to small UAS BVLOS operations, (2) the adoption of a simulation environment (DEGAS) that permits external software integrations (Serres et al., 2020), and (3) the introduction of surveillance source uncertainty for cooperative and non-cooperative aircraft.

Currently, the requirements in the DAA MOPS, DO-365 (SC-228, 2021), do not apply to small UAS that are less than 55 lbs. operating below 400 ft. or other segmented areas (SC-228, 2021). Additionally, the current Part 107 regulations include small UAS flying under Visual Line of Sight operations only. Therefore, when conducting this research, sUAS BVLOS operations did not have a comprehensive solution, such as RTCA MOPS, to comply with see-and-avoid regulations. The FAA TCAS Office (Bender, 2021) provides a DAA solution; ACAS sXu, which is an extension of the ACAS Xu concept (Owen et al., 2019) for smaller UAS. ACAS sXu intends to provide DAA capabilities to sUAS operating BVLOS by receiving multiple surveillance inputs and adapting these to performance requirements that are unique to sUAS operations. Figure 9 is a general overview of the entire ACAS X concept. The ACAS sXu logic was furthered developed independent of this effort, with a Minimum Operational Performance Standard approved by the RTCA Program Management Committee (PMC) in December 2022. ACAS sXu is also the reference architecture for the ASTM F38 DAA performance standard. (ASTM F3442/F3442M-20, 2020).

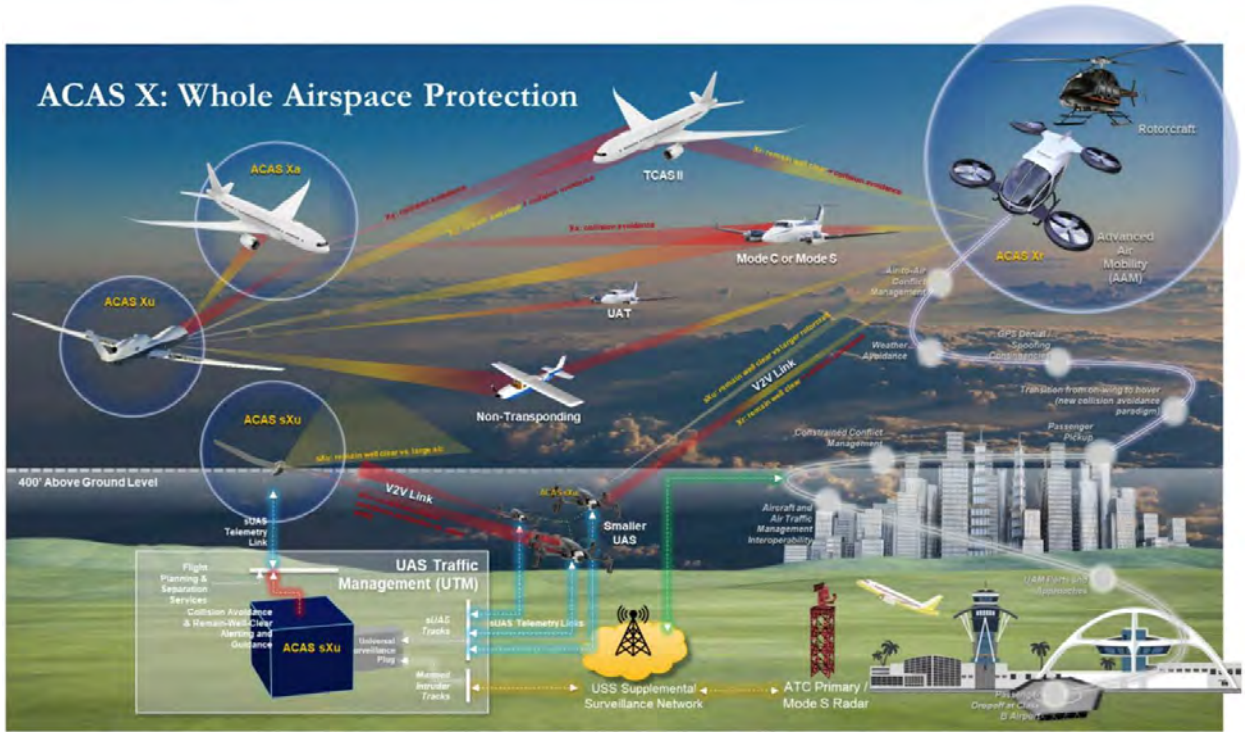

Figure 9. Overall ACAS X Concept (Bender, 2021).

ACAS sXu provides the primary tactical mitigation of collision risk between an sUAS, larger UAS, and manned aircraft. It utilizes cooperative and non-cooperative surveillance that may be onboard the sUAS (ownship), provided by a ground-based link system or a combination of onboard and ground-based sources. (Bender, 2021). ACAS sXu uses a larger protection volume for manned aircraft and larger unmanned aircraft, and a smaller protection volume is used for other sUAS. The logic is structured so that communication with ATC is non-existent; therefore, a single alert level is produced. sXu produces warning alerts and directive guidance in the form of RA. Therefore, immediate awareness of the alert and response is expected. One of the benefits of sXu's directive guidance is that response can be automatic, and no *pilot-in-the-loop* is required. Table 3 and Table 4 highlight the types of RA sXu issues. These can be issued in one-second intervals until the conflict is resolved.

Table 3. ACAS sXu Horizontal RA (Alvarez, 2021).

Action	Description
Clear-of-conflict	No maneuver necessary
Turn Right	At least 3˚/s
Turn Left	At least 3˚/s
Maintain	Maintain target track angle

Table 4. ACAS sXu Vertical RA (Alvarez, 2021).

Action	Description
Clear-of-conflict	No maneuver necessary
Do Not Climb	Used for level-off or preventive guidance
Do Not Descent	Used for level-off or preventive guidance
Climb	Climb with a suggested 1000 ft/min rate
Descend	Descend with a suggested 1000 ft/min rate
Increase Climb	Climb with a vertical rate greater than 1000 ft/min (2500 ft/min suggested)
Increase Descend	Descend with a vertical rate greater than 1000 ft/min (2500 ft/min suggested)
Maintain Vertical Rate	Used to maintain current vertical rate
Multi-threat Level Off	Used to maintain altitude when encountering multiple threats

2.6.1.1 **DAA Tracking and Surveillance Module**

ACAS sXu V4R1 offers a variety of surveillance and tracking entry points that could be used depending on the encounter being analyzed (Jared Wikle et al., 2022). Information related to the position and velocity of the intruder are received as inputs. Table 5 and Table 6 summarize the entry points used in this research for both *1200code-exclude* and *1200code-only* encounter models, respectively. Each entry point receives specific information that describes the encounter geometry and its characteristics.

Table 5. ACAS sXu surveillance modules for *1200-exclude* encounter models (Bender, 2021; Jared Wikle et al., 2022).

Ownship Discretes

toa	v2v uid	opflag	opmode	turn rate	vert rate	wind relative	perform poa	diable gpoa
-	1	TRUE	3	0.053	16.67	FALSE	FALSE	FALSE

Heading OBS

toa	psi rad	heading degraded
-	-	FALSE

Pressure Altitude OBS

toa	alt
-	-

Height AGL OBS

toa	alt hae
-	-

WGS84 OBS

toa	lat	lon	vel_ew	vel_ns	alt	alt rate	nacp	nacv
-	-	-	-	-	-	-	8	2

Airborne Position Report

toa	mode s	non-icao	rebroadcast	lat	lon	alt	alt geo	q int	nic
-	2	FALSE	FALSE	-	-	-	FALSE	25	8

Airborne Velocity Report

toa	mode s	non-icao	rebroadcast	vel_ns	vel_ew	nic
-	2	FALSE	FALSE	-	-	8

Mode Status Report

toa	mode s	non-icao	rebroadcast	adsb version	nacp	nacv	sil	gva	sda	uat
-	2	FALSE	FALSE	2	8	2	3	2	1	FALSE

Externally Validated ADSB

toa	externally validated	mode s	non-icao
-	TRUE	2	FALSE

Table 6. ACAS sXu surveillance modules for *1200-only* encounter models (Bender, 2021; Jared Wikle et al., 2022).

Ownship Discretes

toa	v2v uid	opflag	opmode	turn rate	vert rate	wind relative	perform poa	diable gpoa
-	1	TRUE	3	0.053	16.67	FALSE	FALSE	FALSE

Heading OBS

toa	psi rad	heading degraded
-	-	FALSE

Pressure Altitude OBS

toa	alt
-	-

Height AGL OBS

toa	alt hae
-	-

WGS84 OBS

toa	lat	lon	vel_ew	vel_ns	alt	alt rate	nacp	nacv
-	-	-	-	-	-	-	8	2

Absolute Geodetic Track (AGT)

toa	agt id	mode s	v2v uid	track status	externally validated	classif	lat	lon
-	1	2	2	0	TRUE	1	-	-
vel_ew	vel_ns	covariance hor	baro alt	alt_rate	covariance alt	geo hae	geo hae rate	covariance geo hae
-	-	*[1x16]*	-	-	*[1x4]*	-	-	*[1x4]*

2.6.1.2 **Software Integration**

The adopted DAA logic for this research is ACAS sXu V4R1, which was developed by the FAA TCAS Program Office (Bender, 2021). An early developmental version of V2R0 was leveraged by MIT LL in 2020. .As previously mentioned, modifications to the simulation environment DEGAS were possible because it is open-source software. ACAS sXu has a Julia native coding language (Bezanson et al., 2017), and its integration within the DEGAS environment was achieved through a wrapper written in C++.

Modifications were made within the DEGAS environment to execute ACAS sXu at any given time; due to the nature of the analysis, ACAS sXu was programmed to be executed at a 1-second time step. However, DEGAS cannot directly communicate with the ACAS environment because of the different programming languages. Figure 10 illustrates the integration process that allowed ACAS sXu to be executed in a Matlab/Simulink environment, such as DEGAS.

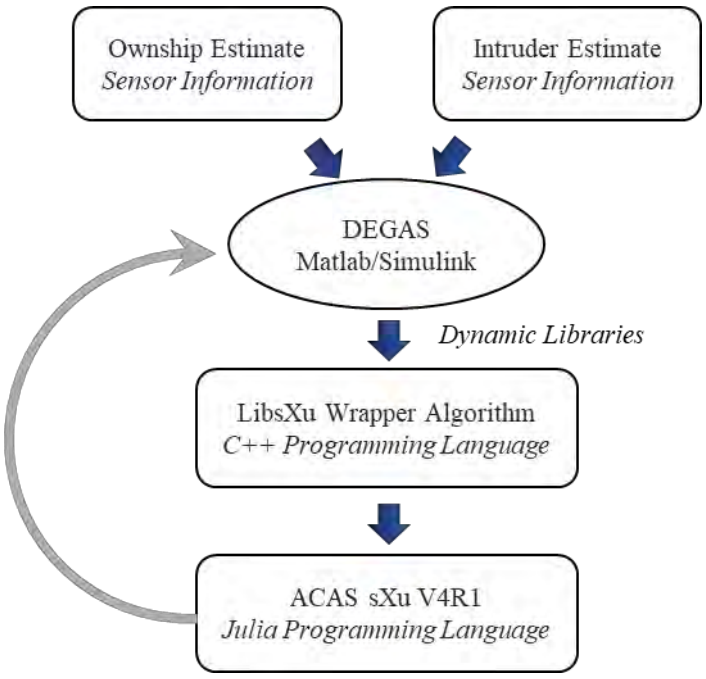

Figure 10. ACAS sXu software integration flowchart.

As illustrated, DEGAS was programmed to communicate or execute the C++ wrapper algorithm, namely *"LibsXu Wrapper"*, by directly calling C/C++ shared libraries or Dynamic-Link Libraries (DLL). The *LibsXu Wrapper* is a wrapper around the base *LibsXu* libraries originally written in the Julia programming language. However, languages such as Python, Matlab, C++, etc., cannot directly access the internal methods of the *LibsXu* library. Hence, the *LibsXu Wrapper* offers a solution by housing sXu objects and providing static entry points to the different object's methods (Young, 2021).

Matlab offers the user capabilities to directly call C and C++ library functionalities (DLL) to create an interface using *"prototype files"* (The MathWorks Inc 2021). This interface allows DEGAS to execute and access the *LibsXu Wrapper* classes and functions, which provides control of the information passed to the sXu objects. This methodology resulted in the most memory and runtime-efficient process when analyzing more than one million encounters.

2.6.1.3 **Software Integration Testing**

The software integration guide provides recommendations on how to test an ACAS sXu integration (Young, 2021). The sXu software integration in a Matlab/Simulink environment was tested and compared against the Test Suite encounters provided in the software package (Katherine Wu et al., 2021). In this research, two main surveillance sources were studied for cooperative and non-cooperative aircraft. Therefore, the respective entry points in the Surveillance Tracking Module (STM) were utilized to construct the encounter appropriately.

For sUAS – cooperative manned aircraft encounter, the following sXu V4R1 entry points were utilized during the analysis. The specifics of each entry point are discussed in Section 2.6.1.1.

- Ownship – GPS
  - Ownship Discretes
  - Pressure Altitude Estimation
  - Heading Estimation
  - Height above Ground Level Estimation
  - WGS84 State Estimation
- Intruder – Automatic Dependent Surveillance-Broadcast (ADS-B)
  - State Vector Position Report
  - State Vector Velocity Report
  - Mode Status Report
  - Externally Validated ADSB Report

For sUAS – non-cooperative manned aircraft encounter, the following sXu V4R1 entry points were utilized during the analysis. The specifics of each entry point are discussed in Section 2.6.1.1.

- Ownship – GPS
  - Ownship Discretes
  - Pressure Altitude Estimation
  - Heading Estimation
  - Height above Ground Level Estimation
  - WGS84 State Estimation
- Intruder – Absolute Geodetic Track Surveillance (AGT)
  - Absolute Geodetic Track

The Test Suite (Katherine Wu et al., 2021) is a set of encounters divided into test groups that are used to validate the correct implementation and functional requirements of the algorithms described in the Algorithm Design Description (ADD) (Jared Wikle et al., 2022). To validate the software integration in DEGAS, a selected set of encounters from the Test Suite were analyzed and compared to assess the functional algorithm correctness through DEGAS. The STM and Threat Resolution Modules (TRM) reports generated from the DEGAS integration were compared to the expected outputs in the Test Suite.

From the STM reports, the following information was checked for proper outputs:

- ground_speed
- psi (heading)
- degraded_own_surveillance
- degraded_surveillance
- belief_vert
- Only one intruder was present in the encounter (stm_report.trm_input)
- The expected surveillance source (stm_report.trm_input.intruder.source)

From the TRM reports, the type of alert and its behavior were compared:

- display_vert
- target_rate
- dz_min, dz_max, ddz_min
- display_horiz

Some of the encounters used to validate the sXu software integration are presented in Table 7 and Table 8. The ACAS sXu V4R0 release was employed in the initial phases of this research, and therefore, the Test Suite encounters from this release were utilized to validate the software integration. As the V4R1 update became available, the integration and analysis were performed with the upgraded logic.

In Table 7 and Table 8, information about the encounter test group, its description, and the surveillance source are presented. Moreover, the vertical and horizontal resolution advisories (RAs) are compared. In all encounters, the alerts issued and reported in the TRM from DEGAS agreed with the ones reported in the Test Suite encounters.

The Test Suite encounters from the V4R1 software update were unavailable when writing this document. Therefore, testing the sXu V4R1 software integration with the V4R1 Test Suite encounters was not possible. However, encounters from the Test Suite V4R0 were analyzed using the sXu V4R1 logic. As a result, outputs from the sXu V4R1 STM and TRM reports are slightly different from V4R0 and, therefore, not included in Table 7 and Table 8. The difference in the information reported in STM and TRM reports is attributed to changes and improvements in the V4R1 logic.

The *Simple.sXu.Runner* is an application part of the sXu V4R1 software package. The application demonstrates the processing steps and scheduling needed to run the logic properly (Young, 2021). It is a Python-based algorithm that parses JSON format files as inputs to the sXu logic. Because this application was available in the sXu V4R1 update, it was utilized to verify that the V4R0 Test Suite encounters analyzed in the DEGAS software integration (with sXu V4R1) yielded the same TRM and STM reports. After this verification process, the sXu V4R1 software integration in DEGAS was deemed correct and valid.

Table 7. Test Suite encounters analyzed in DEGAS – AGT intruder surveillance.

Encounter	Test Group	*Intruder Surveillance*			*Test Suite sXu V4R0*		*DEGAS Integration sXu V4R0*		Multi-Threat	Prescriptive	Description
		AGT (HAE)	AGT (PRES)	ADS-B	Vertical RA	Horizontal RA	Vertical RA	Horizontal RA			
1000001	100	X			4020 6020 1000		4020 6020 1000			X	V4R0: Different RA combinations, no horizontal RA
3110000	311		X		1000 5001 6002	2 3 4	1000 5001 6002	2 3 4			Ownship correlation/decorrelation V4R0: Intruder track disappears, alerting stops at t=24
3120000	312	X								X	Intruder correlation/decorrelation Intruder has V2V-UID matching ownship's V2V-UID No alerting in V4R0
3130000	313		X		1000 5001	1 2	1000 5001	1 2			Intruder correlation/decorrelation V4R0: Intruder track appears at t=34 and alerting begins at t=39
3242005	324	X				3 4		3 4		X	Intruder tracks with different MODE S address Tracks do not correlate throughout the duration of encounter
3242001	324	X		X		1 3		1 3		X	Intruder Track 1: AGT with AGT-ID, anonymous Mode S Intruder Track 2: ADS-B with anonymous Mode S Tracks do not correlate throughout the duration of encounter

Table 8. Test Suite encounters analyzed in DEGAS – ADS-B intruder surveillance.

Encounter	Test Group	*Intruder Surveillance*			*Test Suite sXu V4R0*		*DEGAS Integration sXu V4R0*		Multi-Threat	Prescriptive	Description
		AGT (HAE)	AGT (PRES)	ADS-B	Vertical RA	Horizontal RA	Vertical RA	Horizontal RA			
1000005	10			X	6020 4010 4020 1000					X	Vertical RA combinations, no horizontal RAs
10000009	10			X	6020 4410 1000	1 2	6020 4410 1000	1 2		X	Horizontal and Vertical RA combinations
10000010	10			X	5401 4020 4210 5201 4110 4010	1 2	5401 4020 4210 5201 4110 4010	1 2	X	X	Horizontal and Vertical RA combinations
3241002	324	X		X		3 1		3 1		X	ICAO Mode S correlation Track 1: AGT intruder with AGT ID, V2V-UID ICAO Mode S Track2: ADS-B with ICAO Mode S
4210000	42			X	5001		5001			X	Ownship: Valid pressure altitude and valid HAE Intruder: Valid pressure altitude and no HAE
4210019	42			X						X	Ownship: No valid pressure altitude and in valid HAE Intruder: No pressure altitude and no valid invalid HAE

The numeric codes presented in the vertical RAs fields in Table 7 and Table 8 are a concatenation of fields that describe the vertical resolution advisories (RA). Table 9 introduces the description of every vertical RA that is issued by the logic as well as its description and vertical rate to be maintained. Moreover, the codes describing the horizontal RAs are described in Table 10.

Table 9. ACAS sXu vertical RAs label and definition codes, adapted from (Young, 2021).

Label 270 Code	RA Label	RA Text	Vertical Rate (ft/min)
4010	CL1000	Climb	≥1000
4020	DND	Do Not Descend	≥0
4022	MTLO	Level Off (Issued While Descending)	0
4110	CL1000	Altitude Crossing Climb	≥1000
4210	CL1000	RA Reversal (Descend to Climb)	≥1000
5001	DES1000	Descend	≤-1000
5002	DNC	Do Not Climb	≤0
5022	MTLO	Level Off (Issued While Climbing)	0
5101	DES1000	Altitude Crossing Descend	≤-1000
5201	DES1000	RA Reversal (Climb to Descend)	≤-1000
6002	DNC	Do Not Climb	≤0
6020	DND	Do Not Descend	≥0
6422	MTLO	Level Off	0
4310	SCL2000	Increase Climb	≥2000
4410	MAINTAIN	Maintain Climb Rate	-
5301	SDES2000	Increase Descent	≤-2000
5401	MAINTAIN	Maintain Descent Rate	-
1000	COC	Clear of Conflict	N/A
0	NONE	None	N/A

Table 10. ACAS sXu horizontal RAs label codes.

Label Code	RA Label	RA Text
0	Clear-of-conflict	No maneuver necessary
1	Turn Right	At least 3˚/s
2	Turn Left	At least 3˚/s
3	Maintain	Maintain target track angle

2.6.2 *Resolution Advisory (RA) Execution*

ACAS sXu issues warning alerts only as directive guidance. Therefore, the integration of sXu into DEGAS (Serres et al., 2020) is intended to conserve this functionality. No *pilot-in-the-loop* was developed for this part of the research. Instead, an additional Simulink subsystem block was constructed to process all the RAs. This block calculates new aircraft commands to execute the maneuver and subsequently alter the sUAS nominal trajectory. The *"New Aircraft Commands"* subsystem block, as shown in Figure 11, was developed to communicate to DEGAS all issued alerts (RA's), as well as the target vertical and/or horizontal rates reported in the TRM (Luis Alvarez & Neal A. Suchy, 2021). The new commands are intended to perform the actions shown in Table 3 and Table 4. The commands could involve double (vertical and horizontal) or single maneuvers, depending on the RAs.

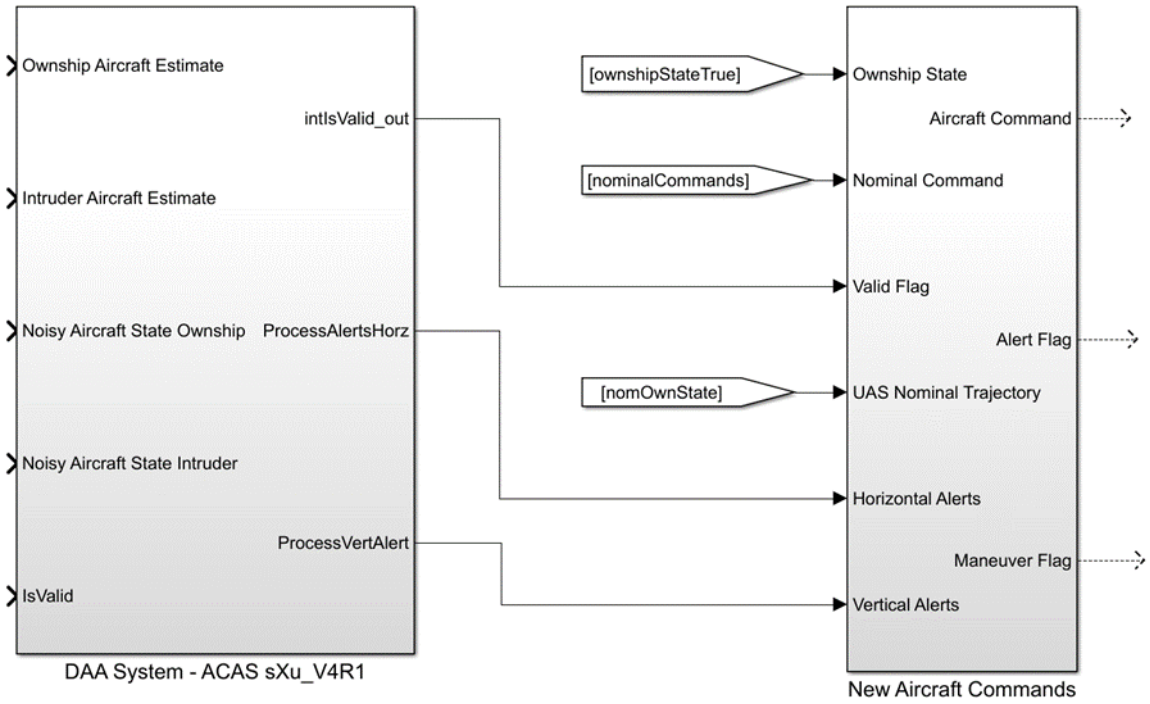

Figure 11. Simulink blocks to process DAA Resolution Advisories (RA) ACAS sXu V4R1.

The subsystem blocks presented in Figure 11 represent a schematic of how the mitigated analysis was performed. A unique subsystem, called *"DAA System – ACAS sXu_v4r1"*, was developed to integrate the DAA logic. The block has input ports in which information about the state and state rate of the sUAS (ownship) and the manned aircraft (intruder) is required. This information can be the true position/altitude or signals from the surveillance sensor in use (noisy).

2.6.3 *Surveillance Sensors*

Section 2.3.1 introduced the type of manned aircraft encounter models that are analyzed in this research. These are categorized based on the transponder code in use when squawking *1200*-code (non-cooperative surrogate) or when squawking something different than the *1200-code* (cooperative). Model-appropriate surveillance sensors were employed in DEGAS (Serres et al., 2020) to introduce position and velocity errors to the manned aircraft trajectories. These signals are then sent to the surveillance and tracking module in ACAS sXu V4R1 (Bender, 2021; Jared Wikle et al., 2022). Table 11 summarizes the types of surveillance used for each encounter model.

Table 11. Surveillance sensors implemented for each encounter model (Serres et al., 2020).

Transponder	Encounter Model	Surveillance Sensor
1200-exclude	FWSE	1090ES ADS-B
	FWME	1090ES ADS-B
	Rotorcraft	1090ES ADS-B
1200-only	FWSE	Ground-based surveillance
	FWME	Ground-based surveillance
	Rotorcraft	Ground-based surveillance

The surveillance sensors are Simulink models which were developed within the DEGAS framework and according to RTCA SC-228 (SC-228, 2021). The models are highly customizable and allow different error or noise introduction levels. The specific position and velocity error distributions used in this analysis are presented in Section 4.

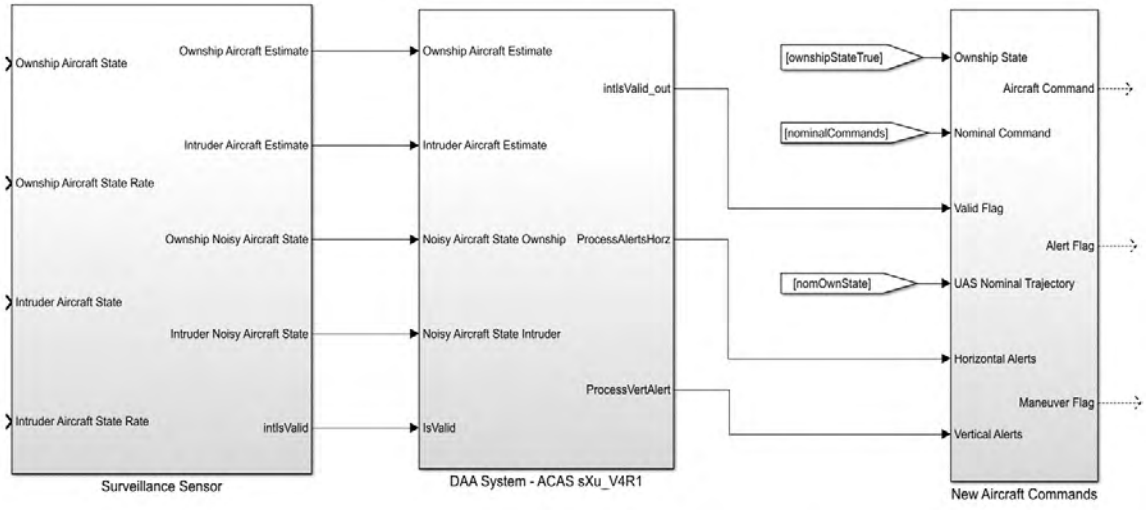

Figure 12. Simulation architecture for mitigated analysis using ACAS sXu V4R1 as DAA logic.

2.6.3.1 **Automatic Dependent Surveillance-Broadcast – ADS-B**

The ADS-B sensor model is included in the DEGAS framework as specified by RTCA SC-228 (SC-228, 2021; Serres et al., 2020). This surveillance model relies on a satellite-based system utilizing navigation sources such as. Global Navigation Satellite Systems (GNSS) and Inertial Navigation Systems (INS). The Simulink model provides one second updates (1 Hz) of precise location and speed of the manned aircraft. The ADS-B Simulink model takes the intruder state, intruder state rate, and the ownship state as inputs and outputs the intruder aircraft estimate (noisy position) and covariance matrix. Positional and velocity errors are added based on the expected accuracy, NACp and NACv respectively. The position signals are then delayed by a random amount to simulate avionic delays before providing information to the DAA or other connected systems.

To illustrate the effects that ADS-B equipment has on aircraft position and velocity, a sensitivity analysis was performed. A manned aircraft trajectory was analyzed using different types of error distributions (NACp and NACv). Figure 13 compares a manned aircraft's north and east position to its true position. Moreover, Figure 14 illustrates an aircraft's airspeed estimate at different NACv error values.

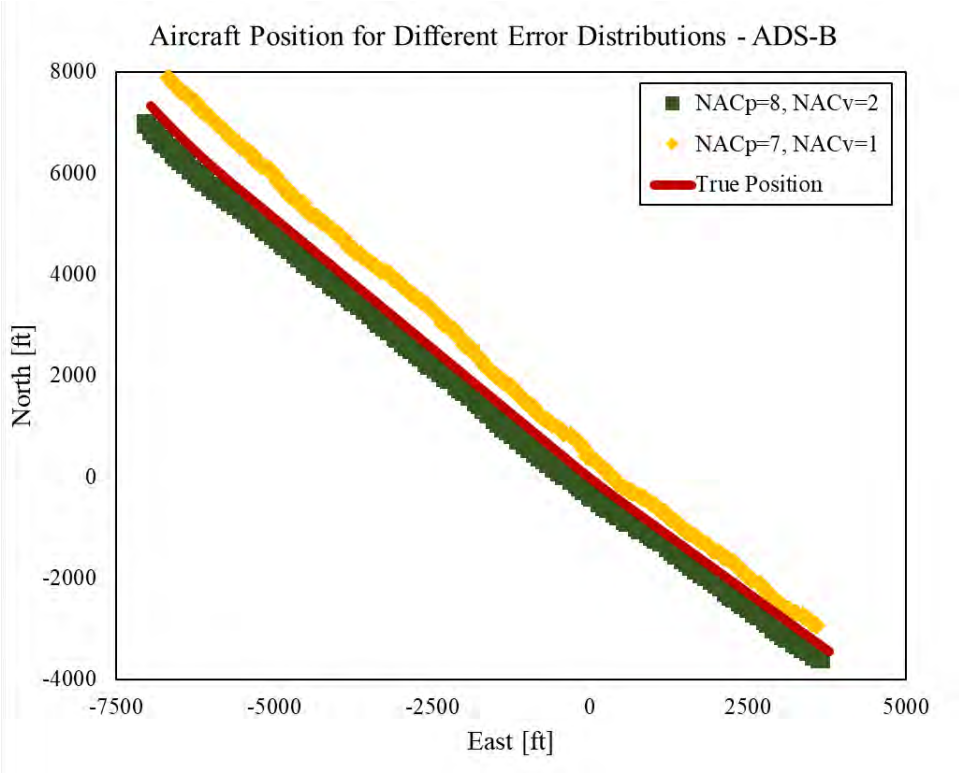

Figure 13. Aircraft position comparison (ADS-B) – DEGAS v1.0 (Serres et al., 2020).

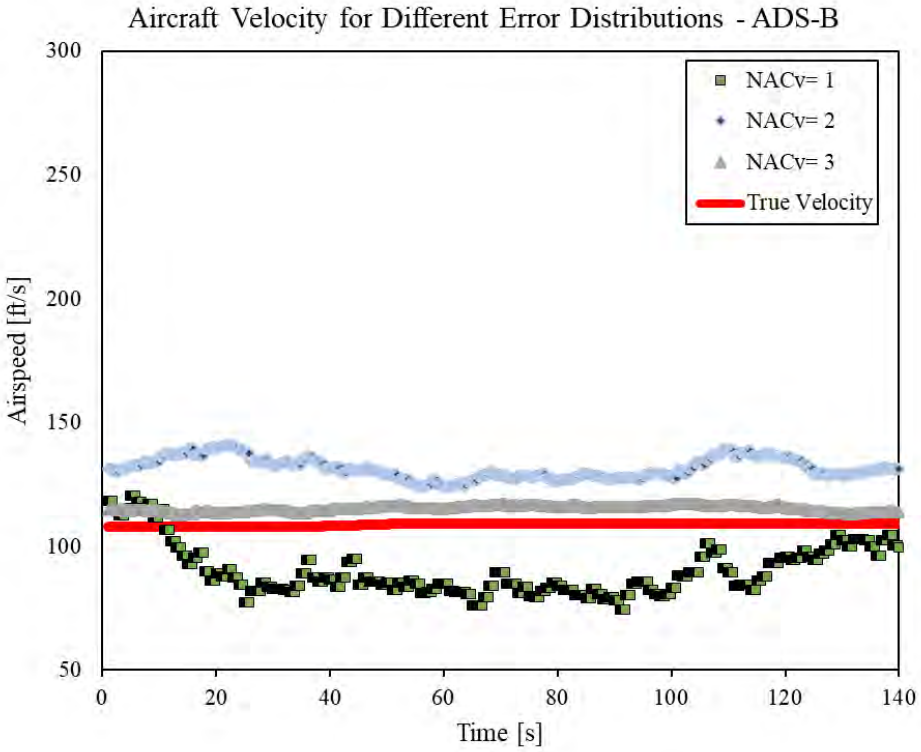

Figure 14. Aircraft velocity comparison (ADS-B) – DEGAS v1.0 (Serres et al., 2020).

2.6.3.2 **Ground-Based Surveillance System – GBSS**

The Ground-Based Surveillance System (GBSS) was modeled using a three-dimensional Gauss-Markov model for position and velocity as defined by the minimum operational performance standards for DAA systems (SC-228, 2021). Bias for position and velocity errors were included. For the mitigated analysis of this research, the noise and bias values were selected from the ACAS sXu MOPS (SC-147, 2022a). Table 12 introduces the error models applied to each parameter for the AGT requirements; these tracks are drawn from Gaussian distributions with a bias for position only.

Table 12. Error models for the AGT ground-based surveillance requirements, adapted from (SC-147, 2022a).

Parameter	Error Model	Bias μ	Sigma σ
Latitude / Longitude	*N(horBias, horSigma)* ft	biasHorM	pHorM
Velocity NS/EW	*N(0, horVelSigma)* ft/s		vHorMS
Geo Altitude	*N(vertBias, vertSigma)* ft	biasAltM	pAltM
Geo Altitude Rate	*N(0, vertVelSigma)* ft/s		vAltMS
Horizontal Covariance	*Diag(horSigma, horVelSigma)*^{2}	covRatio	
Vertical Covariance	*Diag(vertSigma, vertVelSigma)*^{2}	covRatio	

The GBSS radar is implemented as a Simulink model that receives true position signals from DEGAS and sends the noisy signals to the ACAS sXu's AGT surveillance. The specifics of the error models are explained in Section 4 for the *1200-only* (non-cooperative) encounters. In this study, the detection range is at least 1.5 NM along the trajectory of the sUAS. The sensor scans and updates new tracks every second or 1Hz. Moreover, the tracks are set to always be valid with a 100% of probability of track update within the detection range.

To highlight the error and bias effects of this sensor model, a sensitivity analysis was performed on the position and altitude of a manned aircraft, as shown in Figure 15 and Figure 16. The error models shown in Table 13 were used for the sensitivity analysis.

Table 13. Error models used for sensitivity analysis.

	Model 1		**Model 2**	
Parameter	Bias μ	Sigma σ	Bias μ	Sigma σ
Latitude / Longitude	481.3	338.9	649.6	899.0
Velocity NS/EW		31.6		39.4
Geo Altitude	663.6	678.0	1128.6	5902.2
Geo Altitude Rate		63.8		8.5

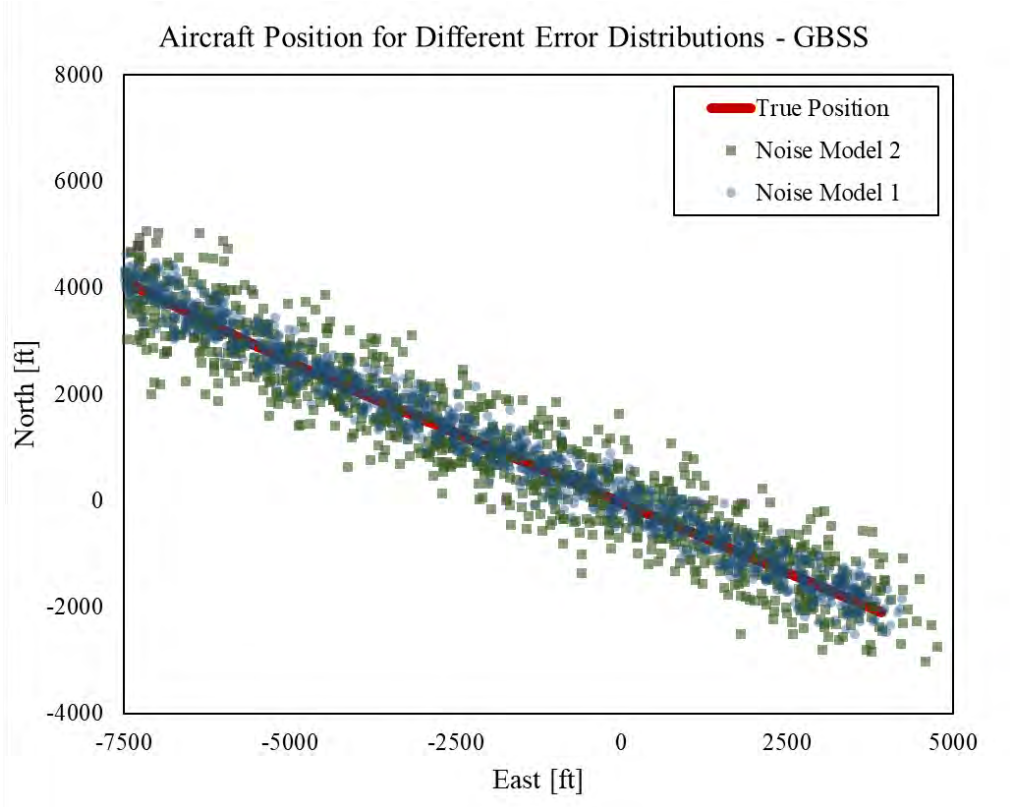

Figure 15. Aircraft position comparison (GBSS) – DEGAS v1.0 (Serres et al., 2020).

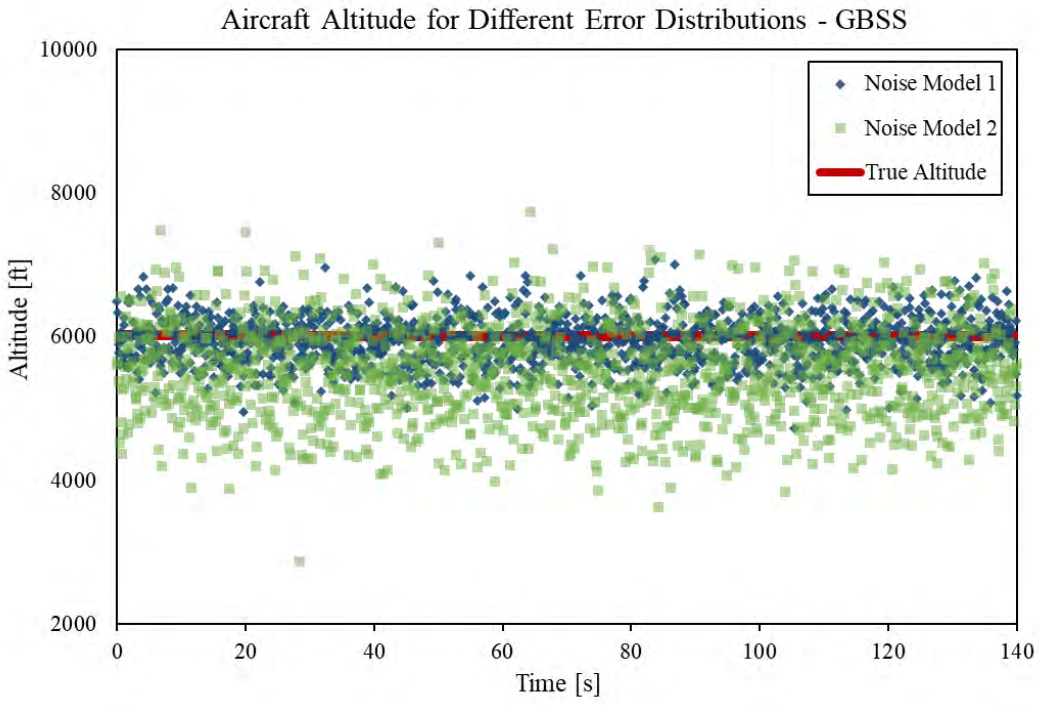

Figure 16. Aircraft altitude comparison (GBSS) –DEGAS v1.0 (Serres et al., 2020).

2.6.3.3 **Global Positioning System – GPS/INS**

The GPS sensor was also developed as part of DEGAS according to SC-228 guidelines (SC-228, 2021; Serres et al., 2020). The sensor is modeled as a Simulink block and allows for error or noise defined by the user. The sensor is based on the Inertial Navigation System (INS) performance and provides information related to the position, velocity, and altitude of the sUAS (ownship). The GPS sensor is based on the expected ADS-B performance. A Gaussian distribution model is used for the roll and pitch, and a Gauss Markov model is used for the position and velocity errors.

2.6.4 ***Unmitigated vs. Mitigated Encounter***

Figure 17 and Figure 18 illustrate an encounter when there is no DAA equipment in-use and when the DAA is enabled, respectively. The change in the trajectory of the sUAS can be observed in the East vs. North plots, which means that the logic issued horizontal RAs. However, no vertical maneuvers were issued in this case. Metrics such as the VMD, HMD, NMAC, and Well Clear Violation (WCV) are shown for both nominal and mitigated cases. After a *Clear of Conflict (COC)* resolution is issued, the sUAS trajectory is allowed to continue with its nominal commands; however, no *return-to-course* was implemented in this research.

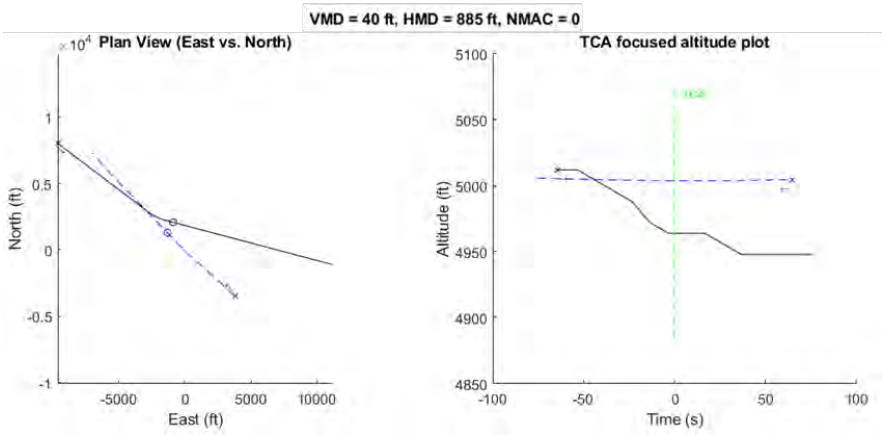

Figure 17. Unmitigated encounter (no DAA) – DEGAS v1.0(Serres et al., 2020).

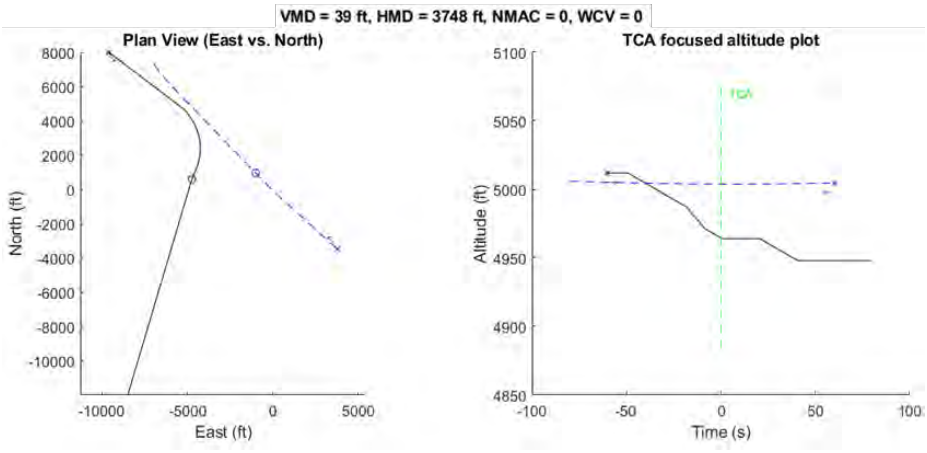

Figure 18. Mitigated encounter (DAA: sXu V4R1) – DEGAS v1.0(Serres et al., 2020).

2.7 Collision Detection

A methodology for identifying the MAC impact location was developed. It will be used to determine the distribution of impact locations on the manned aircraft and the performance of the DAA system in mitigating them. Figure 19 illustrates examples of MACs on different types of manned aircraft.

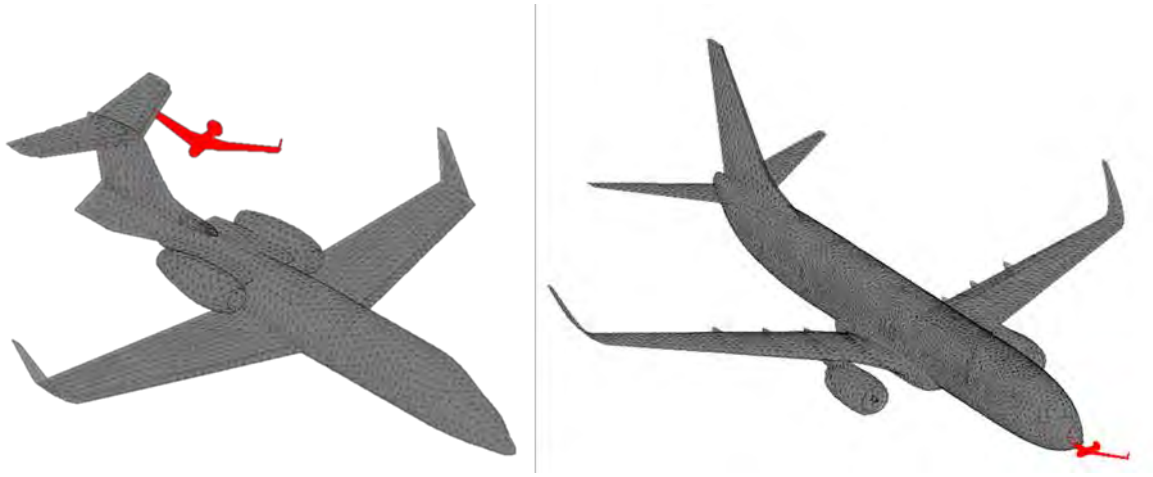

Figure 19. Example of mid-air collision cases detected.

This section explains the methodology employed and the algorithm in use. Additionally, a library of the manned aircraft and sUAS models that are considered in this study is presented. The same methodology and models are used for the unmitigated and mitigated cases.

2.7.1 *Algorithm Description*

The collision detection was separated into two phases, (1) to detect a collision and (2) to determine its corresponding location on the manned aircraft. The analysis method is shown in Figure 20. Additional information describing the state of both aircraft at the time of the collision was stored in a database. The information recorded is as follows.

- Manned aircraft position and orientation at the time of MAC.
- sUAS position and orientation at the time of MAC.
- Manned aircraft and sUAS velocity vectors at the time of MAC.
- Collision location on the manned aircraft at the time of MAC.

The unmitigated and mitigated collision databases will serve as the basis for severity assessment in future analyses.

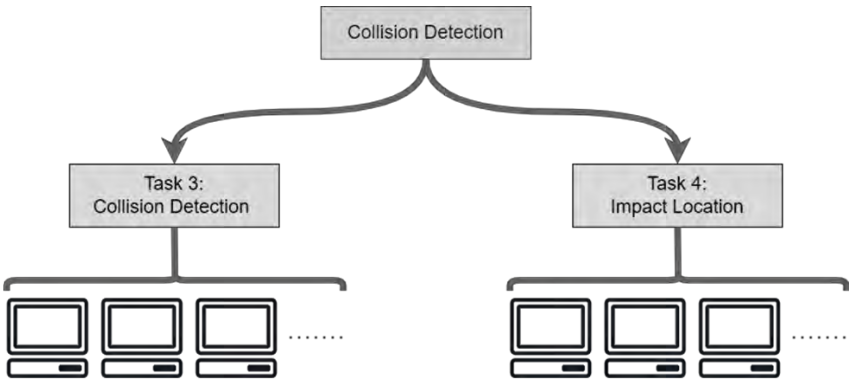

Figure 20. Collision detection and impact location analysis schematic.

2.7.1.1 **Collision Detection**

As previously stated, DEGAS (Serres et al., 2020) is an environment capable of analyzing trajectories using 6-DOF point mass equations. Therefore, it cannot detect a MAC as no information regarding the aircraft geometries can be introduced. For collision detection, encounters that resulted in NMACs were recorded. These encounters are then analyzed through a separate algorithm for collision detection. Since the position and orientation of both aircraft were recorded from DEGAS, it is possible to recreate the entire encounter at every time step. Figure 21 illustrates an encounter where geometries for the ownship (green) and intruder (black) were introduced.

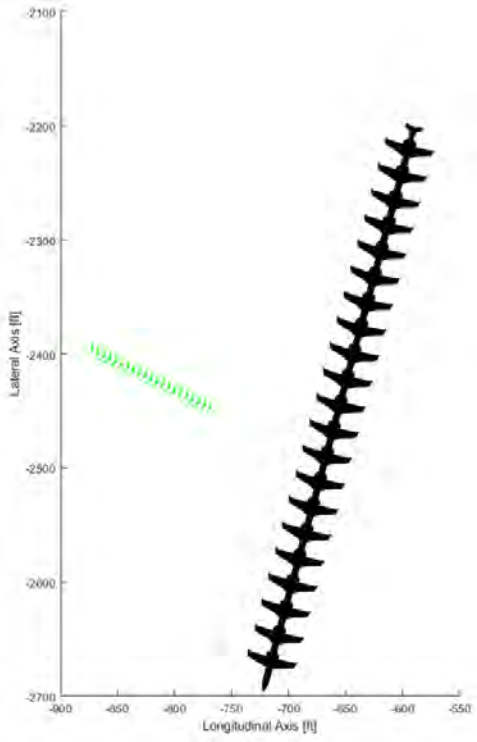

Figure 21. sUAS-manned encounter with their geometric representations.

Once the geometry, relative position, and state of both aircraft are accurately represented, the aircraft bodies are subjected to collision detection for several time steps. The V-COLLIDE algorithm (Hudson et al., 2000) was implemented for detecting collisions between bodies. V-COLLIDE is an algorithm that allows collision analysis of arbitrary polygonal models undergoing rigid body motions. It unifies previous large-scale collision detection techniques and hierarchical data structures (Hudson et al., 2000).

V-COLLIDE's library was developed in C++ and was released in February 1998. A Matlab interface for executing the C++ codes is needed. COLDETECT is an open-source code that utilizes Matlab Executable (MEX) function capabilities (Mykel Kochenderfer, 2008) to execute V-COLLIDE. The MEX function takes object geometries as inputs from Matlab and executes V-COLLIDE's library for collision detections. The input geometries are discretized with rigid polygons. Eq. (1) is the execution line in Matlab.

$$\mathrm{T} = COLDETECT(TRI1, TRI2, TRANS1, TRANS2) \tag{1}$$

Where *T* is an index output of the function that indicates whether a collision was detected or not (0-1), *TRI1* and *TRI2* are (N by 9) matrices describing the object geometries; and *TRANS1* and *TRANS2* are transformation matrices.

The trajectory of each aircraft during an encounter is 140 seconds long and is recorded at 10 Hz. Frequency plays an important role in determining collisions from one time step to the next. The frequency should be high enough to capture all the possible MACs. However, it should not be extremely high to incur significant computational time. For this reason, position, state, and time values were interpolated to 100 Hz (time step of 0.01 s). Figure 22 illustrates the same encounter at different frequencies. The collision was only detected at 100 Hz. The intruder's airframe is shown in a black mesh-like style at the time of the collision.

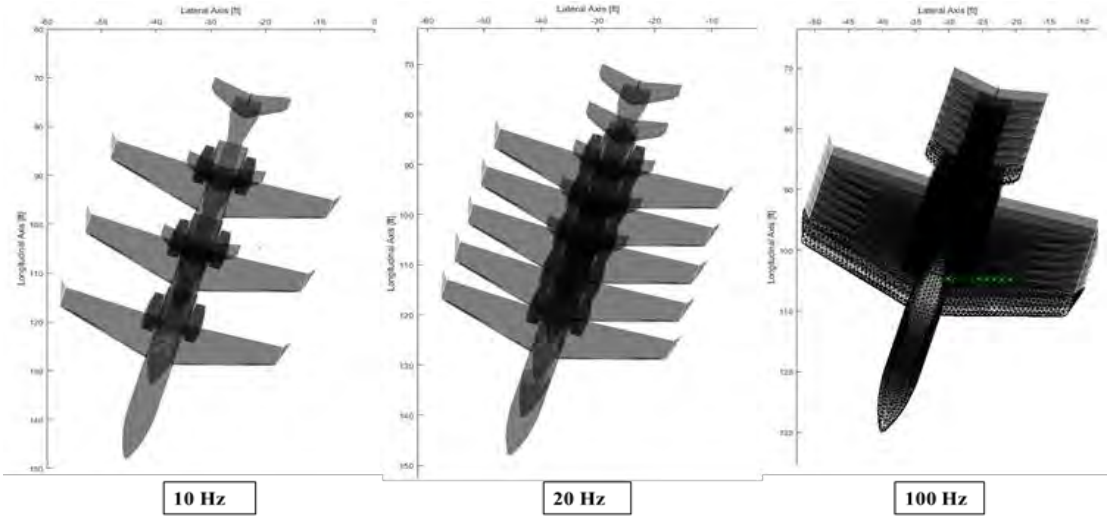

Figure 22. Collision evaluation at different frequencies.

Additionally, Table 14 summarizes the specific instances when V-COLLIDE was executed. For example, if the encounter Time of the Closest Approach (TCA) is at *Time* = 100, V-COLLIDE

would be executed 21 times. Its execution would start at *Time* = 99.90 (s) until *Time* = 100.10 (s) at 0.01s step. This avoids wasting computational resources when the aircraft are far apart.

Table 14. Collision detection execution times.

Time	Collision Check
TCA-10t	V-COLLIDE
TCA	**V-COLLIDE**
TCA+10t	V-COLLIDE

Note: *TCA* is the time of closest approach
t is the simulation time step (0.01 seconds)

2.7.1.2 Impact Locations on Manned Aircraft

Specific locations and areas of a collision on manned aircraft are of high interest for the current research. Relationships between size, speed, and additional flight characteristics can inform the severity of a MAC.

The methodology developed to detect the specific impact locations was derived from Section 2.7.1.1. From the previous section, the encounters which resulted in a MAC were recorded. V-COLLIDE (Hudson et al., 2000) was once again utilized for this subsequent analysis. The objective was to identify all the polygonal elements on the manned aircraft body under collision. To accomplish this, every element composing the manned aircraft body was analyzed using Eq. (1). Once the intersecting elements were detected, their corresponding location ID was determined. Figure 23 illustrates the identification of an intersecting element on the manned aircraft.

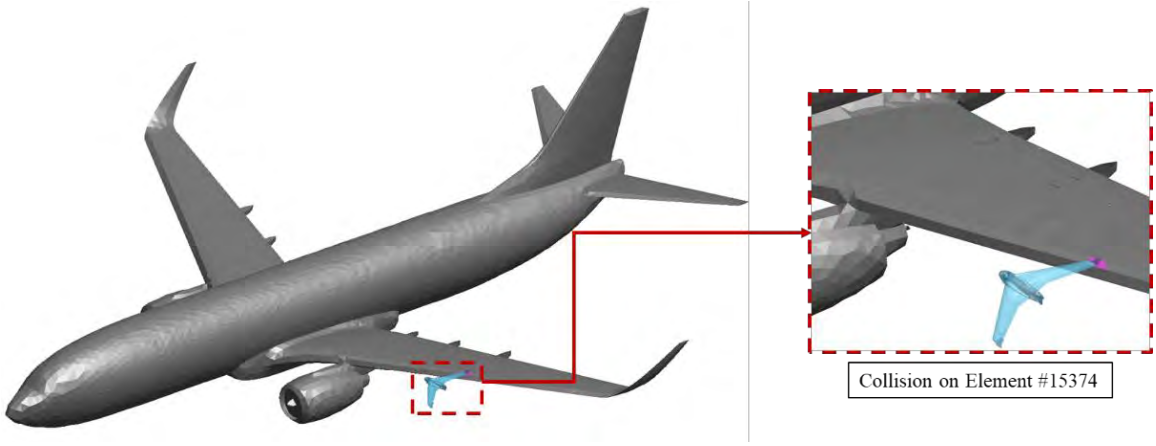

Figure 23. Identification of intersecting elements on manned aircraft geometry.

2.7.2 *Model Description*

The aircraft geometries considered to perform the collision detection analysis were informed by previous collision severity studies (Olivares et al., 2020; Olivares, Gomez, et al., 2017; Olivares, Lacy, et al., 2017).

2.7.2.1 **Intruder Models**

From the uncorrelated encounter models described in Section 2.3, trajectories representing four different types of aircraft were generated. The aircraft types are rotorcraft, fixed-wing multi-engine, and fixed-wing single-engine. Figure 24 illustrates the intruder models used for the analysis.

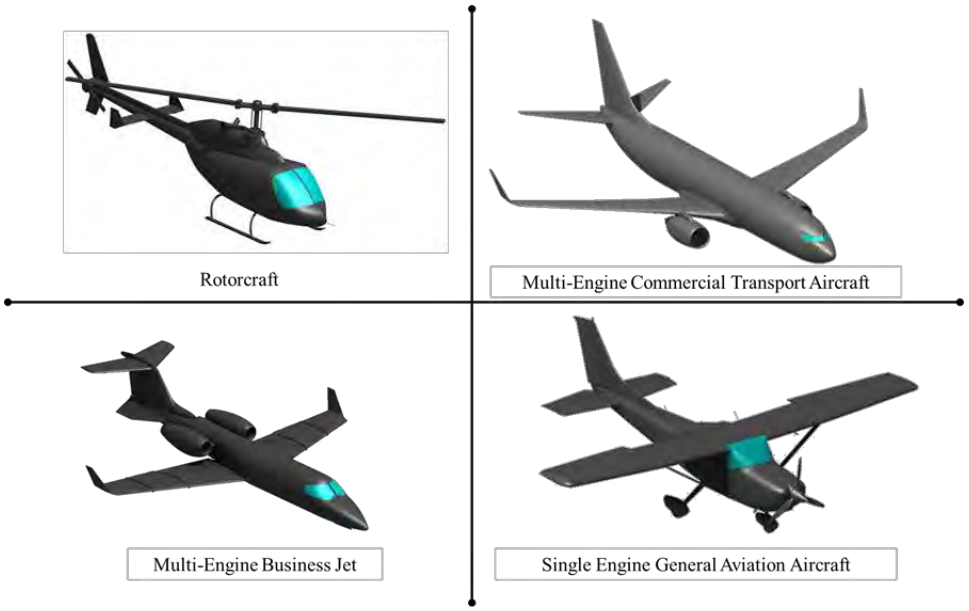

Figure 24. Manned aircraft models for collision detection.

Moving parts of the manned aircraft models, such as propellers and rotors, were represented as static disk-like objects in the polygon models for the collision detection analysis, as shown in Figure 25. Moreover, the size of all intruder models analyzed is shown in Table 15. The measurements for all the models are based on the illustration in Figure 25.

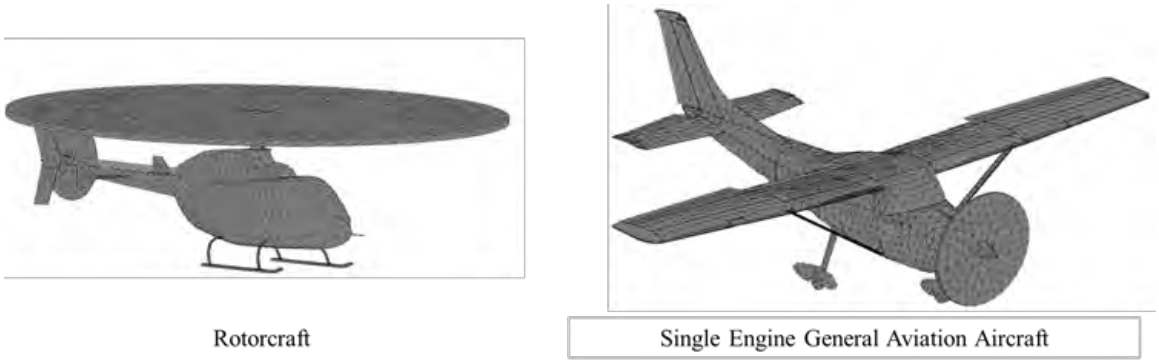

Figure 25. Representation of propellers and rotor parts in the manned aircraft models.

Table 15. Intruder models' dimensions.

Intruder Model	# Seats	Wing Span* (ft)	Body Length (ft)	Exterior Height (ft)
General Aviation	[1,4]	35.8	26.2	10.6
Rotorcraft	[1,4]	40.7	38.4	12.8
Business Jet	[2,10]	42.6	45.6	10.2
Commercial Transport	[1,140]	111.0	124.0	38.8

**Rotorcraft measurement is the main rotor diameter*

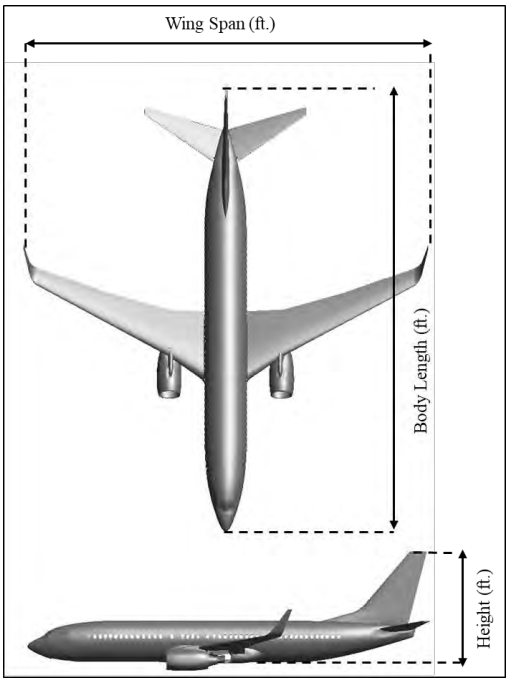

Figure 26. Intruder model size measurements – Commercial transport.

These manned aircraft models were used to develop MAC severity studies in previous research projects (Olivares et al., 2020; Olivares, Gomez, et al., 2017; Olivares, Lacy, et al., 2017). Collision severity levels were determined via finite element simulations for the same models. The research aims to correlate the collision results from the present study with the severity results from past studies based on the mass and velocity of the collision.

2.7.2.2 **Ownship Models**

Previous ASSURE research also informed the sUAS models selected for the collision detection analysis. These studies used the same sUAS models to determine MAC severity levels (Olivares et al., 2020; Olivares, Gomez, et al., 2017; Olivares, Lacy, et al., 2017). The smaller size sUAS models are 4 and 25 lbs. and the large size sUAS models are 55 lbs. These sUAS models are shown in Figure 27 and Figure 28, respectively.

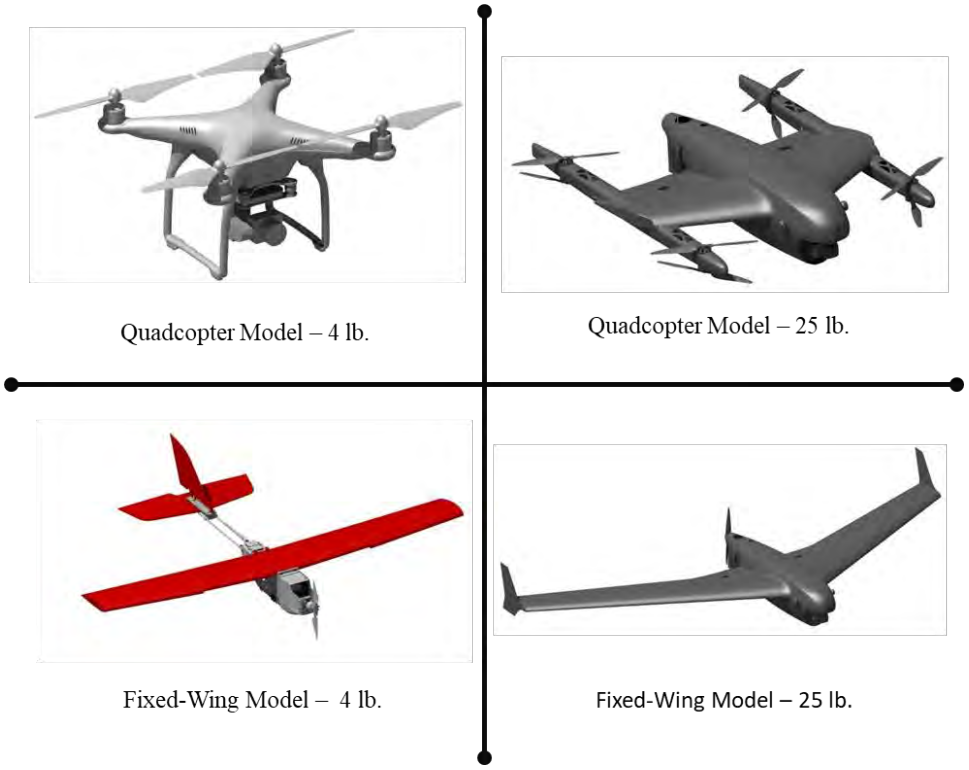

Figure 27. Smaller size sUAS models for collision detection (Olivares et al., 2020; Olivares, Gomez, et al., 2017; Olivares, Lacy, et al., 2017).

Figure 28. Larger size sUAS models for collision detection (Olivares et al., 2020).

Similarly, the ownship polygon models for collision analysis were modified. The modifications were made to capture the moving parts better when the sUAS is in-flight. All propellers were modified to static disk-like objects using the original radii.

The size of all sUAS models analyzed is shown in Table 16. The measurements for fixed-wing and multicopter are based on the illustrations in Figure 29 and Figure 30, respectively. Because all sUAS trajectories are pre-defined in the encounter set, the sUAS models are assumed to be capable of achieving all performance specifications related to the trajectory, such as altitude ceiling, min/max speeds, and turn/climb rates. Therefore, the dimension of the sUAS is the characteristic that determines whether a collision occurs or not in the same encounter. The likelihood of each sUAS performing any particular trajectory was not assessed. When a DAA system is in use, the minimum expected performance characteristics of the sUAS are employed. These are specified in Section 4.

Table 16. Ownship models' dimensions.

Ownship Model	Type	Wing Span (in)	Body Length (in)	Height (in)
sUAS - 4 lb	Quadcopter	19.2	11.2	7.9
sUAS - 25 lb	Quadcopter	44.2	37.1	9.3
sUAS - 55 lb	Quadcopter	57.4	48.3	12.1
sUAS - 4 lb	Fixed-Wing	64.2	42.6	5.3
sUAS - 25 lb	Fixed-Wing	127.1	47.7	11.6
sUAS - 55 lb	Fixed-Wing	165.3	62.0	15.1

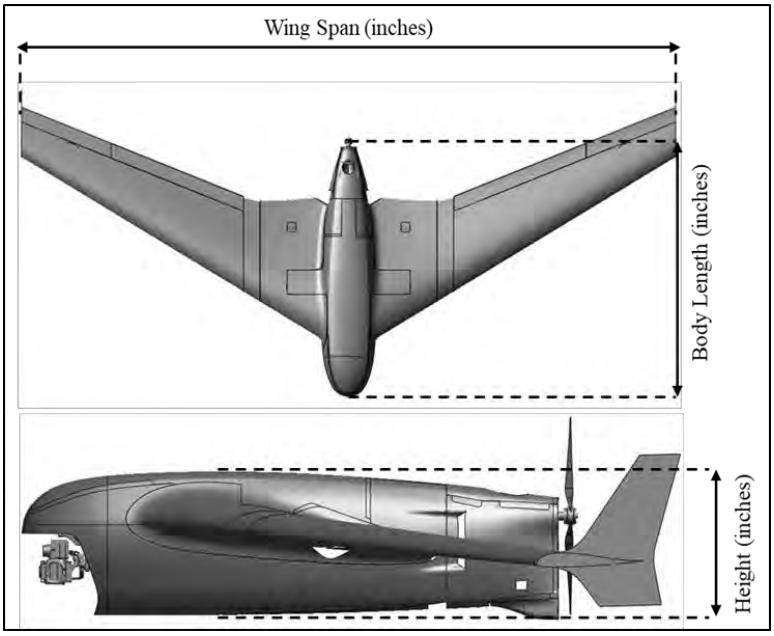

Figure 29. sUAS size measurements – Fixed-wing.

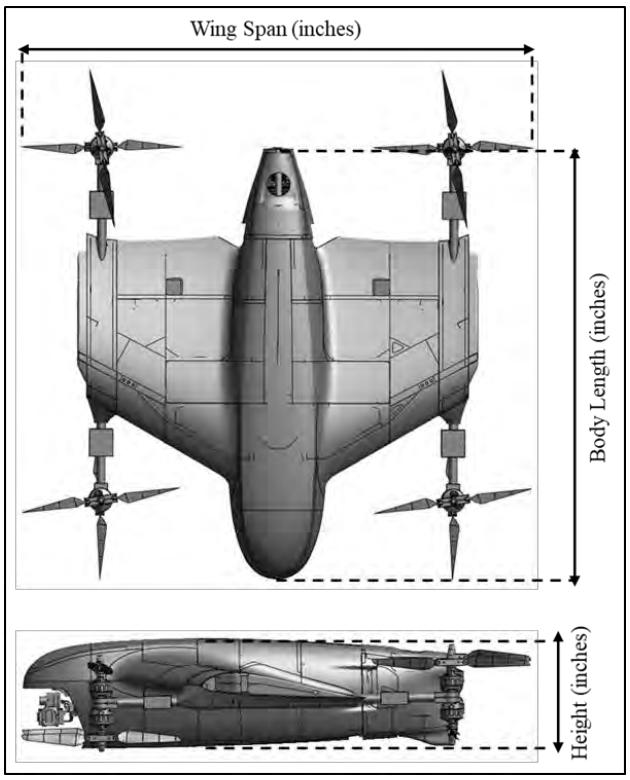

Figure 30. sUAS size measurements – Quadcopter.

A methodology for detecting collisions between manned and unmanned aircraft has been presented. Extended capabilities consist of determining the exact impact location on the manned aircraft. The entire process can be summarized as:

1. Collect encounters from DEGAS that resulted in NMAC
2. Detect if a collision occurred based on the position and orientation of both aircraft
3. Detect where the collision occurred on the manned aircraft (wings, cockpit, fuselage, etc.)

Table 17 presents the collision analysis matrix that combines the encounter models with their corresponding intruder and ownship models.

Table 17. Analysis matrix for collision detection.

Encounter Model	Intruder	Ownship		Analysis Type
Rotorcraft Non-Cooperative Surrogate	Rotorcraft	Quadcopter	DJI Phantom 4 lb.	Unmitigated + Mitigated
			Search & Rescue 25 lb.	Unmitigated + Mitigated
			Search & Rescue 55 lb.	Unmitigated + Mitigated
		Fixed-Wing	Precision Hawk 4 lb.	Unmitigated + Mitigated
			Search & Rescue 25 lb.	Unmitigated + Mitigated
			Search & Rescue 55 lb.	Unmitigated + Mitigated
Rotorcraft Cooperative Surrogate	Rotorcraft	Quadcopter	DJI Phantom 4 lb.	Unmitigated + Mitigated
			Search & Rescue 25 lb.	Unmitigated + Mitigated
			Search & Rescue 55 lb.	Unmitigated + Mitigated
		Fixed-Wing	Precision Hawk 4 lb.	Unmitigated + Mitigated
			Search & Rescue 25 lb.	Unmitigated + Mitigated
			Search & Rescue 55 lb.	Unmitigated + Mitigated
Fixed-Wing Single Engine Non-Cooperative Surrogate	General Aviation	Quadcopter	DJI Phantom 4 lb.	Unmitigated + Mitigated
			Search & Rescue 25 lb.	Unmitigated + Mitigated
			Search & Rescue 55 lb.	Unmitigated + Mitigated
		Fixed-Wing	Precision Hawk 4 lb.	Unmitigated + Mitigated
			Search & Rescue 25 lb.	Unmitigated + Mitigated
			Search & Rescue 55 lb.	Unmitigated + Mitigated
Fixed-Wing Single Engine Cooperative Surrogate	General Aviation	Quadcopter	DJI Phantom 4 lb.	Unmitigated + Mitigated
			Search & Rescue 25 lb.	Unmitigated + Mitigated
			Search & Rescue 55 lb.	Unmitigated + Mitigated
		Fixed-Wing	Precision Hawk 4 lb.	Unmitigated + Mitigated
			Search & Rescue 25 lb.	Unmitigated + Mitigated
			Search & Rescue 55 lb.	Unmitigated + Mitigated
Fixed-Wing Multi-Engine Non-Cooperative Surrogate	Business Jet	Quadcopter	DJI Phantom 4 lb.	Unmitigated + Mitigated
			Search & Rescue 25 lb.	Unmitigated + Mitigated
			Search & Rescue 55 lb.	Unmitigated + Mitigated
		Fixed-Wing	Precision Hawk 4 lb.	Unmitigated + Mitigated
			Search & Rescue 25 lb.	Unmitigated + Mitigated
			Search & Rescue 55 lb.	Unmitigated + Mitigated
Fixed-Wing Multi-Engine Cooperative Surrogate	Business Jet / Commercial transport	Quadcopter	DJI Phantom 4 lb.	Unmitigated + Mitigated
			Search & Rescue 25 lb.	Unmitigated + Mitigated
			Search & Rescue 55 lb.	Unmitigated + Mitigated
		Fixed-Wing	Precision Hawk 4 lb.	Unmitigated + Mitigated
			Search & Rescue 25 lb.	Unmitigated + Mitigated
			Search & Rescue 55 lb.	Unmitigated + Mitigated

2.8 **Common Analytical Metrics**

This section presents the safety metrics calculated and recorded from DEGAS for further analysis. The common metrics to evaluate the safety and performance of the DAA system are Risk Ratio (RR) and LoWCR. Moreover, this research explores the probability of a MAC given an NMAC; *P(MAC|NMAC),* and MAC Ratio.

2.8.1 ***Risk Ratio and Loss of Well Clear Ratio***

The risk ratio is a quantity that helps measure the performance of the Collision Avoidance System or DAA logic in use for a given encounter set. The risk ratio compares the number of encounters that resulted in an NMAC equipped with DAA to the number of encounters that resulted in an NMAC without a DAA, as given by Eq. (2). Therefore, this quantity describes the capability of a DAA system to mitigate an NMAC within the context of the encounter sets used.

$$Risk\ Ratio = \frac{mitigated\ P(NMAC)}{unmitigated\ P(NMAC)} \tag{2}$$

where an NMAC is defined as penetration of a cylindrical volume of fewer than 500 feet horizontally and 100 feet vertically. This NMAC definition is often used in modeling and simulation and differs slightly from a policy-based definition of a loss of 500 ft of separation that is intended for incident reporting, investigation of dangerous encounters, and characterizing trends of airborne risk. For example, a 0.4 risk ratio translates to a 60% reduction in the number of NMACs given an encounter for a given encounter set when a DAA system is equipped. When a different encounter set is used, the same DAA system may result in a different risk ratio value. P(NMAC) for a weighted encounter set is calculated using Eq. (4). w_i represents the weight of an individual encounter. An unweighted encounter set assumes a weight of 1 for each encounter ($w_i = 1$)

$$P(NMAC) = \frac{\sum_{i=1}^{N} NMAC_i * w_i}{\sum_{i=1}^{N} w_i} \tag{3}$$

The LoWCR is also utilized as a metric to assess the performance of the DAA logic for a given encounter set. In the same manner, it establishes a relationship between the number of encounters that incurred a well-clear violation with an equipped DAA system to the number of encounters that incurred a well-clear violation without a DAA system.

$$LoWC\ Ratio = \frac{mitigated\ P(LoWC)}{unmitigated\ P(LoWC)} \tag{4}$$

Similarly, P(LoWC) for an encounter set is calculated using Eq. (5). w_i is the weight of an individual encounter as used in Eq. (4).

$$P(LoWC) = \frac{\sum_{i=1}^{N} LoWC_i * w_i}{\sum_{i=1}^{N} w_i} \tag{5}$$

This research uses the well-clear volume suggested by ASTM F38 (ASTM F3442/F3442M-20, 2020). A separation of fewer than 2000 feet horizontally and 250 feet vertically will determine if an aircraft is in a well-clear violation. Likewise, the LoWCR indicates the performance of the DAA system in mitigating well-clear violations. The well-clear and NMAC volumes are illustrated in Figure 31.

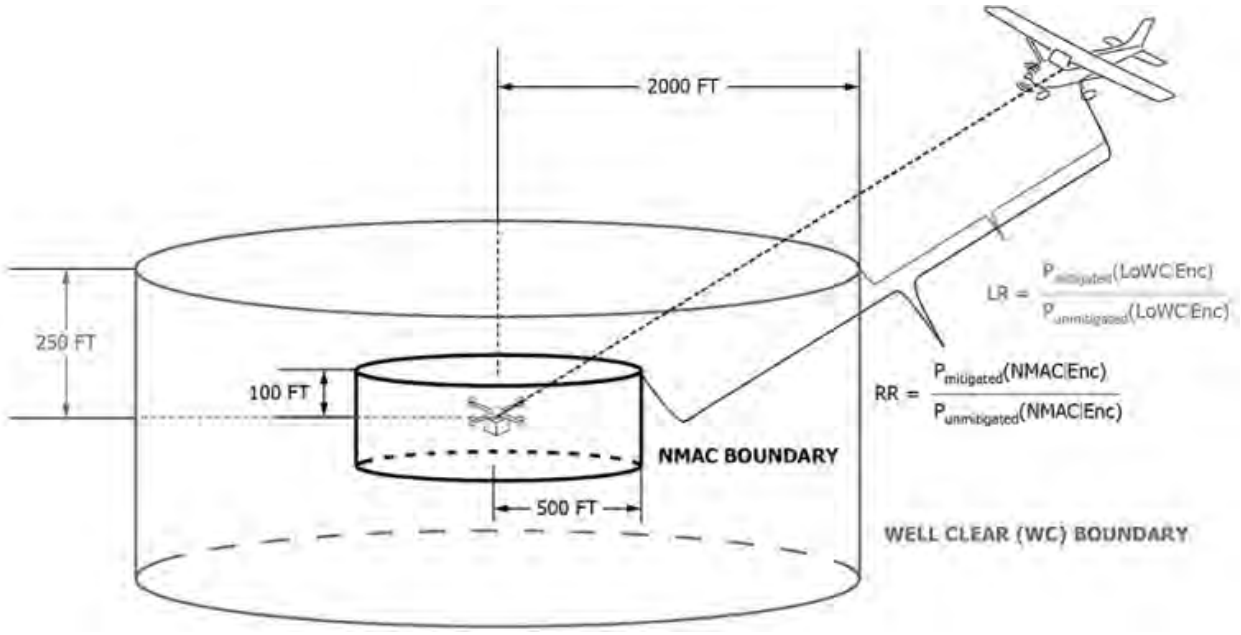

Figure 31. Well-clear and NMAC volume (ASTM F3442/F3442M-20, 2020).

Lastly, Table 18 lists the risk ratio target requirements dictated by the ASTM F3442 for DAA systems (ASTM F3442/F3442M-20, 2020).

Table 18. Risk ratio and loss of well-clear requirements for cooperative and non-cooperative aircraft (ASTM F3442/F3442M-20, 2020).

	Cooperative Intruder	**Non-cooperative Intruder**
ASTM NMAC RR	0.18	0.30
ASTM LoWCR	0.40	0.50

2.8.2 *MAC Ratio*

For this research, the MAC ratio compares the number of NMACs that resulted in a MAC equipped with DAA to the number of NMACs that resulted in a MAC without a DAA. This metric is not an ASTM requirement; however, it was used in this study to quantify the capability of a DAA system to reduce MACs within the context of an NMAC that is unresolved or induced by the DAA system.

$$MAC\ Ratio = \frac{P(MAC|NMAC; mitigated)}{P(MAC|NMAC; unmitigated)} \tag{6}$$

Where P(MAC|NMAC) is calculated by Eq (7).

$$P(MAC|NMAC) = \frac{P(MAC)}{P(NMAC)}; and\ P(MAC) = \frac{\sum_{i=1}^{N} MAC_i * w_i}{\sum_{i=1}^{N} w_i} \tag{7}$$

2.8.3 *Closest Point of Approach (CPA)*

The closest point of approach is defined as the point at which two aircraft are at the smallest distance from each other. There are several methods to determine the CPA at different points of interest.

- Horizontal Range:

$$r = \sqrt{(x_2 - x_1)^2 + (y_2 - y_1)^2} \tag{8}$$

- Vertical Range:

$$h = z_2 - z_1 \tag{9}$$

- Cylindrical Distance:

$$C = \sqrt{(r^2) + (5h)^2} \tag{10}$$

- Slant Range:

$$\rho = \sqrt{r^2 + h^2} \tag{11}$$

Where x, y, and z are in Cartesian Coordinates.

Equations (8) through (11) can be used to calculate the CPA at the following:

- Minimum Horizontal Distance r_{min}
- Minimum Slant Range ρ_{min}
- Minimum Cylindrical Distance C_{min}

2.8.4 *Horizontal Miss Distance (HMD)*

The horizontal miss distance is the horizontal range between two aircraft measured at the CPA.

2.8.5 *Vertical Miss Distance (VMD)*

The vertical miss distance is the vertical range between two aircraft measured at the CPA. The vertical miss distance is often calculated as the minimum vertical range while both aircraft are within 500 ft. horizontal distance.

2.8.6 *Altimetry Bias*

An NMAC is usually described as a discrete probability value of zero or one when the condition is met. It occurs when the horizontal separation distance is less than 500 ft. and the vertical separation distance is less than 100 ft. In this case, the NMAC probability is equal to one. Therefore, encounters that have a horizontal separation distance greater than 500 ft. are not considered NMAC, or probability equal to 0. This mathematical concept causes a unit step-like function when plotting *P(NMAC) vs. Separation Distance,* as shown in Figure 32. This approach is correct when the sensor error is considered during the encounter simulation. However, the encounters can also be evaluated without any altitude error, and the results are later adjusted during post-processing. In this case, the Standard Altimetry Error Model from the International Civil Aviation Organization (ICAO) is used during post-processing (International Civil Aviation Organization, 2014).

The altimetry error model is a function of aircraft CAS equipage and absolute altitude. As described in Section 2.5, all the encounters in this research have an altitude of fewer than 1200 ft. Therefore, the altimetry error model uses the first altitude layer category (International Civil Aviation Organization, 2014). The errors in the measurement are distributed as a Laplacian distribution (International Civil Aviation Organization, 2014), as described in Eq. (12).

$$p(e) = \frac{1}{2\lambda} e^{\left(\frac{|e|}{\lambda}\right)} \tag{12}$$

Where the parameter λ is a requirement for the definition of the statistical distribution of the altimetry error. For altitudes up to 2300 ft., the parameter λ is shown in Table 19.

Table 19. Parameter λ for the standard altimetry error model (International Civil Aviation Organization, 2014).

Layer	***0-2300 ft***	
	m	*ft*
λ	10	35

The intruders in the cooperative encounters are equipped with ADS-B out in the present research. However, no altitude error model was employed during each encounter simulation. On the other hand, the non-cooperative intruders have altitude errors integrated into the sensor model during the simulation. Therefore, the correction model presented above was only applied to the *1200-exclude* (cooperative) encounters during post-processing. Figure 32 and Figure 33 provide a comparison of the probability distribution of the discrete error model and the standard altimetry error model for the NMAC and well-clear volumes, respectively.

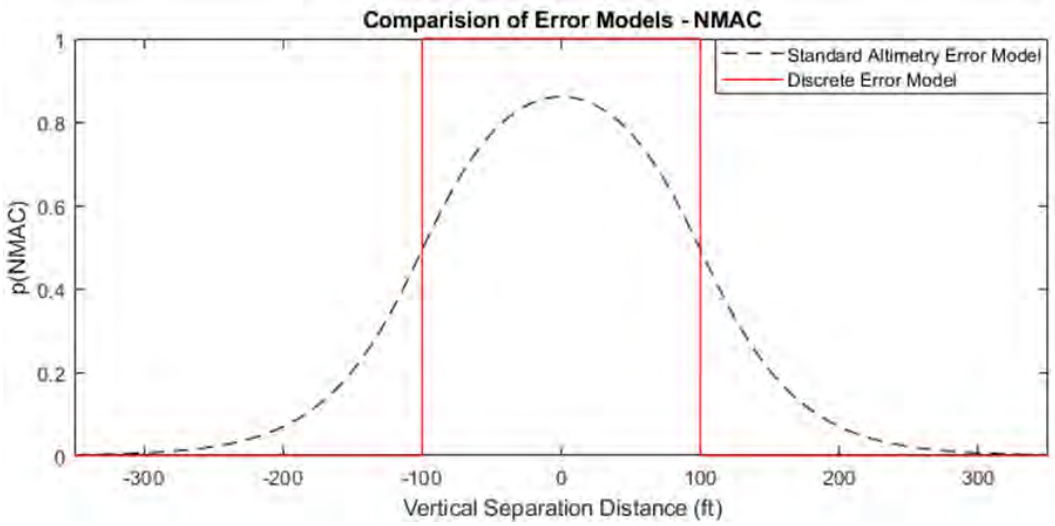

Figure 32. Discrete and standard altimetry error model comparison – NMAC.

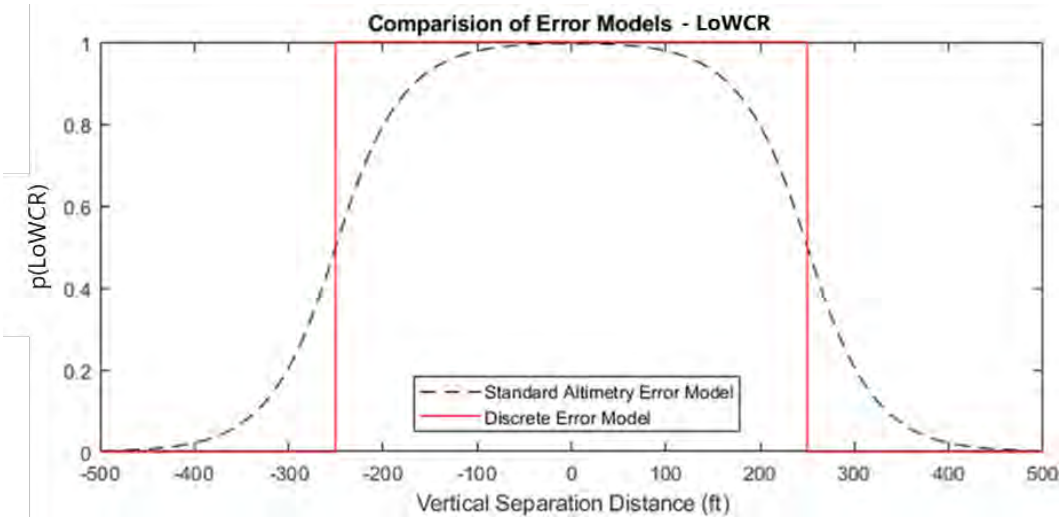

Figure 33. Discrete and standard altimetry error model comparison – LoWCR.

2.9 Assumptions and Limitations

The list below encompasses the assumptions and limitations of this research. It is not sorted by importance

- The trajectories are simulated without any wind and without any deviations from their nominal trajectory.
- The sUAS trajectories are generated from assumed surveillance targets. Actual observed trajectories were not used.
- The encounters are uncorrelated, and the burden of collision avoidance/remain well clear falls to the sUAS operator.
- The surveillance systems are assumed to function within their design parameters during an encounter. Individual system failures are not accounted for.
- sUAS are assumed to be capable of performing avoidance maneuvers at the specified rates.
- The manned aircraft trajectories are representative of en-route aircraft within an airspace class and altitude range. However, they are not specific to a geographic location or to a time of day.
- The manned aircraft is assumed to not react to the presence of the sUAS and to continue with its nominal trajectory
- sUAS trajectories are assumed to be independent of the sUAS platform.
- On-going development of ACAS sXu. ACAS sXu continues to be improved and modified. The current publicly available version at the time of conducting this research is V4R1.
- An altitude distribution of encounters was not estimated. The encounters were uniformly distributed in the expected altitude range of the sUAS (50 ft. to 1200 ft.).

3 UNMITIGATED ENCOUNTER SET EVALUATION

3.1 Simulation Parameters and Setup

The unmitigated encounters were evaluated in DEGAS without performing any avoidance maneuver. The sUAS and the intruder both follow their nominal trajectories during the encounter. No surveillance source or DAA logic were used for the unmitigated encounters.

Each encounter model represents a trajectory from a type of manned aircraft (i.e. Rotorcraft, fixed-wing single-engine, and fixed-wing multi-engine). Therefore, the intruder wireframe models were only checked for collisions when the encounter set coincides with its aircraft type. For instance, the commercial transport wireframe model was used with encounters generated with the fixed-wing multi-engine encounter model.

The metric of interest for the unmitigated results is the probability of a MAC given an NMAC, *P*(MAC|NMAC). Even though the team is estimating these values for each airframe pair, this metric should not be interpreted independently. This is because the metric is ultimately dependent on how the encounter set was generated. For the present study, the encounter set is intended to contain a random VMD and HMD distribution within the NMAC volume. More details on how the encounter sets were generated are provided in Section 2.5.

3.2 Prototype MIT LL results

For the prototype 2020 analysis, MIT LL assumed a maximum effective wingspan for the sUAS ownship of 25 feet. For ownship, six unique fixed wing sUAS and six unique rotary wing wireframe models were simulated. Each unique ownship wireframe was scaled to 10%, 20%, 40%, 60%, 80% and 100% of the 25-ft sUAS maximum wingspan. The intruder aircraft were organized based on aircraft type and the number of seats. MIT LL assumed that the number of seats can be used as surrogate for aircraft size, as aircraft size typically increases with the quantity of seats. Intruder wireframe models were organized by number of estimated seats by correlating the wireframe model name with the FAA aircraft registry (Weinert, Brittain, et al., 2020).

For each intruder type, hundreds of thousands of encounters were simulated to identify unmitigated NMACs. The encounter set was design to maximize P(NMAC|Encounter) and not designed to be representative of the observed P(NMAC) rate in the NAS. Accordingly, P(NMAC|LoWC) was not estimated by MIT LL because, by design, an overwhelmingly majority of unmitigated encounters resulted in a LoWC. The A47 ASSURE team had a different approach to encounter design because of the slightly different research objectives.

For each encounter set, 1000 NMACs were selected to estimate P(MAC|NMAC) using VCOLLIDE. NMACs with less horizontal and vertical separation were prioritized when down sampling to the 1000 NMAC encounters. Each of the 1000 encounters were assessed for each combination of manned aircraft and sUAS wireframes. Table 20 presents the unmitigated *P*(MAC|NMAC) for this 2020 MIT LL study. Notably, there was no statistical difference between the fixed wing and rotary wing sUAS models.

Table 20: Unmitigated evaluation results from 2020 MIT LL study

Intruder	Crewed Aircraft # Seats	Unmitigated P(MAC|NMAC)
Fixed-Wing Multi-Engine	[1,10]	4.0E-03
Fixed-Wing Multi-Engine	[11,31]	5.1E-03
Fixed-Wing Multi-Engine	[32, ∞]	1.2E-02
Fixed-Wing Single-Engine	[1,6]	1.9E-03
Fixed-Wing Single-Engine	[7,10]	3.2E-03
Fixed-Wing Single-Engine	[11, ∞]	2.9E-02
Rotorcraft	[1,4]	2.8E-03
Rotorcraft	[5,8]	3.0E-03
Rotorcraft	[9, ∞]	4.1E-03

Additionally, MIT LL organized encounters based on ownship speeds of either 10-60 knots or 60-90 knots. They observed unresolved NMAC encounters are skewed to lower ownship speeds and higher intruder speeds. However, the P(MAC|NMAC) rate was not statistically dependent on ownship speed. Like the Kochenderfer et al. (2010) study, 2020 MIT LL demonstrated that P(MAC) decreases as the sum of wingspans decreased.

Furthermore, reported in Table 21, MIT LL estimated the percent difference in P(MAC) between fixed-wing single-engine encounters with rotorcraft versus fixed-wing single-engine encounters with sUAS. This was estimated not using a separate manned vs manned encounter set, but rather replacing the sUAS wireframe model with a manned rotorcraft wireframe. Significant percent decreases ranging from 56 to 72% were calculated for fixed-wing aircraft with less than 10 seats, indicating that the physical smaller size of a sUAS compared to a manned rotorcraft had a statistically important effect on reducing P(MAC).

Table 21: P(MAC) decrease based on wireframe models from 2020 MIT LL study

Fixed-Wing Single Engine # Seats	Rotorcraft # Seats	Unmitigated P(MAC): Fixed-Wing Single Engine vs Rotorcraft	Unmitigated P(MAC) vs Fixed-Wing Single Engine sUAS	Percent Decrease
[1,6]	[1,4]	5.2E-03	1.9E-03	-64%
[1,6]	[5,8]	5.4E-03	1.9E-03	-65%
[1,6]	[9, ∞]	6.7E-03	1.9E-03	-72%
[7,10]	[1,4]	7.2E-03	3.2E-03	-56%
[7,10]	[5,8]	7.2E-03	3.2E-03	-56%
[7,10]	[9, ∞]	9.0E-03	3.2E-03	-64%
[11, ∞]	[1,4]	6.8E-03	2.9E-02	327%
[11, ∞]	[5,8]	6.9E-03	2.9E-02	320%
[11, ∞]	[9, ∞]	8.6E-03	2.9E-02	237%

3.3 MAC Results

The results presented in this section are from the unmitigated simulations. The sUAS models are described in Section 2.7.2.2 and were paired with all the intruder models described in Section 2.7.2.1; 24 airframe combinations were checked for collisions.

Table 22 through Table 25 present the unmitigated *P*(MAC|NMAC) and *P*(MAC|LoWC) from encounters derived from all six Lincoln Lab Uncorrelated Encounter Models (LLUEM). Figure 34 and Figure 35 summarize the *P*(MAC|NMAC) results from the tables for the cooperative and non-cooperative (surrogate) encounter sets, respectively.

The results show that the unmitigated *P*(MAC|NMAC) is a function of the size of both the sUAS and the manned aircraft. For instance, the larger manned aircraft in the analysis (commercial transport) has more than twice *P*(MAC|NMAC) compared to the smaller GA aircraft. However, this does not indicate that the commercial transport aircraft will have twice the MAC rate of the GA aircraft. MAC rate (MAC/flight hr) is a function of aircraft density which varies over time and airspace. The difference in *P*(MAC|NMAC) merely indicates that once an unmitigated NMAC occurs, an sUAS is more likely to collide with a larger aircraft than a smaller one. Similarly, larger sUAS are more likely to have a MAC given an NMAC.

Table 22. Rotorcraft unmitigated evaluation results.

Ownship	Intruder	Unmitigated P(LoWC)	Unmitigated P(NMAC)	Unmitigated P(MAC)	Unmitigated P(MAC|LoWC)	Unmitigated P(MAC|NMAC)
Q4	Rotorcraft 1200exclude_v2p1 Encs = 501204	7.34E-01	2.00E-01	6.74E-04	9.19E-04	3.37E-03
Q25				8.62E-04	1.17E-03	4.31E-03
Q55				9.70E-04	1.32E-03	4.84E-03
FW4				8.54E-04	1.16E-03	4.27E-03
FW25				1.10E-03	1.50E-03	5.49E-03
FW55				1.28E-03	1.74E-03	6.38E-03
Q4	Rotorcraft 1200only_v2p1 Encs = 505946	7.25E-01	1.98E-01	5.10E-04	7.04E-04	2.57E-03
Q25				6.78E-04	9.35E-04	3.42E-03
Q55				7.73E-04	1.07E-03	3.90E-03
FW4				6.80E-04	9.38E-04	3.43E-03
FW25				8.91E-04	1.23E-03	4.49E-03
FW55				1.07E-03	1.48E-03	5.39E-03

Table 23. General aviation unmitigated evaluation results.

Ownship	Intruder	Unmitigated P(LoWC)	Unmitigated P(NMAC)	Unmitigated P(MAC)	Unmitigated P(MAC|LoWC)	Unmitigated P(MAC|NMAC)
Q4	General Aviation 1200exclude_v2p1 Encs = 527721	7.17E-01	2.00E-01	3.58E-04	4.99E-04	1.79E-03
Q25				4.96E-04	6.92E-04	2.49E-03
Q55				5.55E-04	7.74E-04	2.78E-03
FW4				4.79E-04	6.68E-04	2.40E-03
FW25				6.37E-04	8.88E-04	3.19E-03
FW55				7.26E-04	1.01E-03	3.64E-03
Q4	General Aviation 1200only_v2p1 Encs = 529766	7.14E-01	2.02E-01	3.02E-04	4.23E-04	1.49E-03
Q25				4.08E-04	5.71E-04	2.02E-03
Q55				4.83E-04	6.76E-04	2.39E-03
FW4				3.83E-04	5.36E-04	1.90E-03
FW25				5.49E-04	7.69E-04	2.72E-03
FW55				6.78E-04	9.48E-04	3.35E-03

Table 24. Business jet unmitigated evaluation results.

Ownship	Intruder	Unmitigated P(LoWC)	Unmitigated P(NMAC)	Unmitigated P(MAC)	Unmitigated P(MAC|LoWC)	Unmitigated P(MAC|NMAC)
Q4	Business Jet 1200exclude_v2p1 Encs = 503050	6.97E-01	1.93E-01	3.54E-04	5.08E-04	1.83E-03
Q25				5.07E-04	7.27E-04	2.62E-03
Q55				6.00E-04	8.61E-04	3.11E-03
FW4				5.05E-04	7.24E-04	2.61E-03
FW25				7.16E-04	1.03E-03	3.70E-03
FW55				8.55E-04	1.23E-03	4.42E-03
Q4	Business Jet 1200only_v2p1 Encs = 524177	7.13E-01	2.00E-01	4.31E-04	6.05E-04	2.15E-03
Q25				5.69E-04	7.98E-04	2.84E-03
Q55				6.54E-04	9.18E-04	3.27E-03
FW4				5.88E-04	8.25E-04	2.94E-03
FW25				7.33E-04	1.03E-03	3.66E-03
FW55				8.81E-04	1.24E-03	4.41E-03

Table 25. Commercial transport unmitigated evaluation results.

Ownship	Intruder	Unmitigated P(LoWC)	Unmitigated P(NMAC)	Unmitigated P(MAC)	Unmitigated P(MAC|LoWC)	Unmitigated P(MAC|NMAC)
Q4	Commercial 1200exclude_v2p1 Encs = 503050	6.97E-01	1.93E-01	2.07E-03	2.97E-03	1.07E-02
Q25				2.52E-03	3.61E-03	1.30E-02
Q55				2.80E-03	4.02E-03	1.45E-02
FW4				2.52E-03	3.61E-03	1.30E-02
FW25				3.11E-03	4.46E-03	1.61E-02
FW55				3.60E-03	5.17E-03	1.87E-02

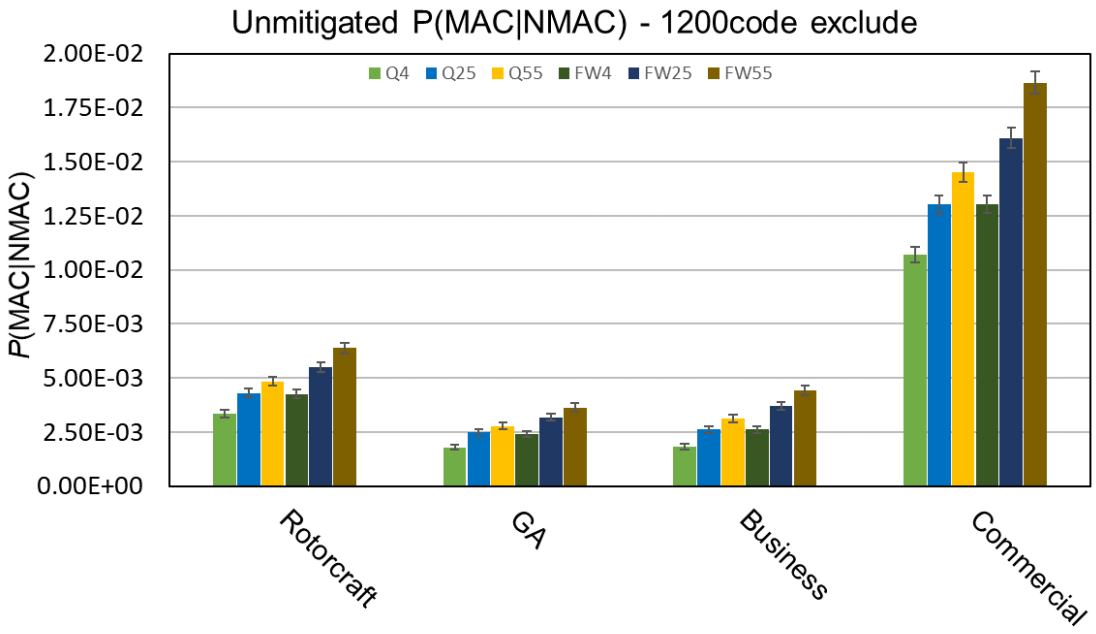

Figure 34. 1200code exclude (cooperative surrogate) *P*(MAC|NMAC) summary for all aircraft and sUAS evaluated.

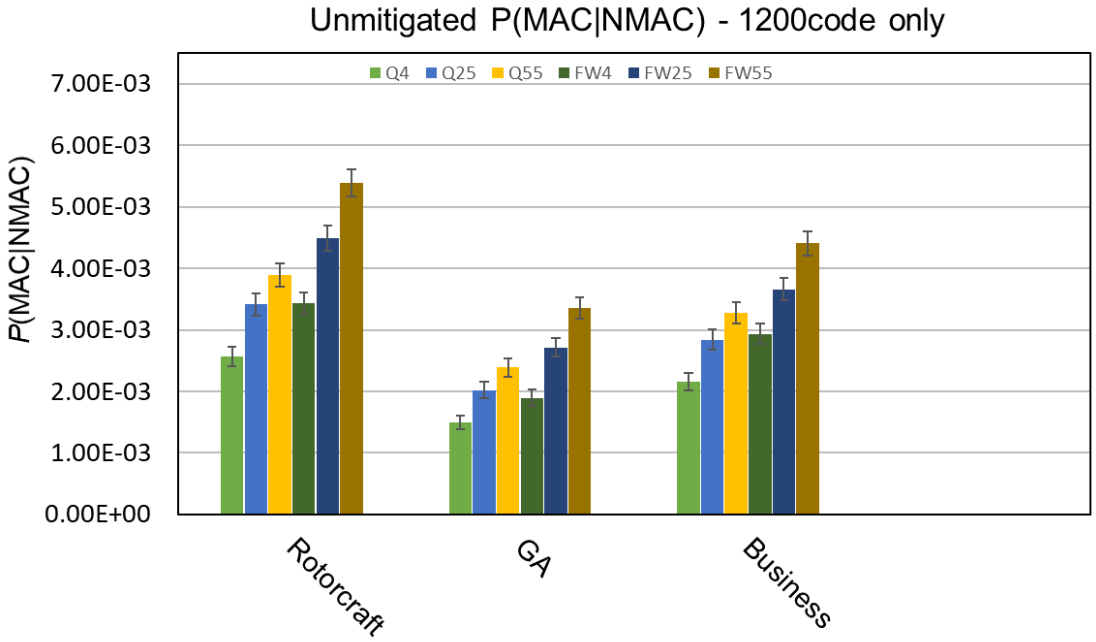

Figure 35. 1200code only (non-cooperative surrogate) *P*(MAC|NMAC) summary for all aircraft and sUAS evaluated.

The standard error bars shown in Figure 34 and Figure 35 are calculated from the analytical standard error of the simulations. The numerical standard error was calculated by Eq. (13) provided by Geweke (1989, p. 1321).

$$\sigma^2 = \frac{\sum_{i=1}^{n} [\mathrm{MAC}_i - \overline{MAC_n}]^2 \cdot w_i^2}{[\sum_{i=1}^{n} w_i]^2} \tag{13}$$

Where MAC_i is 1, if a MAC occurred during an encounter, w_i is the encounter weight, and $\overline{MAC_n}$ is given by:

$$\overline{MAC_n} = \frac{\sum_{i=1}^{n} \mathrm{MAC}_i \cdot w_i}{\sum_{i=1}^{n} w_i} \tag{14}$$

3.3.1 *Derivation of other metrics*

A secondary metric of interest is the probability of a MAC given a LoWC, *P*(MAC|LoWC). Additionally, *P*(MAC|enc) also provides a general understanding of a given encounter from LoWC to MAC. These values can be calculated from Bayes' theorem described by Eq. (15). For instance, *P*(MAC|LoWC) is given by Eq. (16). In the case of a MAC, the likelihood probability is known, *P*(LoWC|MAC) = 1. This property allows us to multiply multiple conditional probabilities to obtain a different probability of MAC given an "event", *P*(MAC|"event"). This is shown in Eq. (18) for *P*(MAC|LoWC).

$$P(A \mid B) = \frac{P(B \mid A) \cdot P(A)}{P(B)} \tag{15}$$

$$P(MAC \mid LoWC) = \frac{P(LoWC \mid MAC) \cdot P(MAC)}{P(LoWC)} = \frac{P(MAC)}{P(LoWC)} \tag{16}$$

$$P(MAC \mid LoWC) = P(MAC \mid NMAC) \cdot P(NMAC \mid LoWC) \tag{17}$$

Eq. (17) reduces to

$$P(MAC \mid LoWC) = \frac{P(NMAC \mid MAC) \cdot P(MAC)}{P(NMAC)} \cdot \frac{P(LoWC \mid NMAC) \cdot P(NMAC)}{P(LoWC)} = \frac{P(MAC)}{P(LoWC)} \tag{18}$$

For instance, the ASTM well-clear volume (2000' horizontal and 250' vertical) was recommended analytically from an unmitigated *P*(NMAC|LoWC) ≈ 0.1 (Weinert et al., 2018). Therefore, a *P*(MAC|NMAC) = 0.05 would result in a *P*(MAC|LoWC) ≈ 0.005 by applying Eq. (17).

The analytical *P*(MAC|LoWC) presented in Table 22 through Table 25 does not conform to the *P*(NMAC|LoWC) ≈ 0.1 estimated by Weinert et al. (2018). This is due to how the encounter sets used in this study were generated. The main objective of this task was to estimate *P*(MAC|NMAC). Hence, the encounter sets were sampled to obtain more NMACs, as explained in Section 2.5. As a result, the encounter sets used in this study have an unmitigated *P*(NMAC|LoWC) ≈ 0.27. This highlights the importance of interpreting the metrics holistically rather than independently.

Mitigation ratios (i.e., risk ratio) provide a relative measure of the performance of a DAA system in the context of the encounter sets used.

3.3.2 *Impact Location on the Manned Aircraft*

The MACs recorded in Section 3.3 were further analyzed to determine the impact location on the manned aircraft for each airframe pair. Figure 36 through Figure 42 highlight the impact location for the cases described in Table 17. For this analysis, the collision location is determined as the location where the sUAS first collides with the manned aircraft. Therefore, this analysis does not record a MAC that could result in multiple impact locations.

The fuselage for the commercial transport aircraft had the highest share of MACs (~35-40%). MACs with the engines represented ~13% (any MAC with the engine nacelles is also recorded as an engine MAC in this case). No differentiation was made for cases that could result in sUAS engine ingestion. This also applies to the business jet and rotorcraft results.

Around 40% of MACs were with the rotor blades of the rotorcraft. The nose, windshield, fuselage, engine cowling, vertical tail, and landing gear had roughly an equal share of MACs, around 8-10% each.

For the GA single-engine aircraft, MACs with wings and propeller represented roughly 30 to 40% of all collisions each. In this case, even though MACs with the windshield are <1%, a large share of the MACs with the propeller are also expected to result in a MAC with the windshield, by extension.

For the business jet, wings and wing tips represented ~20-25% and ~12-15% of all MACs, respectively.

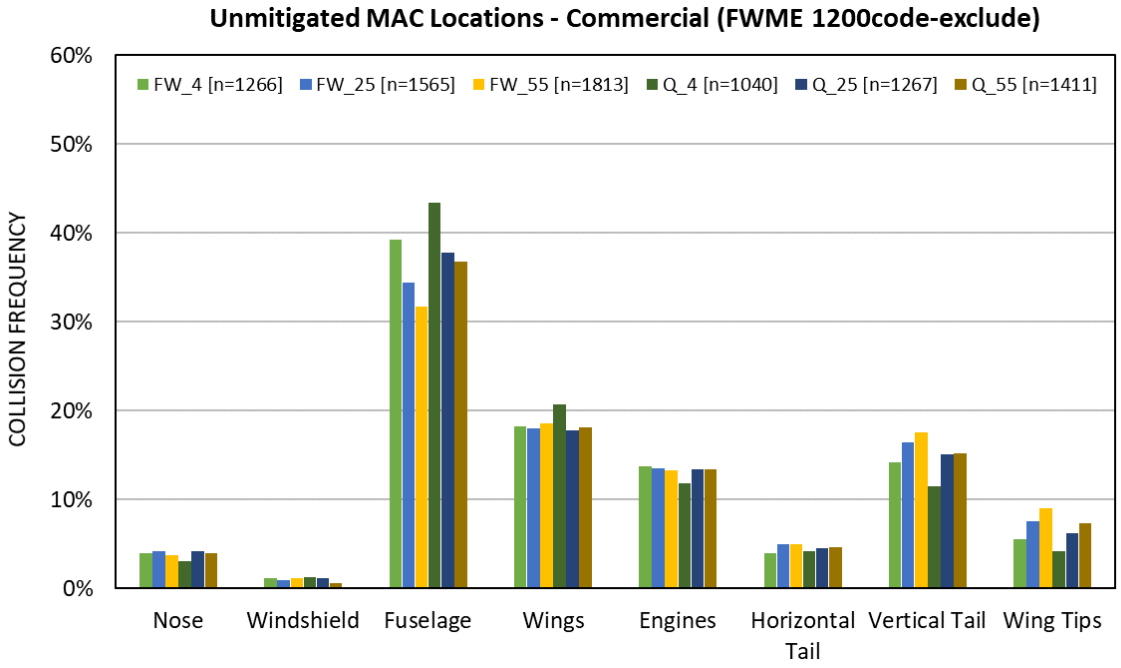

Figure 36. sUAS impact locations on the manned aircraft (commercial transport).

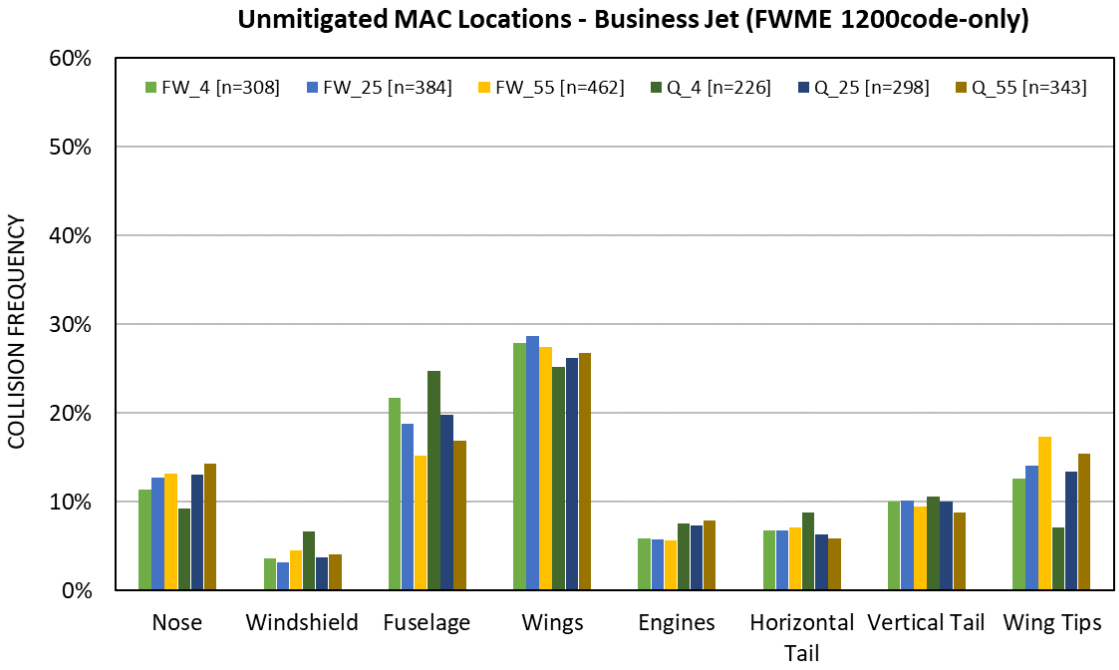

Figure 37. sUAS impact locations on the manned aircraft (business jet non-coop).

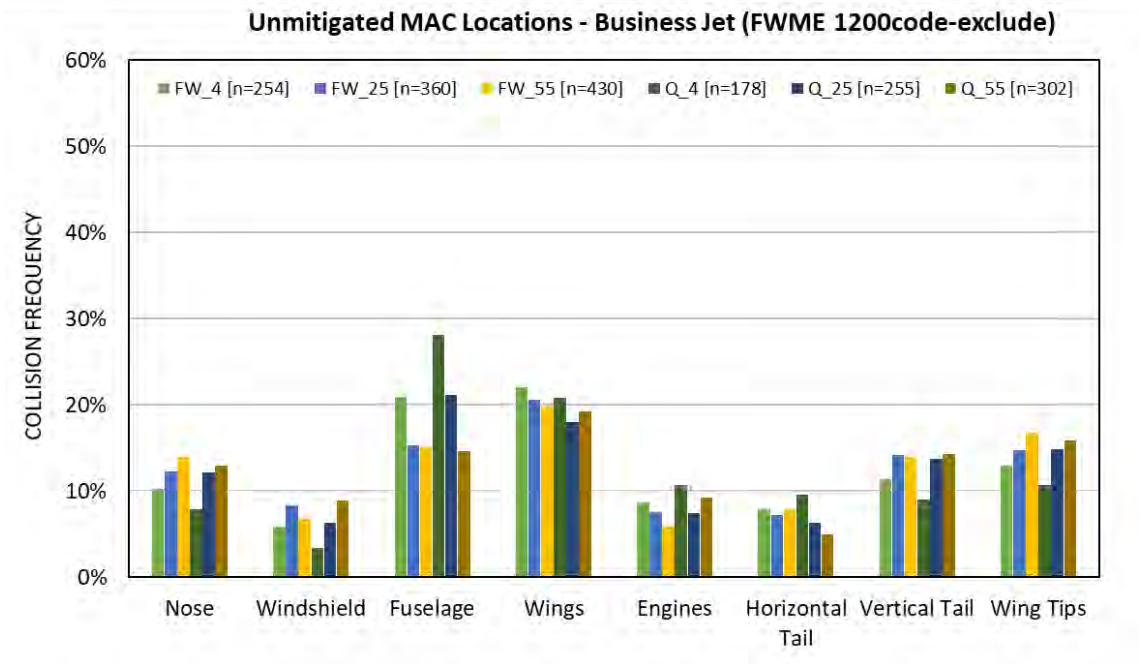

Figure 38. sUAS impact locations on the manned aircraft (business jet coop).

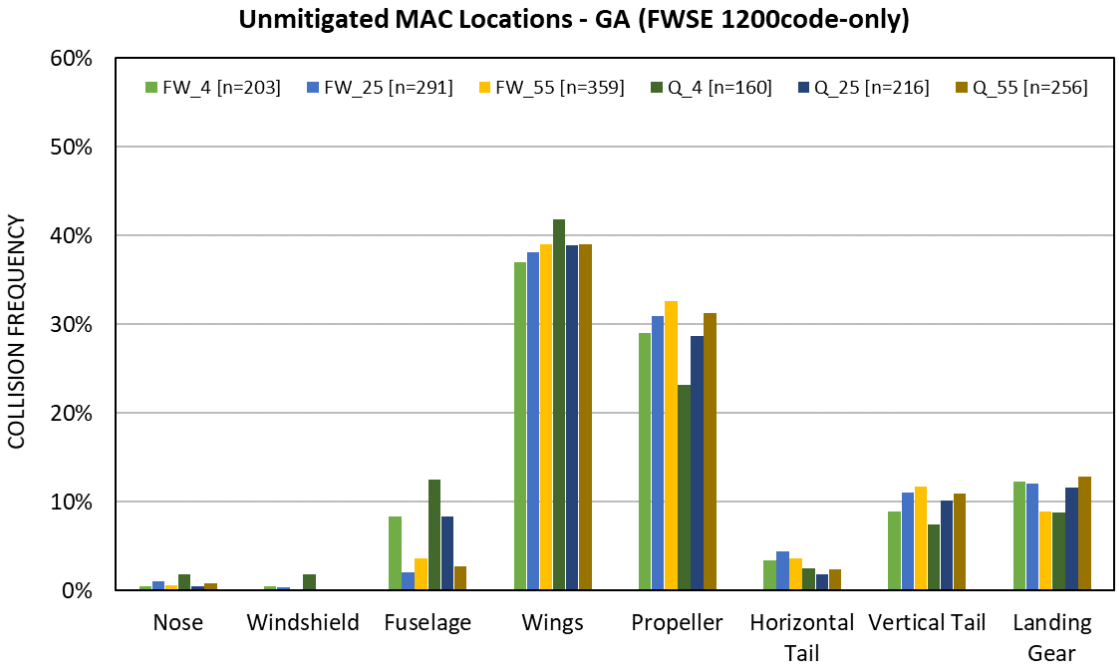

Figure 39. sUAS impact locations on the manned aircraft (GA single-engine non-coop).

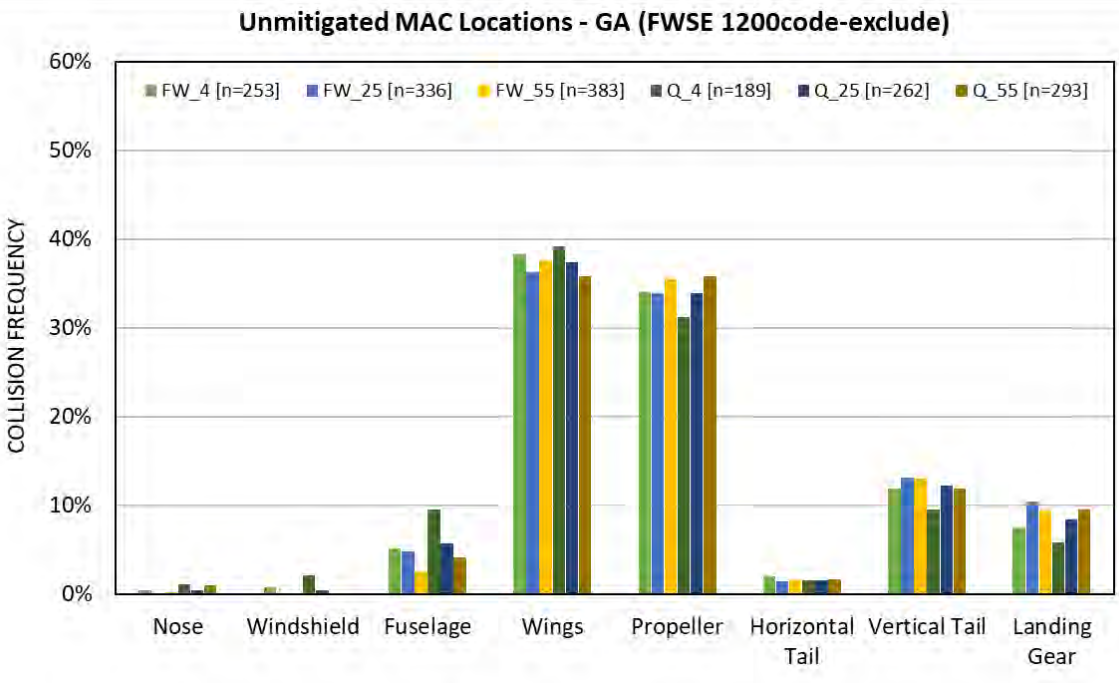

Figure 40. sUAS impact locations on the manned aircraft (GA single-engine coop).

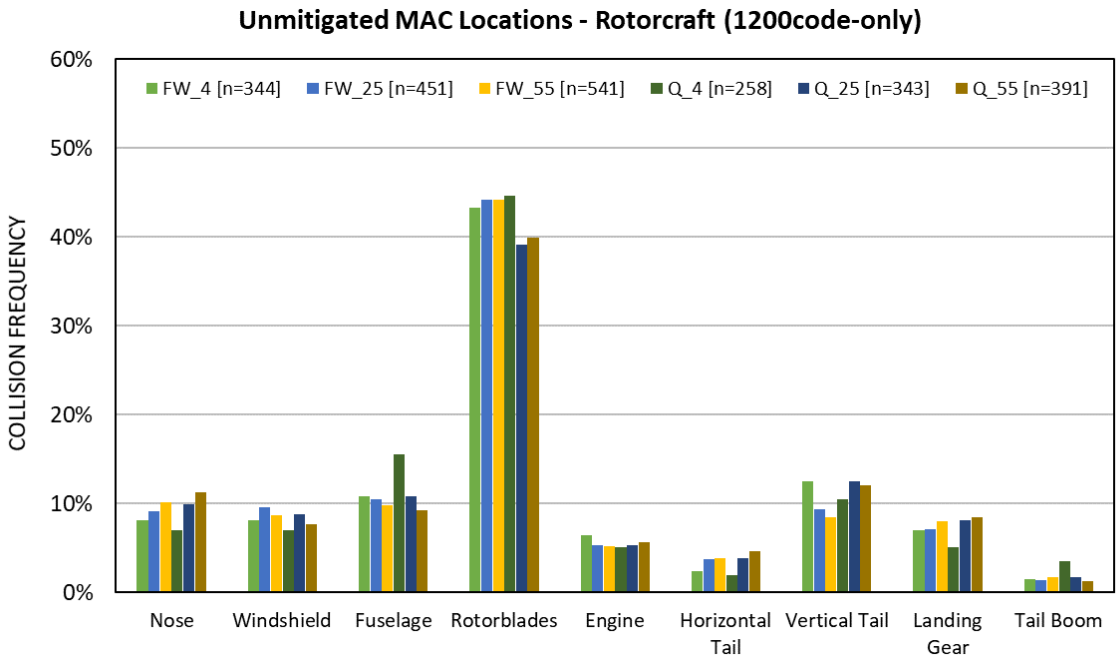

Figure 41. sUAS impact locations on the manned aircraft (rotorcraft non-coop).

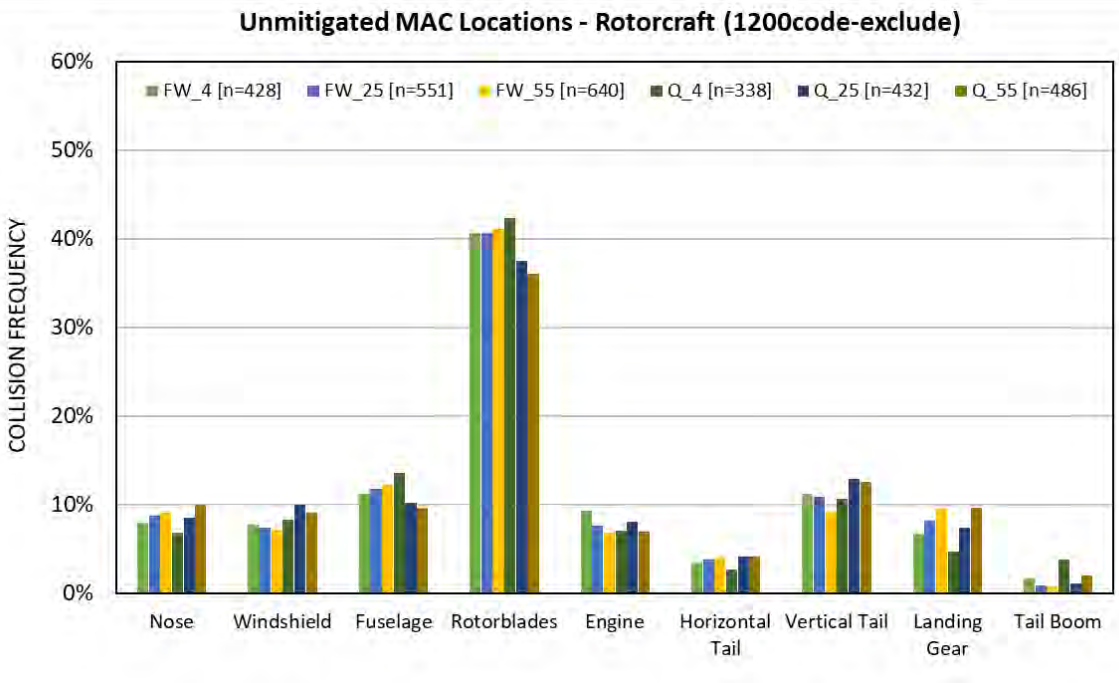

Figure 42. sUAS impact locations on the manned aircraft (rotorcraft coop).

4 MITIGATED ENCOUNTER SET EVALUATION

4.1 Prototype MIT LL results

MIT LL assessed the efficacy of the ACAS sXu V2R0 algorithm to mitigate P(MAC) and P(NMAC) with a surveillance sensor model with uncertainty representative of UAT surveillance. MIT LL assumed only the sUAS ownship will maneuver to mitigate an airborne hazard; there was no collision avoidance maneuvering by the manned aircraft. The mitigated simulations used the same encounter set and downsampling of NMAC approach as the MIT LL unmitigated simulations. Table 26 summarizes the mitigated P(MAC|NMAC) results, organized by intruder aircraft type and seats.

Table 26: Mitigated evaluation results from 2020 MIT LL study

Manned Intruder	**Manned Aircraft # Seats**	**Mitigated P(MAC|NMAC)**
Fixed-Wing Multi-Engine	[1,10]	7.5E-04
Fixed-Wing Multi-Engine	[11,31]	9.1E-04
Fixed-Wing Multi-Engine	[32, ∞]	1.8E-03
Fixed-Wing Single-Engine	[1,6]	7.3E-04
Fixed-Wing Single-Engine	[7,10]	1.2E-04
Fixed-Wing Single-Engine	[11, ∞]	1.2E-03
Rotorcraft	[1,4]	7.3E-05
Rotorcraft	[5,8]	7.0E-05
Rotorcraft	[9, ∞]	2.2E-04

MIT LL observed that large fixed-wing aircraft are generally faster, resulting in faster closing rates with more aircraft surface to collide against and subsequently increasing the P(MAC) risk. Conversely, rotorcraft are generally slower, resulting in slower closing rates and less stressing encounters for DAA system to resolve. Figure 43 illustrates the P(MAC|NMAC) results for all combinations of ownship and intruder wireframes, along with different encounter sets, as a function of the sum of wingspans. ACAS sXu V2R0 reduced P(MAC|NMAC) by as much as a factor of ten. However, many aircraft pairs with combined wingspan less than 150 ft had no MACs in the downsampled NMAC encounters when mitigating with ACAS sXu V2R0. For low altitude encounters, where the sum of wingspans is likely to be 50-100 feet, MIT LL estimated an upper P(MAC|NMAC) upper bound of 1.0 x 10-3.

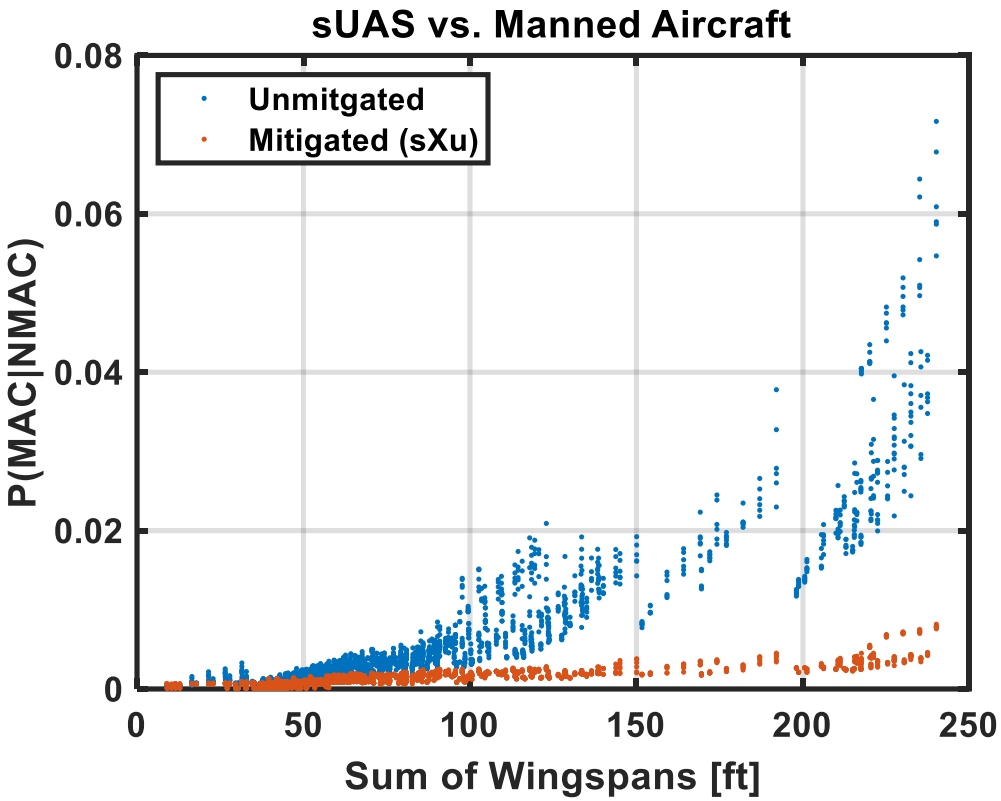

Figure 43: P(MAC|NMAC) as a function of the sum of wingspans from the 2020 MIT LL study.

4.2 Encounter Configurations

Three different sensor models were utilized in the mitigated analysis: ADS-B for cooperative intruders, GBSS for non-cooperative intruders, and GPS/INS for the ownship's location. The errors of these surveillance models are intended to follow the MOPS specified in the ACAS sXu MOPS (SC-147, 2022a) or DAA MOPS DO-365 (SC-228, 2021). Table 27 and

Table 28 summarize the simulation parameters used in this analysis.

Table 27. Simulation parameters for the *1200code-exclude (*cooperative) encounter models.

	Ownship	Intruder
DAA Logic	sXu V4R1	None
Vertical Maneuvers	+/- 1000 fpm	None
Horizontal Maneuvers	+/- 3 deg/s	
Surveillance	*ADSB 1090ES* NACp = 8 , NACv = 2 *GPS WGS84* NACp = 10 , NACv = 3	None
DAA Alerts	Horizontal and vertical RAs	None
Pilot Response	< 1s	None
Safety Target	NMAC Risk Ratio ≤ 0.18, LoWC Ratio ≤0.4	

Table 28. Simulation parameters for the *1200code-only* (non-cooperative surrogate) encounter models.

	Ownship	Intruder
DAA Logic	sXu V4R1	None
Vertical Maneuvers	+/- 1000 fpm	None
Horizontal Maneuvers	+/- 3 deg/s	
Surveillance	*Ground-Based Radar (AGT)* $\sigma_{lat,lon}$ = 246 ft , bias = 164 ft σ_{vel} = *25 ft/s ,* bias = *0* $\sigma_{altitude}$ = *328 ft ,* bias = *492 ft* $\sigma_{alt\text{-}rate}$ = *33 ft/s ,* bias = *0* *GPS WGS84* NACp = 10 , NACv = 3	None
DAA Alerts	Horizontal and vertical RAs	None
Pilot Response	< 1s	None
Safety Target	NMAC Risk Ratio ≤ 0.30, LoWC Ratio ≤0.50	

4.3 Encounter Set Metrics

Given the various encounter models and surveillance sources used in this analysis, results from all encounter models are presented in Table 29 for the 2020 MIT LL study and Table 30 for the present A47 research. Risk ratio contours for each encounter model are also presented in Figure 44 through Figure 49.

ACAS sXu, as evaluated in both MIT LL and ASSURE research with the parameters described in Section 2.6, can meet the risk ratio target requirements dictated by the ASTM F3442 for DAA systems (ASTM F3442/F3442M-20, 2020). These requirements are listed in Table 18.

Table 29. DAA performance summary.- sUAS vs manned aircraft – MIT LL.

Manned Intruder	Manned Aircraft # Seats	MAC Risk Ratio
Fixed-Wing Multi-Engine	[1,10]	**1.9E-01**
Fixed-Wing Multi-Engine	[11,31]	**1.8E-01**
Fixed-Wing Multi-Engine	[32, ∞]	**1.5E-01**
Fixed-Wing Single-Engine	[1,6]	**3.8E-01**
Fixed-Wing Single-Engine	[7,10]	**3.8E-02**
Fixed-Wing Single-Engine	[11, ∞]	**4.1E-02**
Rotorcraft	[1,4]	**2.6E-02**
Rotorcraft	[5,8]	**2.3E-02**
Rotorcraft	[9, ∞]	**5.4E-02**

Table 30. DAA performance summary.- sUAS vs. manned aircraft.

Encounter Model	Number of Encounters	Unmitigated P(NMAC)	Mitigated P(NMAC)	Unmitigated P(LoWC)	Mitigated P(LoWC)	NMAC Risk Ratio	LoWC Risk Ratio
FWSE 1200code-exclude_v2p1 (Coop)	527,721	2.00E-01	1.50E-03	7.17E-01	1.27E-01	**7.50E-03**	**1.77E-01**
FWME 1200code-exclude_v2p1 (Coop)	503,050	1.93E-01	1.70E-03	6.97E-01	1.22E-01	**8.81E-03**	**1.75E-01**
Rotorcraft 1200code-exclude_v2p1 (Coop)	501,204	2.00E-01	1.50E-03	7.34E-01	1.19E-01	**7.50E-03**	**1.53E-01**
FWSE 1200code-only_v2p1 (Non-coop)	529,766	2.02E-01	1.80E-02	7.14E-01	2.62E-01	**8.91E-02**	**3.67E-01**
FWME 1200code-only_v2p1 (Non-coop)	524,177	2.00E-01	2.25E-02	7.13E-01	2.92E-01	**1.13E-01**	**4.10E-01**
Rotorcraft 1200code-only_v2p1 (Non-coop)	505,946	1.98E-01	1.25E-02	7.25E-01	2.25E-01	**6.31E-02**	**3.10E-01**

Foremost both A47 and MIT LL demonstrated that ACAS sXu mitigates P(MAC) by one order of magnitude for small drone vs manned aircraft encounters. This conclusion is consistent across different aircraft sizes and encounter dynamics. MIT LL estimated an upper bound of 1.0 x 10-3 while the more recent A47 estimated a upper bound of 1.0 x 10-4. Given the differences, by design, of the encounter generation approaches and ACAS sXu version, this order of magnitude difference of P(MAC) is not problematic. The A47 research validates the upper bound by MIT LL while also verifying that both the LoWC and NMAC risk ratio requirements, prescribed in the ASTM F38 DAA performance standard and RTCA SC-147 MOPS, can be satisfied by ACAS sXu. We emphasize that the mitigated P(MAC) results and risk ratios are only applicable to ACAS sXu. It is possible that a less capable DAA system may have a more frequent P(MAC|NMAC) rate

The risk ratio contours shown in Figure 45 through Figure 49 highlight the risk ratio at different volumes. The contour lines represent risk ratio levels at 0.1 increments. There is a distinct difference between the cooperative cases and the non-cooperative cases. The non-cooperative cases are not as sensitive to different VMD values, i.e., the risk ratio contour does not change significantly as altitude increases. The significant altitude error most likely explains this in the non-cooperative surveillance. Therefore, ACAS sXu attempts more horizontal maneuvers to achieve the safety targets. Further analysis of the types of alerts issued by ACAS sXu will reveal if this is indeed the case.

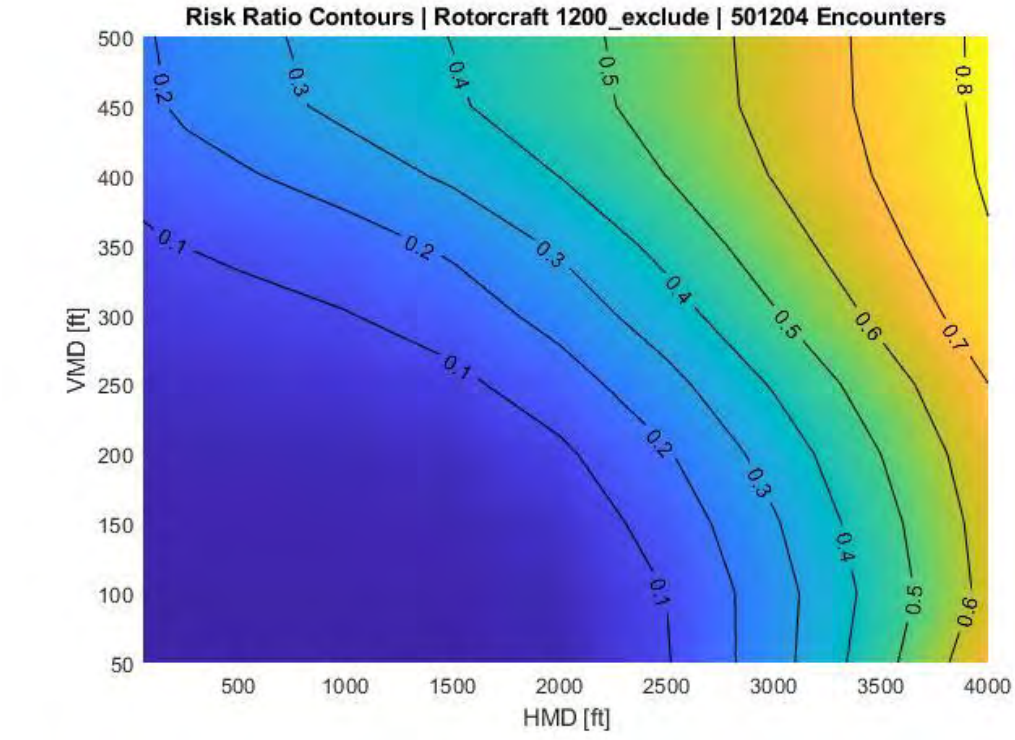

Figure 44. Rotorcraft 1200code-exclude (cooperative) risk ratio contours.

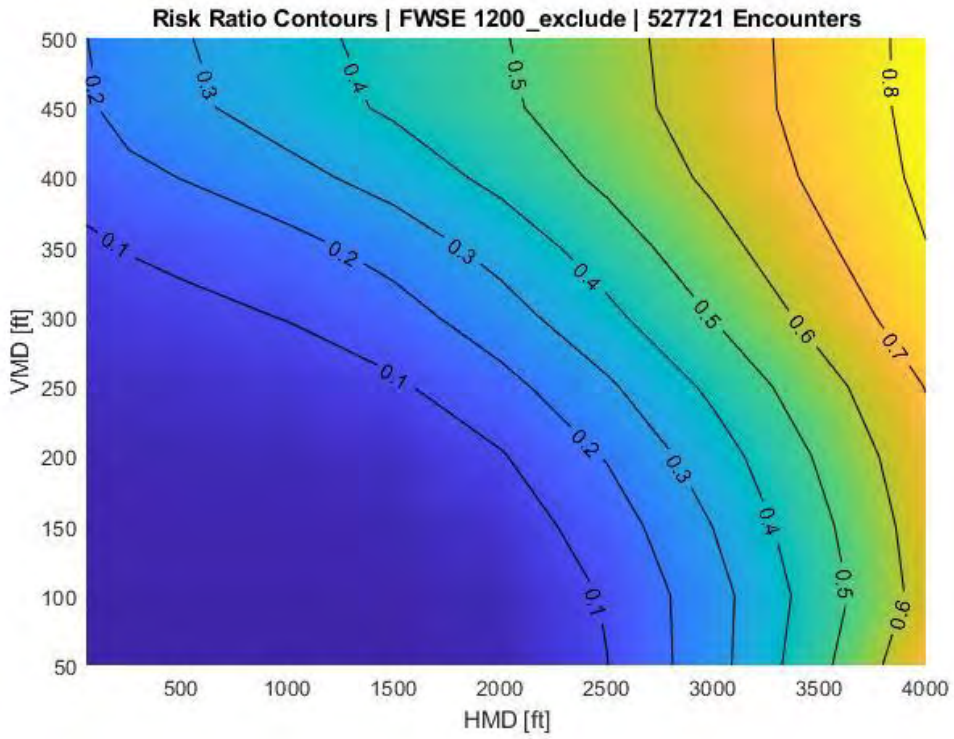

Figure 45. FWSE 1200code-exclude (cooperative) risk ratio contours.

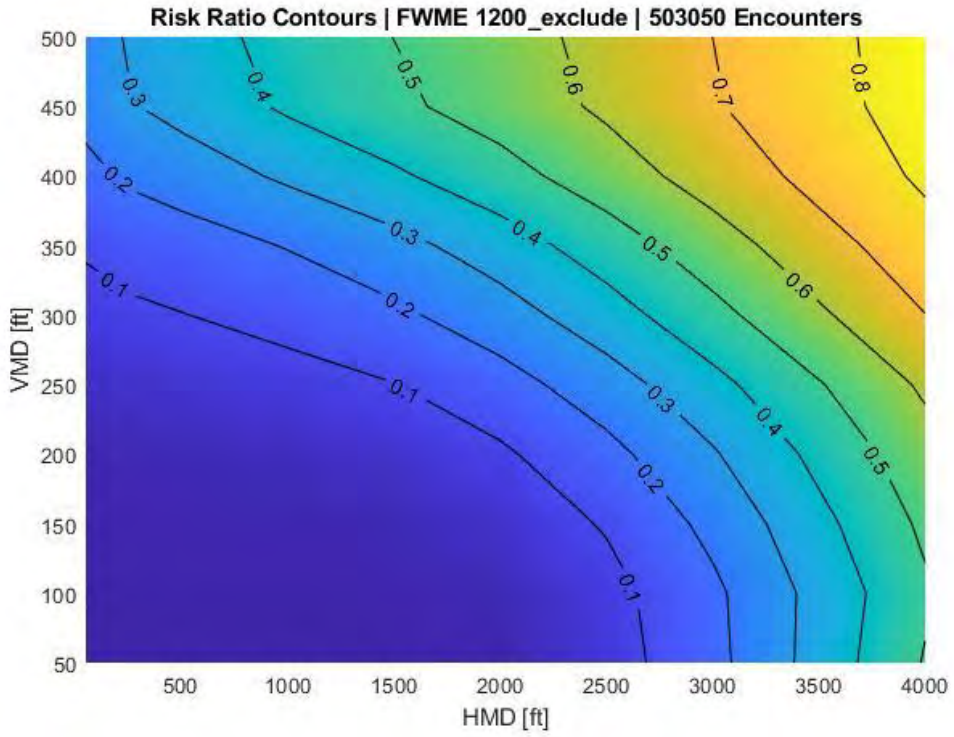

Figure 46. FWME 1200code-exclude (cooperative) risk ratio contours.

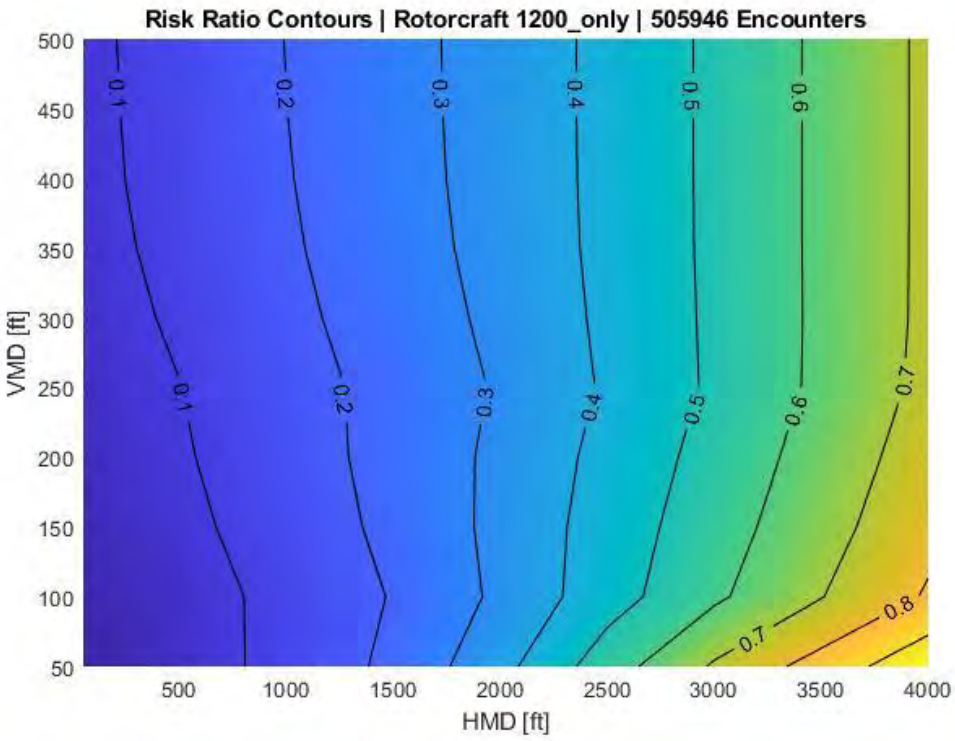

Figure 47. Rotorcraft 1200code-only (non-cooperative surrogate) risk ratio contours.

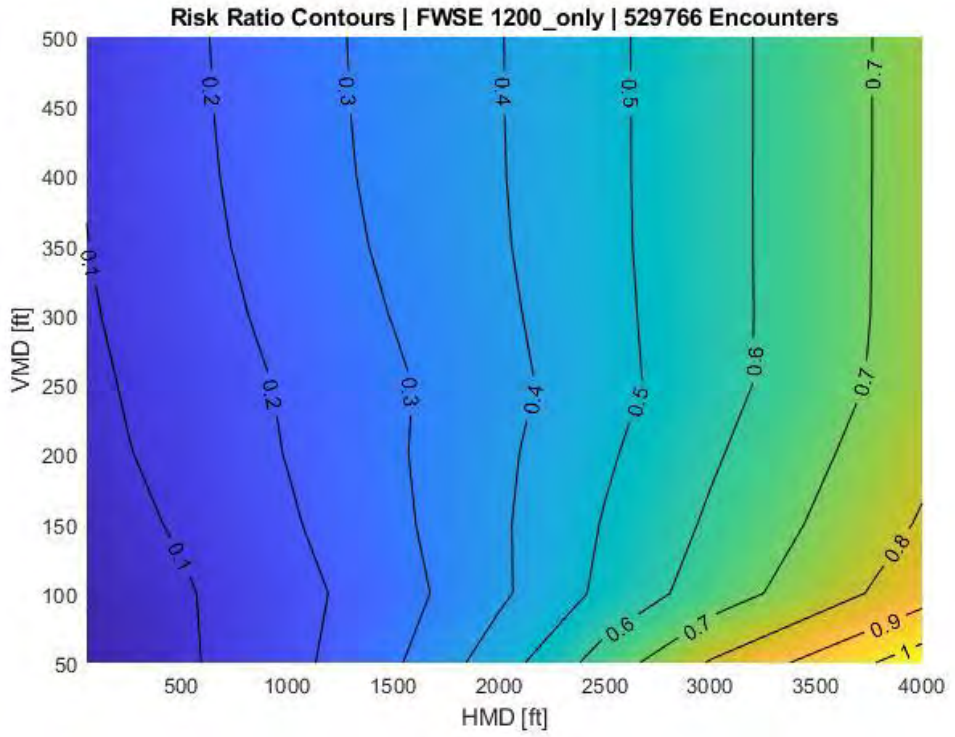

Figure 48. FWSE 1200code-only (non-cooperative surrogate) risk ratio contours.

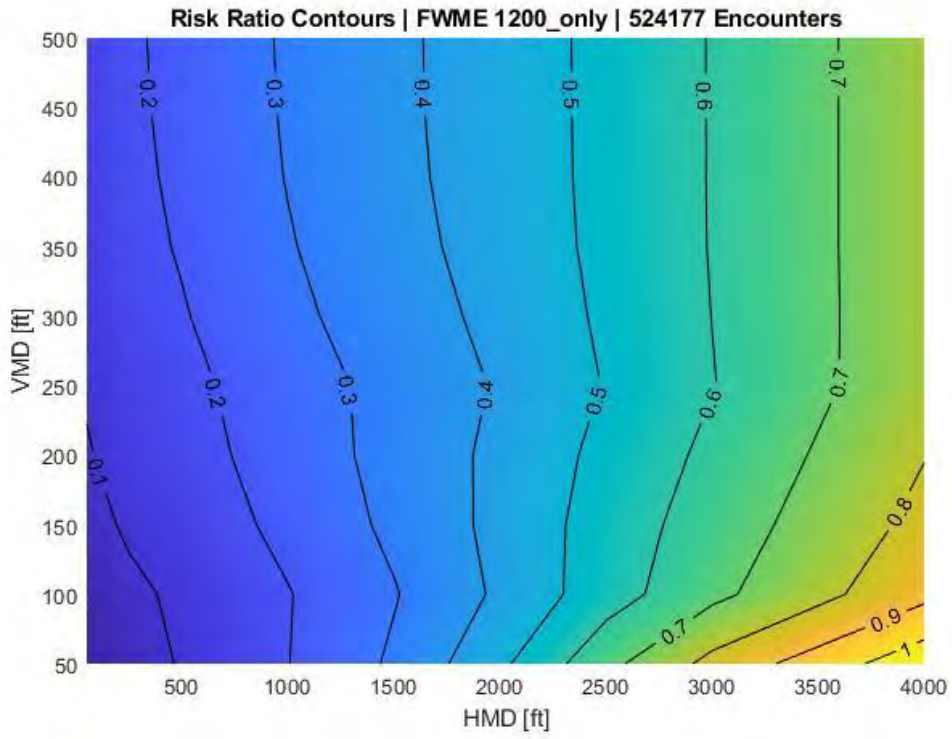

Figure 49. FWME 1200code-only (non-cooperative surrogate) risk ratio contours.

4.4 MAC Results

The results presented in this section are from the mitigated simulations. For these cases, the sUAS performs maneuvers according to the RAs provided by ACAS sXu. As such, the sUAS trajectory is modified every time a new RA is issued. No return-to-course was implemented once a COC was issued. The manned aircraft follows the nominal trajectory initially defined in the encounter set. Similar to the unmitigated cases, the sUAS models described in Section 2.7.2.2 were paired with all the intruder models described in Section 2.7.2.1. 24 airframe combinations were checked for collisions.

Table 31 through Table 34 present the mitigated *P*(MAC|NMAC), *P*(MAC|LoWC), and MAC ratio from encounters derived from all six LLUEM. Figure 50 and Figure 51 summarize the mitigated *P*(MAC|NMAC) and MAC ratio results from the tables for the non-cooperative (surrogate) encounter sets, respectively. For the cooperative cases, there was only 1 MAC across the 24 aircraft combinations; this was between the commercial transport and FW55 models. The upper bound P(MAC) and MAC ratio were estimated for the cases with no MAC.

The MAC ratio for the 1200code-only (non-cooperative surrogate) rotorcraft model is between 0.37 and 0.49, depending on the sUAS geometry. The GA aircraft has a broader range between 0.25 and 0.56. On the other hand, the business jet has a MAC ratio between 0.27 and 0.35. Overall, all the 1200code-only models showed a net benefit when ACAS sXu is employed, even after an NMAC has occurred. The MAC ratio indicates that the *P*(MAC|NMAC) is less than half of the mitigated cases.

Similarly, the upper bound MAC ratio for the 1200code-exclude (cooperative) rotorcraft model is between 0.39 and 0.21, as shown in Figure 52. The GA aircraft upper bound MAC ratio is between 0.7 and 0.35. The business jet is between 0.64 and 0.26. The smallest upper bound MAC ratio was between 0.11 and 0.06, which was observed in the commercial transport model. This is due to a large unmitigated *P*(MAC|NMAC) compared to the other manned aircraft models. The upper bound mitigated *P*(MAC|NMAC) for all 1200code-exclude models was estimated at approximately < 1.3E-3. This result is expected to be conservative since all, but one airframe pair for the cooperative cases had zero MACs recorded. Even though the upper bound MAC ratio of the 1200code-exclude is comparable to the 1200code-only results, ACAS sXu overall MAC mitigation effectiveness is higher in the 1200code-exclude models. This is because of the significantly smaller RR results (i.e., 8.91E-02 vs. 7.5E-03).

The total reduction of MACs in an encounter set with a DAA system can be quantified by multiplying the MAC ratio with the NMAC RR. For the 1200code-only models, the total MAC reduction is between 95% and 97.8%. On the other hand, for the 1200code-exclude models, the estimated overall MAC reduction is > 99.4%.

Table 31. Rotorcraft mitigated evaluation results.

Ownship	Intruder	Mitigated P(LoWC)	Mitigated P(NMAC)	Mitigated P(MAC)	Mitigated P(MAC|LoWC)	Mitigated P(MAC|NMAC)	MAC Ratio
Q4	Rotorcraft 1200exclude_v2p1 Encs = 501204	1.19E-01	1.50E-03	<2.00E-06	<1.67E-05	<1.33E-03	<3.95E-01
Q25				<2.00E-06	<1.67E-05	<1.33E-03	<3.09E-01
Q55				<2.00E-06	<1.67E-05	<1.33E-03	<2.75E-01
FW4				<2.00E-06	<1.67E-05	<1.33E-03	<3.12E-01
FW25				<2.00E-06	<1.67E-05	<1.33E-03	<2.42E-01
FW55				<2.00E-06	<1.67E-05	<1.33E-03	<2.09E-01
Q4	Rotorcraft 1200only_v2p1 Encs = 505946	2.25E-01	1.25E-02	1.58E-05	7.04E-05	1.27E-03	4.94E-01
Q25				1.78E-05	7.92E-05	1.43E-03	4.18E-01
Q55				1.78E-05	7.92E-05	1.43E-03	3.67E-01
FW4				1.98E-05	8.80E-05	1.59E-03	4.63E-01
FW25				2.37E-05	1.06E-04	1.90E-03	4.24E-01
FW55				2.57E-05	1.14E-04	2.06E-03	3.83E-01

*For cases where no MACs were recorded, the upper bound (<) was reported instead

Table 32. General aviation mitigated evaluation results.

Ownship	Intruder	Mitigated P(LoWC)	Mitigated P(NMAC)	Mitigated P(MAC)	Mitigated P(MAC|LoWC)	Mitigated P(MAC|NMAC)	MAC Ratio
Q4	General Aviation 1200exclude_v2p1 Encs = 527721	1.27E-01	1.50E-03	<1.89E-06	<1.50E-05	<1.26E-03	<7.04E-01
Q25				<1.89E-06	<1.50E-05	<1.26E-03	<5.08E-01
Q55				<1.89E-06	<1.50E-05	<1.26E-03	<4.54E-01
FW4				<1.89E-06	<1.50E-05	<1.26E-03	<5.26E-01
FW25				<1.89E-06	<1.50E-05	<1.26E-03	<3.96E-01
FW55				<1.89E-06	<1.50E-05	<1.26E-03	<3.47E-01
Q4	General Aviation 1200only_v2p1 Encs = 529766	2.62E-01	1.80E-02	1.51E-05	5.77E-05	8.41E-04	5.63E-01
Q25				1.51E-05	5.77E-05	8.41E-04	4.17E-01
Q55				1.51E-05	5.77E-05	8.41E-04	3.52E-01
FW4				1.51E-05	5.77E-05	8.41E-04	4.44E-01
FW25				1.51E-05	5.77E-05	8.41E-04	3.09E-01
FW55				1.51E-05	5.77E-05	8.41E-04	2.51E-01

*For cases where no MACs were recorded, the upper bound (<) was reported instead

Table 33. Business jet mitigated evaluation results.

Ownship	Intruder	Mitigated P(LoWC)	Mitigated P(NMAC)	Mitigated P(MAC)	Mitigated P(MAC|LoWC)	Mitigated P(MAC|NMAC)	MAC Ratio
Q4	Business Jet 1200exclude_v2p1 Encs = 503050	1.22E-01	1.70E-03	<1.99E-06	<1.62E-05	<1.17E-03	<6.38E-01
Q25				<1.99E-06	<1.62E-05	<1.17E-03	<4.46E-01
Q55				<1.99E-06	<1.62E-05	<1.17E-03	<3.76E-01
FW4				<1.99E-06	<1.62E-05	<1.17E-03	<4.47E-01
FW25				<1.99E-06	<1.62E-05	<1.17E-03	<3.16E-01
FW55				<1.99E-06	<1.62E-05	<1.17E-03	<2.64E-01
Q4	Business Jet 1200only_v2p1 Encs = 524177	2.92E-01	2.25E-02	1.34E-05	4.58E-05	5.92E-04	2.75E-01
Q25				1.91E-05	6.54E-05	8.46E-04	2.98E-01
Q55				2.29E-05	7.85E-05	1.02E-03	3.10E-01
FW4				1.91E-05	6.54E-05	8.46E-04	2.88E-01
FW25				2.67E-05	9.16E-05	1.18E-03	3.24E-01
FW55				3.43E-05	1.18E-04	1.52E-03	3.46E-01

*For cases where no MACs were recorded, the upper bound (<) was reported instead

Table 34. Commercial transport mitigated evaluation results.

Ownship	Intruder	Mitigated P(LoWC)	Mitigated P(NMAC)	Mitigated P(MAC)	Mitigated P(MAC|LoWC)	Mitigated P(MAC|NMAC)	MAC Ratio
Q4	Commercial 1200exclude_v2p1 Encs = 503050	1.22E-01	1.70E-03	<1.99E-06	<1.62E-05	<1.17E-03	<1.09E-01
Q25				<1.99E-06	<1.62E-05	<1.17E-03	<8.97E-02
Q55				<1.99E-06	<1.62E-05	<1.17E-03	<8.05E-02
FW4				<1.99E-06	<1.62E-05	<1.17E-03	<8.98E-02
FW25				<1.99E-06	<1.62E-05	<1.17E-03	<7.26E-02
FW55				1.99E-06	1.62E-05	1.17E-03	6.27E-02

*For cases where no MACs were recorded, the upper bound (<) was reported instead

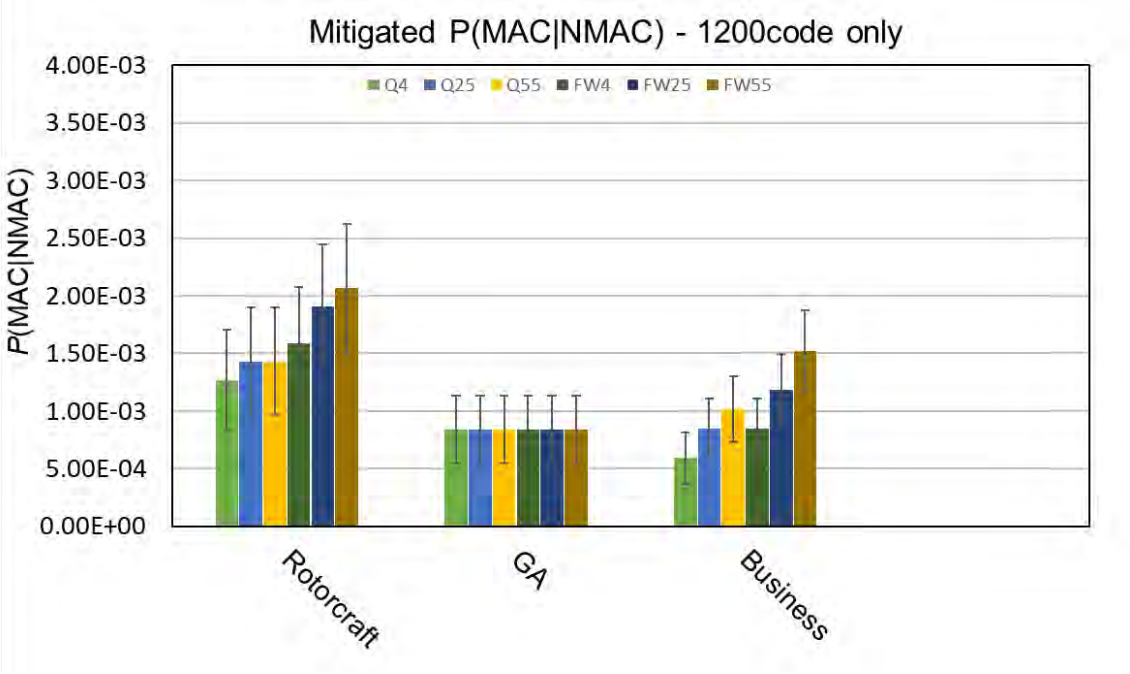

Figure 50. 1200code-only (non-cooperative surrogate) mitigated *P*(MAC|NMAC) summary for all aircraft and sUAS evaluated.

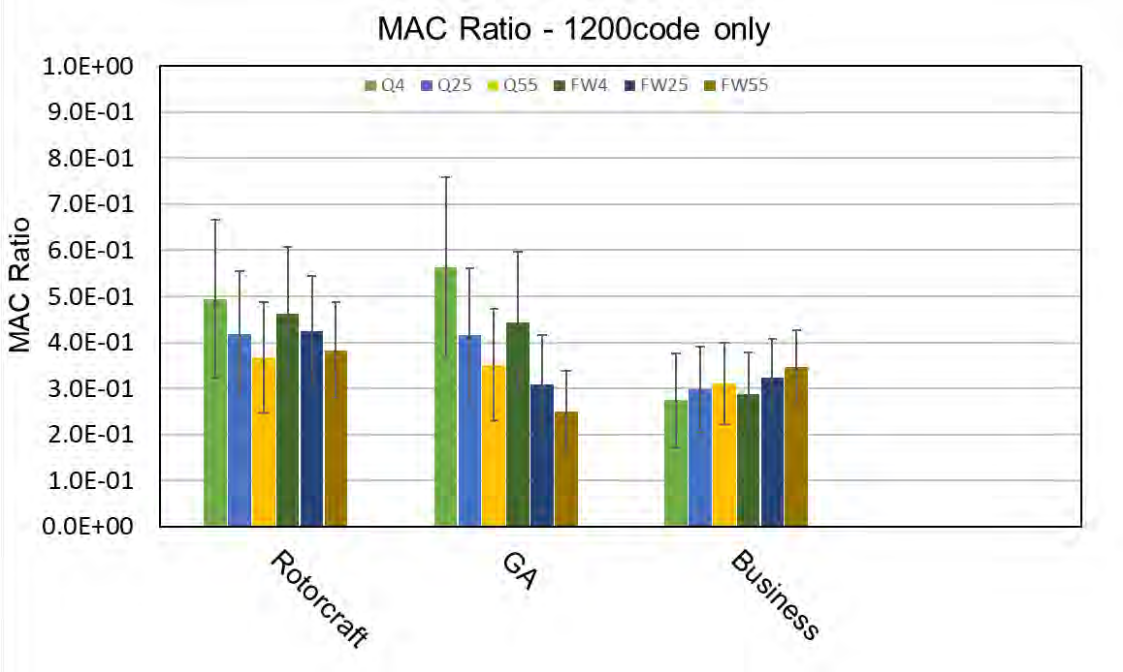

Figure 51. 1200code-only (non-cooperative surrogate) MAC Ratio for all aircraft and sUAS evaluated.

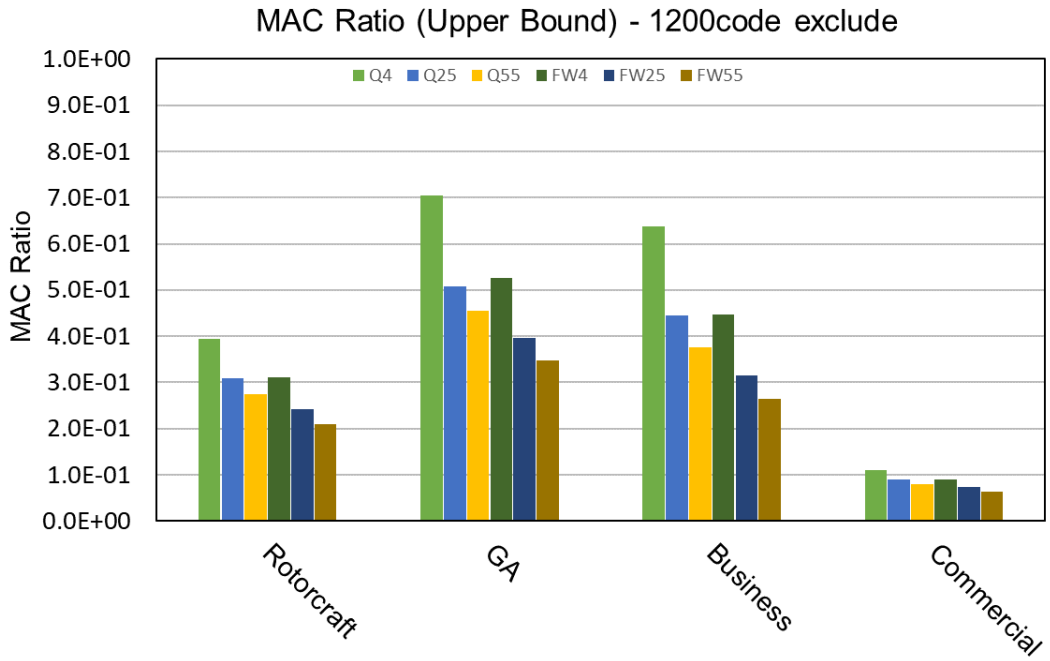

Figure 52. 1200code-exclude (cooperative) MAC Ratio for all aircraft and sUAS evaluated. The estimated upper bound was plotted since no MACs were recorded in these cases.

4.4.1 *Impact Location on the Manned Aircraft*

The impact location distribution for the mitigated and unmitigated MACs are compared in Figure 53 through Figure 55. Only the 1200code-only (non-cooperative) models were compared, given that the 1200code-exclude only had 1 MAC. The aggregate of all sUAS MACs instead of each

individual sUAS was used in the comparison. Similarly, the total mitigation ratio per impact location and its corresponding 95% bootstrap confidence interval are shown in Figure 56 through Figure 58.

There were no mitigated MACs with the engines and horizontal tail of the business jet. The wings had the highest proportion of MACs in both the mitigated and unmitigated cases at 37% and 27%, respectively.

There were mitigated MACs with the wings, propeller, vertical tail, and landing gear of the GA single-engine aircraft. The propeller represented the largest share at 58% compared to 30% in the unmitigated cases.

For the rotorcraft, the most significant proportion of mitigated MACs is with the rotor blades at 56% compared to 43% in the unmitigated cases.

For the 1200code-exclude models, only 1 MAC was found. The MAC occurred in the commercial transport and fixed-wing 55 lb. (FW55) sUAS pair. The collision was identified in the manned aircraft's engine.

The total (in the encounter set) MAC mitigation ratio upper bound is less than 1.00E-1 for all impact locations (except for the GA aircraft windshield), with many impact locations less than 5.00E-2, as shown in Figure 56 through Figure 58. This highlights the high MAC reduction efficiency of ACAS sXu, as indicated previously.

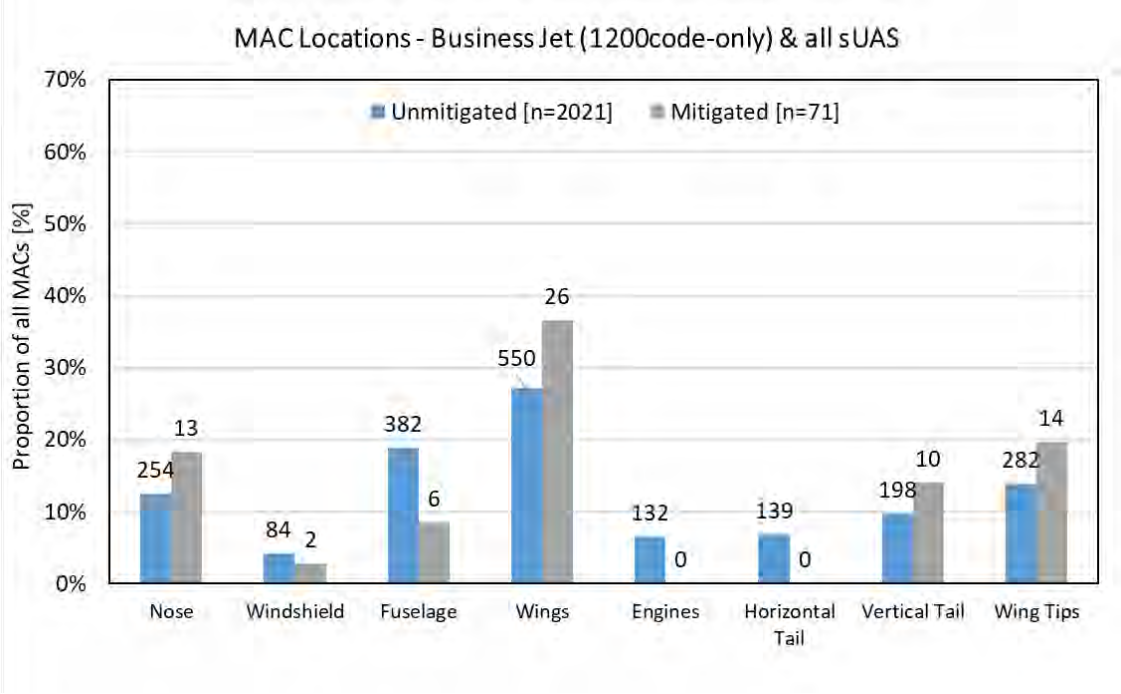

Figure 53. 1200code-only (non-cooperative surrogate) MAC location comparison between mitigated and unmitigated – Business jet and all sUAS aggregate.

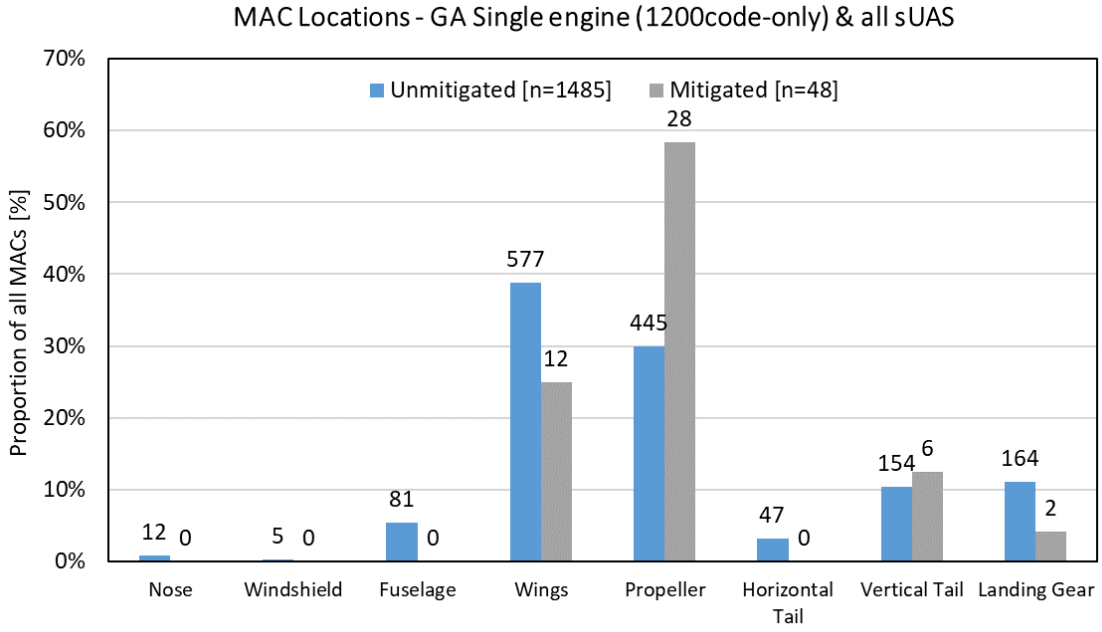

Figure 54. 1200code-only (non-cooperative surrogate) MAC location comparison between mitigated and unmitigated – GA aircraft and all sUAS aggregate.

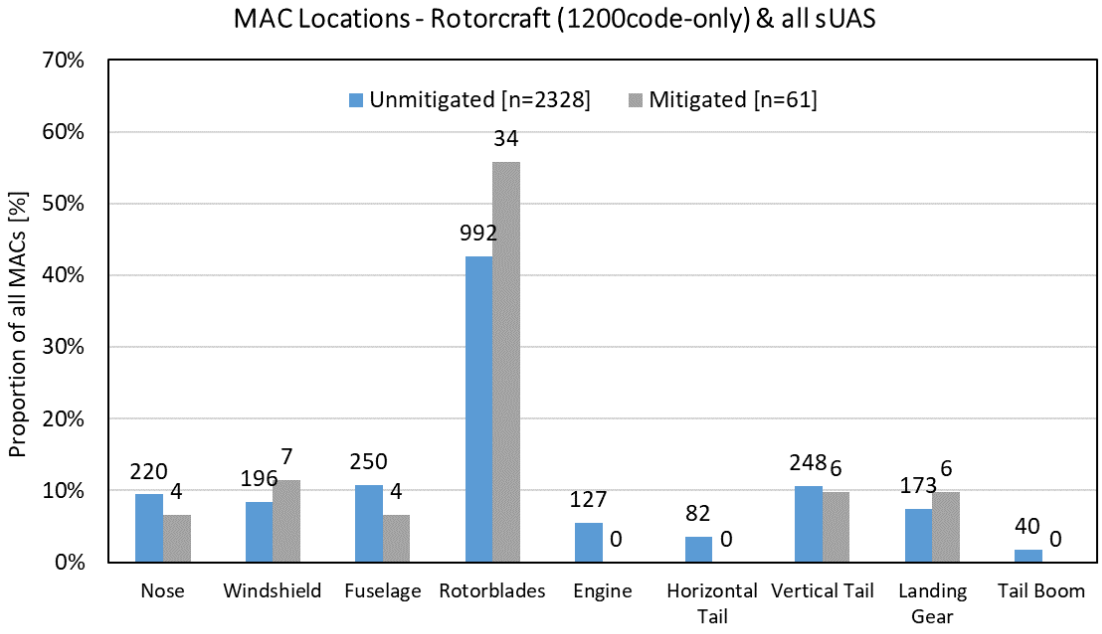

Figure 55. 1200code-only (non-cooperative surrogate) MAC location comparison between mitigated and unmitigated – Rotorcraft and all sUAS aggregate.

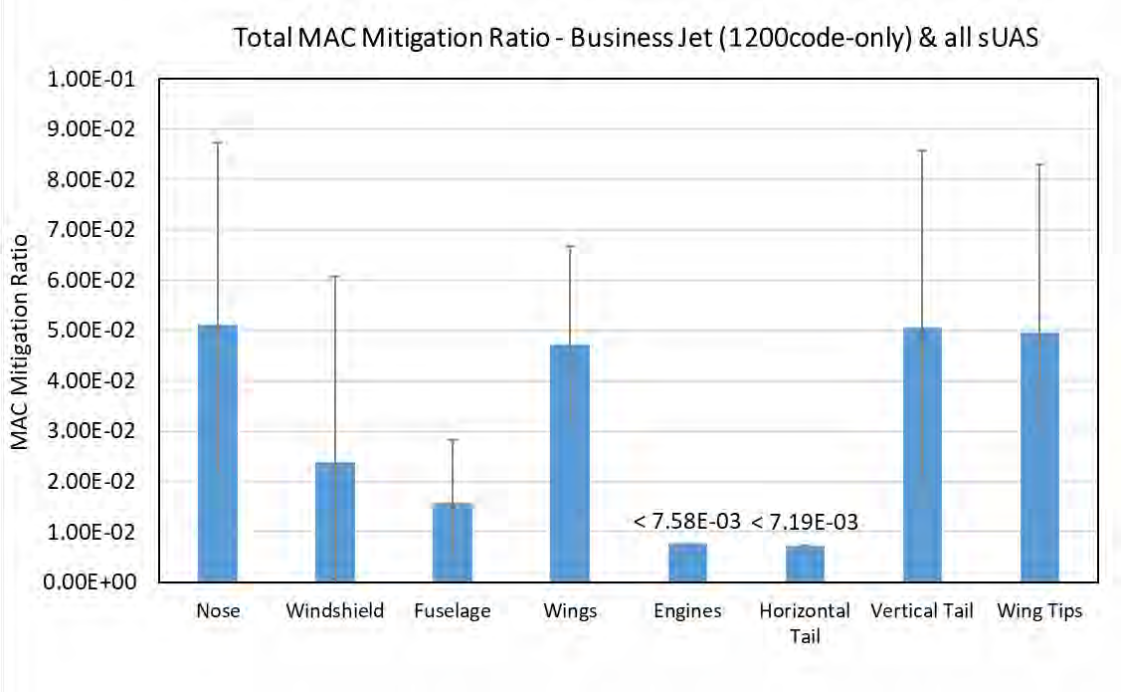

Figure 56. 1200code-only (non-cooperative surrogate) MAC mitigation ratio (upper bound shown for locations with 0 mitigated MAC) – Business jet and all sUAS aggregate.

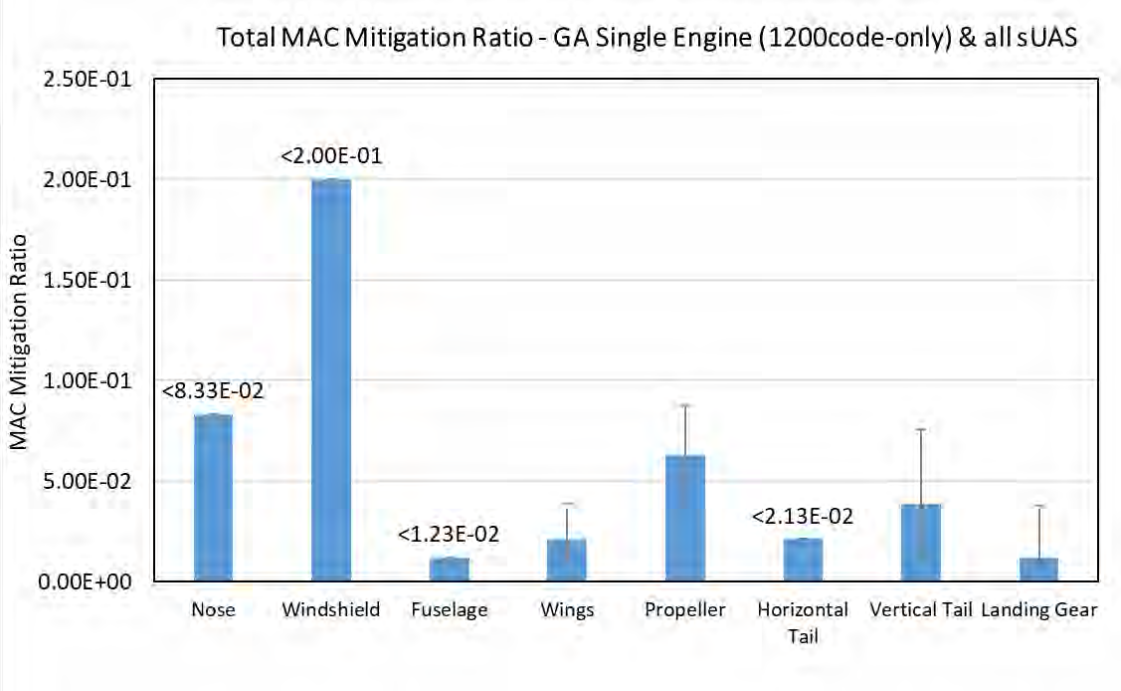

Figure 57. 1200code-only (non-cooperative surrogate) MAC mitigation ratio (upper bound shown for locations with 0 mitigated MAC) – GA aircraft and all sUAS aggregate.

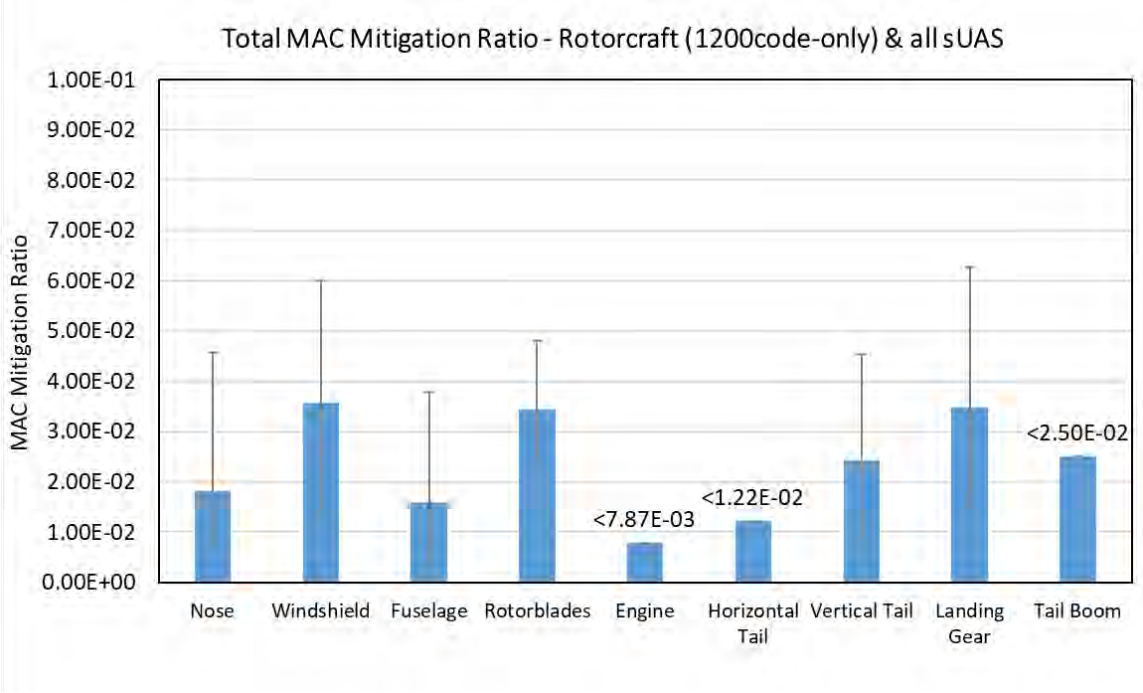

Figure 58. 1200code-only (non-cooperative surrogate) MAC mitigation ratio (upper bound shown for locations with 0 mitigated MAC) – Rotorcraft and all sUAS aggregate.

4.4.2 *Comparison to Manned-Manned encounters*

The unmitigated *P*(MAC|NMAC) results from Table 22 through Table 24, and the mitigated *P*(MAC|NMAC) results from Table 31 through Table 33 are plotted as a function of the sum of wingspans in Figure 63. *P*(MAC|NMAC) is reduced as the sum of wingspans decreases. This is more evident in the unmitigated cases. The sum of wingspans is typically dominated by the manned aircraft wingspan. However, the size effect is also observed when only the sUAS size is considered. The results of each manned aircraft were normalized to the smallest sUAS size to remove the effect of the manned aircraft size. Figure 60 and Figure 61 show the normalized unmitigated *P*(MAC|NMAC results) of the cooperative and non-cooperative encounter sets, respectively. *P*(MAC|NMAC) increases by a factor between 1.75 and 2.4 for the largest sUAS (13.9 ft. wingspan), depending on the manned aircraft pair. The effect is also observable in the mitigated dataset, as shown in Figure 62. The 13.9 ft. wingspan is larger than nearly the entirety of sUAS in the Association for Unmanned Vehicle Systems International (AUVSI) database (Weinert et al., 2018), as shown in Figure 63. Weinert et al. (2018) reported that the majority of wingspans in the database were less than 8 ft. These results assume that all sUAS models are capable of performing the same flight trajectory defined in the encounter sets (i.e., flying at 5 kt. to 100 kt.). The likelihood of each sUAS performing a trajectory was not assessed. However, this should be considered when generating an encounter set for a specific sUAS performance envelope. In this report, the results show the benefit of a smaller size, everything else being equal. The results also indicate that even if the RR and the LoWCR are the same (because the encounter set is the same), a smaller size sUAS ultimately translates into a lower *P*(MAC|NMAC). These could be further explored by generating sUAS-specific encounter sets or weighing the encounters in this research based on the likelihood of sUAS-specific speeds.

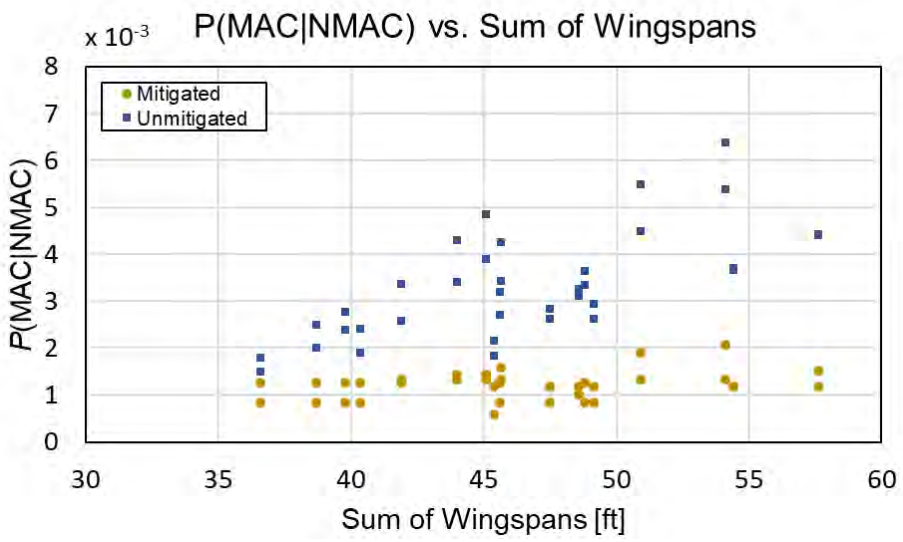

Figure 59. *P*(MAC|NMAC) as a function of wingspan. sUAS-Manned airframe pairs.

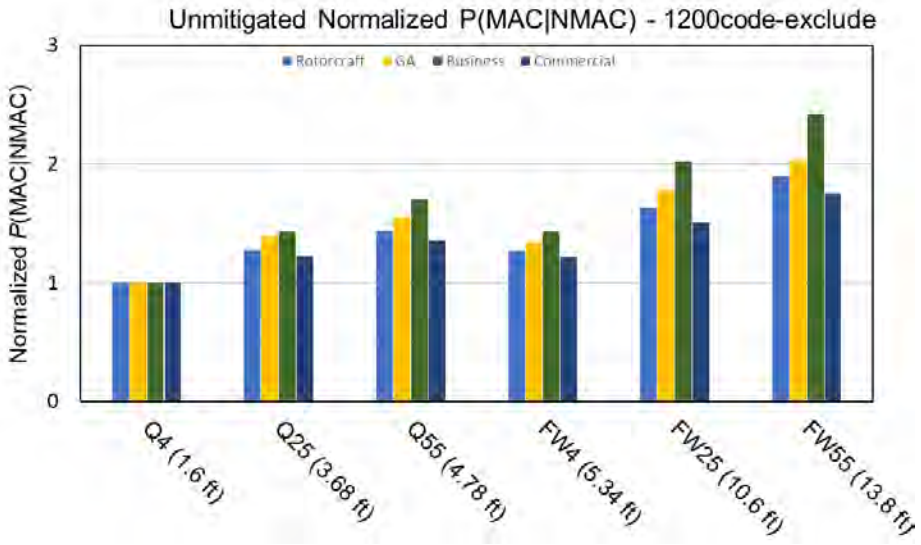

Figure 60. Unmitigated normalized *P*(MAC|NMAC) of the cooperative encounter sets (1200code-exclude). In parenthesis is the wingspan of each sUAS model.

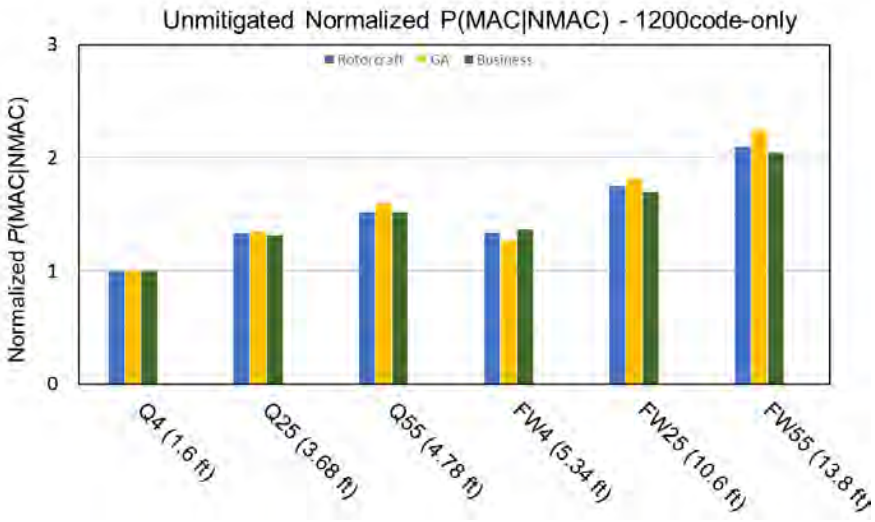

Figure 61. Unmitigated normalized *P*(MAC|NMAC) of the non-cooperative (surrogate) encounter sets (1200code-only). In parenthesis is the wingspan of each sUAS model.

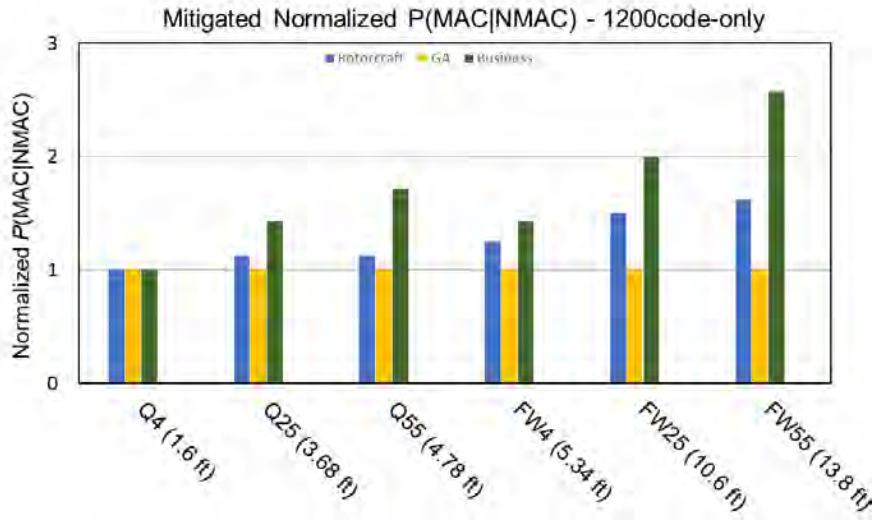

Figure 62. Mitigated normalized *P*(MAC|NMAC) of the non-cooperative (surrogate) encounter sets (1200code-only). In parenthesis is the wingspan of each sUAS model.

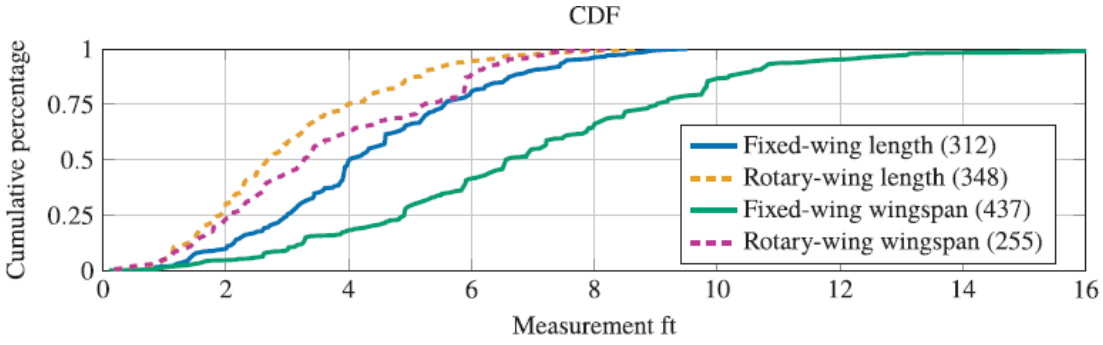

Figure 63. Distribution of sUAS wingspan in AUVSI air platform database as reported by Weinert et al. (2018).

Kochenderfer et al. (2010) estimated *P*(MAC|NMAC) for 173x173 combinations of wireframe airframe models. 400 NMAC encounters were used to determine *P*(MAC|NMAC) for each airframe pair. Kochenderfer et al. (2010) demonstrated that smaller wingspans result in a significant reduction of *P*(MAC|NMAC). The *P*(MAC|NMAC) of manned aircraft without TCAS was compared with the unmitigated *P*(MAC|NMAC) of sUAS-manned encounters in Figure 64. The small size of sUAS results in an overall lower unmitigated *P*(MAC|NMAC), as previously assumed by Weinert et al. (2018).

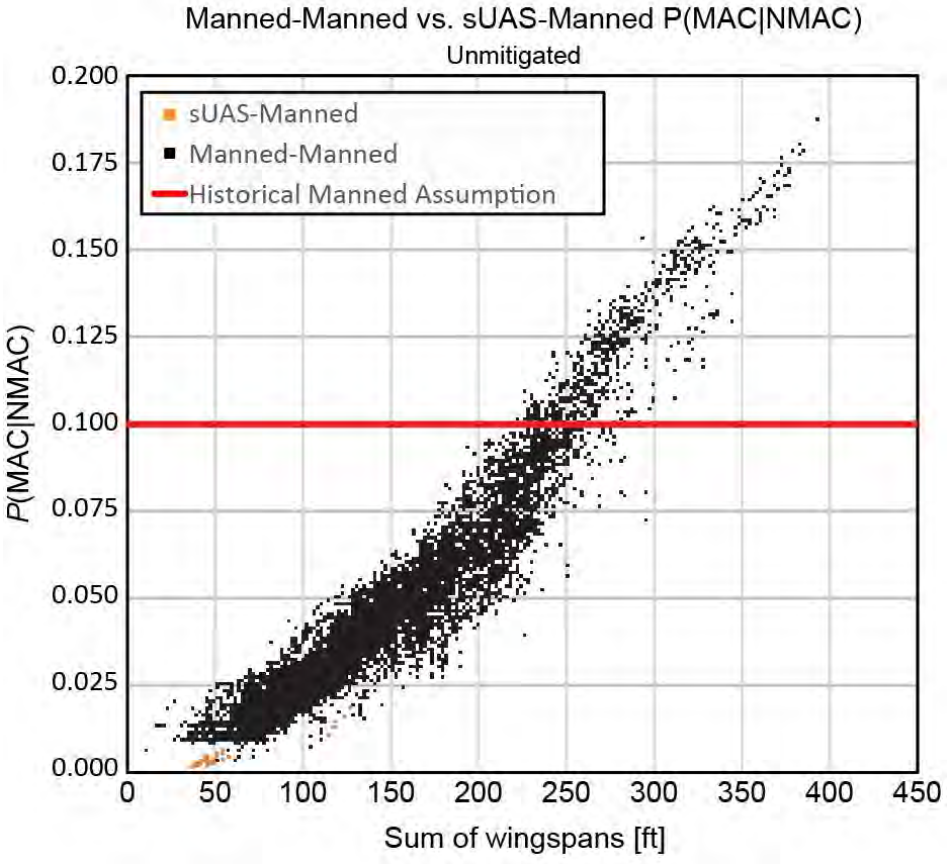

Figure 64. *P*(MAC|NMAC) as a function of wingspan. sUAS-Manned vs. Manned-Manned (without TCAS) airframes. Adapted from Kochenderfer et al. (2010).

Similarly, the *P*(MAC|NMAC) of manned aircraft when only one aircraft has TCAS (TCAS-none) was compared with the mitigated *P*(MAC|NMAC) of sUAS-manned encounters in Figure 65. In this case, the sUAS datapoints are within the lower bound of the manned-manned aircraft dataset. However, the reduction in *P*(MAC|NMAC) due to sUAS size is not as significant as in the unmitigated case. A major difference between Kochenderfer et al. (2010) and the present research is the number of datapoints. The present research only included datapoints for 6x4 airframe pairs. This is intentional because the MAC severity evaluation utilizes these airframe pairs. It would not have been possible to evaluate the severity for more airframe pairs. The severity evaluation is further discussed in Section 5.

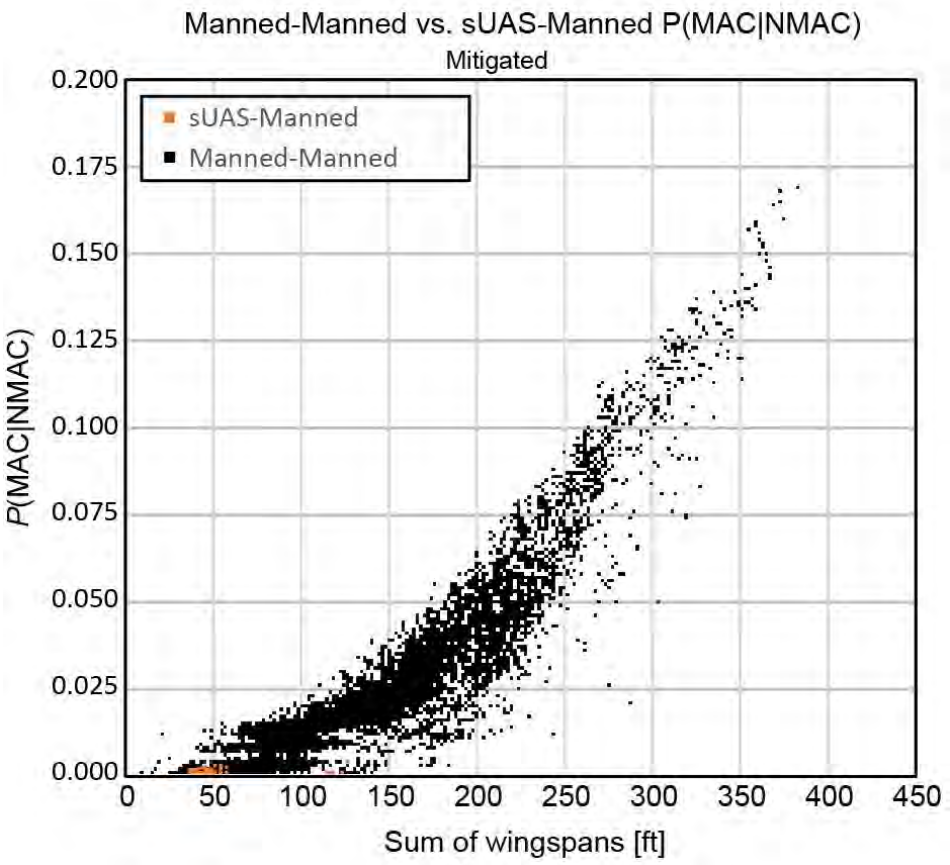

Figure 65. *P*(MAC|NMAC) as a function of wingspan. sUAS-Manned vs. Manned-Manned (TCAS-none pair) airframes. Adapted from Kochenderfer et al. (2010).

4.4.3 *Mitigation Ratio Curves*

Mitigation ratios at multiple volumes can also be calculated to determine the overall relationship between MAC, NMAC, and LoWC. Figure 66 through Figure 68 showcase mitigation curves at multiple VMDs for all the encounter sets analyzed. The mitigation ratio was calculated according to Eq. (19), where Volume can be any HMD and VMD combination.

$$Mitigation\ Ratio = \frac{P_{mitigated}(Volume\ Violation\ |Encounter)}{P_{Unmitigated}(Volume\ Violation\ |Encounter)} \tag{19}$$

The ratio represents the total mitigation at any given volume given an encounter set. The MAC mitigation ratio was also plotted at HMD equal to the sum of wingspans. Each aircraft pair was added as an individual point in Figure 66 through Figure 68. The MAC mitigation ratio differs from the MAC ratio (presented in Figure 51 and Figure 52) in the sense that it uses probabilities given an encounter rather than probabilities given an NMAC.

The effect of sensor uncertainty is evident between the 1200code-only and the 1200code-exclude models. The more accurate altitude estimates of ADS-B results in higher mitigation sensitivity in the vertical domain. This is true for the three 1200code-exclude models.

The MAC mitigation ratio correlates well with the mitigation curves at 50 ft. and 100 ft. VMD. Figure 69 highlights the Root Mean Square Error (RMSE) between the MAC data points and the mitigation curves. Lower RMSE indicates less error on average. The 1200code-only models had an overall lower RMSE with the 50 ft. VMD curves. The rotorcraft model had a slightly better fit with the 100 ft. VMD curve. However, both the 50 ft. and 100 ft. VMD curves had similar results at 50 ft. HMD, 2.04E-2 vs. 2.78E-2, respectively. On the other hand, the 1200code-exclude models have a better fit with the 100 ft. VMD curves. In this case, the upper bound of the MAC mitigation ratio was estimated since no MACs were recorded in these models. This could explain why the MAC mitigation ratio better fits with the 100 ft. as opposed to the 50 ft. VMD curve.

These results indicate that the mitigation ratio curves at 50 ft. and 100 ft. VMD can be used to roughly estimate the MAC mitigation ratio in an encounter set without performing a collision detection analysis with discrete aircraft geometries. Similarly, the 100 ft. VMD and 50 ft. HMD volume could be used to conservatively estimate the overall DAA MAC reduction efficiency in an encounter set. However, a collision detection analysis is recommended to estimate more accurate MAC mitigation ratios.

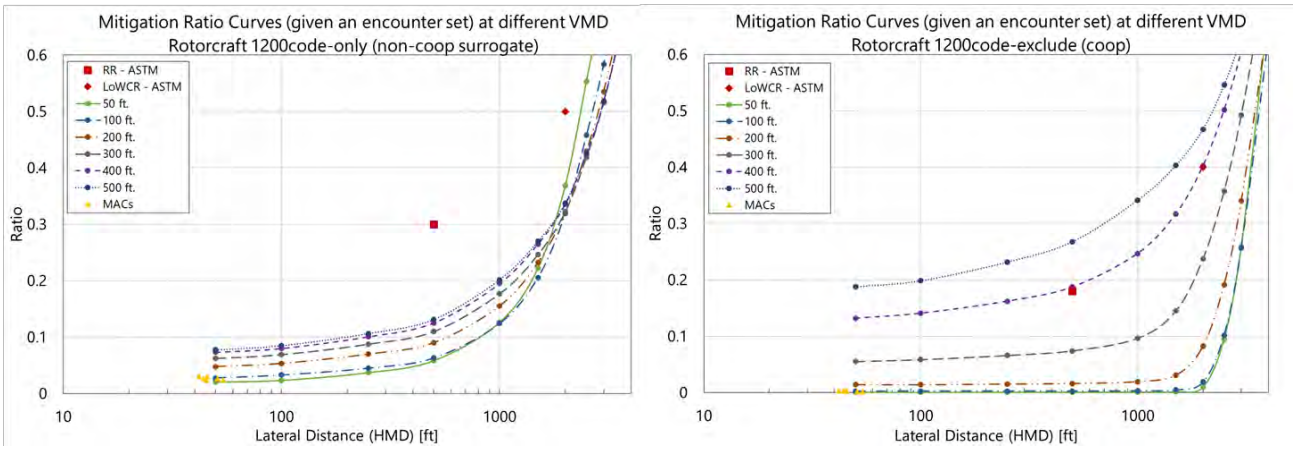

Figure 66. Mitigation ratio curves for the rotorcraft models. 1200code-only (left) and 1200code-exclude (right).

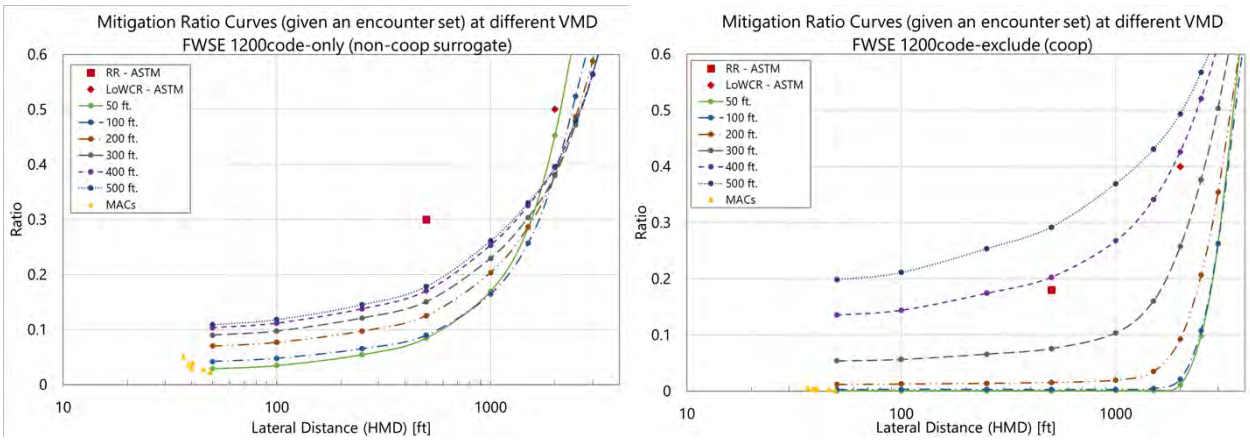

Figure 67. Mitigation ratio curves for the FWSE models. 1200code-only (left) and 1200code-exclude (right).

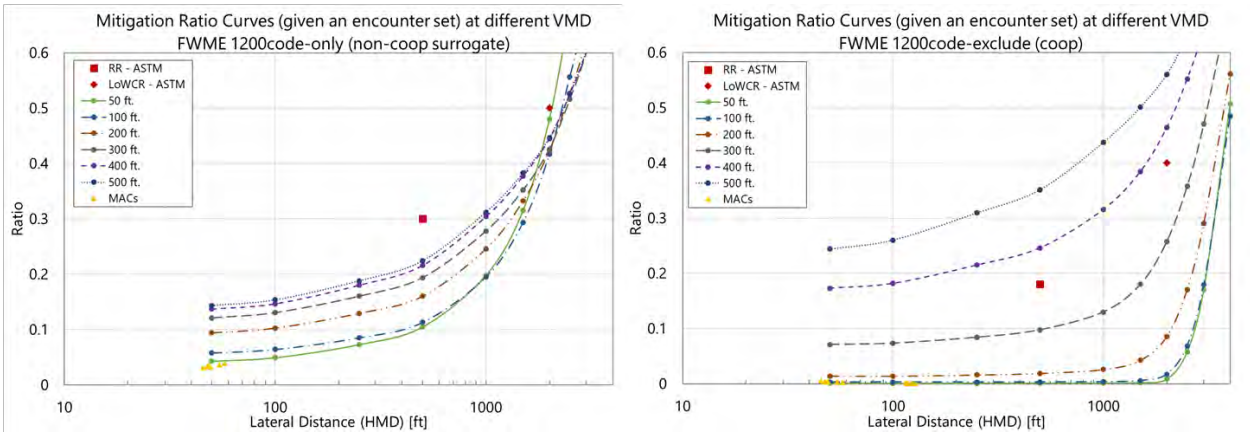

Figure 68. Mitigation ratio curves for the FWME models. 1200code-only (left) and 1200code-exclude (right).

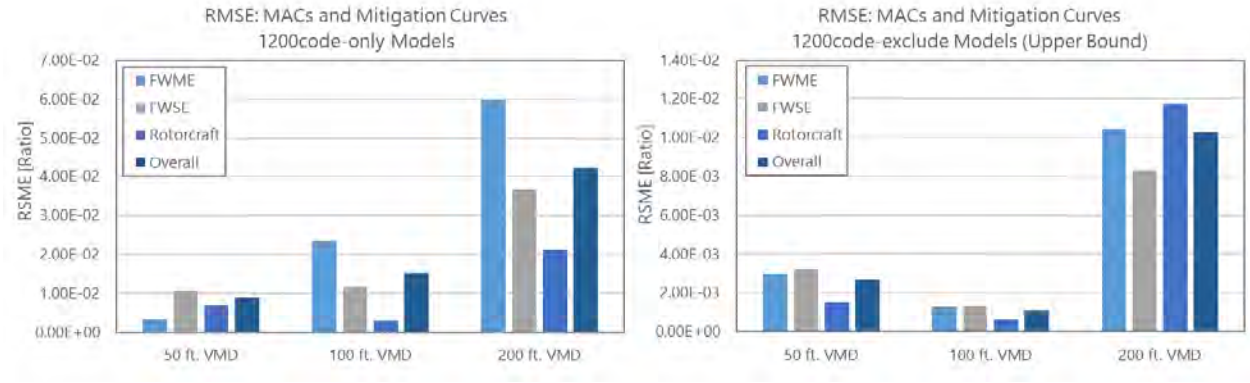

Figure 69. Root Mean Square Error (RMSE) between mitigation ratio curves and MAC mitigation ratio. 1200code-only (left) and 1200code-exclude (right).

4.5 Effect of Encounter Weights

The actual encounter frequency between sUAS and manned aircraft is unknown. Weinert, Edwards, et al. (2020) suggest a weighting scheme based on the encounter relative speed at CPA.

Weinert, Edwards, et al. (2020) also indicate that a uniform weighting scheme is more simplistic and provides a conservative approach. The weighting scheme does not significantly affect the results of this research. The RR and LoWCR comparison between uniform weights and relative speed weights results is shown in Figure 70 and Figure 71, respectively. Head-on encounters are weighted more heavily in the relative speed approach. This can be observed in the relative speed distribution shown in Figure 72.

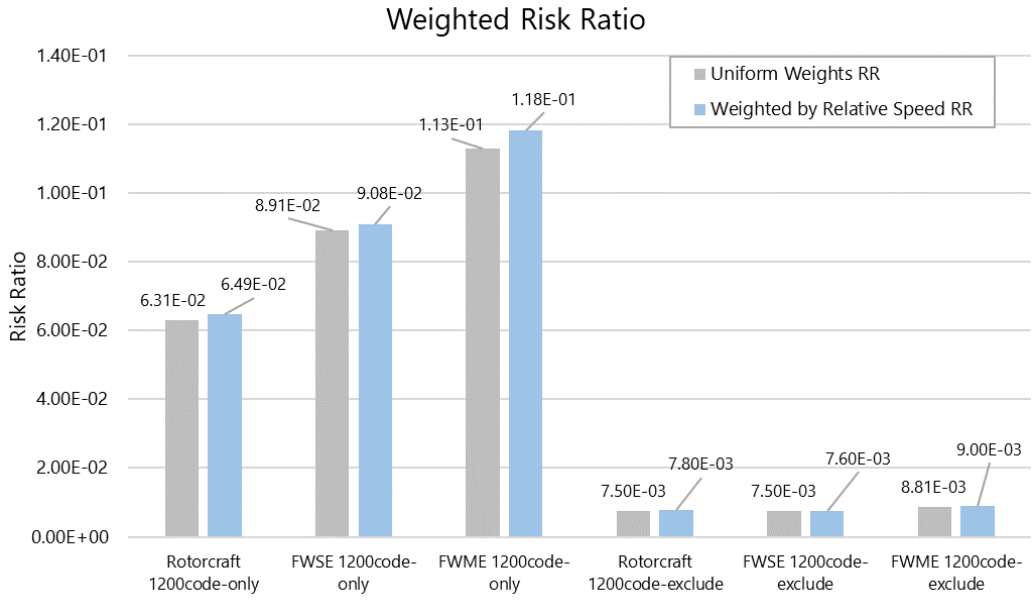

Figure 70. Risk ratio comparison with different weighting schemes.

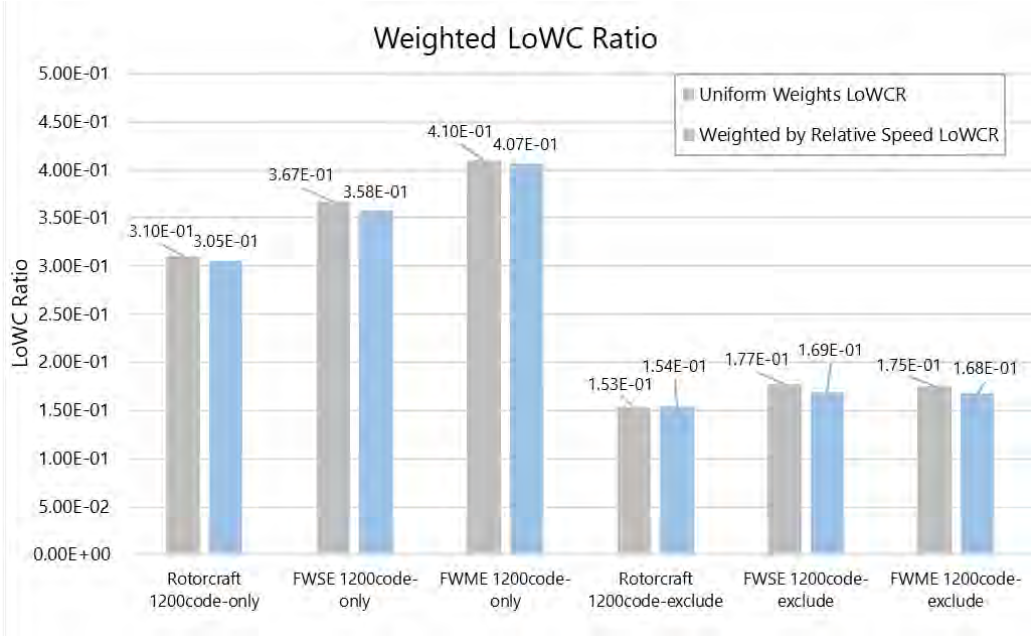

Figure 71. LoWC ratio comparison with different weighting schemes.

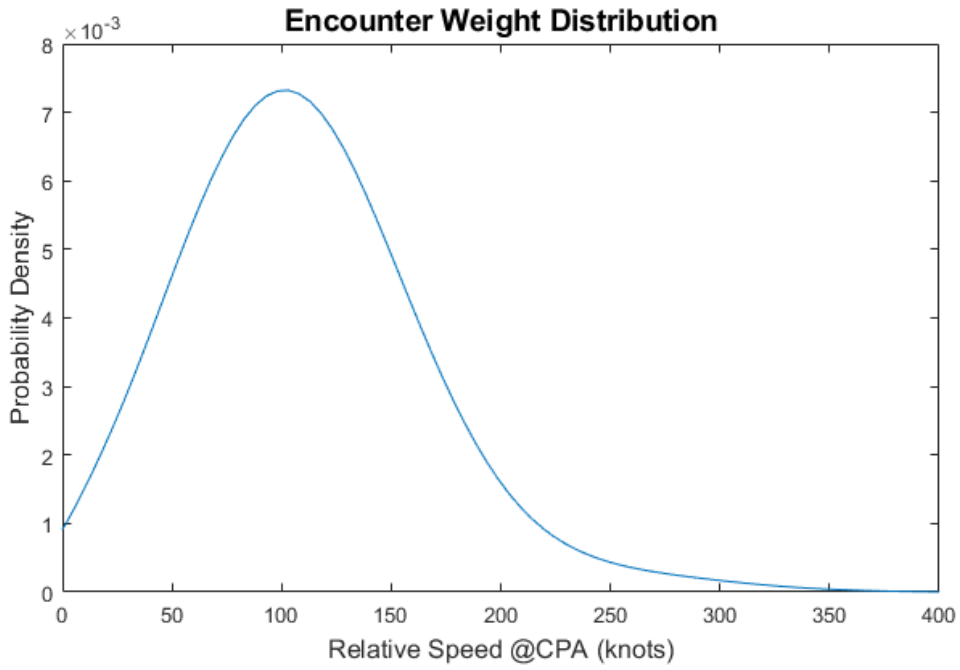

Figure 72. Relative speed distribution (used as encounter weights) at CPA.

4.6 Other DAA Metrics

This section discusses other DAA metrics that are not requirements in the ASTM F3442 or the ACAS sXu MOPS. However, these metrics provide an overall description of the behavior of the DAA logic.

4.6.1 *Alert Metrics*

This section summarizes the Resolution Advisories (RAs) issued by ACAS sXu V4R1. The RAs were collected from each analyzed encounter, as presented in Section 4.3. Table 35 introduces the alert rate metric. This metric reflects the number of encounters that issued any alert over the total number of encounters analyzed, as shown in Eq. (20).

$$Alert\ Rate = \frac{\#Encounters\ with\ any\ RA}{Total\ Number\ of\ Encounter} \tag{20}$$

The alert rate metric is important to understand how alerting works when the DAA logic is supplied with different types of sensor modules or surveillance sensors. Roughly 95.3% of all *1200-only* (non-cooperative) encounters issued an alert. On the other hand, 86% of all *1200-exclude* (cooperative) encounters issued an alert. This highlights that greater sensor uncertainty generally results in more DAA alerts, even when they might not be necessary.

Table 35. Summary of ACAS sXu alerts per encounter model.

Encounter Model	Alert Rate	Horz Alert Rate	Vert Alert Rate	Horz RAs Per Encounter with Horz RAs	Vert RAs Per Encounter with Vert RAs	Avg. Duration of Horizontal RAs	Avg. Duration of Vertical RAs
FWSE 1200-exclude	0.85	0.71	0.46	2.88	3.12	27.97	17.78
FWME 1200-exclude	0.86	0.70	0.54	2.99	3.14	25.07	17.45
Rotorcraft 1200-exclude	0.87	0.73	0.46	2.91	3.12	29.47	19.23
FWSE 1200-only	0.95	0.95	0.34	4.86	5.04	47.60	12.53
FWME 1200-only	0.95	0.95	0.37	4.65	4.68	44.41	12.06
Rotorcraft 1200-only	0.96	0.96	0.30	4.83	4.87	48.17	10.87

Moreover, the number of unique horizontal and vertical alerts issued per encounter is greater for the 1200-only encounter models. ACAS sXu also relied more heavily on horizontal alerts in these encounter models. This is indicative of the large altitude error present in the AGT inputs. This data highlights what can be expected from the ACAS sXu logic behavior when this type of sensor is used. It also explains the difference observed in the risk ratio contours shown in Section 4.3. The number of alerts distribution given encounters with an alert for the 1200-only and 1200-exclude models are shown in Figure 73 Figure 74, respectively. These figures confirm that the errors in the AGT position result in encounters with more numerous alerts.

The type of horizontal and vertical alerts was also identified for each encounter model. These are shown in Figure 75 through Figure 80. There is not a clear trend on a predominant horizontal action issued. ACAS sXu decided to turn either right or left equally, roughly 30% each. The remaining horizontal alert was to maintain heading (approximately 34% to 38% of all horizontal alerts). Similarly, the vertical alert distribution shows a preference for either do-not-climb or do-not-descend alerts.

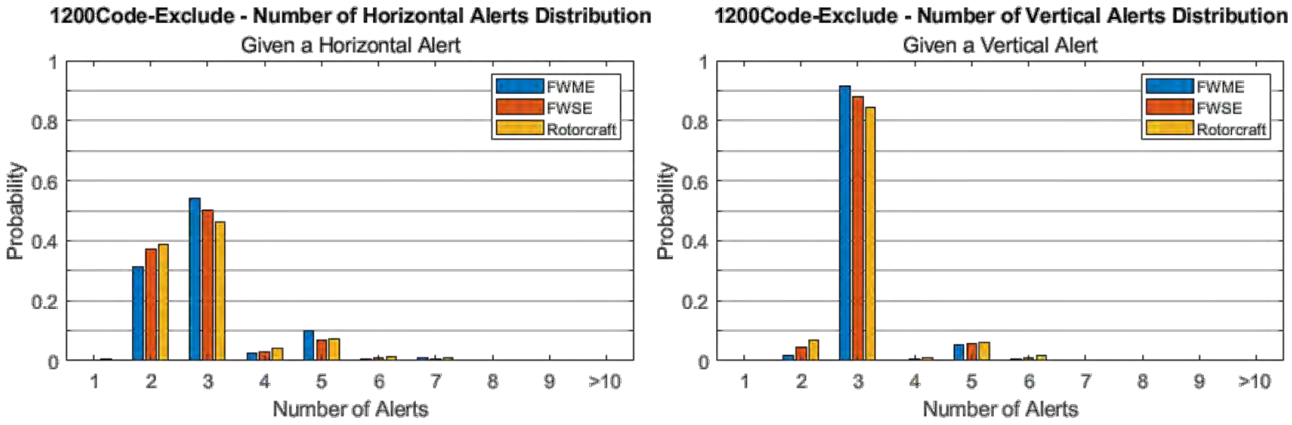

Figure 73. Number of alerts distribution given an encounter with an alert – 1200code-exclude encounter models.

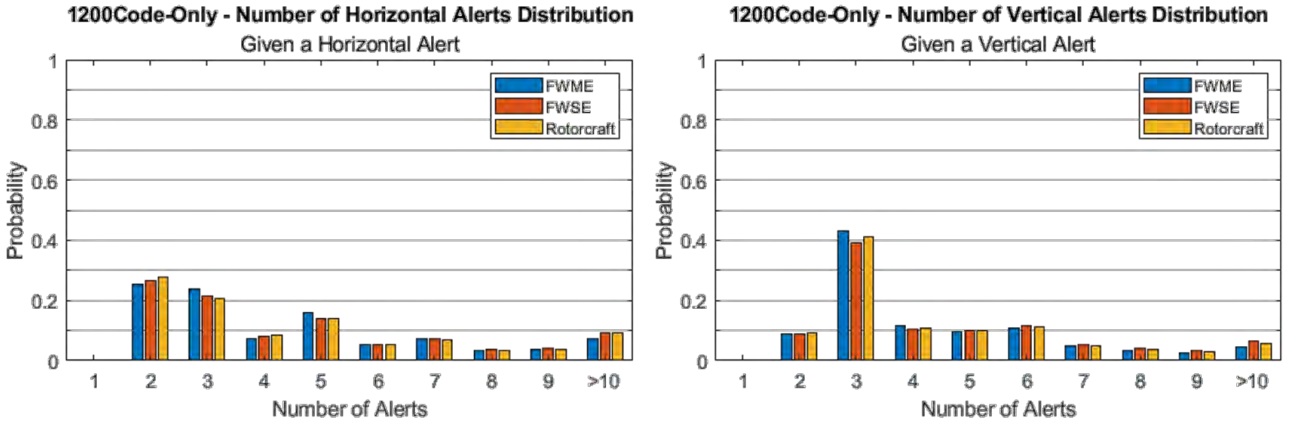

Figure 74. Number of alerts distribution given an encounter with an alert – 1200code-only encounter models.

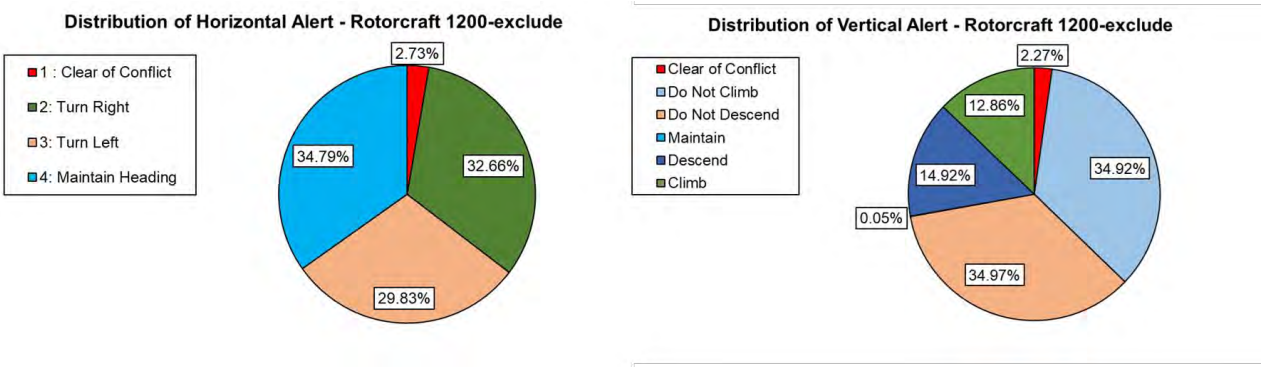

Figure 75. Distribution of horizontal and vertical alerts – Rotorcraft 1200-exclude (cooperative) encounters.

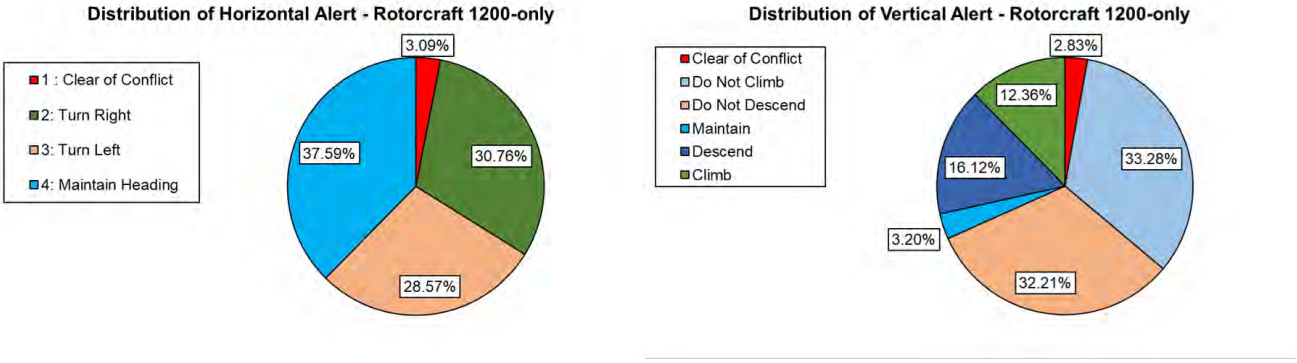

Figure 76. Distribution of horizontal and vertical alerts – Rotorcraft 1200-only (non-cooperative) encounters.

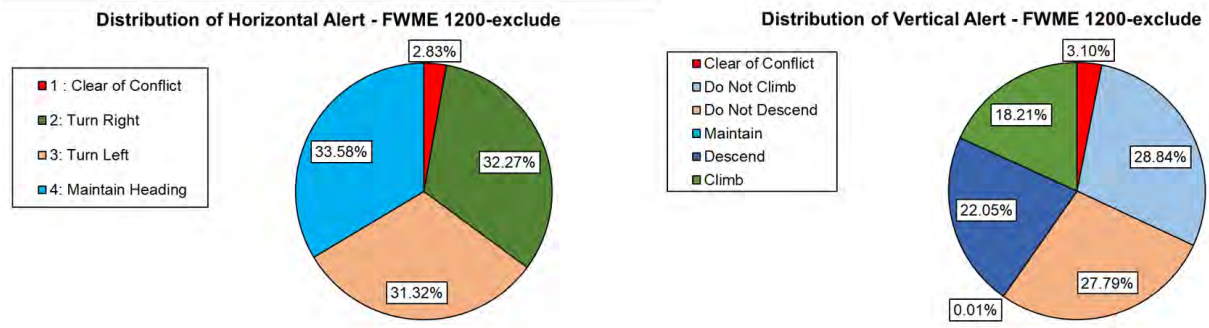

Figure 77. Distribution of horizontal and vertical alerts – FWME 1200-exclude (cooperative) encounters.

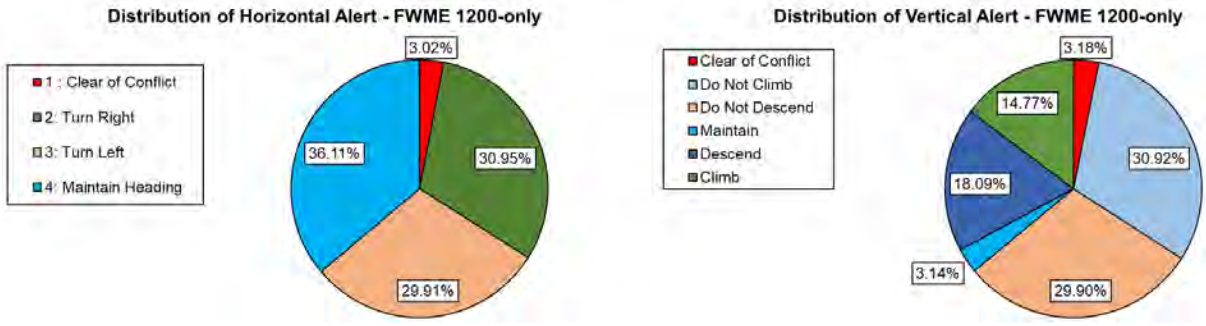

Figure 78. Distribution of horizontal and vertical alerts – FWME 1200-only (non-cooperative) encounters.

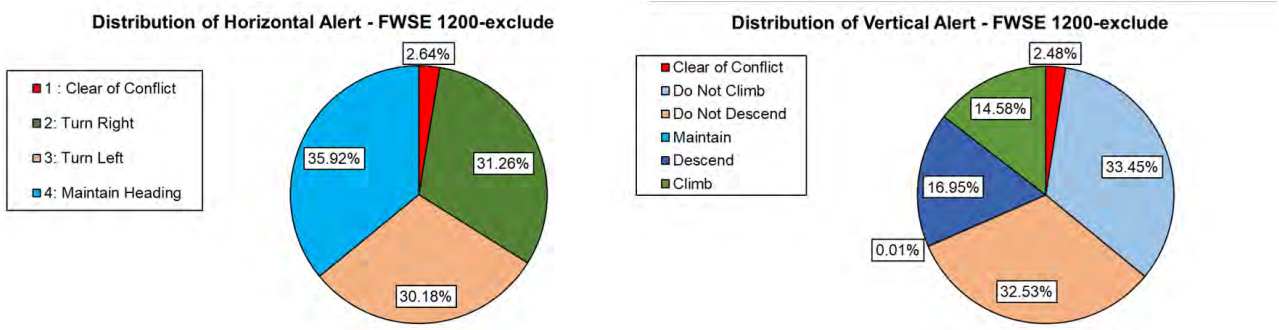

Figure 79. Distribution of horizontal and vertical alerts – FWSE 1200-exclude (cooperative) encounters.

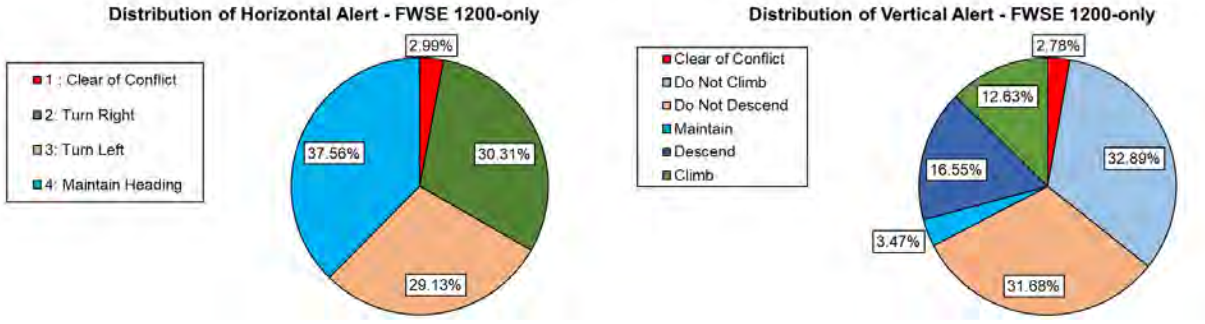

Figure 80. Distribution of horizontal and vertical alerts – FWSE 1200-only (non-cooperative) encounters.

4.6.2 *Induced and Unresolved Metrics*

Another metric to understand the overall DAA performance is the induced and unresolved RR and LoWCR. The induced ratio quantifies the encounters that resulted in an NMAC or LoWC violation after performing a maneuver advised by the DAA logic. These encounters would not have resulted in an NMAC or LoWC without performing any action. On the other hand, the unresolved ratio refers to the DAA logic failing to prevent an NMAC or LoWC violation that would have occurred regardless of the DAA action. Figure 81 and Figure 82 present this metric for RR and LoWCR, respectively.

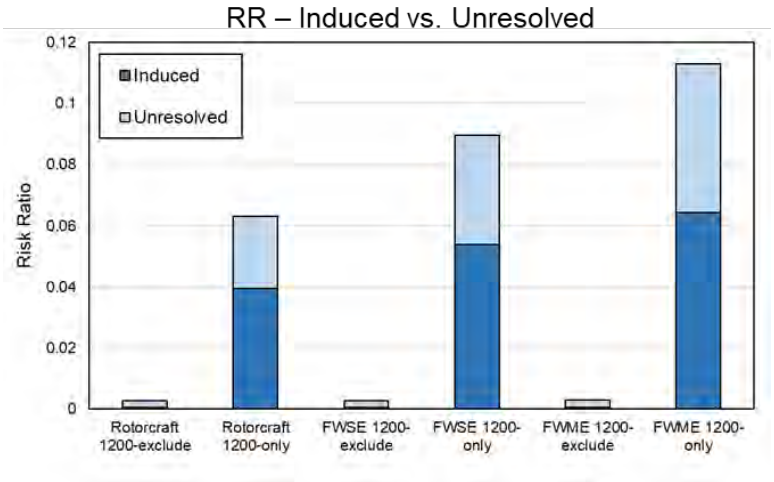

Figure 81. NMAC risk ratio – Induced vs. Unresolved.

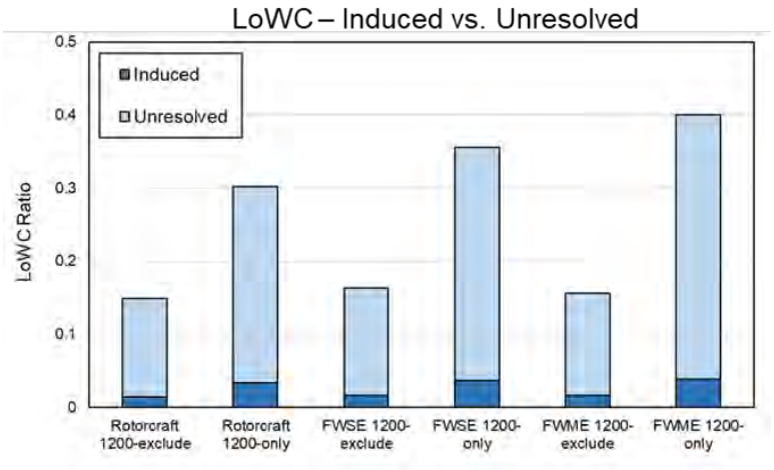

Figure 82. Loss of well-clear ratio – Induced vs. Unresolved.

In general, the DAA logic had no difficulties mitigating all 1200-exclude code (cooperative) encounter NMACs, as shown in Figure 81. For the 1200-only code (non-cooperative) encounters, most NMACs (60% to 70%) were induced by the logic due to significant sensor uncertainties. On the other hand, most well-clear violations were unresolved in all encounter sets, as shown in Figure 82.

5 MAC SEVERITY EVALUATION

This chapter discusses the severity evaluation of the MACs recorded in Sections 3.3 and 4.4. Section 5.1 explains the factors that affect the severity of a MAC. Section 5.2 presents the previous MAC severity assessment research and defines the approach used to evaluate the severity in this research.

Section 5.3 defines a methodology to account for the overly conservative approach described in Section 5.2. This is done by defining an energy scale factor for each MAC. Section 5.4 provides validation and comparison of the severity evaluation methodology to actual severity results from Finite Element Analyses (FEA). The severity assessment of all MACs recorded in Sections 3.3 and 4.4 is discussed in Section 5.5.

Finally, Section 5.7 discusses the research gaps identified in this chapter and emphasizes the need for further research required for a comprehensive severity analysis

5.1 Components of Severity

The severity of a MAC is dependent on several factors. sUAS mass, vehicle stiffness, and impact velocity (relative to manned aircraft) are the main drivers of severity. In general, higher kinetic energy impacts tend to be more severe.

sUAS architecture and construction also affect the severity of a MAC. Olivares, Lacy, et al. (2017) demonstrated that fixed-wing architectures tend to concentrate more loads on the manned aircraft (for head-on collisions). Research also shows that larger-size sUAS with an evenly distributed mass (distribution of internal components) can generate less damage than smaller-size sUAS with the same mass (more concentrated mass).

In the same manner, depending on the orientation of the sUAS relative to the manned aircraft at the time of impact, the severity level can be vastly different. This is more apparent for fixed-wing configurations, as highlighted in Figure 83, i.e., a MAC with only the wings of the sUAS will result in a considerably lower severity compared to a head-on collision.

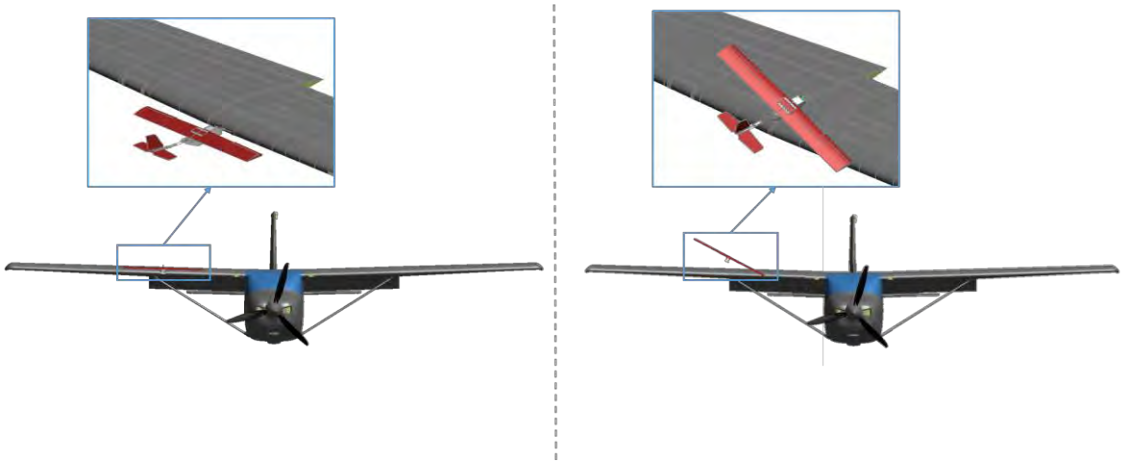

Figure 83. MACs with different relative orientations.

Severity, in this report, refers to the level of damage observed in the manned aircraft in a MAC. It does not evaluate the severity of an encounter (how close the aircraft get to each other). Similarly,

the damage to the sUAS is not evaluated since the main risk is to people on board the manned aircraft. The typical severity levels are shown in Table 36.

Table 36. UAS MAC Severity Categories (Olivares, Lacy, et al., 2017).

Severity	Description	Example
Level 1	• The airframe is undamaged. • Small deformations.	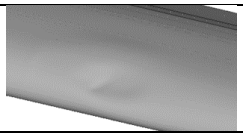
Level 2	• Extensive permanent deformation on external surfaces. • Some deformation in internal structure. • No failure of skin.	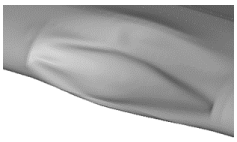
Level 3	• Skin fracture. • Penetration of at least one component into the airframe.	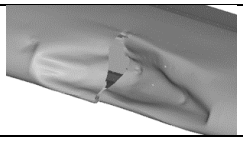
Level 4	• Penetration of UAS into the airframe. • Failure of parts of the primary structure.	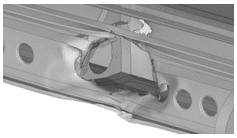

5.1.1 *Relative Heading*

The unmitigated relative heading distribution is discussed in this section. The relative heading is the difference in heading at the time a collision is detected. A visual representation of the relative headings of the business jet-Q4 pair's MACs is shown in Figure 84. The arrowheads indicate the sUAS heading, and they are plotted at the center of gravity of the sUAS. All the other sUAS-manned aircraft pairs are documented in Appendix E.

The relative heading distribution of all the business jet MACs is shown in Figure 85. Depending on the impact location, the number of cases in the head-on range changes. For instance, there are roughly 12% of wing MACs in the head-on range compared to only 3% of fuselage MACs, as shown in Figure 86. This is expected as the exposed surface of the fuselage, while airborne, does not facilitate a head-on MAC. The relative heading distributions for all the sUAS-manned aircraft pairs are presented in Appendix D.

In general, head-on collisions are expected to be more severe because the impact speed is the sum of both aircraft's speeds. Further analysis of the relative impact speed vs. relative heading is provided in Section 5.1.2.

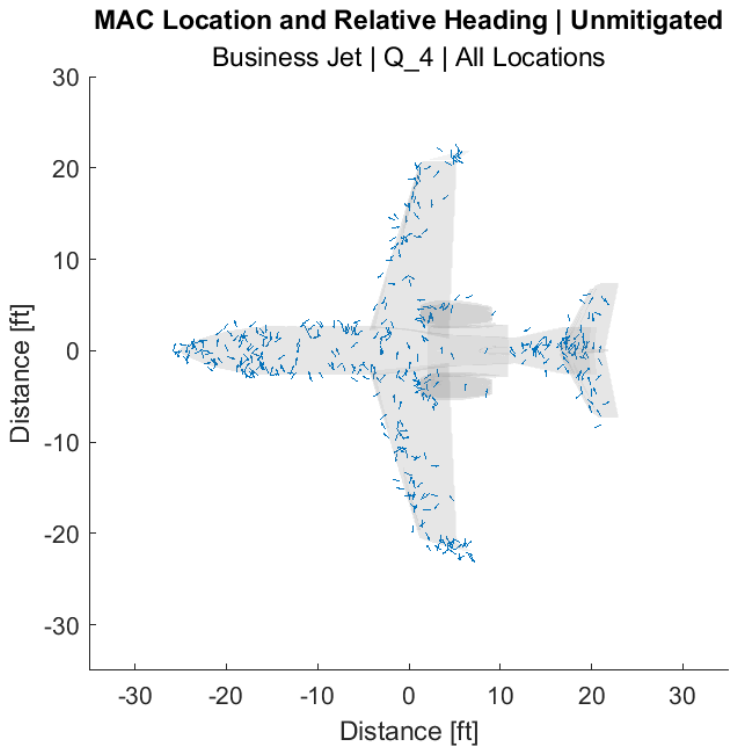

Figure 84. MAC location and relative heading – Unmitigated business jet-Q4 pair.

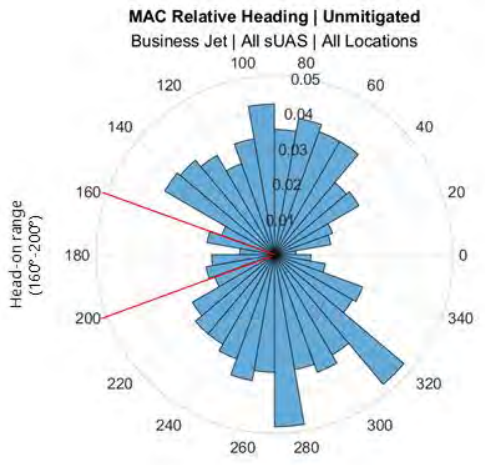

Figure 85. MAC relative heading distribution – All unmitigated business jet MACs.

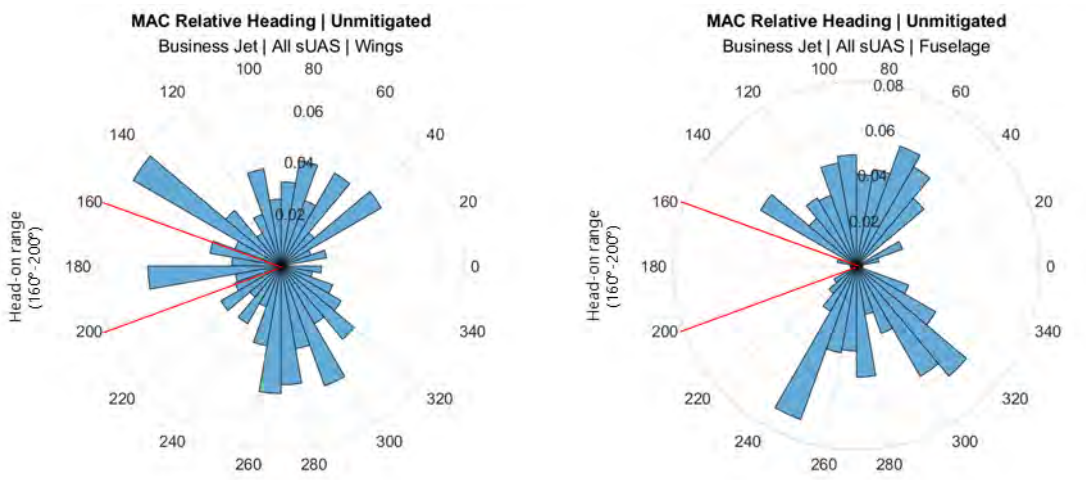

Figure 86. MAC relative heading distribution – Unmitigated business jet wing (left) and fuselage (right) MACs.

The relative heading for the business jet- Q4-pair mitigated unresolved MACs is shown in Figure 87. The distribution is shown in Figure 88. The mitigated cases consist of a limited number of cases, lowering the confidence in the relative heading distribution. For the mitigated cases, the relative heading breakdown by impact location on the manned aircraft is not possible due to the limited number of MACs.

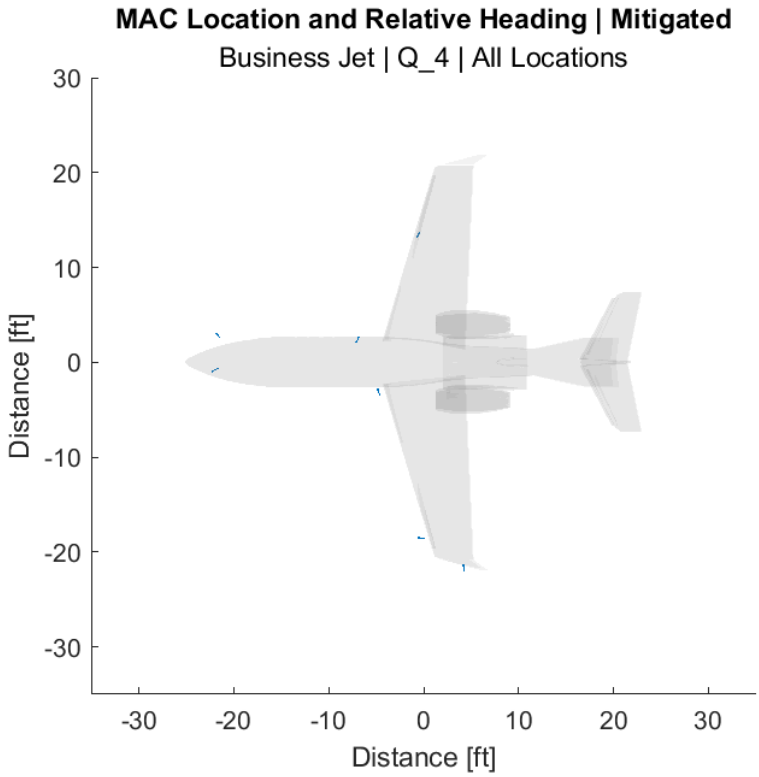

Figure 87. MAC location and relative heading – Mitigated business jet-Q4 pair.

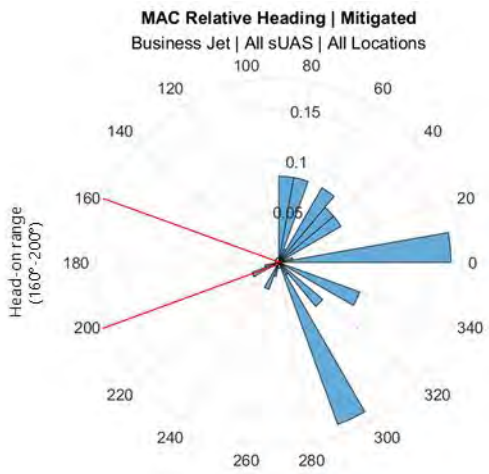

Figure 88. MAC relative heading distribution – All mitigated business jet MACs.

5.1.2 *Relative Impact Speed*

The relative speed is the addition of the manned aircraft's speed and the projection of the sUAS speed in the heading direction of the manned aircraft. The relative speed as a function of relative heading is shown in Figure 89 through Figure 92; the relative speed can be approximated with a 2nd-degree polynomial fit. As expected, the local maximum relative speed is at 180deg (head-on), and the minimums are at 0deg/360deg (manned aircraft overtaking the sUAS).

For the mitigated cases, there is an overall reduction in relative speed for the unresolved MACs. The maximum relative speed for the mitigated was 150 knots. While for the unmitigated cases, it is ~350 knots. Interestingly, there is a weaker relationship between relative speed and relative heading. The unresolved MACs occurred in a tighter 100 knots relative speed band (50-150 knots) for all the encounter models as opposed to the much wider 0-200 knots for the rotorcraft and Fixed-Wing Single Engine Aircraft (FWSE) encounter models and to the even broader 50-350 knots range of the 1200-exclude (cooperative) Fixed-Wing Multiple Engine Aircraft (FWME) cases. This overall reduction in the relative speed range indicates that ACAS sXu was able to resolve overtaking encounters with similar speed (low relative speed at 300-360deg and 0-60deg ranges) as well as high-speed head-on encounters. Reductions in relative impact speed could result in lower severity for the unresolved MACs. The severity of the MACs is discussed in Section 5.2.

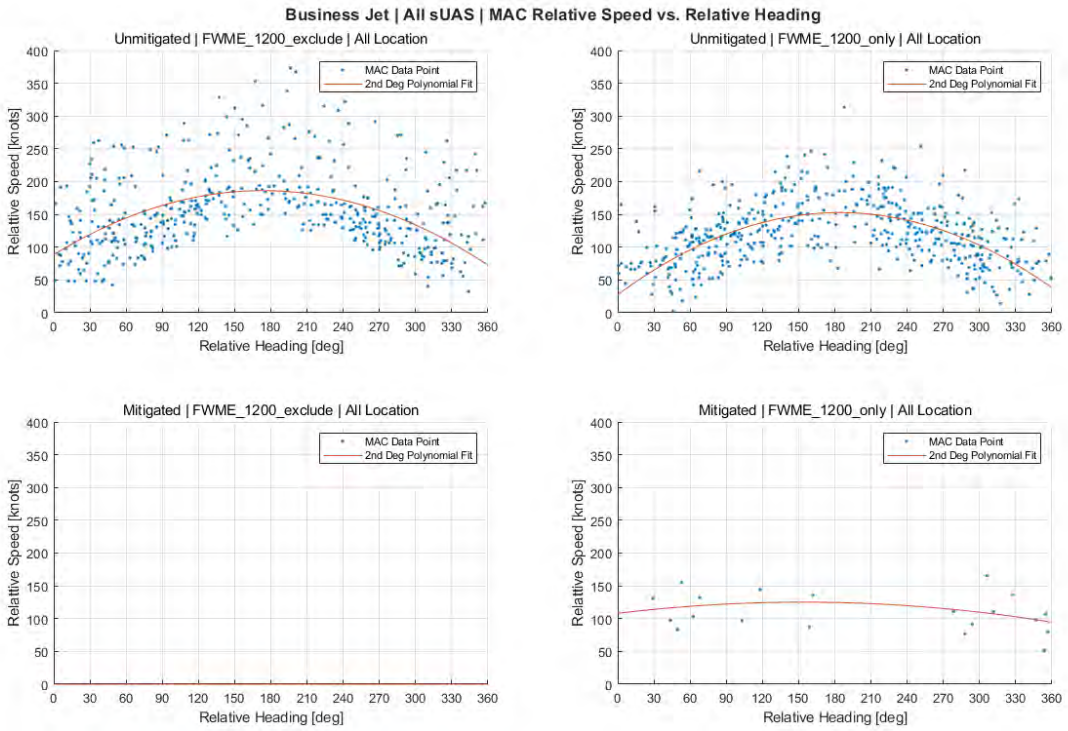

Figure 89. MAC relative speed as a function of relative heading – Business jet & all sUAS.

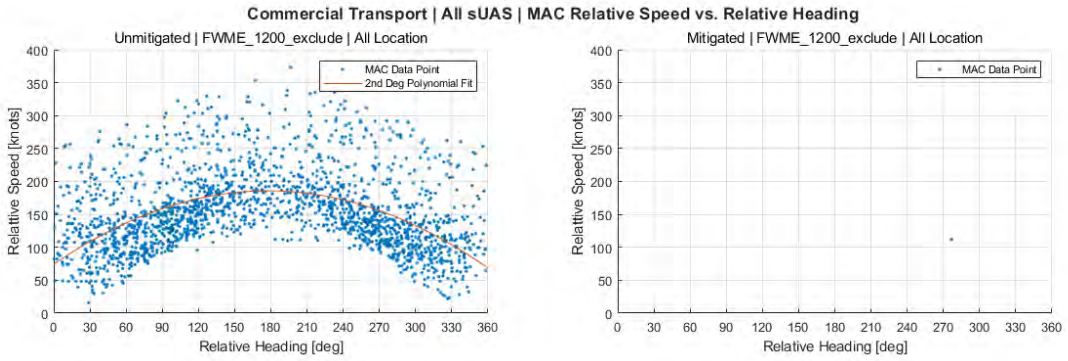

Figure 90. MAC relative speed as a function of relative heading –Commercial transport & all sUAS.

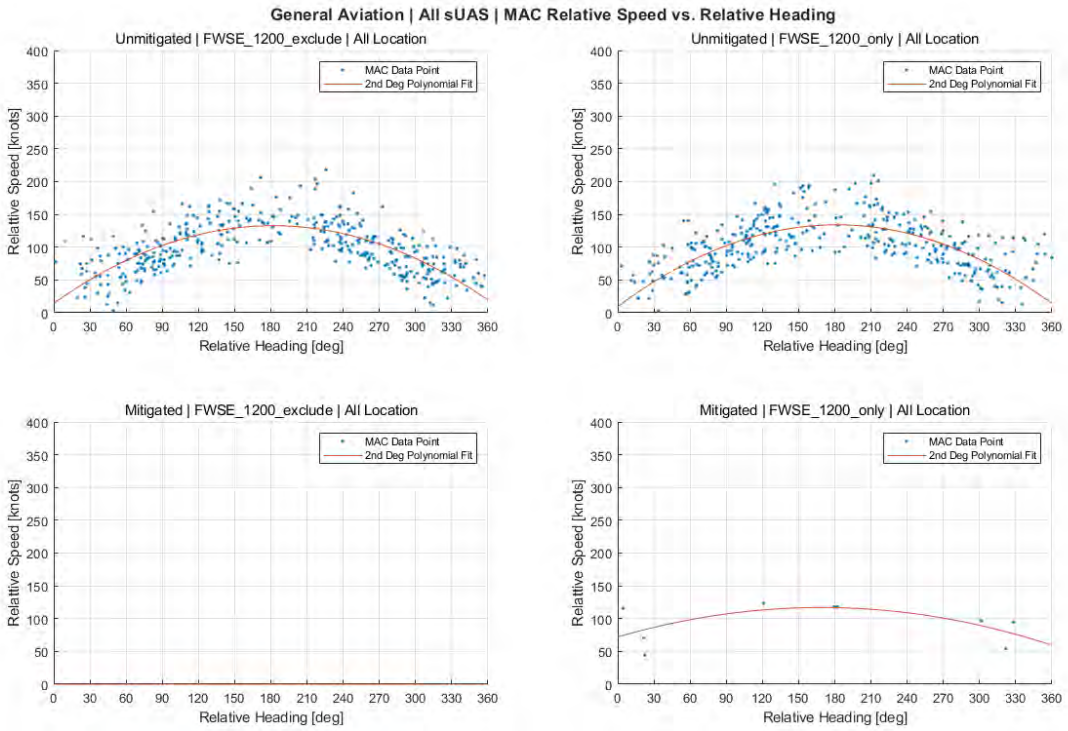

Figure 91. MAC relative speed as a function of relative heading – General aviation & all sUAS.

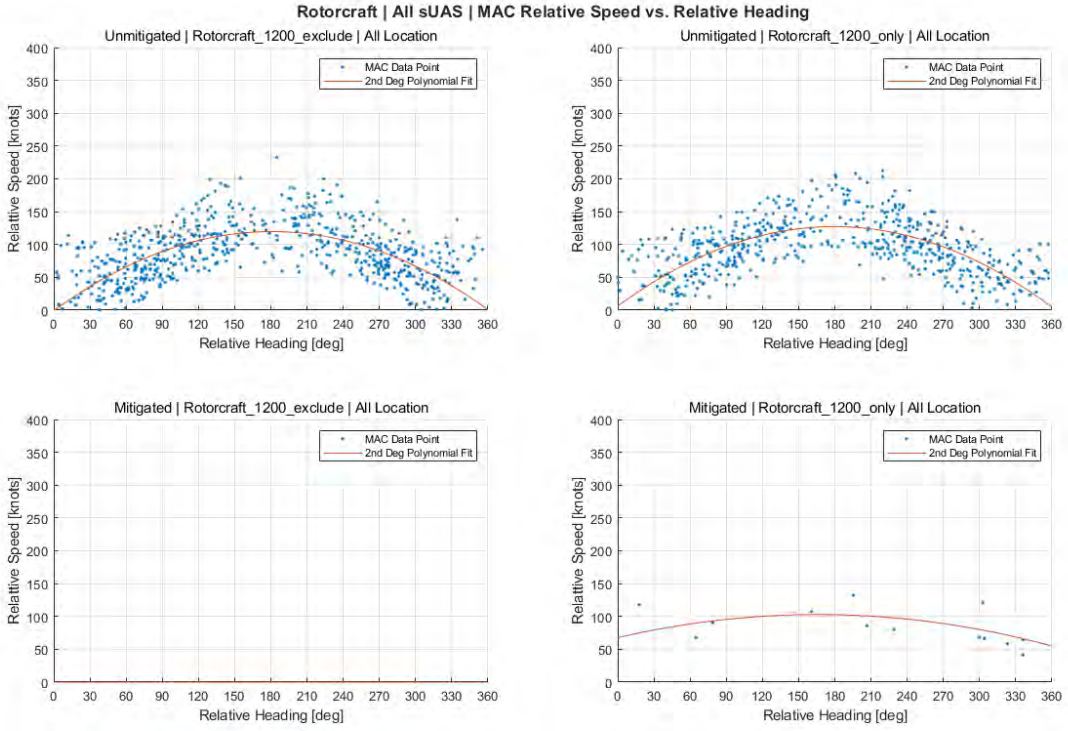

Figure 92. MAC relative speed as a function of relative heading – Rotorcraft & all sUAS.

The average sUAS and manned aircraft speed are lower for the unresolved MAC mitigated cases. The reduction is more significant for the sUAS, as shown in Figure 93. The standard deviation is also reduced for both aircraft speeds and, in turn, for the relative impact speed. ACAS sXu was able to resolve most MACs when the sUAS was flying at higher speeds. Figure 94 shows a histogram of the sUAS speed for unmitigated and unresolved mitigated MACs. Over 50% of unresolved MACs occurred when the sUAS was flying at less than 30 knots. Even though ACAS sXu does an excellent job at reducing MACs at all sUAS speeds, this is an important consideration for sUAS operators and DAA manufacturers. The effect of the sUAS acceleration capability was not investigated in this research. The DAA MOPS and operational validation reports provide more information on the effects the sUAS capabilities (turn acceleration, turn rate, and vertical speed) have on RR and LoWCR (Das, 2021b; SC-147, 2022b). However, the reports did not address the effect on the MAC ratio. It is worth noting that sXu expects a 25 knots minimum ground speed when performing horizontal maneuvers (Das, 2021b).

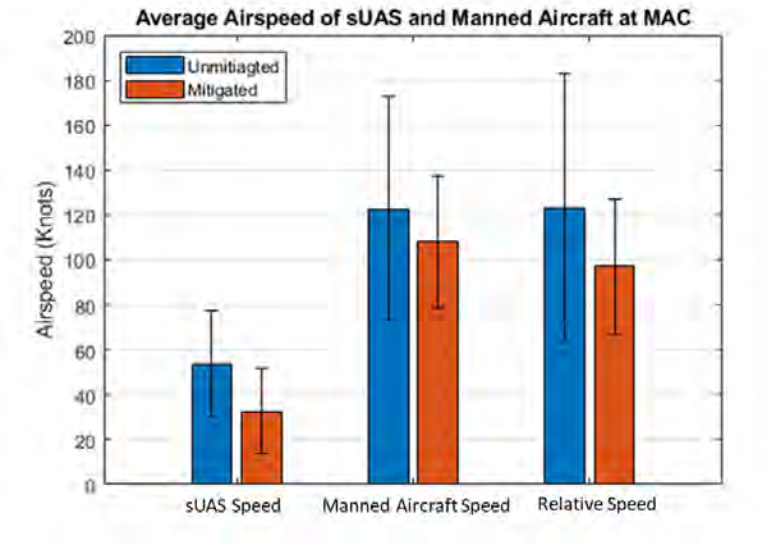

Figure 93. MAC average speed – Unmitigated & mitigated.

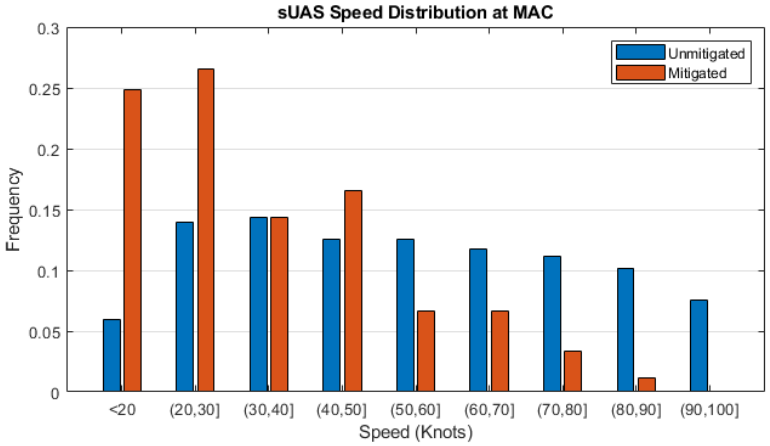

Figure 94. sUAS speed distribution at MAC – Unmitigated & mitigated.

5.2 Severity Approximation Functions

Olivares et al. (2020; 2022; 2021; 2017) conducted several mid-air collision damage assessments in the past. These served as the foundation to assess the severity of the MACs recorded in the present research. The available database, however, is limited to only head-on collisions. Similarly, the assessments only apply to select manned aircraft impact locations. Table 37, Table 38, Table 39, and Table 40 summarize the severity data points available for each manned aircraft and sUAS model. This database's impact conditions represent the worst-case condition during a MAC between sUAS and manned aircraft. Moreover, MACs during three main phases of flight were evaluated (at different impact speeds); take-off, holding, and landing.

On the other hand, the MAC cases recorded in the present research are not limited to only worst-case conditions, and their corresponding impact speeds are based on the flight condition during the encounter. Therefore, a relationship between severity level and impact energy was developed to evaluate the severity of unknown cases through interpolation of known data. In this manner, all vehicles' size, weight, and velocity are no longer a variable, and all mid-air collision cases can be studied as a function of impact energy. For sUAS architectures where a single interpolated function did not capture the behavior of all data points, multiple functions were created instead; an example is shown in Figure 185 in Appendix B.

Table 37. Available mid-air collision severity levels for commercial transport aircraft. Data from (Olivares et al., 2020; Olivares, Gomez, et al., 2017; Olivares, Lacy, et al., 2017).

Commercial	Q4	Q25	Q55	FW4	FW25	FW55
Nose	○ (Large sUAS data)	✓	✓	○ (Large sUAS data)	✓	✓
Windshield	✓	✓	✓	✓	✓	✓
Fuselage	×	×	×	×	×	×
Wings	✓	✓	✓	✓	✓	✓
Engines	○ (Fan Blades only, 2.7 lb sUAS)	×	×	×	×	×
Horizontal Tail	✓	✓	✓	✓	✓	✓
Vertical Tail	✓	✓	✓	✓	✓	✓
Wing Tips	○ (Wing data)	○ (Wing data)	○ (Wing data)	○ (Wing data)	○ (Wing data)	○ (Wing data)

✓ Acceptable Data × No Data ○ Limited Data

Table 38. Available mid-air collision severity levels for business jet aircraft. Data from (Olivares et al., 2020; Olivares, Gomez, et al., 2017; Olivares, Lacy, et al., 2017).

Business Jet	Q4	Q25	Q55	FW4	FW25	FW55
Nose	✓	✓	✓	✓	✓	✓
Windshield	✓	✓	✓	✓	✓	✓
Fuselage	×	×	×	×	×	×
Wings	✓	✓	✓	✓	✓	✓
Engines	×	×	×	×	×	×
Horizontal Tail	✓	✓	✓	✓	✓	✓
Vertical Tail	✓	✓	✓	✓	✓	✓
Wing Tips	○ (Wing data)	○ (Wing data)	○ (Wing data)	○ (Wing data)	○ (Wing data)	○ (Wing data)

✓ Acceptable Data × No Data ○ Limited Data

Table 39. Available mid-air collision severity levels for general aviation single-engine aircraft. Data from (Olivares, Gomez, & Marco, 2022; Olivares et al., 2021).

GA Single Engine	Q4	Q25	Q55	FW4	FW25	FW55
Nose	×	×	×	×	×	×
Windshield	✓	✓	✓	✓	✓	✓
Fuselage	×	×	×	×	×	×
Wings	✓	✓	✓	✓	✓	✓
Propeller	○ (Same severity levels)	○ (Same severity levels)	○ (Same severity levels)	○ (Same severity levels)	○ (Same severity levels)	○ (Same severity levels)
Horizontal Tail	✓	✓	✓	✓	✓	✓
Vertical Tail	✓	✓	✓	✓	✓	✓
Landing Gear	×	×	×	×	×	×

✓ Acceptable Data × No data ○ Limited Data

Table 40. Available mid-air collision severity levels for rotorcraft. Data from (Olivares, Gomez, Marco, et al., 2022).

Rotorcraft	Q4	Q25	Q55	FW4	FW25	FW55
Nose	×	×	×	×	×	×
Windshield	✓	×	×	✓	×	×
Fuselage	×	×	×	×	×	×
Rotor blades	○ (Same severity levels)	×	×	○ (Same severity levels)	×	×
Engine/Cowling	✓	×	×	✓	×	×
Horizontal Tail	✓	×	×	✓	×	×
Vertical Tail	○ (Rear servo only)	×	×	○ (Rear servo only)	×	×
Landing Gear	×	×	×	×	×	×
Tail Boom	×	×	×	×	×	×

✓ Acceptable Data × No data ○ Limited Data

Olivares et al. (2020; 2022; 2021; 2017) analyzed a total of four manned aircraft models and six sUAS architectures. Impacts between the sUAS and manned aircraft are aligned along the global longitudinal axis for a head-on collision at five different aircraft locations (for each manned aircraft model). Table 41 and Table 42 summarize the total number of impact conditions analyzed per manned aircraft part.

Table 41. MAC analysis data points between manned fixed-wing aircraft and sUAS.

Aircraft \ Part	Vertical Stabilizer	Horizontal Stabilizer	Wing	Windshield	Nosecone	Propeller
Commercial Transport	27	27	27	26	18	-
Business Jet	28	28	28	27	18	-
General Aviation	24	24	56	26	-	24

Table 42. MAC analysis data points between rotorcraft and sUAS.

Aircraft \ Part	Front Cowling	Horizontal Stabilizer	Rear Servo	Windshield	Rotorblades
Rotorcraft	7	6	6	7	6

Table 43 illustrates an example of the results of the single-engine general aviation damage assessment study on different parts of the aircraft. The information collected to develop the interpolation functions includes:

- Manned aircraft part
- Impact speed
- sUAS mass and type
- Severity level.

Table 43. GQ2.7 airborne collision simulation assessment – damage severity levels (Olivares, Gomez, & Marco, 2022).

	GA Aircraft and Quadcopter 2.7 lb. Impact (GQ2.7)																			
	H-Stab			V-Stab			Wing Locations 1, 2 and 3									Windshield			Propeller		
Case	GQ2.7-H1T	GQ2.7-H1H	GQ2.7-H1C	GQ2.7-V1T	GQ2.7-V1H	GQ2.7-V1C	GQ2.7-W1T	GQ2.7-W1H	GQ2.7-W1C	GQ2.7-W2T	GQ2.7-W2H	GQ2.7-W2C	GQ2.7-W3T	GQ2.7-W3H	GQ2.7-W3C	GQ2.7-C1T	GQ2.7-C1H	GQ2.7-C1C	GQ2.7-P1T	GQ2.7-P1H	GQ2.7-P1C
Severity	Level 2	Level 2	Level 3	Level 2	Level 3	Level 3	Level 3	Level 3	Level 3	Level 2	Level 2	Level 4	Level2	Level 3	Level 3	Level 4	Level 4	Level 4	Level 1	Level 1	Level 1

In some cases, such as the propeller shown in Table 43, the severity is level one in all three impact conditions, regardless of the impact speed. This is also the case for other sUAS architectures and speed combinations with the propeller. As noted in Table 34, a severity approximation function cannot be developed in this case. Therefore, MACs with these parts were not assessed in the present research. Moreover, some aircraft parts had multiple impact locations within the same part, such as the manned aircraft wing. These data points were grouped during the development of the approximation function to reduce the complexity. This approach increases data scatter but significantly simplifies the MAC severity evaluation. As a result, the approximations function does not distinguish between different impact location within the same manned aircraft part, for instance, an impact with the wing tip vs an impact with the wing root. It is also evident that additional severity assessment studies have to be conducted for a full envelope of all MACs observed. However, these studies are out of the scope of this research.

The research team attempted to define a severity level as a function of variables representative of a MAC event. These variables can then be expressed as a set of dependent variables. The dependent variables considered for this study are:

- sUAS architecture (fixed-wing and quadcopter)
- sUAS mass (i.e., 4 lb, 25 lb, 55 lb.)
- sUAS and manned aircraft heading angle
- Impact speed

- Manned aircraft type (i.e., commercial transport, business jet, rotorcraft, general aviation)
- Impact location on the manned aircraft (i.e., as shown in Table 37 through Table 40)

However, having each parameter as a variable increased the functions' complexity and reduced accuracy. As a result, the methodology was adjusted to simplify all dependent variables into one; impact kinetic energy. Figure 95. illustrates the process of combining and simplifying the independent variables to produce the approximation functions. The impact kinetic energy also allows the function to be easily applied to all MAC cases regardless of orientation and type of sUAS. The impact kinetic energy for each MAC is calculated based on the relative speed and mass of the sUAS, as shown in Eq (21).

$$Impact\ K.E. = \frac{1}{2}(mass_{sUAS}) * (relative\ speed)^2 \tag{21}$$

Where relative speed is calculated by Eq (22):

$$relative\ speed = (speed_{Manned\ Aircraft}) - (speed_{sUAS} * \cos(heading_{sUAS} - heading_{Manned\ aircraft})) \tag{22}$$

Multiple second-order polynomials were created with the available data points for each manned aircraft location. Figure 96 and Figure 97 are examples of the second-order approximation functions for the commercial transport horizontal tail and business jet vertical tail, respectively. All the severity approximation functions developed in this study are documented in Appendix B. A summary of the available functions is shown in Table 44.

Overall, the approximation functions provide a conservative severity level estimate and do not distinguish between a head-on collision and a collision with different heading angles (if both cases have the same relative impact speed). The following section presents a methodology to scale the impact kinetic energy to address this limitation.

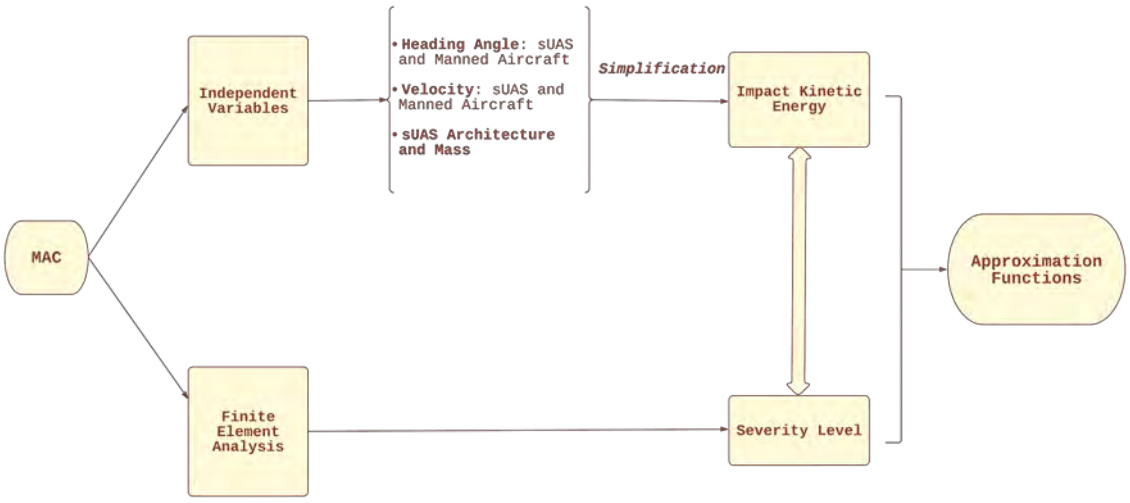

Figure 95. Process flowchart to produce approximation functions.

Table 44. Severity approximation functions developed in this study.

	Commercial	Business Jet	GA Single-Engine	Rotorcraft
Nose	✓	✓	×	×
Windshield	✓	✓	✓	✓
Fuselage	×	×	×	×
Wing / Rotor blades	✓	✓	✓	×
Engine / Cowling / Propeller	×	×	×	✓
Horizontal Tail	✓	✓	✓	✓
Vertical Tail	✓	✓	✓	✓
Landing Gear	NA	NA	×	×
Tail Boom	NA	NA	NA	×

✓ Available function × No Function

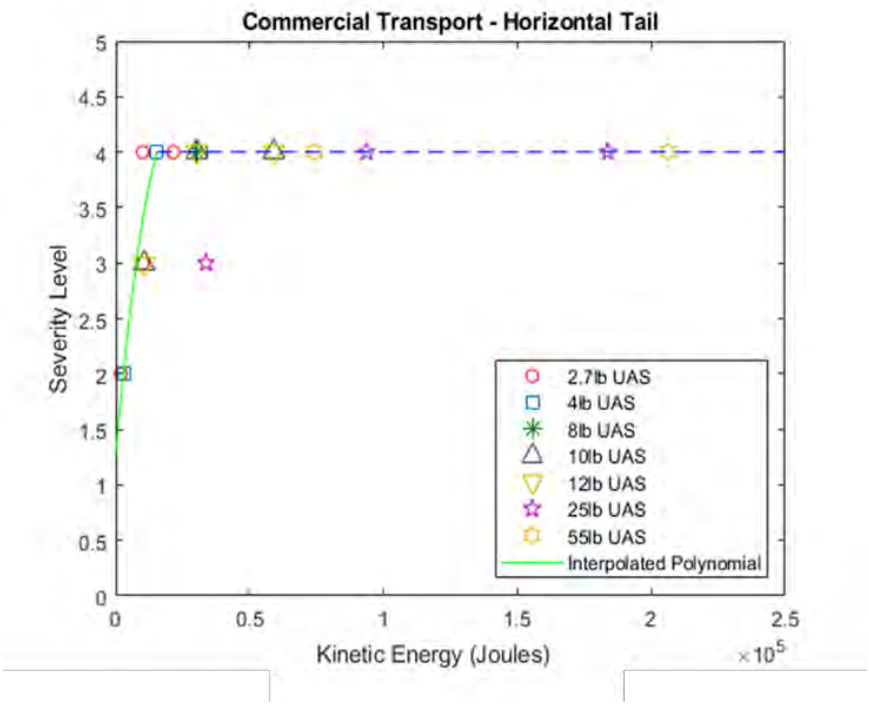

Figure 96. Approximation function – Commercial transport horizontal tail.

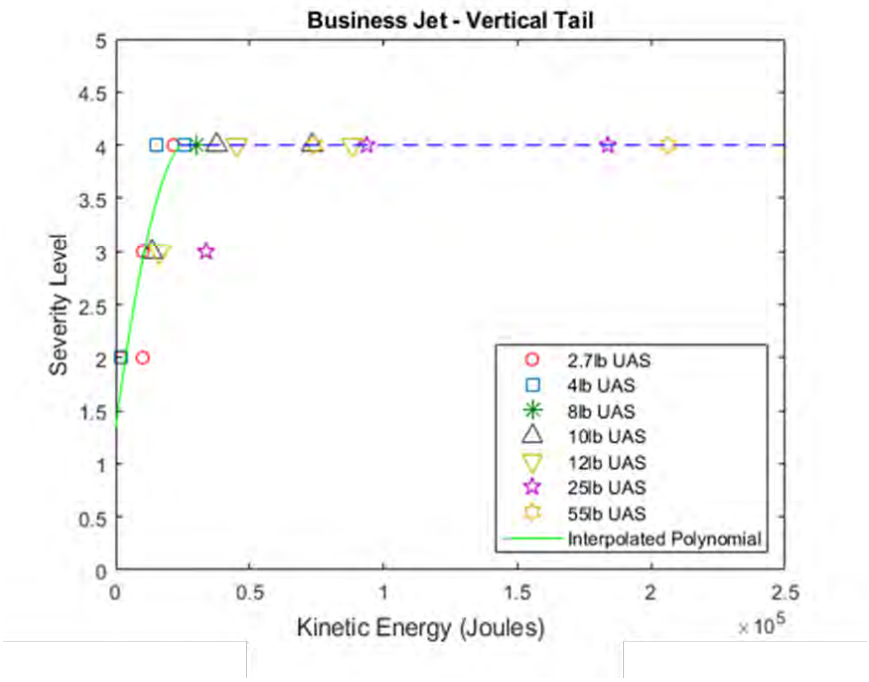

Figure 97. Approximation function – Business jet vertical tail.

5.3 Energy Scale Factor

The relationship between impact kinetic energy and severity levels was discussed in Section 5.2. This relationship was derived from previous studies that aimed to estimate mid-air collision severity levels for sUAS and manned aircraft (Olivares et al., 2020; 2022; 2021; 2017). For the present research, the MAC cases recorded from Sections 3.3 and 4.4 need to be evaluated using the approximation functions developed in Section 5.2.

The severity level is a function of impact kinetic energy. Each manned aircraft impact location has an appropriate approximation function. However, these equations were derived from worst-case condition data. The worst-case condition occurs when the sUAS and the manned aircraft are perfectly aligned for a head-on collision, as shown in Figure 98. The functions provide overly conservative severity estimates for non-head-on MACs. Therefore, an energy scale factor was devised to adjust the severity based on the relative orientation of each MAC.

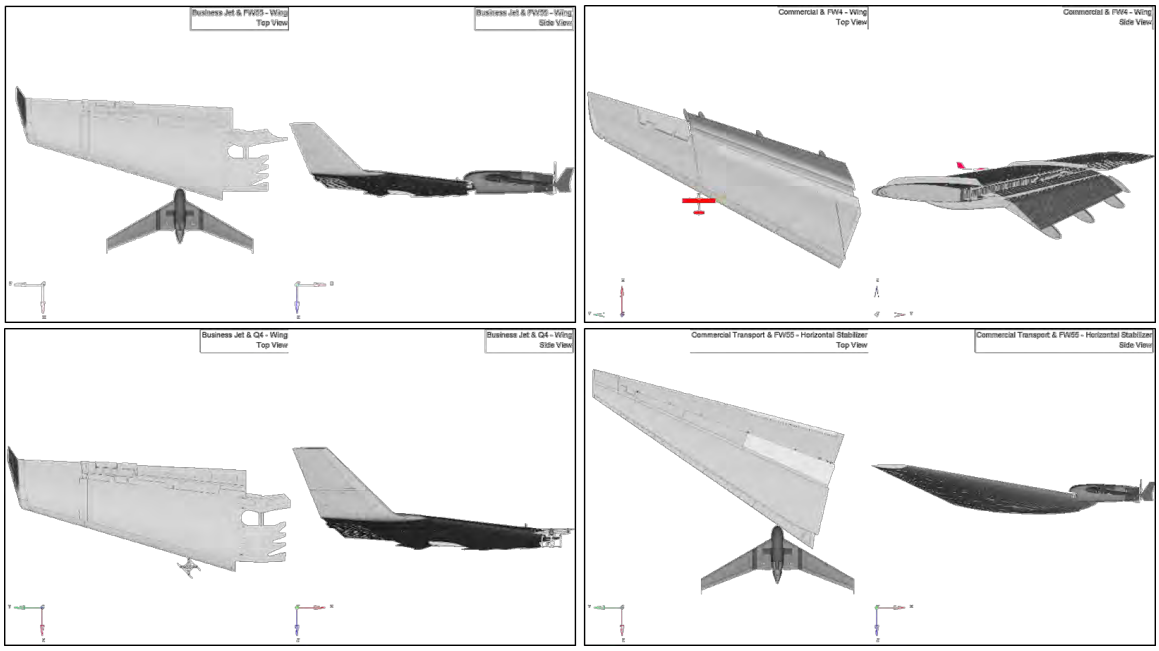

Figure 98. Head-on collision configuration (Olivares et al., 2020).

5.3.1 *Energy Reduction as a function of sUAS Position and Heading*

The previous section introduced the challenges faced when using worst-case condition MAC risk studies to assess the severity of the MACs recorded in Sections 3.3 and 4.4. For worst-case conditions, most of the impacting energy is transferred to the manned aircraft, depending on the sUAS geometric features. Olivares, Gomez, et al. (2017) conducted a parametric study to determine the effects of impact location (vertical offset) and sUAS orientation (yaw only). They determined that slight offsets in the vertical position resulted in no penetration of sUAS components into the wing. The yaw study revealed that a 45deg yaw resulted in more damage than the other cases. Olivares, Gomez, et al. (2017) explained that this is the effect of having three masses (two motors and the battery) aligned in the impact direction, increasing the concentrated loads on the manned aircraft. However, the parametric study was limited to only a few conditions and does not encompass the wide range of impact conditions discussed in Section 5.1.1.

For example, a business jet and a commercial transport MAC recorded in Section 3.3 are shown in Figure 99 and Figure 100, respectively. In both scenarios, the MAC is not head-on. The sUAS have different orientations, and only a portion of the sUAS's mass collides with the manned aircraft. This will result in reduced impact energy transferred to the manned aircraft and, by extension, a reduced severity.

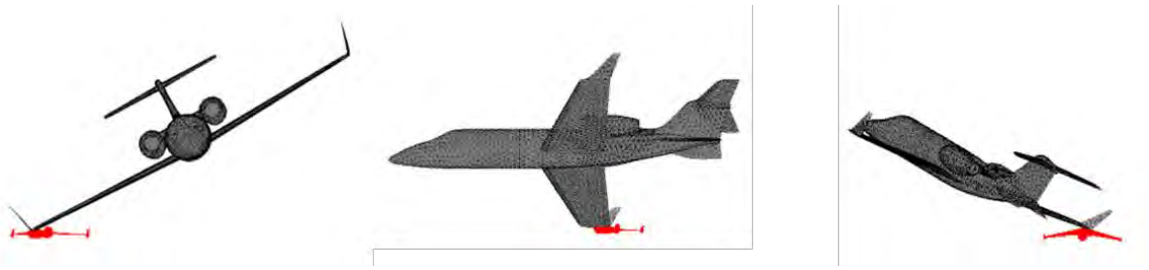

Figure 99. Business jet and fixed-wing 55 lb. mid-air collision case.

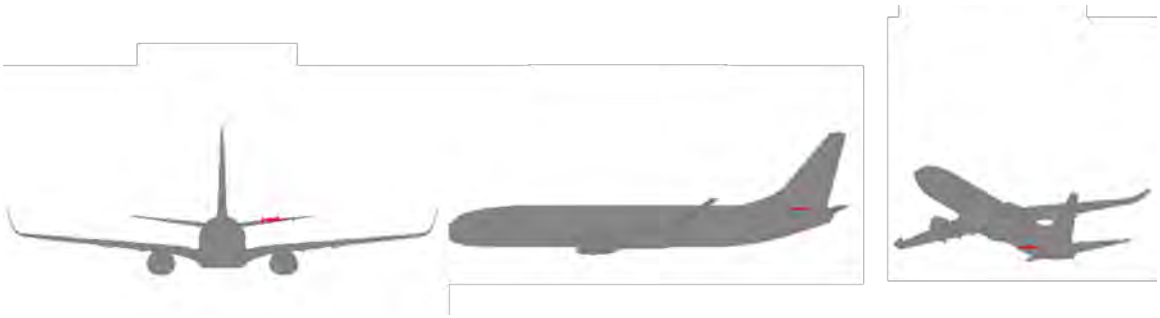

Figure 100. Commercial transport and fixed-wing 25 lb. mid-air collision case.

To overcome this challenge, a methodology to reduce the impact energy of each MAC based on its relative orientation was developed. This methodology consists of estimating a factor to scale or reduce the impact energy. The estimated factor encompasses the position and orientation of the sUAS relative to the manned aircraft; the closer it is to a head-on orientation, the higher the scale factor is. In this manner, the impact kinetic energy is recalculated for each MAC. The severity level is then estimated with the recalculated impact energy and the approximation functions presented in Section 5.2. Eq.(23) is used to recalculate kinetic energy at the time of impact.

$$KE_1 = c * KE_0 \tag{23}$$

$$KE_0 = \frac{1}{2} m * v^2 \tag{24}$$

Where c is the scale factor, v is the relative impact speed, and m is the mass of the sUAS. Eq. (24) is the classic method to calculate the kinetic energy of a moving object.

5.3.2 *Machine Learning Approach*

This part of the research employs a machine learning approach to estimate scale factors that are used to modify the impact kinetic energy of each MAC. Over 20,000 unmitigated and mitigated MACs were recorded in Sections 3.3 and 4.4. Manually assigning an energy scale factor to every

MAC would be extremely time-consuming. However, a machine learning algorithm can leverage a small known dataset and make predictions at a large scale for all MACs.

This research features a *Random Forest Regression* algorithm, a supervised machine learning approach (Dutta, 2022). A random forest is an ensemble technique that performs decisions based on the aggregated decision of multiple decision trees (Pedregosa et al., 2011). This specific technique is capable of performing regression or classification tasks through an open-source package, *scikit-learn,* in Python (Pedregosa et al., 2011).

Pedregosa et al. (2011) state that a random forest regressor is an estimator that fits multiple classifying decision trees on various sub-samples of the main dataset. This technique is called *Bootstrap*, where row sampling is randomly performed from the main dataset to form sample datasets or sub-samples. Each sub-sample is then used to form multiple decision trees as base learning models. Figure 101 illustrates the basic logic of how a random forest regressor operates.

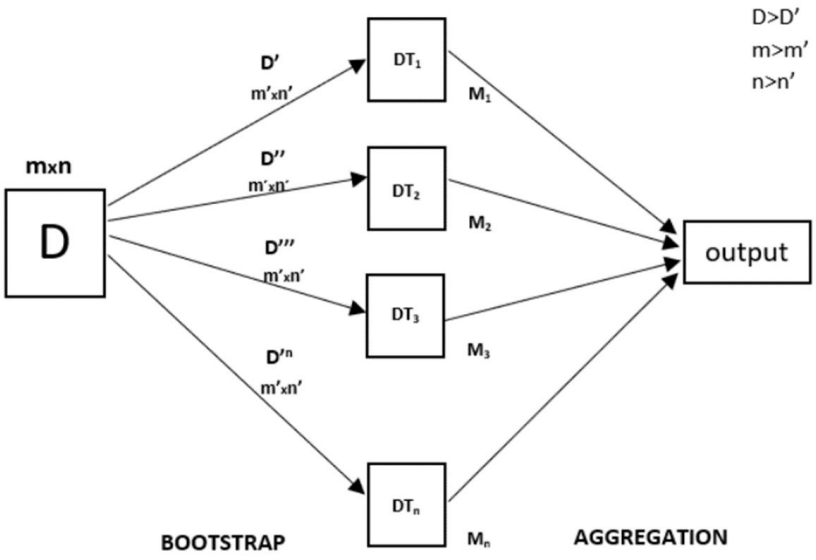

Figure 101. Random forest regression diagram logic, adapted from Dutta (2022).

In Figure 101, the main data set or "training data" is shown in block *D* of size *mxn*; subsamples of this main dataset are then created and labeled as DT_i. The number of subsamples created is user-defined, and each one outputs a decision block. Once a decision in each tree has been made, an *Aggregation* technique is then performed. This technique outputs a final decision or prediction on the main dataset. The technique uses averaging to improve accuracy and control data over-fitting.

Figure 99 and Figure 100 illustrate MAC cases where the sUAS and manned aircraft fly at different speeds and orientations. From the MAC detection analysis, the following information was recorded at the time of the collision between the sUAS and manned aircraft.

- Horizontal and vertical position
  - *x,y,x*
- Attitude Angles
  - Roll, φ
  - Pich, θ
  - Yaw (heading), Ψ

As illustrated in Figure 102, the information recorded for each vehicle serves as inputs for the random forest. Each MAC was identified with an ID, and variables such as *x-position*, *y-position*, *z-altitude*, and *heading-angle* were used to collectively define a relationship with the scale factor. The training dataset consists of ~100 MAC cases with known scale factors to build all the decision trees in the random forest. The relative variables, shown in Figure 102, are calculated using Eq (25), where *Var* can be any "variable" listed above.

$$Var_{rel} = Var_{sUAS} - Var_{Manned\ aircraft} \tag{25}$$

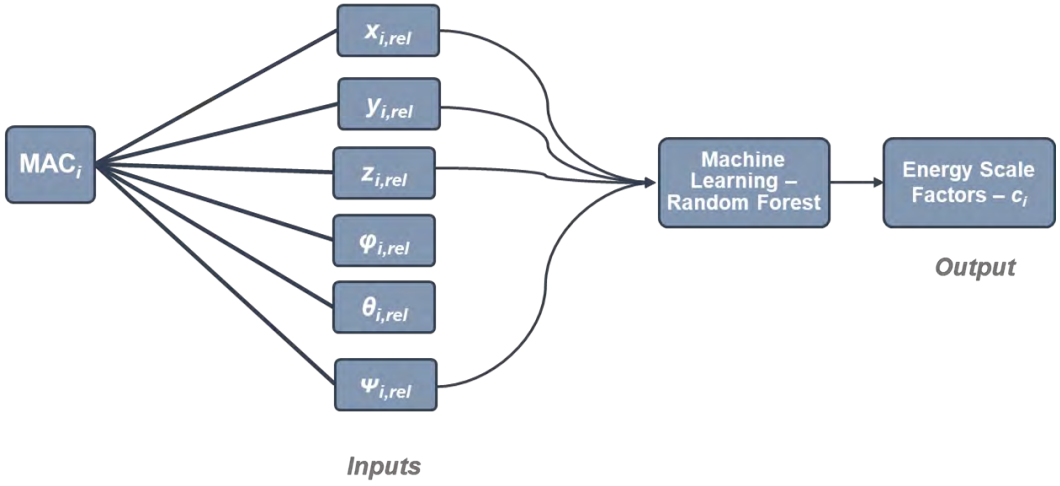

Figure 102. Input-Output schematic of the random forest model.

The training data had to be assigned "true" scale factors. These were manually assigned by visually analyzing every MAC case based on the qualitative judgement of the researchers. This step of the process is subject to human interpretation of how close each MAC is to a worse-case condition MAC. This analysis did not consider the relative roll and pitch angles for simplification purposes. The addition of these variables into the random forest resulted in the need for a larger training dataset and reduced the accuracy of the predictions.

Once the algorithm is trained, the patterns and behavior within the training data (main data set) are learned. The algorithm can then be used to predict other MACs that share similar patterns. A test dataset was also defined in the same manner as the training dataset to test the accuracy of the predictions. The accuracy is measured by calculating the root mean square error of all predictions from true data. Figure 103 illustrates a comparison of the "true" assigned scale factors to the predicted scale factors using the random forest regression algorithm. The test dataset was not previously exposed to the algorithm in this scenario.

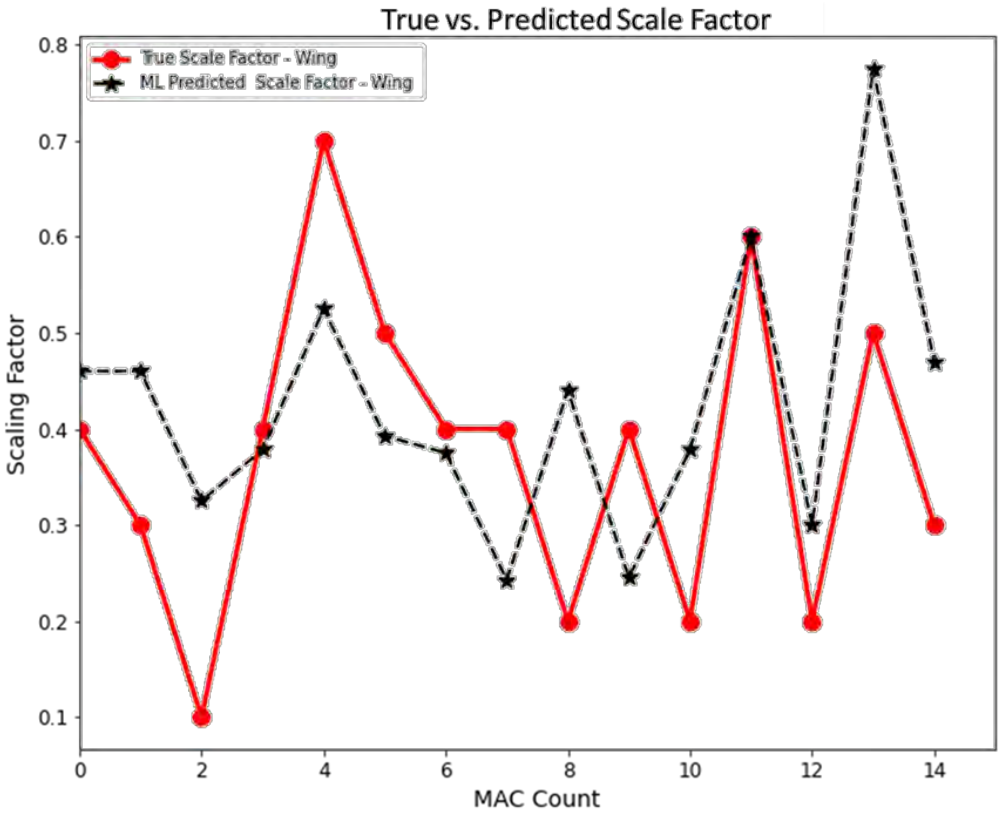

Figure 103. Comparison of scaled factor predictions to true factor assignments.

Once scale factors are assigned to the entire MAC dataset, the kinetic energy can be re-calculated using Eq.(23). Additionally, a new "scaled" estimated severity level can be computed using the approximation functions presented in Section 5.2. This value is now also a function of the sUAS conditions relative to the manned aircraft.

Lastly, to assess the effects of the scale factors, Figure 104 and Figure 105 illustrate a comparison of severity level vs. unscaled energy on a set of MACs for the commercial transport horizontal stabilizer and wing, respectively. The plots help understand the effects of the scale factor on the severity approximation.

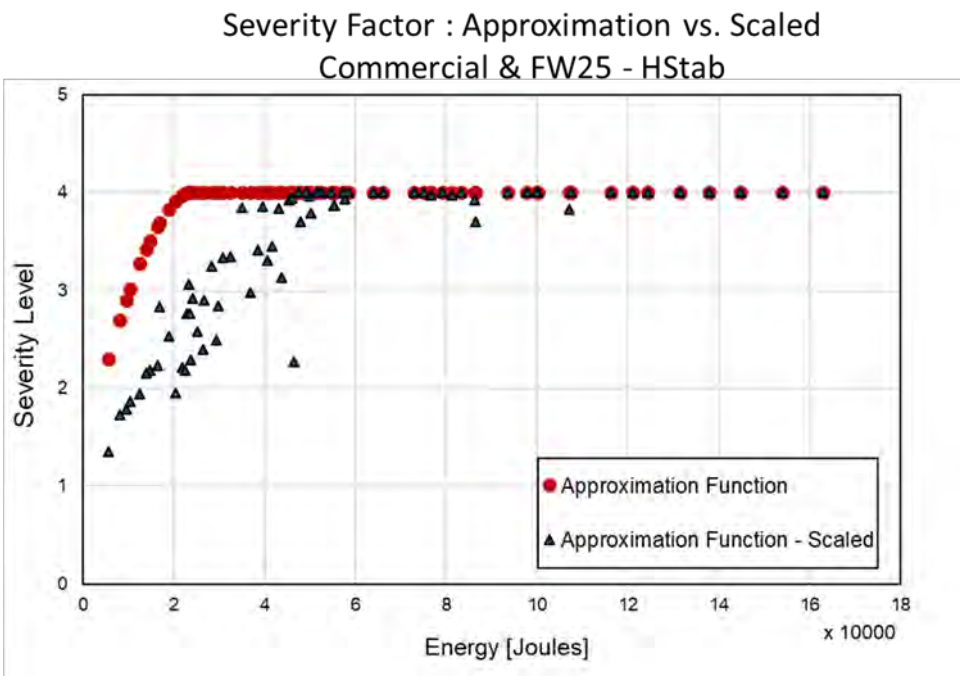

Figure 104. Severity level vs. unscaled impact energy on testing data set – Commercial transport horizontal stabilizer and fixed-wing 25lb. sUAS.

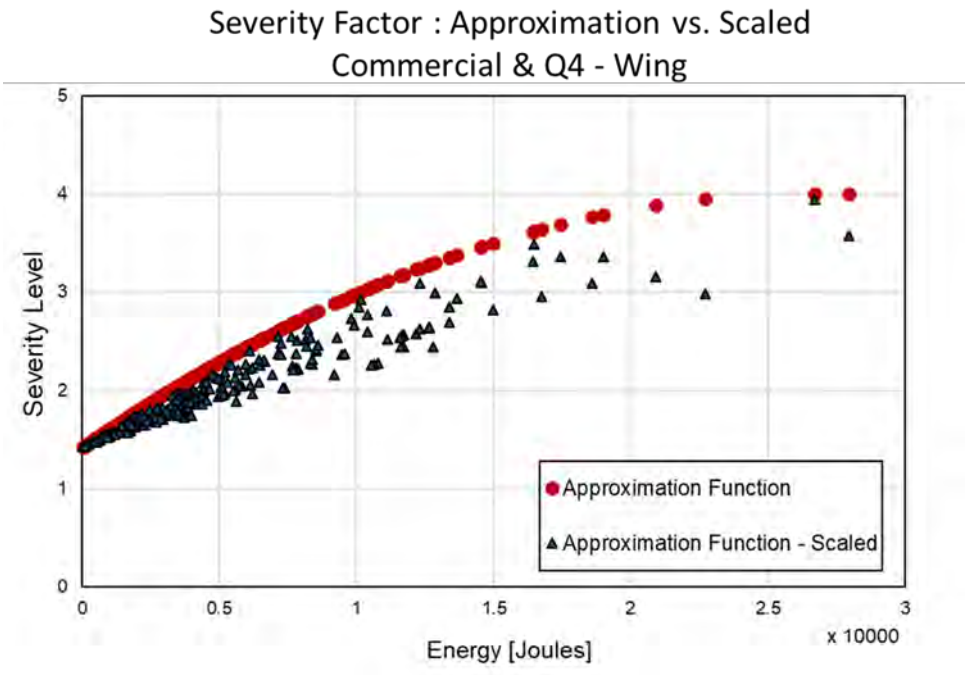

Figure 105. Severity level vs. unscaled impact energy on testing data set – Commercial transport wings and quadcopter 4lb. sUAS.

This section has presented the conditions and limitations of using the MAC assessments from previous research projects (Olivares et al., 2020; 2022; 2021; 2017). These damage assessments are a function of MAC conditions which produce only worst-case outcomes. However, the MAC data obtained in the present research is not limited to only worst-case conditions. Therefore, a methodology to adapt data from previous research was developed. The approach consists of predicting energy scale factors as a function of patterns and behaviors of individual MACs through a supervised machine learning algorithm. Individual MAC patterns and behaviors with a known output were fed into the algorithm to be learned and later used on predictions of similar MAC conditions. Figure 106 presents a step-by-step flowchart needed to train the random forest algorithm successfully. Several cases were further analyzed using FEA to assess the overall effectiveness and accuracy of the algorithm. The results are discussed in the next section.

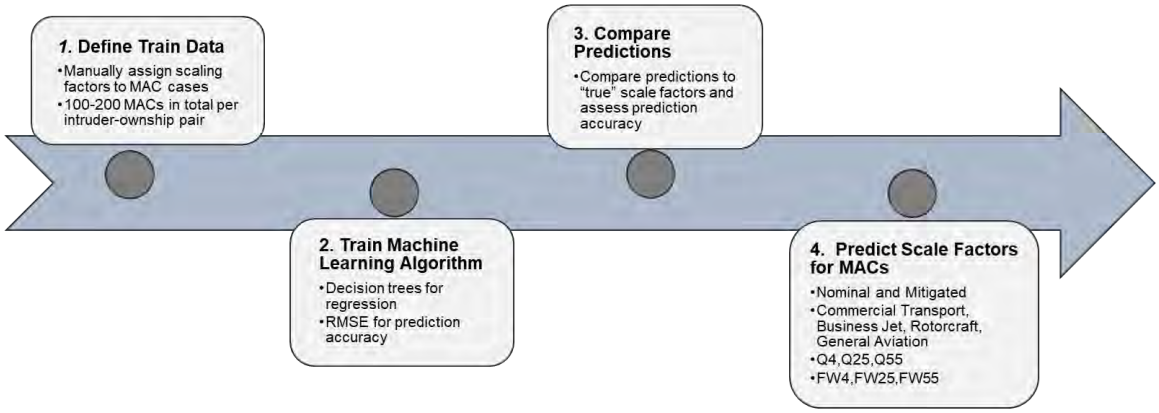

Figure 106. Flowchart of developed methodology to predict energy scale factors.

5.4 FEA vs. Approximation Functions

This section compares select MAC cases subjected to a severity assessment through FEA. The methodologies and models previously developed by Olivares, Gomez, et al. (2017) were used for this assessment. This analysis provides a physics-based severity assessment of the selected MAC cases.

The MAC cases were selected to test the validity of the severity approximation functions and scale factors calculated from Sections 5.2 and 5.3. Figure 107 shows an example MAC case that was used for this comparison. The manned aircraft's horizontal stabilizer collides with the right wing of the sUAS. The approximation functions from Section 5.2 assume that this is a "head-on" collision, which results in an overestimated severity level of 3.7.

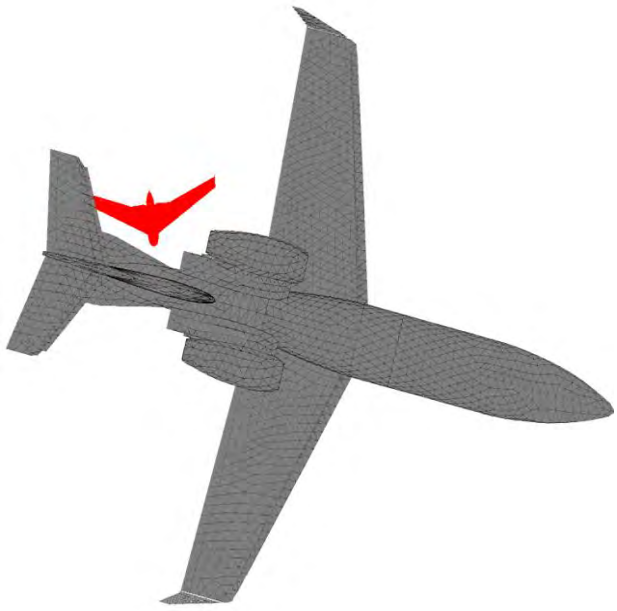

Figure 107. Selected MAC case for finite element analysis.

Figure 108 illustrates the FEA kinematic sequence. In the analysis, the manned aircraft's horizontal stabilizer is fixed in space, and the sum of the velocity vectors is applied to the sUAS. Additionally, Figure 109 displays the damage to the horizontal stabilizer of the manned aircraft. Based on Table 36, the severity is assessed as level 2. While the approximation functions from Section 5.2 predict a severity level of 3.7, the severity is adjusted to 2.3 with the addition of the scale factors from Section 5.3, which is in agreement with the FEA results.

Table 45 and Figure 110 summarize all the MAC cases that were analyzed to test the validity of the results. Overall, the approximation functions are overly conservative and result in most MACs being assessed as a level 4. The addition of a scale factor substantially improves the accuracy of the approximation functions, especially for cases that significantly deviate from a "head-on" collision. The 21 MAC cases used in this study are documented in Appendix C.

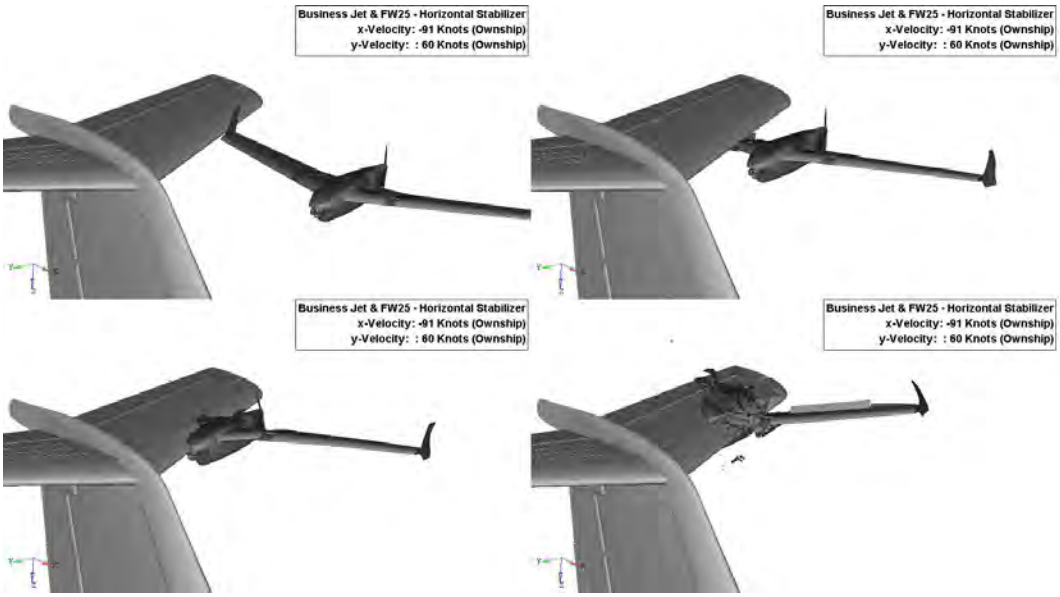

Figure 108. Mid-air collision kinematics sequence – Business jet & FW25.

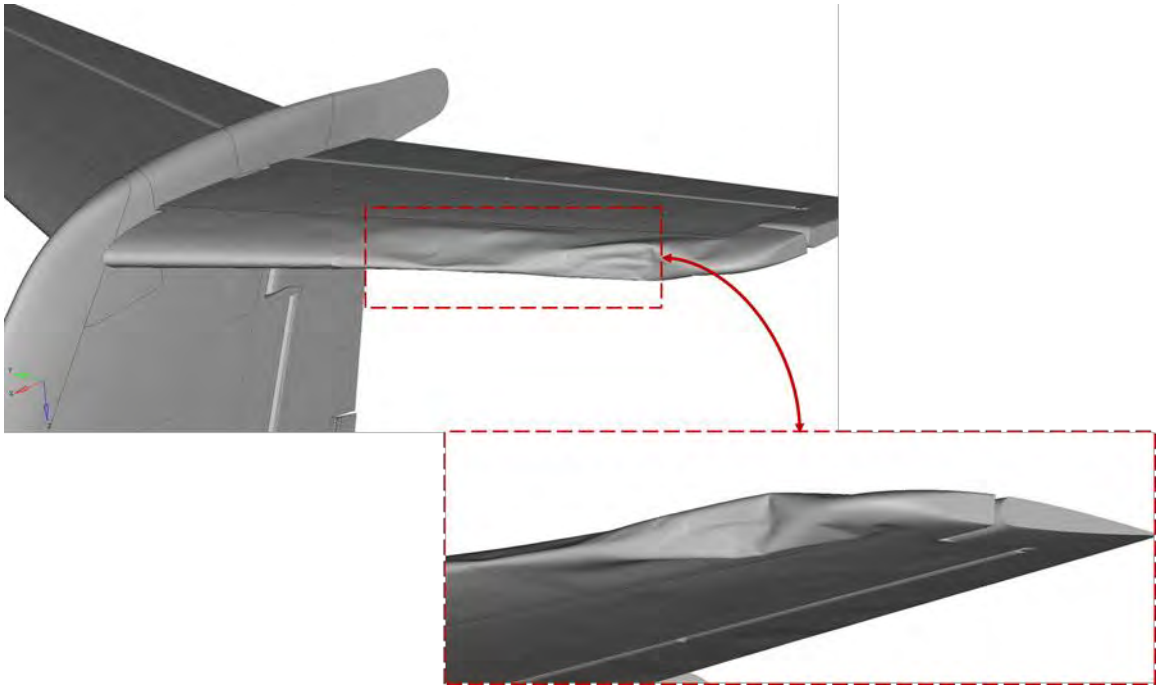

Figure 109. Business jet horizontal stabilizer damage assessment.

Table 45. Severity comparison of select MAC cases – Approximation function vs. FEA.

MAC	Manned Aircraft	sUAS	Manned Aircraft Part	Impact Kinetic Energy [J]	Severity Level [1]	Severity Level [2]	Severity Level [3]
1	GA	Q4	Wing	2.90E+03	4.0	2.0	2.0
2	Business	Q4	Wing	2.40E+04	4.0	2.2	3.0
3	GA	FW55	Wing	2.80E+03	4.0	2.0	2.0
4	Commercial	FW55	Wing	2.20E+05	2.1	1.3	1.0
5	Business	FW55	Wing	2.40E+05	4.0	2.1	3.0
6	Business	FW4	Windshield	2.30E+04	3.5	2.5	3.0
7	Commercial	Q25	Windshield	3.20E+04	3.6	1.9	2.0
8	Commercial	FW4	Horizontal Stabilizer	1.40E+04	3.9	1.9	3.0
9	Business	FW25	Horizontal Stabilizer	1.20E+04	3.7	2.3	2.0
10	Business	FW55	Wing	1.00E+05	4.0	1.5	1.0
11	GA	Q25	Vertical Stabilizer	8.00E+03	4.0	2.4	2.0
12	Commercial	FW25	Nose	5.50E+04	3.8	2.1	2.0
13	Business	FW55	Wings	1.60E+05	4.0	1.9	2.0
14	Business	Q25	Vertical Stabilizer	4.20E+04	4.0	4.0	3.0
15	GA	FW4	Wings	9.30E+03	4.0	4.0	3.0
16	Commercial	FW25	Horizontal Stabilizer	7.30E+04	4.0	4.0	4.0
17	Commercial	FW55	Horizontal Stabilizer	1.25E+04	3.7	1.8	2.0
18	Commercial	FW55	Horizontal Stabilizer	1.21E+05	4.0	4.0	2.0
19	Business	Q4	Wing	1.48E+03	1.4	1.3	1.0
20	Business	Q4	Wing	8.17E+03	2.2	1.5	1.0
21	Business	Q4	Wing	2.40E+04	3.0	1.4	2.0
[1] Approximation Function Prediction – Unscaled				**Average**	3.6	2.3	2.3
[2] Approximation Function Prediction – Scaled				**RMSE**	1.8	0.8	-
[3] Severity Level – FEA Simulation							

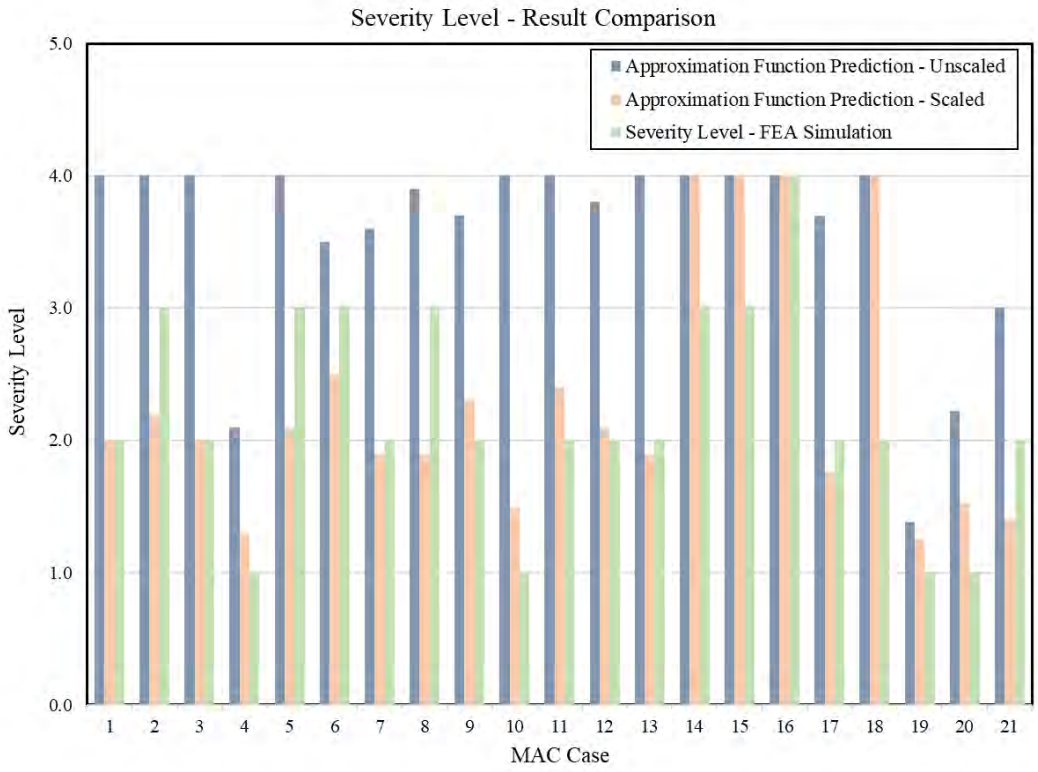

Figure 110. Severity comparison of select MAC cases – Approximation function vs. FEA.

5.5 MAC Severity Estimation (Unmitigated vs. Mitigated)

This section discusses the severity estimation for the unmitigated and mitigated encounters that resulted in a MAC. The section is divided into 4 sub-sections, one for each manned aircraft model.

The severity was estimated using the techniques outlined in Sections 5.2 and 5.3. The results presented in this section include only the scaled severity distributions. Both unscaled and scaled severity scatter plots for unmitigated and mitigated MACs are documented in Appendix A.

The 95% confidence intervals were estimated for the overall aircraft model and each individual manned aircraft location. The unmitigated confidence intervals were estimated using Eq. (26). The mitigated results have a small sample size. In this case, the distribution of both data sets was assumed to be derived from the same population for each impact location. Therefore, the standard deviation of the unmitigated results was used to estimate the mitigated confidence intervals, as shown in Eq. (27).

$$95\ \%\ Confidence\ Interval_{Unmitigated} = \pm \frac{1.96 * Standard\ Deviation_{(Unmitigated)}}{\sqrt{Sample\ Size_{(Unmitigated)}}} \tag{26}$$

$$95\%\ Confidence\ Interval_{Mitigated} = \pm \frac{1.96 * Standard\ Deviation_{(Unmitigated)}}{\sqrt{Sample\ Size_{(Mitigated)}}} \tag{27}$$

5.5.1 *Commercial Transport*

The commercial transport cases are derived from the fixed-wing multi-engine encounter model (1200exclude_fwme). Only cooperative encounters (1200_exclude) were evaluated since all commercial flights are expected to operate with a transponder and/or ADS-B. Only the locations for which a severity function could be approximated were evaluated. Therefore, fuselage and engine MACs were not evaluated.

The average severity level is 2.06 for the aggregated unmitigated cases. The severity distributions for all impact locations are shown in Figure 111 through Figure 117. The highest severity levels were observed in the horizontal stabilizer, with over 60% of the cases equal to severity level 4 for the sUAS greater than 25 lbs. For the mitigated cases, there was only one MAC with the engines, which could not be evaluated.

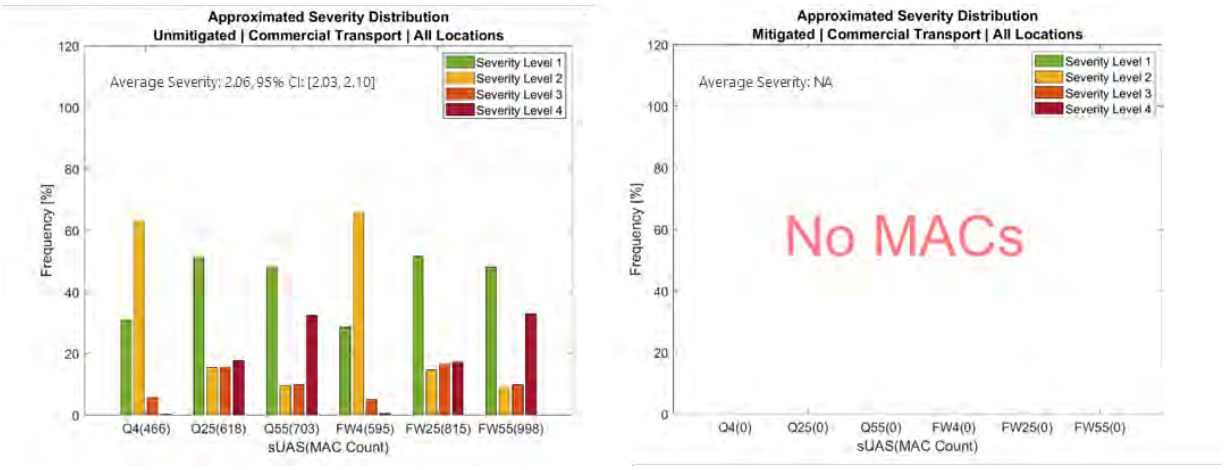

Figure 111. Severity level distribution – Commercial transport & all locations.

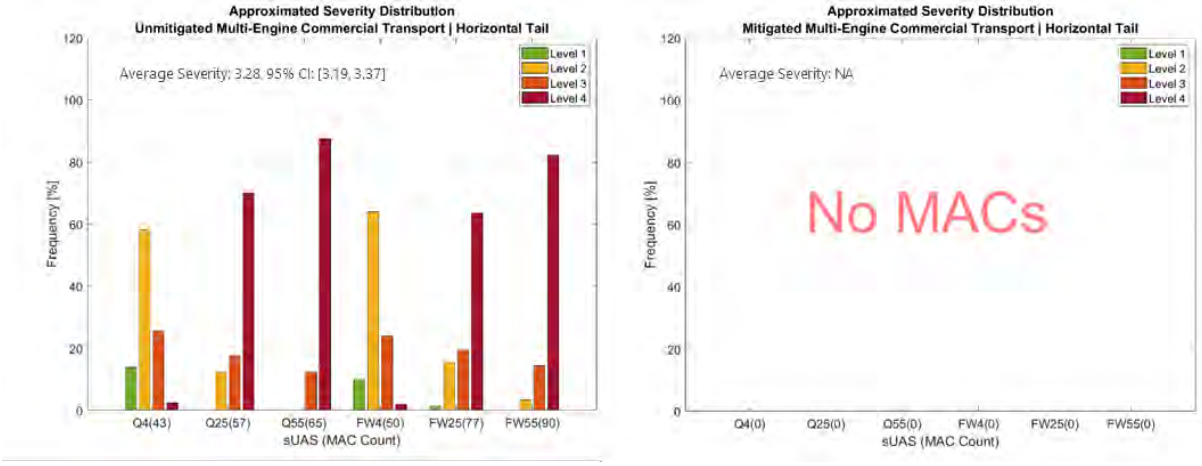

Figure 112. Severity level distribution – Commercial transport & horizontal tail.

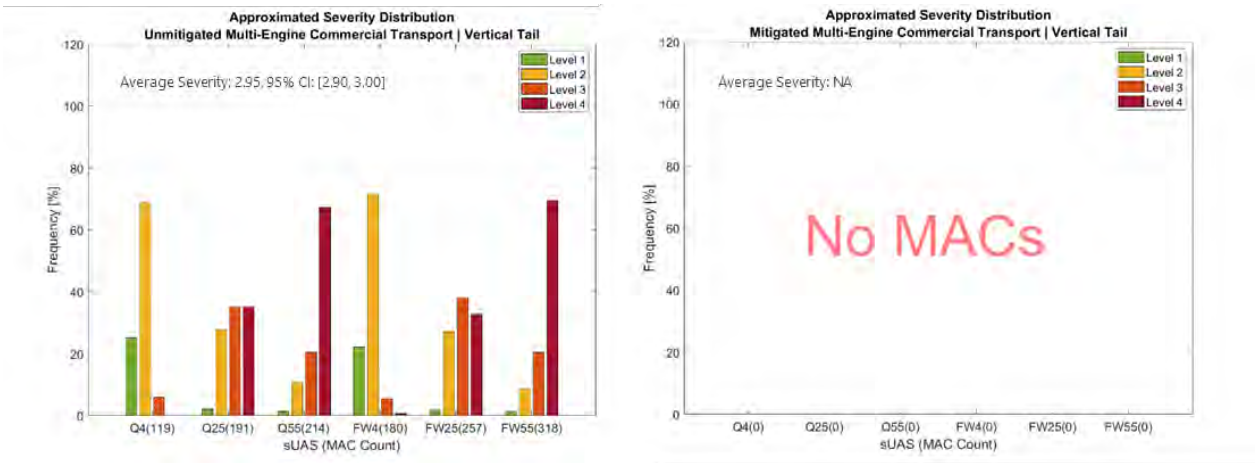

Figure 113. Severity level distribution – Commercial transport & vertical tail.

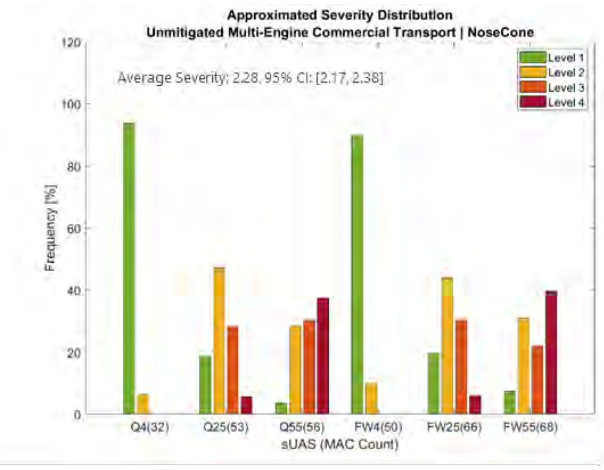

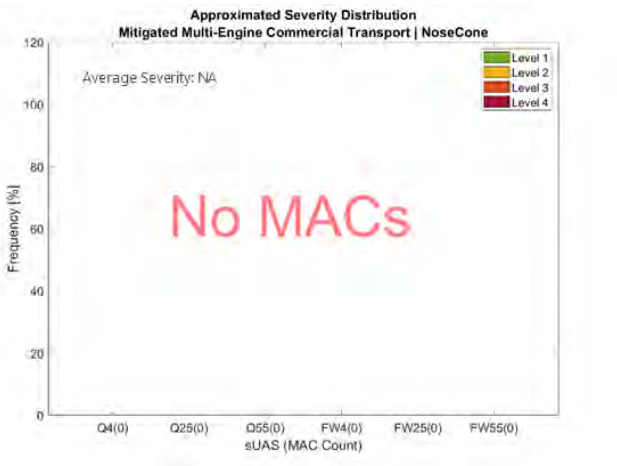

Figure 114. Severity level distribution – Commercial transport & nose cone.

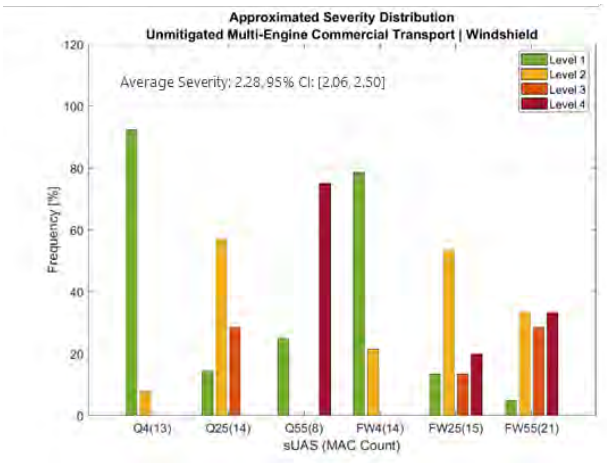

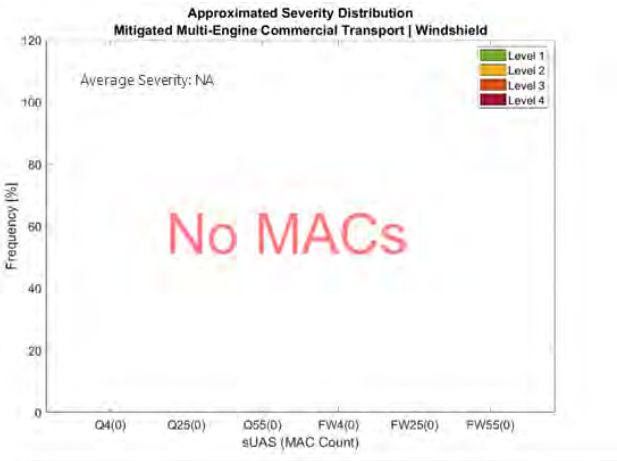

Figure 115. Severity level distribution – Commercial transport & windshield.

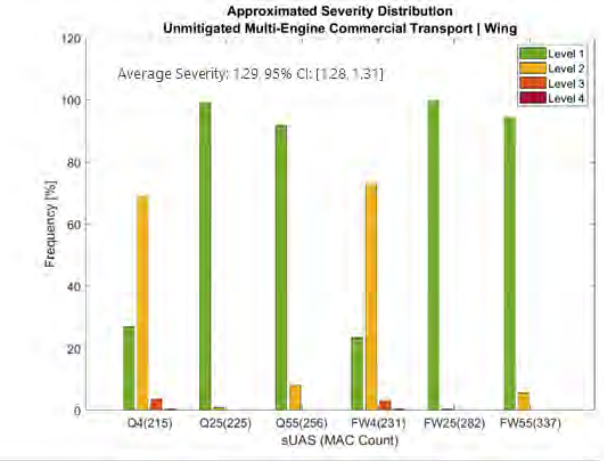

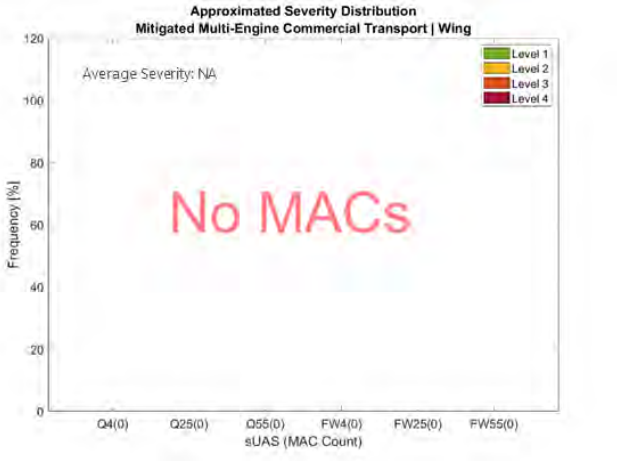

Figure 116. Severity level distribution – Commercial transport & wing.

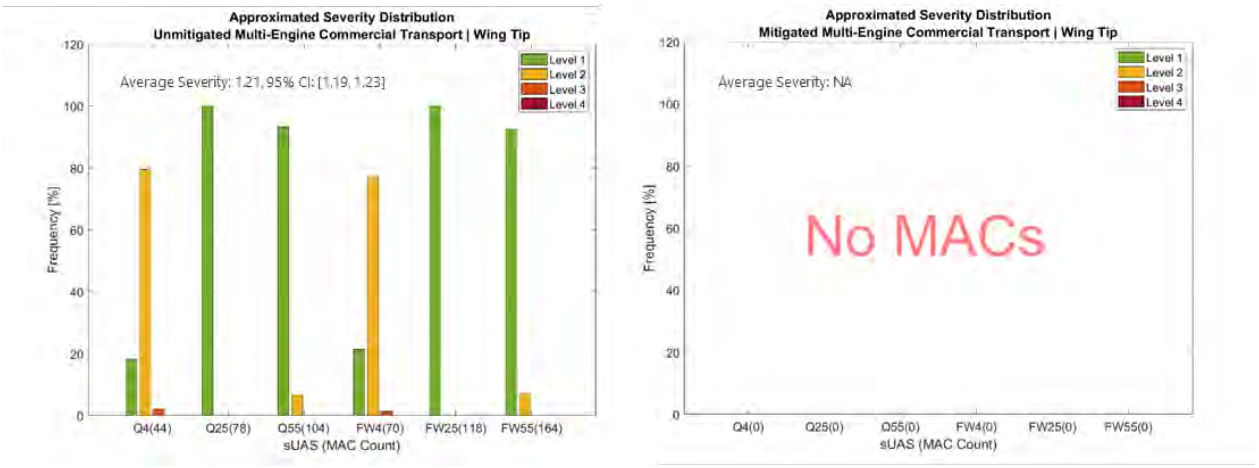

Figure 117. Severity level distribution – Commercial transport & wing tip.

5.5.2 *Business Jet*

The business jet cases are also derived from the fixed-wing multi-engine encounter models. Both cooperative (1200exclude_fwme) and non-cooperative (1200only_fwme) cases were evaluated. Like the commercial transport model, fuselage and engine MACs were not evaluated since severity data was unavailable.

The average aggregated unmitigated severity is 2.06. On the other hand, the average mitigated severity is lower at 1.69. The individual impact location comparisons are shown in Figure 118 through Figure 124. The number of MACs limits the mitigated severity distributions. All locations had less than 5 MACs per sUAS model. This lowers the confidence in the mitigated severity distribution. However, the results still show a severity improvement for unresolved MACs. This is especially highlighted in the wing and wing tip cases, where 98% of the unresolved MACs had a severity equal to one, as shown in Figure 123 and Figure 124. The wing and wing tip cases comprised 56% (40 cases) of all unresolved MACs. As a reminder, all cooperative MACs (1200exclude_fwme) were resolved by ACAS sXu.

The highest unmitigated severity is on the horizontal stabilizer, with 2.84. On the other hand, all the horizontal stabilizer MACs were resolved by ACAS sXu. The highest mitigated severity is on the windshield (3.15), followed by the vertical tail (2.58). However, there were only 2 and 10 cases, respectively, which significantly lowers the confidence in the severity distribution for these impact locations, as indicated by the wide 95% confidence intervals.

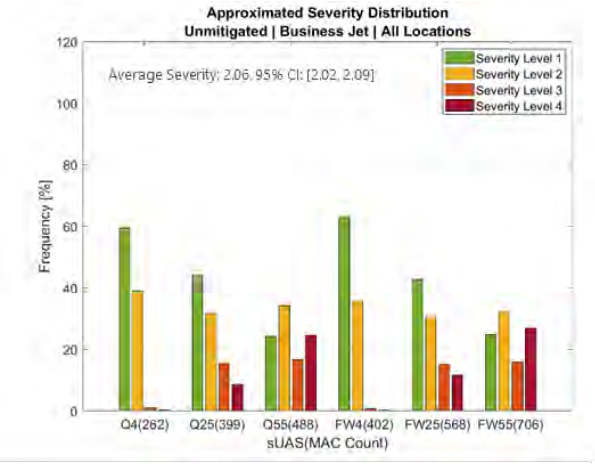

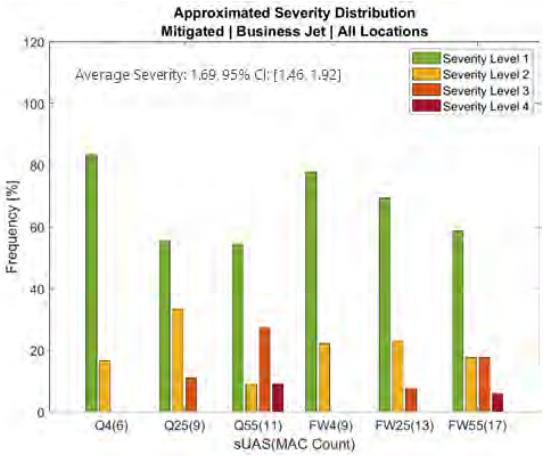

Figure 118. Severity level distribution – Business jet & all locations.

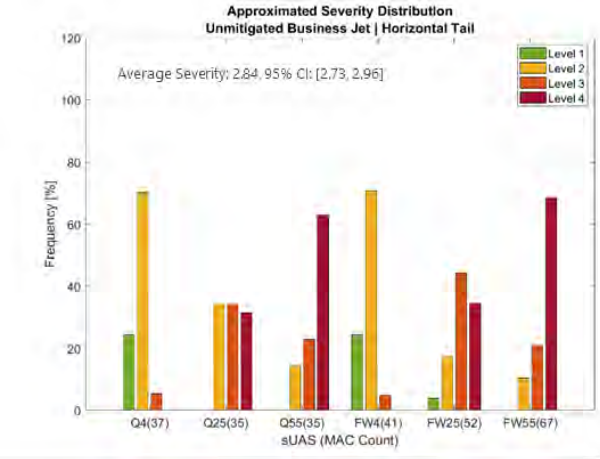

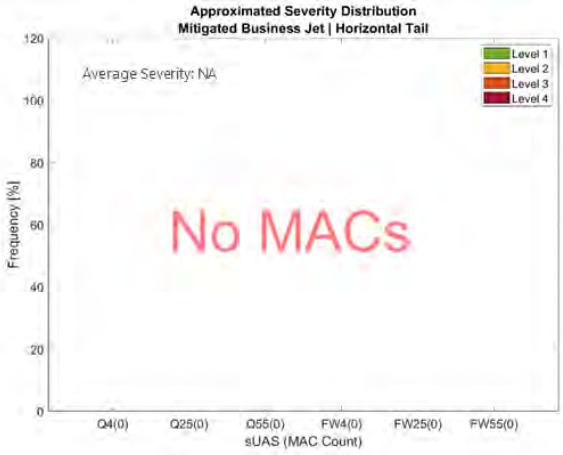

Figure 119. Severity level distribution – Business jet & horizontal tail.

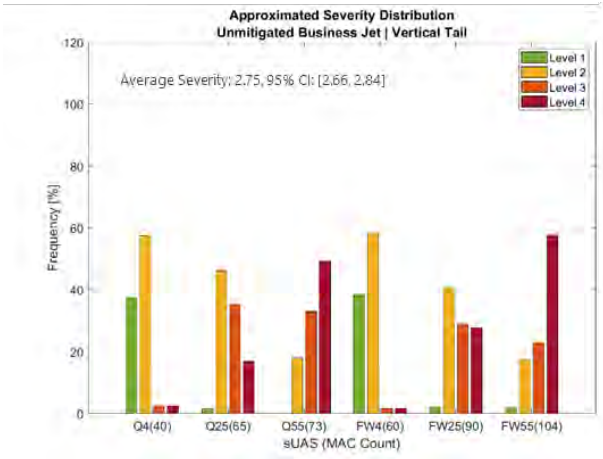

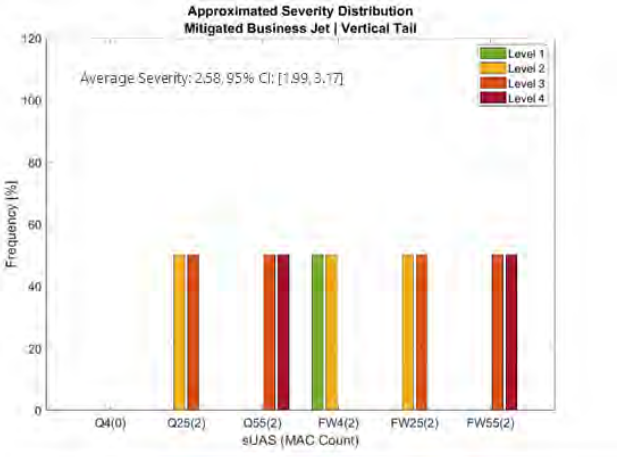

Figure 120. Severity level distribution – Business jet & vertical tail.

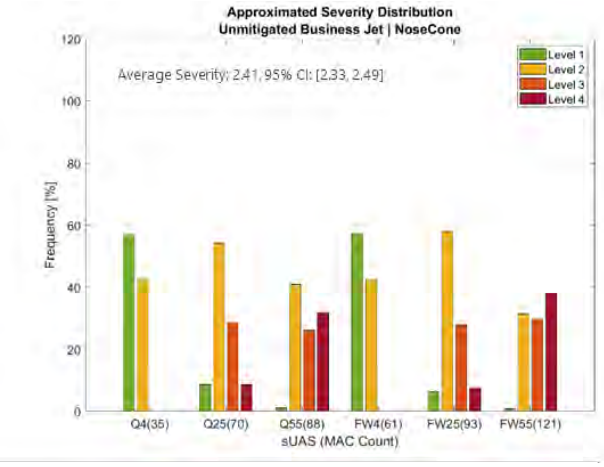

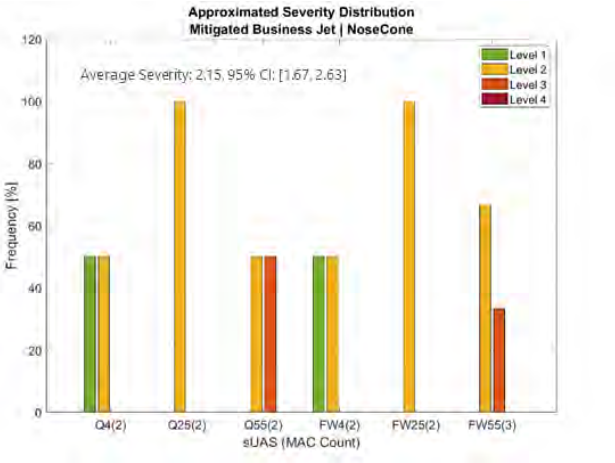

Figure 121. Severity level distribution – Business jet & nose cone.

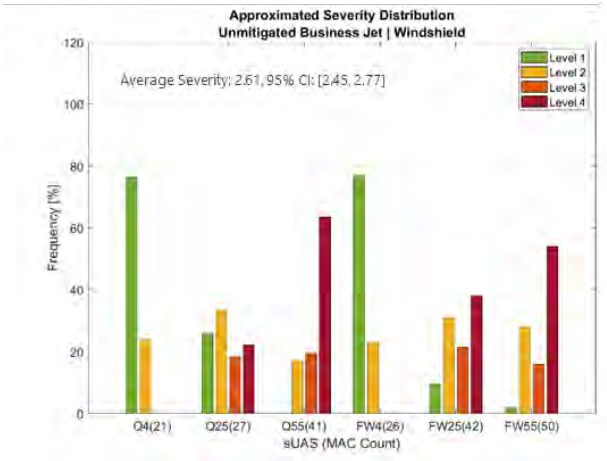

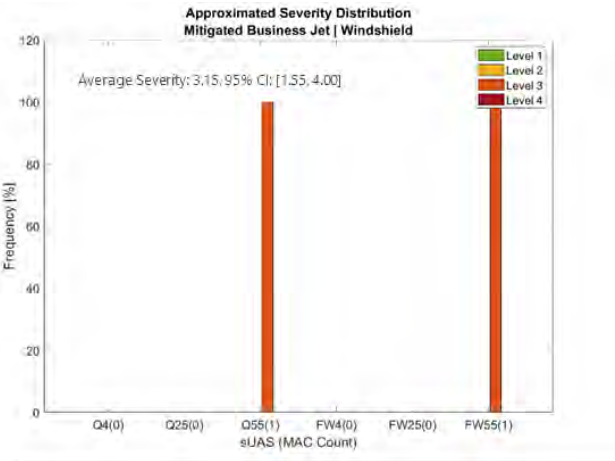

Figure 122. Severity level distribution – Business jet & windshield.

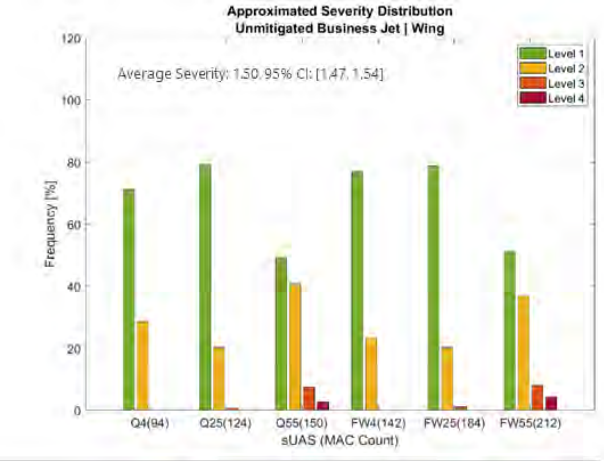

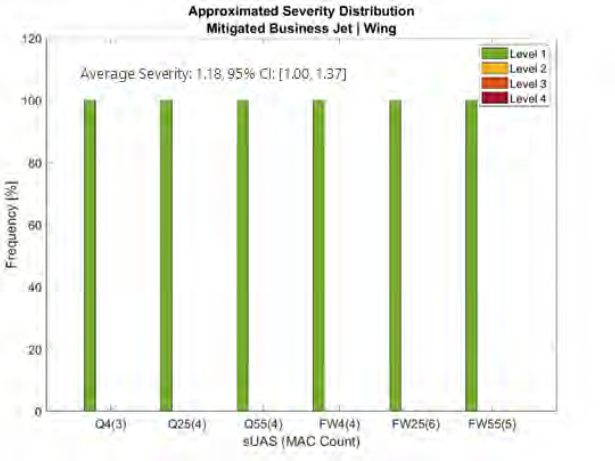

Figure 123. Severity level distribution – Business jet & wing.

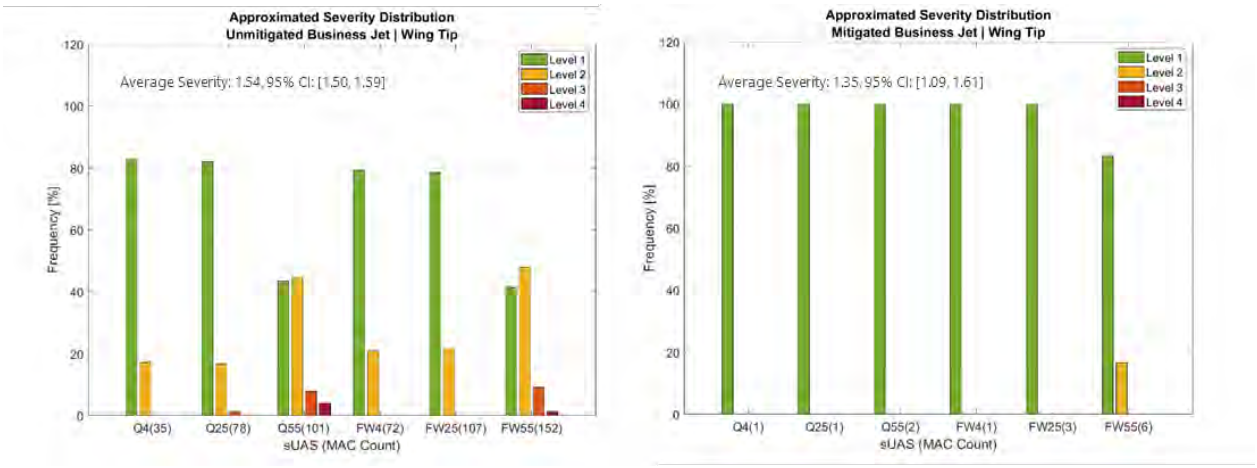

Figure 124. Severity level distribution – Business jet & wing tip.

5.5.3 *General Aviation (Single-Engine)*

The general aviation cases are derived from the fixed-wing single-engine encounter models. Both cooperative (1200exclude_fwse) and non-cooperative (1200only_fwse) cases were evaluated. The fuselage, landing gear, and nose MACs were not evaluated due to a lack of severity data. Similarly, the propeller cases were not evaluated because all the severity data points available are equal to one. This would result in all propeller MACs being estimated as a level one which might not be appropriate for all propeller MACs.

The average aggregated unmitigated severity is 3.31. On the other hand, the average mitigated severity is slightly higher at 3.35. However, only 18 unresolved MACs, which comprise 38% of all unresolved MACs, were evaluated due to the lack of severity data. The comparison between mitigated and unmitigated average severity does not conclusively indicate whether the MACs that occurred with a DAA system are worse (on average) because of the wide 95% confidence interval. Similar to the business jet, all cooperative MACs (1200exclude_fwse) were resolved by ACAS sXu.

The severity distributions for all impact locations are shown in Figure 125 through Figure 129. The highest unmitigated mean severity is on the wings at 3.47. Similarly, the highest mitigated severity is also on the wings at 3.60. Unfortunately, there are only two unresolved MACs with each sUAS model, which significantly lowers the confidence in the mitigated severity distribution, as indicated by the wide 95% confidence interval.

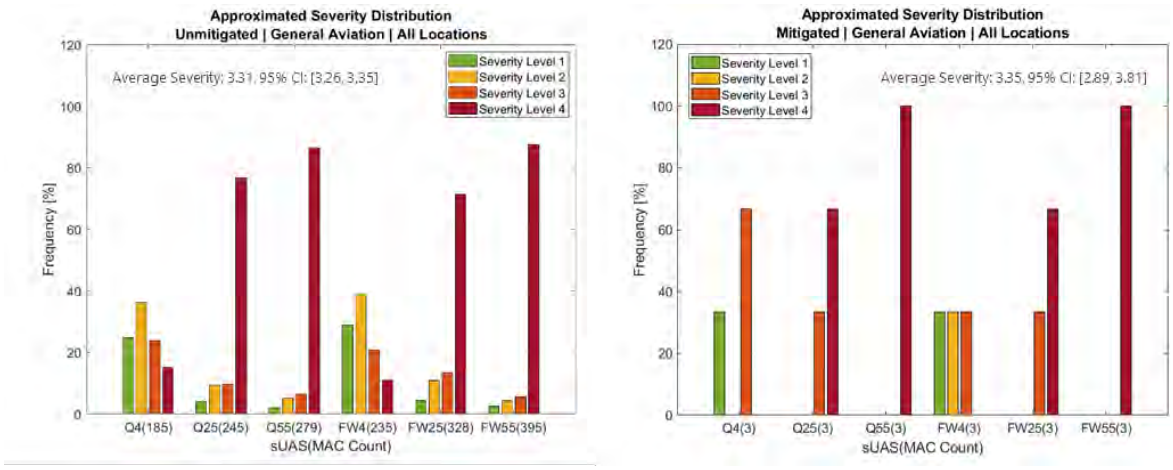

Figure 125. Severity level distribution –General aviation & all locations.

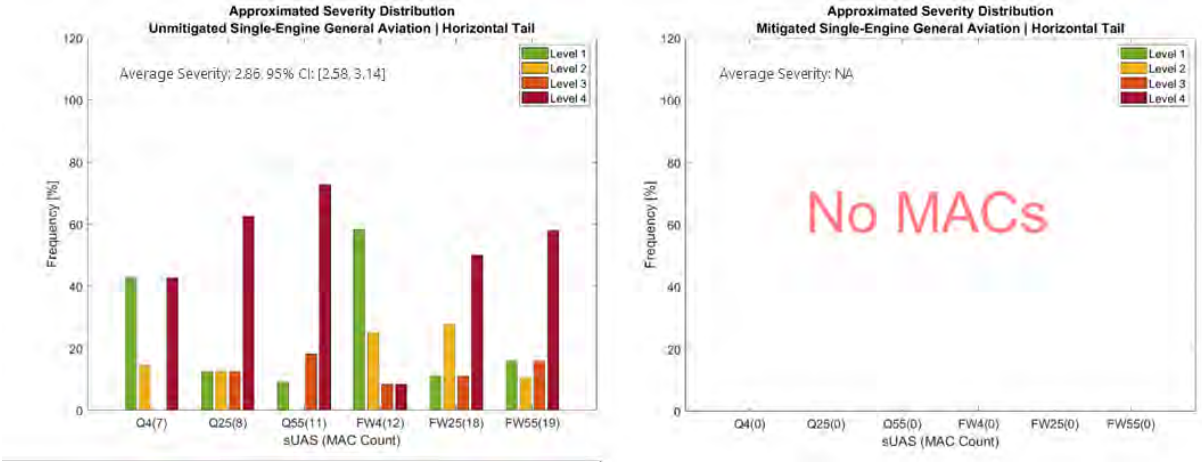

Figure 126. Severity level distribution –General aviation & horizontal tail.

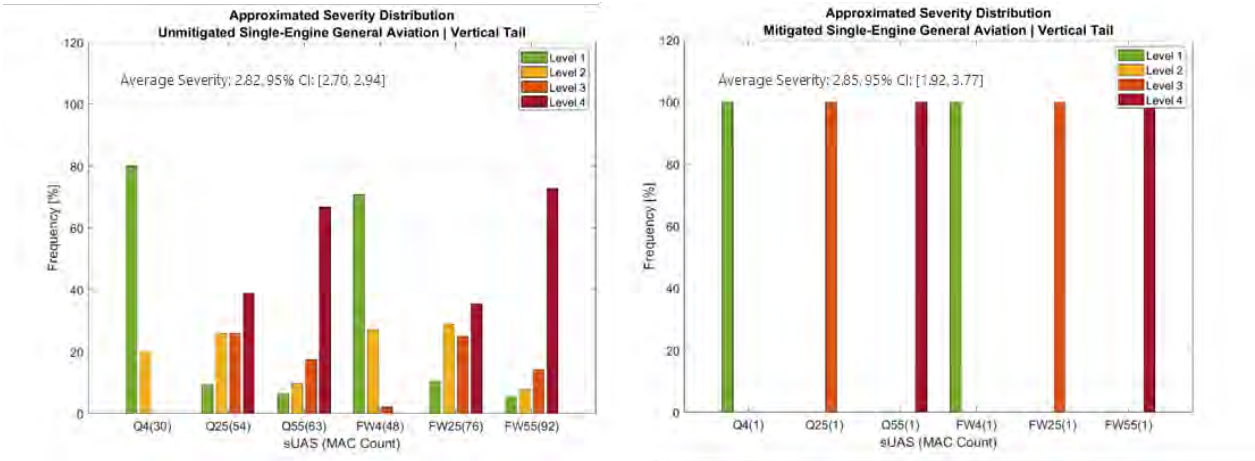

Figure 127. Severity level distribution –General aviation & vertical tail.

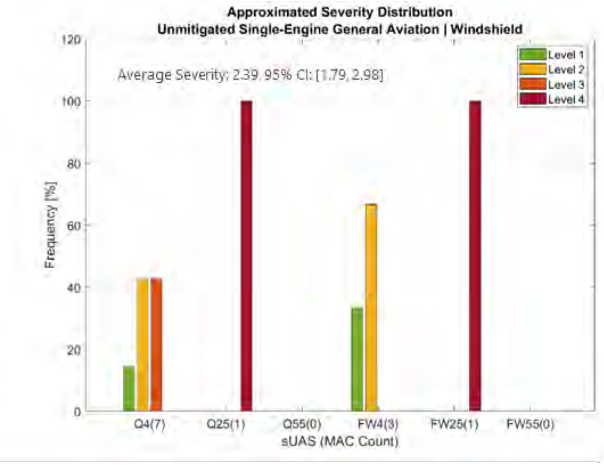

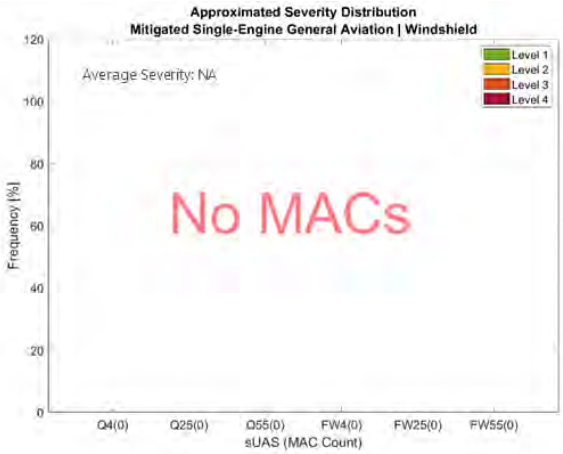

Figure 128. Severity level distribution –General aviation & windshield.

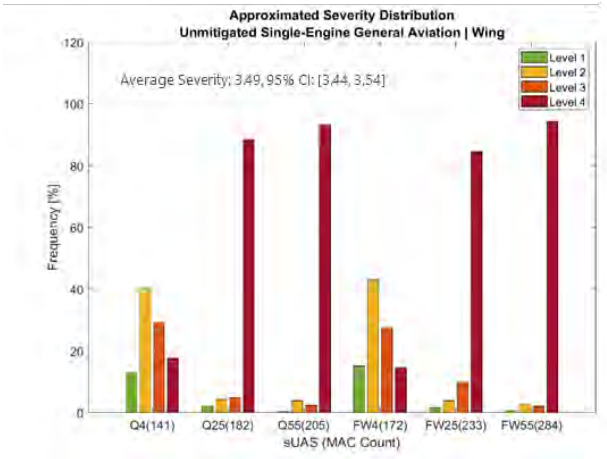

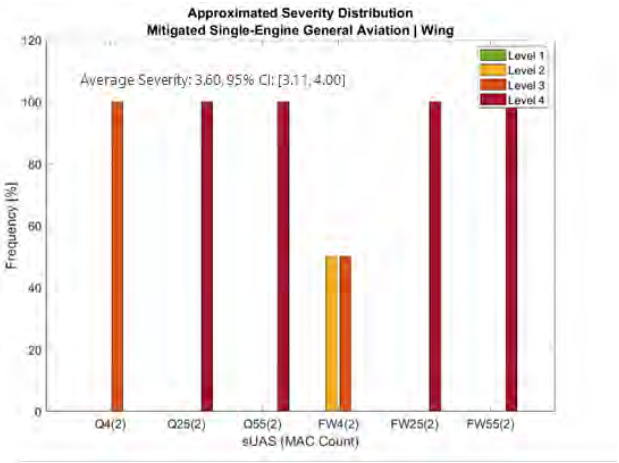

Figure 129. Severity level distribution –General aviation & wing.

5.5.4 *Rotorcraft*

The rotorcraft cases are derived from the rotorcraft encounter models. Both cooperative (1200exclude_rotorcraft) and non-cooperative (1200only_rotorcraft) cases were evaluated. The nose, fuselage, landing gear/skid, and tail boom MACs were not evaluated due to a lack of severity data. The rotor blades were not evaluated because all the severity data points available are equal to two. Additionally, only 2.7 lbs. quadcopter sUAS and 4.0 lbs. fixed-wing sUAS impacts were available from previous research (Olivares, Gomez, Marco, et al., 2022). These cases were extrapolated to estimate the severity of the 25 lbs. and 55 lbs. sUAS models.

Due to the lack of severity approximation functions, only 44% (1536 cases) of the unmitigated and 21% (13 cases) of the mitigated MACs were evaluated. This highlights a need for further severity data points and analysis. The severity distributions are shown in Figure 130 through Figure 134.

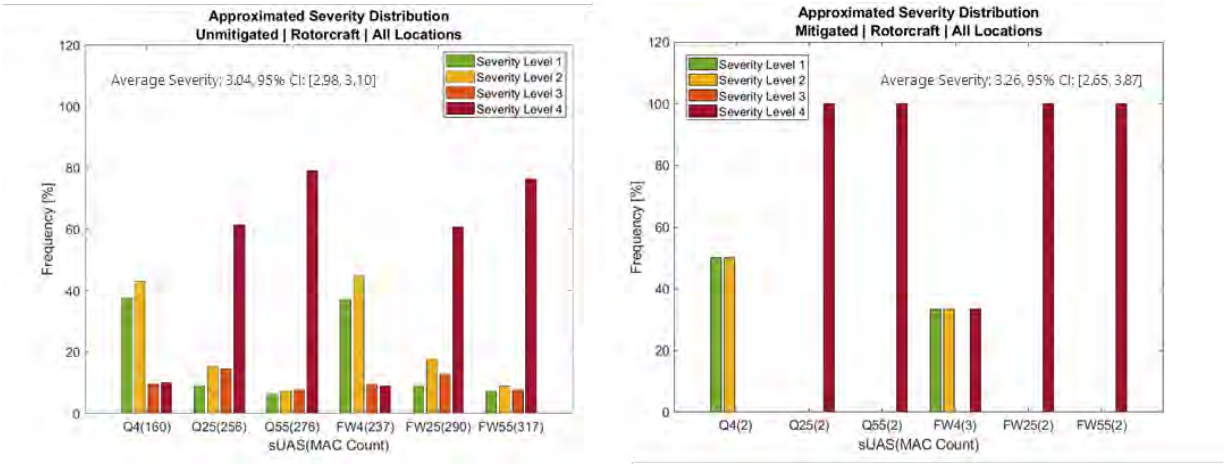

Figure 130. Severity level distribution – Rotorcraft & all locations.

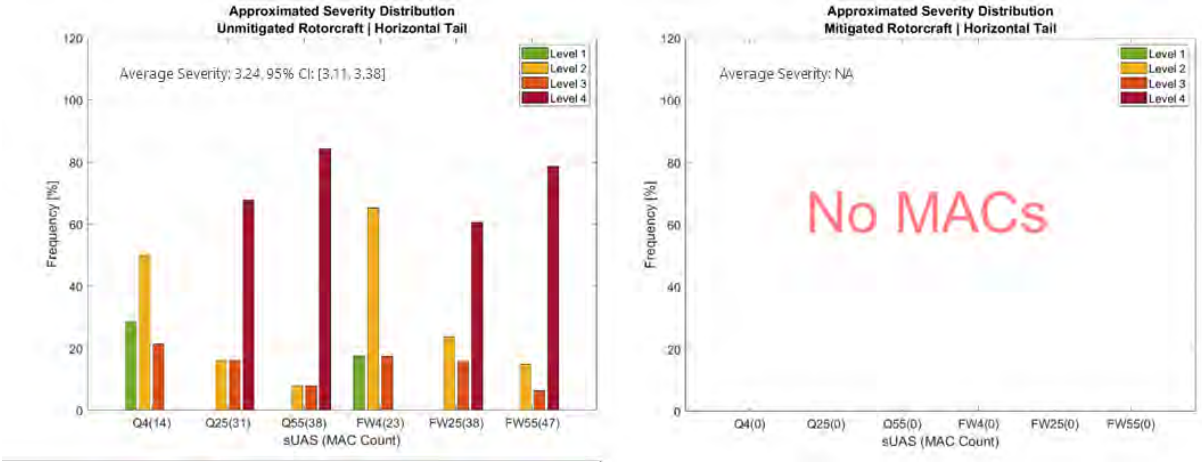

Figure 131 Severity level distribution – Rotorcraft & horizontal tail.

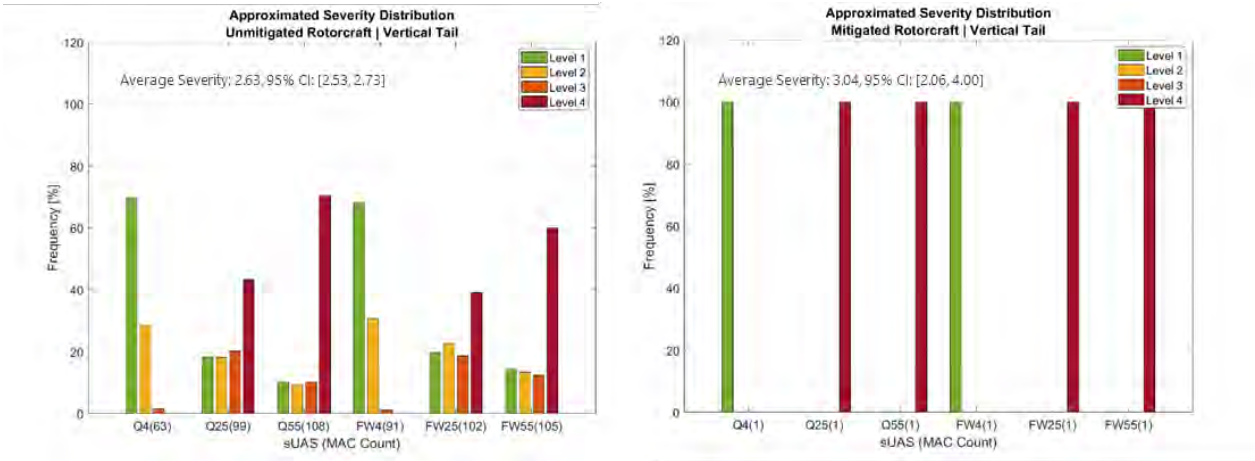

Figure 132. Severity level distribution – Rotorcraft & vertical tail.

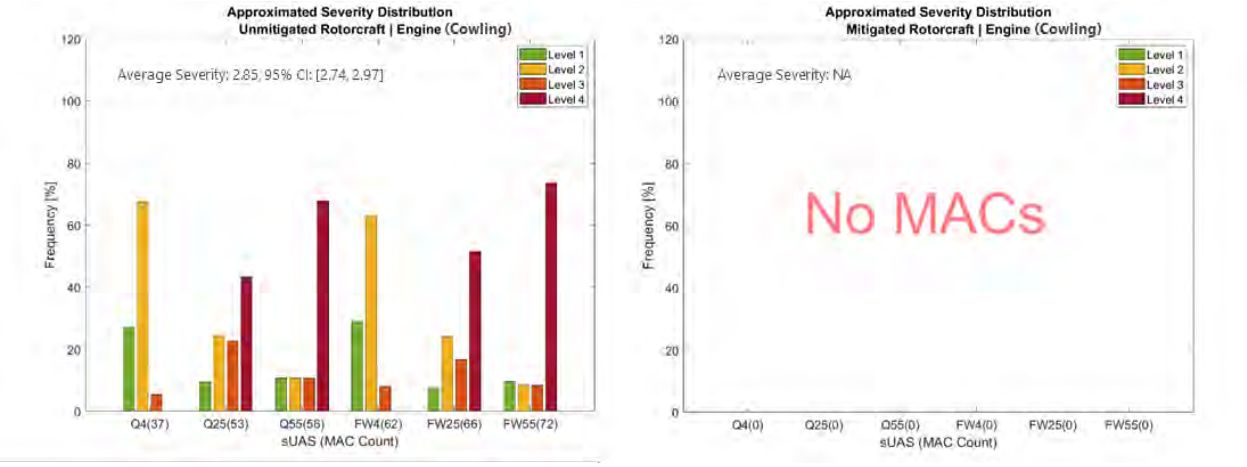

Figure 133. Severity level distribution – Rotorcraft & engine (cowling).

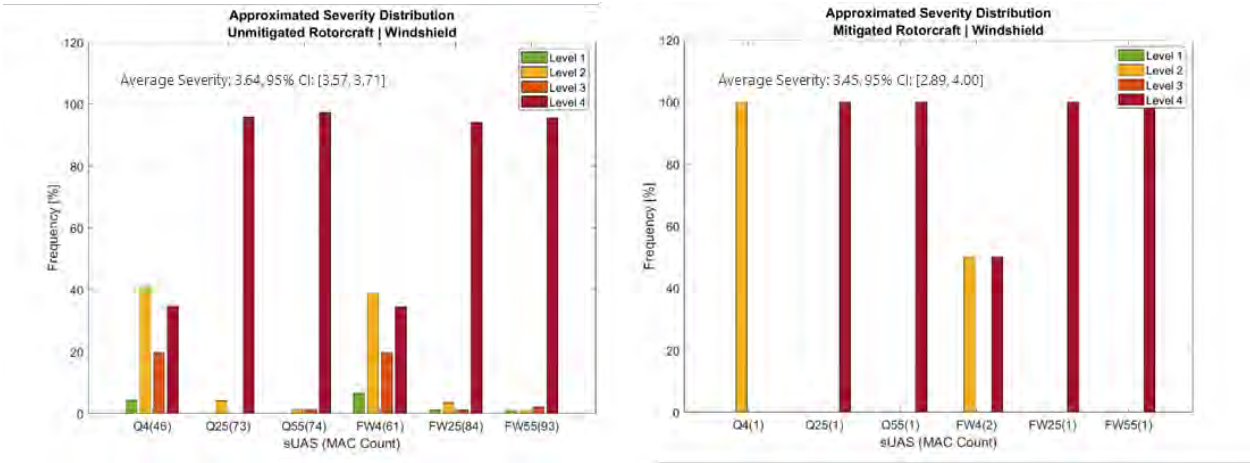

Figure 134. Severity level distribution – Rotorcraft & windshield.

5.6 **Discussion**

Figure 135 summarizes each manned aircraft model's unmitigated and mitigated mean severity level with their corresponding 95% confidence interval. The breakdown of each aircraft location is also shown in Figure 136 through Figure 139. The business jet had a definitive improvement in the aggregate mitigated mean severity level. The general aviation aircraft and rotorcraft had an inconclusive difference between unmitigated and mitigated mean severity because of the large uncertainty in the mitigated MAC dataset. Similarly, even though the mitigated mean severity level of the business jet improved, the same cannot be said when the results are broken down into each impact location, as shown in Figure 137. The business jet's vertical tail, windshield, and nose cone did not show a conclusive change in the mitigated mean severity due to the lack of MACs in the mitigated dataset. This is also the case for the general aviation aircraft and rotorcraft breakdowns, as shown in Figure 138 and Figure 139, respectively.

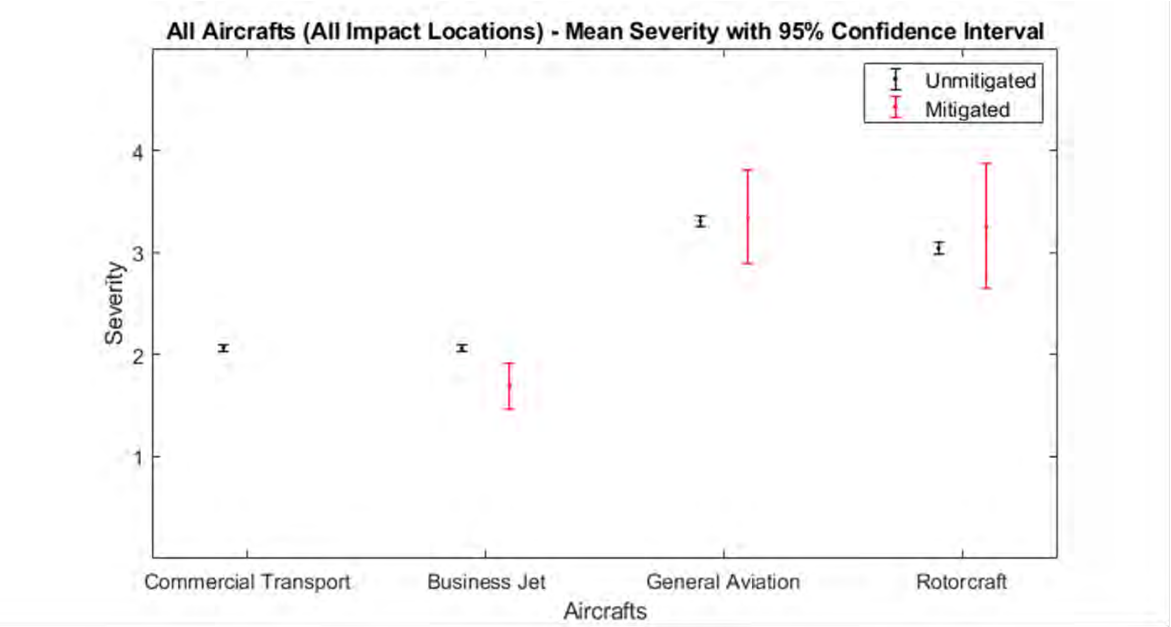

Figure 135. Mean severity level – Manned aircraft aggregate.

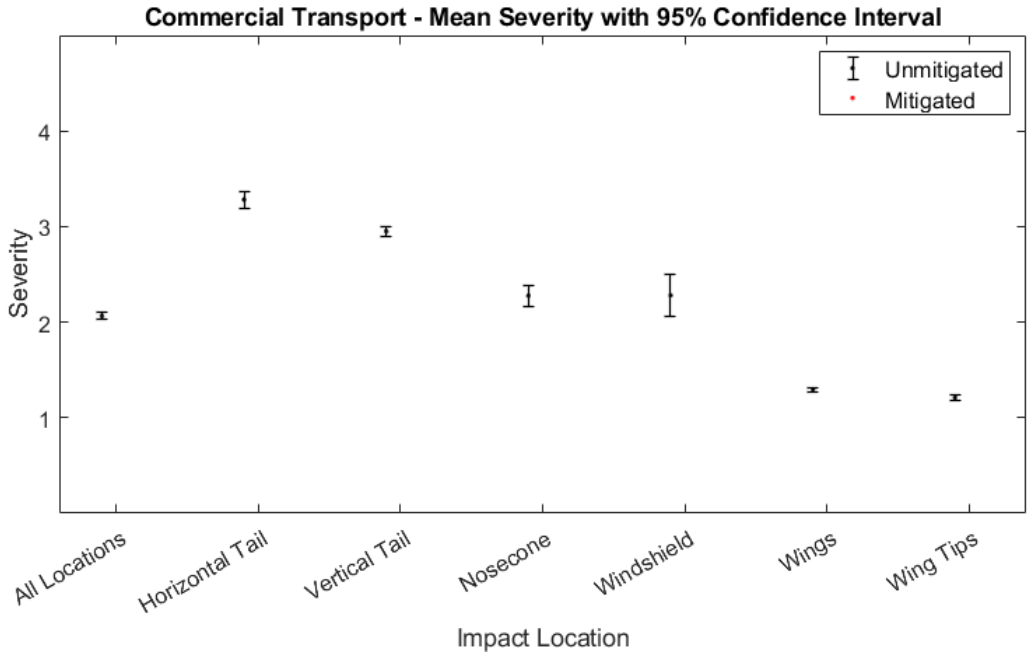

Figure 136. Mean severity level – Commercial transport.

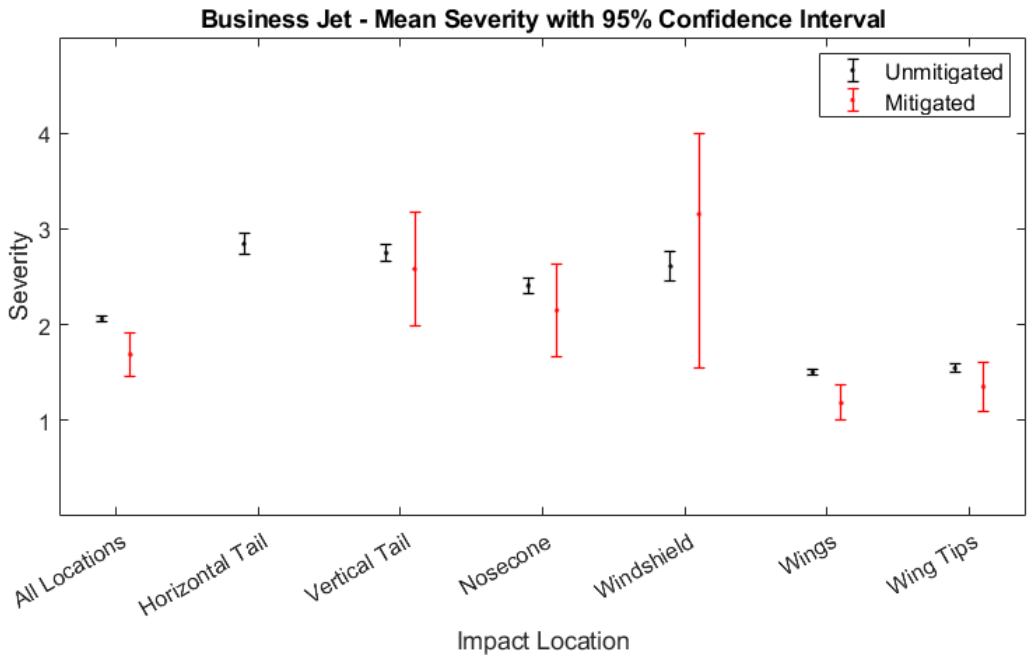

Figure 137. Mean severity level – Business jet.

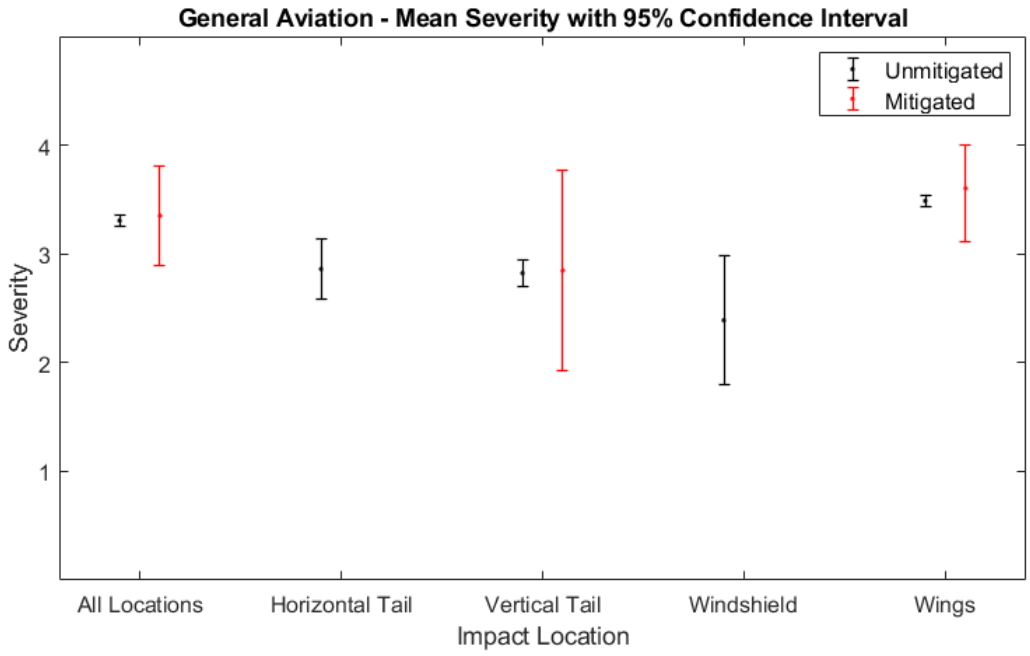

Figure 138. Mean severity level – General aviation (single-engine) aircraft.

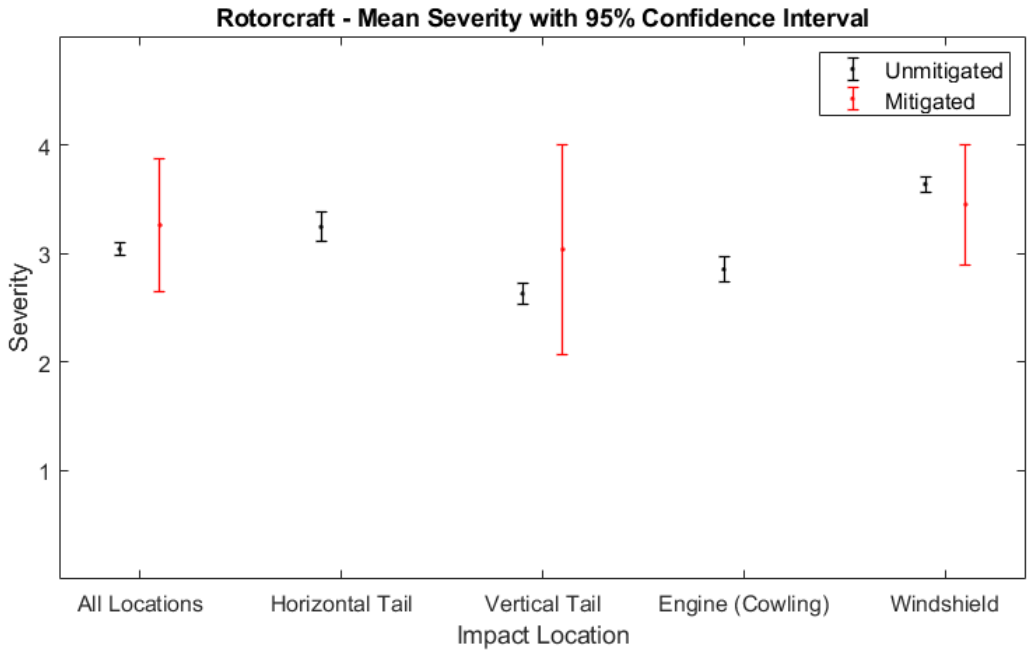

Figure 139. Mean severity level – Rotorcraft.

5.7 Gaps and Further Research

Discrete severity data points were used to create an approximation function. This is a challenge since the severity was effectively converted into a continuous function. Currently, there is no distinction between severity levels 3.4 and 2.7. In both cases, the severity will be rounded to level 3. An examination of all available cases through an image recognition algorithm to assign a new severity on a gliding scale could yield improved severity approximation functions. Results from the set of FEA presented in Section 5.4 could be expanded and used to enrich the datasets. This approach might reduce some of the data scatter observed in the current approximation functions. A new severity scale based on a material "damage parameter" could also be developed. This would allow for a quantitative severity assessment instead of the current qualitative approach. Furthermore, a Design of Experiments (DOE) exercise can be performed to include more varied impact conditions during FEA assessments. This will enable more accurate and representative severity evaluations based on the encounter simulation results discussed in Sections 3 and 4.

Throughout the analysis, the lack of severity data was also evident. Previous research addressed only worst-condition cases in manned aircraft locations where head-on collisions were expected. Therefore, fuselage impact conditions were not assessed. Similarly, ongoing efforts are focusing on engine ingestion severity which is expected to be the worst condition for an engine MAC (ASSURE, 2022a). However, nacelle impacts should also be evaluated for a complete severity evaluation of the engines, even if such cases are expected to be low severity. Other impact locations (with an expected low severity), such as landing gear (general aviation aircraft and rotorcraft), should also be investigated.

The same applies to the rotorcraft severity data points. Currently, the rotor blade MAC severity evaluation is limited by the lack of data variability. Further research should investigate impact conditions that result in greater and lower severity. Future rotorcraft research might address some

of these gaps (ASSURE, 2022b). Likewise, general aviation propeller impacts should be explored further. Different construction types and materials could be considered to include a broader range of available propellers.

In the same way, future analyses could include more sUAS architectures. The present research only included the six sUAS architectures that Olivares, Gomez and Marco (2022) have previously analyzed. A library of the most widely expected sUAS architecture could be analyzed based on a survey of the ever-changing sUAS landscape. This will enable the creation of robust generalized functions that could be extrapolated for future and innovative designs that mix-and-match features of different platforms without the need for a specialized research campaign for each architecture.

The lack of unresolved MACs s hindered the confidence in the severity results of the mitigated datasets. During the encounter sets definition stage, the research team expected a larger number of "mitigated" unresolved MACs based on preliminary analyses with a different DAA system. ACAS sXu proved to be exceptionally capable of reducing MACs, especially in the cooperative encounter sets. Future research should include at least 1,000 mitigated unresolved MACs in each of the encounter models to determine a robust severity distribution when a DAA system is employed. Based on the results presented in this report, 1,000 MACs would require the evaluation of ~300 million encounters. This expansion of the scope was unfeasible in the present research due to limited computational resources allocated and without significantly delaying the timeframe of the *A47_A11L.UAS.87 -002 research (sUAS Mid Air Collision Likelihood)* effort.

6 SUAS MACS VS. BIRD STRIKES

An analysis of simulated sUAS MACs with intruder aircraft and bird strikes provides a means of comparison between sUAS impacts with crewed aircraft and bird strikes. This analysis aims to draw parallels between bird strikes, a well-documented aviation hazard, and sUAS MACs, which are less understood. This analysis explores similarities and differences between simulated sUAS MAC data and historical bird strike data between 1990 and 2020 to inform on the similarity of bird strikes to sUAS MACs.

The following analysis provides an overview of sUAS MAC data obtained from simulated MACs encounters, a brief discussion of bird strike data, key assumptions and limitations, and a comparison of data. The research team will recommend areas of future work based on conclusions from this research. The research team anticipates future work to stem from the limitations of this analysis.

6.1 Simulated sUAS MAC Events

The data set for simulated MACs between sUAS and crewed intruder aircraft consisted of a total of 20,747 collision cases. The team sorted this data between unmitigated and mitigated MACs and further defined whether the sUAS was cooperative or non-cooperative with intruder traffic. Table 46 shows the entire dataset.

Table 46. Breakdown of the dataset for simulated sUAS/crewed aircraft MACs.

Simulated sUAS MACs with Crewed Aircraft			
MITIGATED		**UNMITIGATED**	
Cooperative	*Non-cooperative*	*Cooperative*	*Non-cooperative*
1	180	14,732	5,834
Total Simulated sUAS MACs: 20,747			

Characteristics of intruder aircraft simulated sUAS are also part of the data sets. Intruder aircraft included the following aircraft types, incorporating basic operational considerations:

- GA Aircraft – A model that is representative of a typical single-engine, piston-powered airplane.
- Rotorcraft – A representative model of a typical civilian helicopter.
- Business Jet – A representative model of a typical business jet.
- Commercial Transport – A model of wide-body business jet with two turbofan engines.

Figure 24 shows examples of intruder aircraft used in sUAS encounters and MAC simulations. Likewise, simulated sUAS represented a range of configurations and varying weights to represent a reasonable cross-section of sUAS typically encountered in the NAS. These simulated sUAS consisted of fixed-wing aircraft with weights of 4 lbs., 25 lbs., and 55 lbs., and multirotor with the same weight categories. Figure 27 and Figure 28 show the sUAS used in the simulations.

6.2 Bird Strike Data

To assess how bird strikes compare to the simulated sUAS MACs and to determine correlations between bird strikes with given components on the different intruder aircraft, the research team

relied on data from *Wildlife Strikes to Civil Aircraft in the United States, 1990-2020* Dolbeer et al. (2021) to pull data regarding bird strikes with civil aircraft of various classifications. Table 47 shows data for civil aircraft component bird strikes in the United States between 1990 and 2020 as a function of impact location and damage to the aircraft.

Table 47. Civil aircraft components reported as being struck and damaged by bird strikes, USA, 1990-2020 Dolbeer et al. (2021).

	Bird Strikes (31-year total)				
Aircraft Component	Number of Strikes	Percentage of Total	Number of Damaged	Percentage with damage	Percentage of Total (damaged)
Windshield	30,678	15.4%	1,240	4.0%	6.3%
Nose	27,947	14.0%	1,358	4.9%	6.9%
Wing/Rotor	27,819	13.9%	4,881	17.5%	24.8%
Radome	23,029	11.5%	1,833	8.0%	9.3%
Fuselage	22,150	11.1%	866	3.9%	4.4%
Engine (s)	22,142	11.1%	5,123	23.1%	26.0%
Landing Gear	29,662	14.8%	1,786	6.0%	9.1%
Propeller	8,730	4.4%	634	7.3%	3.2%
Tail	3,962	2.0%	305	7.7%	1.6%
Light	2,439	1.2%	808	33.1%	4.1%
Other	1,211	0.6%	834	68.9%	4.2%
Total	199,769	100%	19,668	-	100%

The data in Table 47 is essential for making comparisons to simulated sUAS MACs because it highlights (1) the total reported aircraft components impacted by bird strikes and (2) of those impacts, the number of components with reported damage. This enables a comparison between simulated MAC events with known impact locations and known damage to the impacted aircraft. Table 47 also provides a total number of bird strikes for comparison, as the bird strikes listed in the table are aggregated from various categories and classes of aircraft struck by birds over a 31-year period.

It is important to note that Dolbeer et al. (2021) captured a total of 233,915 total bird strikes, and the numbers above represent a subset of that total. Researchers chose these totals for analysis because they were traceable to a known data set – i.e., associated with other data points, such as specific aircraft component(s) impacted. This allowed for the most direct comparison to simulated sUAS MACs. The research team omitted comparisons of raw numbers of bird strikes to numbers of simulated sUAS MACs, as the number of simulated MACs was entirely dependent upon the research team and determined by inputs into the simulations.

6.3 **Assumptions and Limitations**

The research team had to make a series of simplifying assumptions to facilitate a reasonable comparison between existing bird strike data and simulated sUAS MACs. These assumptions provided a means to make more direct comparisons. These simplifying assumptions also contribute to limiting factors of the analysis.

6.3.1 ***Assumptions***

Simplifying assumptions for this analysis are as follows:

Assumption 1: Aircraft MACs with sUAS damaged the intruder aircraft in all cases, even if it is not a severe MAC. This was a conservative estimate due to a lack of data regarding real-world damage from sUAS MACs.

Assumption 2: For analysis, certain aircraft components for bird strike data sets were grouped. As such, radome strikes equated to nose strikes since radomes are commonly, but not always, located in an aircraft's nose, particularly in larger commercial transports and business jets. Figure 140 shows a Boeing 777 following a bird strike to its radome, located in its nose.

Figure 140. Boeing 777 with bird strike to radome (Chong, 2015).

Assumption 3: Researchers grouped components and impact points for sUAS MAC data sets to enable direct comparisons – e.g., wing, wingtips, and rotors were grouped, engines were a single category, and tail structures were grouped as well. Similarly, impacts with aircraft lights were categorized as "other."

Assumption 4: For this analysis, researchers did not consider distinctions between cooperative/non-cooperative sUAS MACs when analyzing similarities with bird strikes.

Assumption 5. Specific sUAS types/configurations – e.g., fixed-wing or multirotor, were not considered when comparing to bird strikes. This assumption is based on the notion that with the

bird strike data available, there is no means to directly correlate the flight characteristics of bird strikes and sUAS MACs.

Researchers made the assumptions listed above to enable direct comparisons between data sets to conclude similarities and differences between bird strikes and sUAS MACs.

6.3.2 *Limitations*

In addition to simplifying assumptions, there are inherent limitations in the comparison between simulated sUAS MACs and bird strikes. These limitations stem from the limited availability of data sets, the assumptions listed above, and gaps in data that do not enable a complete comparison, either through non-response or incomplete documentation. Noteworthy limitations of this analysis are as follows:

Limitation 1: While Dolbeer et al. (2021) included data on approximately 233,915 bird strikes, this analysis only addresses a subset of that total attributed to reported impacts with aircraft components.

Limitation 2: Data regarding damage resulting from sUAS MACs was not available for this analysis. As such, every simulated sUAS MAC was assumed to result in damage to the intruder aircraft.

Limitation 3: The available data set for bird strikes is aggregated from multiple types of aircraft – e.g., general aviation aircraft, commercial transports, business jets, or rotorcraft. There is no direct comparison between bird strikes on specific aircraft components and the type of aircraft impacted.

Limitation 4: The research team did not consider sUAS type/configuration/weight in this analysis, as there is no direct relation to bird strikes within the given data set.

As such, available data constrain this analysis to the following parameters.

1. The research team compared bird strikes and sUAS MACs based on impact locations on crewed aircraft using the available bird strike data.
2. Comparisons between bird strikes and sUAS MACs used data sets with common data values – e.g., impact with wing or tail.
3. The research team compared sUAS MACs to bird strikes where correlating data for bird strikes existed – e.g., MAC occurred and impacted ‘x’ component.
4. Comparisons between simulated mitigated/unmitigated sUAS MACs and bird strikes may not extrapolate beyond the available data.

6.4 Historical Bird Strikes and Simulated sUAS Mid-Air Collisions (MACs)

While a direct comparison between simulated sUAS MACs and all available bird strike data is not feasible, comparing data sets with similar variables, such as impact location, is possible. The following subsections outline a comparison of raw numbers of simulated sUAS MACs in relation to aircraft components struck by birds – to include a comparison of sUAS MACs with and without mitigation.

6.4.1 *Simulated sUAS MACs vs. Bird Strikes on Aircraft Components*

Using data from simulated sUAS MACs with intruder aircraft and existing data on bird strikes, it was possible to group simulated sUAS MACs so that the research team could compare them to the

bird strike data. The resulting data, displayed in Figure 141, represents a comparison between simulated sUAS MACs and bird strikes on given aircraft components that resulted in damage. This is in keeping with the assumption that all sUAS MACs will result in damage and are comparable to damaging bird strikes.

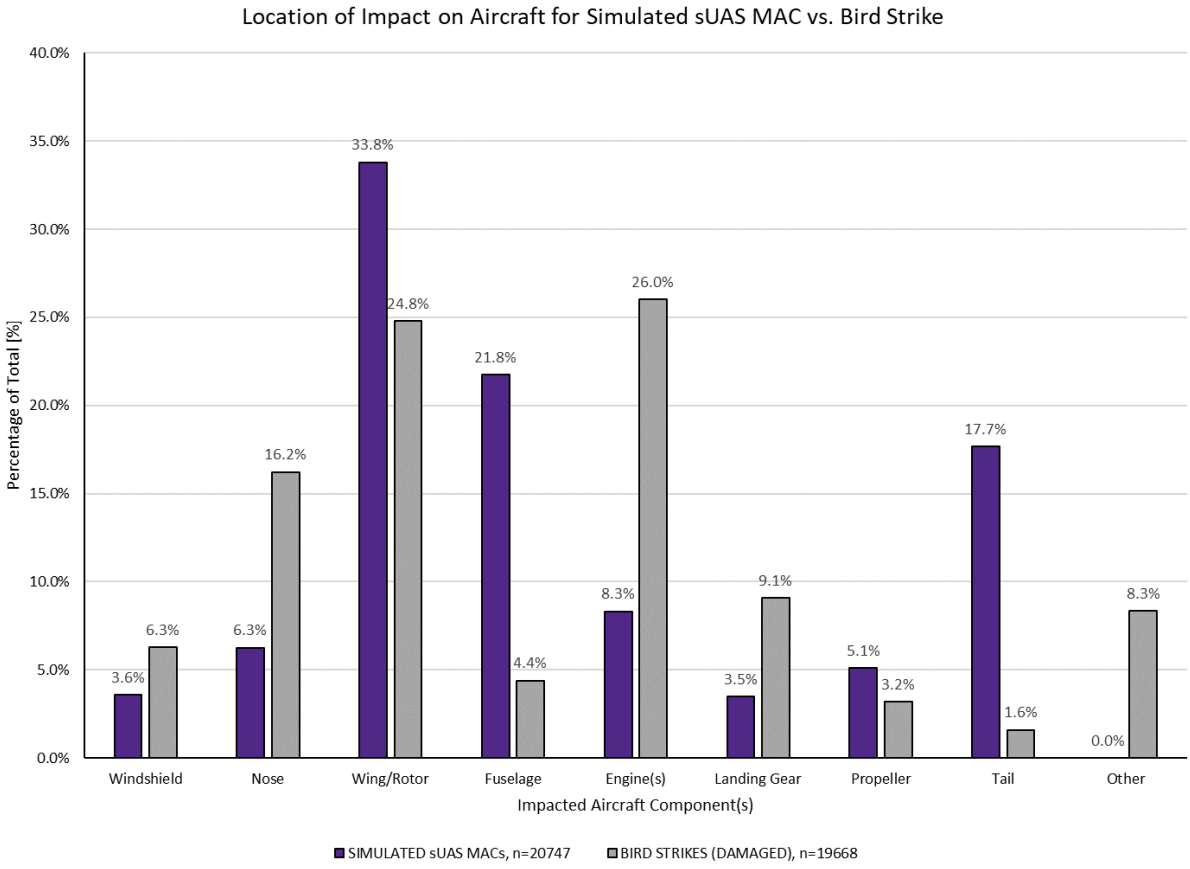

Figure 141. Number of Simulated sUAS MACs vs. Number of Bird Strikes as a percentage of total number of events, USA.

Figure 141 shows that bird strikes occurred to a greater extent than simulated sUAS MACs for aircraft engines, noses, landing gear, windshields, and other components. The figure also shows that simulated sUAS MACs occurred more often on aircraft fuselages and tail components than bird strikes, with the majority of simulated sUAS MACs occurring with wings/rotors.

6.4.2 *Simulated sUAS MACs vs. Bird Strikes on Aircraft Components – Mitigated and Unmitigated*

Simulated sUAS MACs fit into two main categories: mitigated and unmitigated. The research team compared mitigated and unmitigated MACs to aircraft component bird strike data as percentages of their individual totals – i.e., percentage of the total number of simulated sUAS MACs (mitigated) compared to bird strikes on aircraft components and percentage of the total number of simulated sUAS MACs (unmitigated) compared to the same bird strike data for given components. Figure 142 shows the results of this comparison.

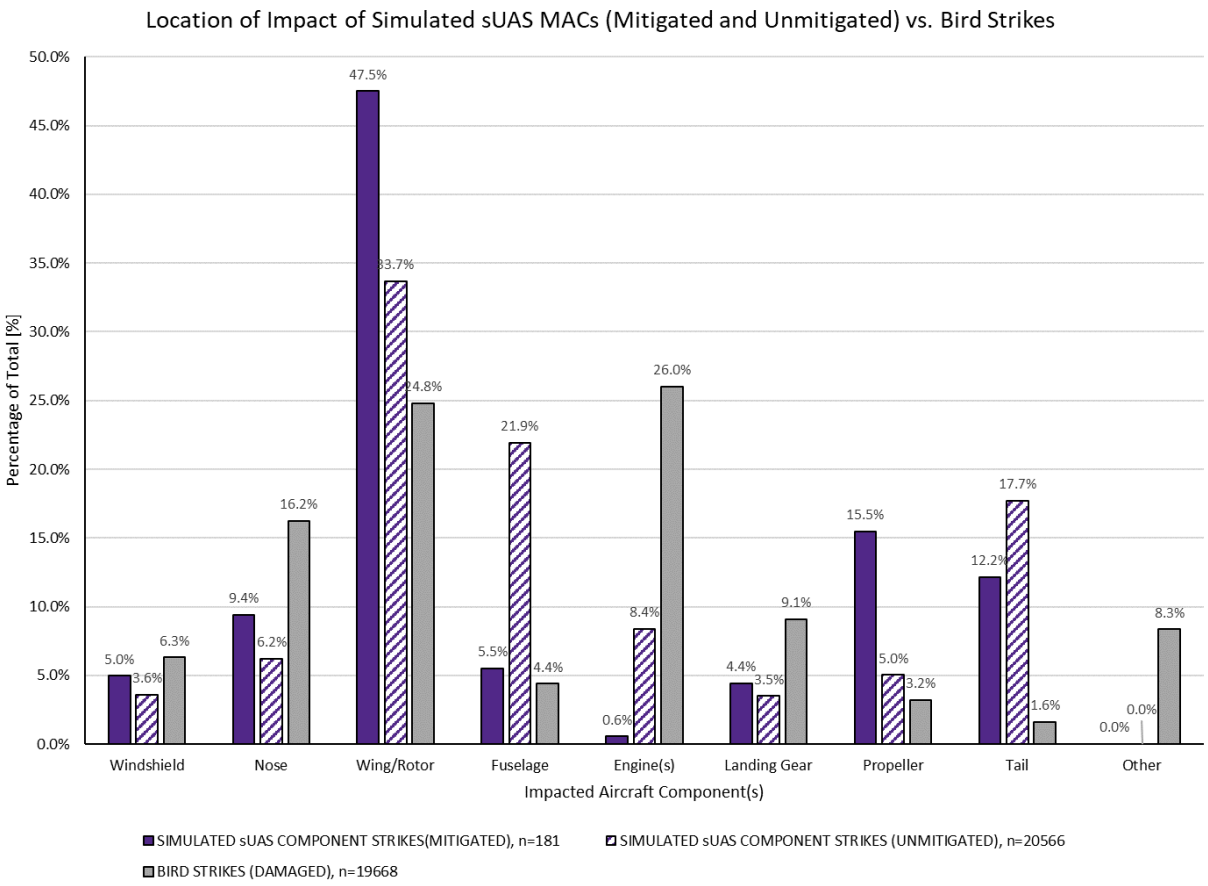

Figure 142. Location of Impact on Aircraft – sUAS MAC (Mitigated and Unmitigated) vs. Bird Strike as Percentage of Totals, USA.

From Figure 142, one can see that there is no obvious correlation between bird strikes and simulated mitigated or unmitigated sUAS MACs on given aircraft components. Figure 142 also shows the differences between mitigated and unmitigated MACs for multiple components. One of the highlights is the low count in the engines. The mitigated sUAS MACs had a 0.6% share compared to 8.4% unmitigated sUAS MACs and 26% bird strikes. On the other hand, the tail share was higher in the mitigated and unmitigated MACs; 12.2% and 17.7%, respectively, compared to bird strikes; 1.6%.

Future analysis regarding comparisons between sUAS MACs and bird strikes should differentiate the aircraft type (rotorcraft, single-engine fixed-wing, etc.). This will allow comparisons of the individual aircraft models instead of an aggregate of all aircraft. Larger mitigated data sets will also enable more direct comparisons. There was no separate data set for rotorcraft or business jets for this analysis. As such, this analysis focused on available data for GA and commercial transport aircraft. Even with available data, comparisons had to be narrowed to consider similar events – e.g., collisions with specified aircraft components and constrained to specified cases with common variables.

7 CONCLUSION

This report highlights how to utilize open-source resources, such as MIT LL encounter models and DEGAS, to generate and evaluate encounter sets. The encounter sets can be used to demonstrate compliance with ASTM F3442. Multiple encounter sets (i.e., using expected sUAS trajectories rather than an encounter model) can be used to determine the robustness of a DAA system under different scenarios.

A DAA system can be integrated into the simulation framework, DEGAS. ACAS sXu was used as the DAA logic in this research. Similarly, the available sensor models can be adjusted to desired parameters (i.e., expected error, refresh rate, and delays). In addition, new sensor models can also be developed and integrated into DEGAS, if they are not available in the surveillance library. Two independent sensor models were used in this research. ADS-B was used for cooperative intruders and a ground-based radar-like system for non-cooperative intruders. RTCA DO-396 informed the expected performance of each sensor.

The analysis showed that ACAS sXu meets the ASTM F3442 RR and LoWCR requirements for cooperative and non-cooperative intruders. ADS-B has smaller positional errors than the non-cooperative sensor, resulting in a much lower RR (8.81E-3 vs. 1.13E-1 respectively in the FWME set) and LoWCR (1.75E-1 vs. 4.10E-1 respectively in the FWME set). The most significant difference between cooperative and non-cooperative is observed in the RR. Less sensor uncertainty results in significantly better RR in all the encounter sets in this study. However, an encounter set defined under different assumptions might result in a different outcome. Similarly, variations in the non-cooperative error values could lead to different conclusions. For instance, more accurate vertical positions (with the same horizontal error) could lead to a better RR in the non-cooperative sets. ACAS sXu reliance on horizontal maneuvers in the non-cooperative sets was discussed in Section 4.6.1

This study also showed that the size of sUAS can be considered a passive MAC mitigation factor. The unmitigated *P(MAC|NMAC)* is lower by a factor of 2 from the smallest to the largest sUAS, assuming both aircraft have the same capabilities. The smallest sUAS in this study is the size of a DJI Phantom 3 (1.6 ft. rotor-to-rotor span), and the largest is a fixed-wing sUAS with a 13.8 ft. wing span.

The *P(MAC|NMAC)* for the 1200code-only intruders (non-coop surrogate) was estimated between 6E-4 and 2E-3. The upper bound mitigated *P(MAC|NMAC)* for all 1200code-exclude models was estimated at < 1.3E-3. This result is expected to be conservative since all, but one airframe pair for the cooperative cases had zero MACs recorded. Even though the upper bound MAC ratio of the 1200code-exclude is comparable to the 1200code-only results, ACAS sXu overall MAC mitigation effectiveness is higher in the 1200code-exclude models. This is because of the significantly smaller RR results (i.e., 8.91E-02 vs. 7.5E-03 in the FWSE sets). When only analyzing non-cooperative NMACs unresolved or induced by the DAA system, *P(MAC|NMAC*) is ~45-75% lower than the unmitigated cases. This is indicated by MAC ratios between ~0.55 and ~0.25. Nevertheless, this is not indicative of the actual realized MAC risk but the comparative risk given an encounter set. Actual encounter rates, and by extension MAC rates, depend on other factors such as aircraft density and airspace segregation. This also highlights the importance of using conditional probabilities and ratios rather than standalone probabilities, such as *P(MAC)*. A

standalone probability can be misleading because its value depends on the definition of an "encounter". An encounter set involving many encounters with large separation distances can dilute the value of *P(MAC)*. This, however, does not indicate that the MAC risk is indeed lower when an NMAC or LoWC occurs. Similarly, ratios, such as RR and LoWCR, highlight the performance of a DAA system in relation to the encounter set rather than meeting a standalone probability target that could be achieved by only modifying the encounter set composition.

ACAS sXu reduced the overall number of collisions with non-cooperative intruders in an encounter set by ~95% to 98%. ACAS sXu also showed an overall MAC reduction with cooperative intruders > 99.4%. These results, along with the MAC ratios, demonstrate that the benefits of ACAS sXu, with sensor errors modeled according to DO-396, continue beyond reducing NMACs. The results presented in this report are based on the performance of the DAA system, assuming the minimum surveillance requirements outlined in Sections 2.6.3 and 4. An assurance analysis of each of the components making up a DAA system and their effect on the performance of the DAA was out of the scope of this research. Therefore, malfunctions and other unexpected errors in the electronic systems were not incorporated into the analysis but should be considered when performing a holistic safety analysis.

A methodology to assess the severity of a MAC was developed. It involved the creation of multiple severity approximation functions and a trained model to scale the severity based on the impact relative position and orientation. Each manned aircraft model's average unmitigated and mitigated severity was estimated on a 1 to 4 scale. However, the low number of MACs in the mitigated cases hindered the mitigated severity distribution. Only the business jet aircraft had a definitive improvement in the mitigated mean severity (1.69 vs. 2.06). The general aviation aircraft and the rotorcraft had an inconclusive change in the mitigated mean severity due to the significant uncertainty in the mitigated datasets. The commercial transport aircraft severity was not compared because there were no MACs that could be assessed. ACAS sXu proved to be exceptionally capable of reducing MACs, especially in the cooperative encounter sets, which resulted in scant MACs in the mitigated datasets.

Throughout the severity analysis, the lack of severity data was also evident. Previous research only addressed worst-condition cases in manned aircraft locations where head-on collisions were expected. However, more impact conditions should be evaluated for a comprehensive severity evaluation of all aircraft parts, even if such cases are expected to be low severity. In the same manner, future analyses should include more sUAS architectures. A library of the most widely expected sUAS architecture could be analyzed. This will enable the creation of robust generalized severity functions that could be extrapolated for future and innovative designs that mix-and-match features of different platforms without the need for a specialized research campaign for each architecture.

8 REFERENCES

Alvarez, L. (2021). *Airborne Collision Avoidance System sXu Threat Resolution Module Design Summary* [V3R0]. Traffic Alert & Collision Avoidance System Program Office & Federal Aviation Administration.

ASSURE. (2022a). *Airborne Collision Severity Evaluation – Engine Ingestion*. Retrieved October, 2022 from https://assureuas.com/projects/airborne-collision-severity-evaluation-engine-ingestion/

ASSURE. (2022b). *Determine The Collision Severity Of Small Unmanned Aircraft Systems (SUAS) In Flight Critical Zones Of Manned Helicopter*. Retrieved October, 2022 from https://assureuas.com/projects/determine-the-collision-severity-of-small-unmanned-aircraft-systems-suas-in-flight-critical-zones-of-manned-helicopter/

ASTM F3442/F3442M-20. (2020). Standard Specification for Detect and Avoid System Performance Requirements. In ASTM International (Ed.). West Conshohocken, PA: ASTM International

Bender, W. (2021). *Concept of Use for the Airborne Collision Avoidance System X for Smaller UAS (ACAS sXu)* [V3R0]. Traffic Alert & Collision Avoidance System Program Office & Federal Aviation Administration.

Bezanson, J., Edelman, A., Karpinski, S., & Shah, V. B. (2017). Julia: A Fresh Approach to Numerical Computing. *SIAM Review*, *59*(1), 65-98. https://doi.org/10.1137/141000671

Chong, A. (2015). *Bird Strike Tears Open Radome of SIA 777*. Retrieved October, 2022 from https://www.flightglobal.com/bird-strike-tears-open-radome-of-sia-777/117957.article

Das, A. (2021a). *Airborne Collision Avoidance System sXu Performance Summary* [V3R0]. Traffic Alert & Collision Avoidance System Program Office & Federal Aviation Administration.

Das, A. (2021b). *Airborne Collision Avoidance System sXu, Operational Validation Report* [V4R0]. Traffic Alert & Collision Avoidance System Program Office & Federal Aviation Administration.

Dolbeer, R. A., Begier, M. J., Miller, P. R., Weller, J. R., & Anderson, A. L. (2021). *Wildlife Strikes to Civil Aviation States, 1990-2020* (Serial Report Number 27). Federal Aviation Administration & United States Department of Agriculture Wildlife Services.

Dutta, A. (2022). *Random Forest Regression in Python*. https://www.geeksforgeeks.org/random-forest-regression-in-python/

Espindle, L. P., Griffith, J. D., & Kuchar, J. K. (2009). *Safety Analysis of Upgrading to TCAS Version 7.1 Using the 2008 U.S. Correlated Encounter Model* (Project Report ATC-349).

Geweke, J. (1989). Bayesian Inference in Econometric Models Using Monte Carlo Integration. *Econometrica*, *57*(6), 1317-1339. https://doi.org/10.2307/1913710

Hudson, T., Lin, M., Cohen, J., Gottschalk, S., & Manocha, D. (2000). *V-COLLIDE: Accelerated Collision Detection for VRML* Association for Computing Machinery, Monterey, California, USA.

International Civil Aviation Organization. (2014). *Annex 10 to the Convention on International Civil Aviation* (Volume IV Surveillance and Collision Avoidance Systems). ICAO.

Jared Wikle, Luis Alvarez, & Neal A. Suchy. (2022). *Algorithm Design Description of the Airborne Collision Avoidance System sXu* (ACAS_ADS_22_001_V4R1, V4R1). Federal Aviation Administration.

Katherine Wu, Barbara Kobzik-Juul, Matthew Lempka, & Daniel Muller. (2021). *Test Suite ACAS sXu V4R0* [Version 1, Revision 0]. Traffic Alert & Collision Avoidance System (TCAS), Program Office (PO), & Federal Aviation Administration.

Kochenderfer, M., Griffith, D., & Olszta, J. (2010). On Estimating Mid-Air Collision Risk. *10th AIAA Aviation Technology, Integration, and Operations (ATIO) Conference*. https://doi.org/10.2514/6.2010-9333

Kochenderfer, M. J., Kuchar, J. K., Espindle, L. P., & Griffith, J. D. (2008). *Uncorrelated Encounter Model of the National Airspace System, Version 1.0* (Project Report ATC-345). MIT Lincoln Laboratory.

Luis Alvarez, & Neal A. Suchy. (2021). *Airborne Collision Avoidance System sXu Threat Resolution Module Design Summary* (ACAS_RPS_21_005_V1R0, V3R0). Federal Aviation Administration (FAA).

Mykel Kochenderfer. (2008). *Fast Collision Detection.* MATLAB Central File Exchange. https://www.mathworks.com/matlabcentral/fileexchange/18473-fast-collision-detection

Olivares, G., Gomez, L., Baldridge, R. J., Marco, R., & Ly, H. (2020). *Large sUAS Airborne Collision Severity Evaluation with 14 CFR 25 Aircraft -ATO Office of Safety* [Assure Report].

Olivares, G., Gomez, L., & Marco, R. (2022). *Volume VII – UAS Airborne Collision Severity Evaluation – 14 CFR Part 23 General Aviation* [Assure Report]. https://assureuas.com/wp-content/uploads/2021/06/Volume-VII-Airborne-Collision-Severity-Evaluation-14-CFR-Part-23-General-Aviation.pdf

Olivares, G., Gomez, L., Marco, R., Ly, H., Calderon, J., Duling, C., Zwiener, M., & Perrin, Z. (2022). *Volume VI – UAS Airborne Collision Severity Evaluation – 14 CFR Part 29 Rotorcraft* [Assure Report]. https://assureuas.com/wp-content/uploads/2021/06/Volume-VI-Airborne-Collision-Severity-Evaluation-14-CFR-Part-29-Rotorcraft.pdf

Olivares, G., Gomez, L., Monteros, J. E. d. l., Baldridge, R. J., Zinzuwadia, C., & Aldag, T. (2017). *UAS Airborne Collision Severity Evaluation – Volume II – Quadcopter* [Assure Report]. https://www.assureuas.org/projects/completed/sUASAirborneCollisionReport.php

Olivares, G., Gomez, L., Zinzuwadia, C., Kadiyala, S. S., & Marco, R. (2021). *Analysis of Collision Severity Between Small Unmanned Aircraft Systems and Fixed Wing, General Aviation Aircraft* [Assure Report].

Olivares, G., Lacy, T., Gomez, L., Zinzuwadia, C., Monteros, J. E. d. l., Baldridge, R. J., Aldag, T., Kota, K. R., Ricks, T., & Jayakody, N. (2017). *UAS Airborne Collision Severity Evaluation – Volume III – Fixed Wing* [Assure Report]. https://www.assureuas.org/projects/completed/sUASAirborneCollisionReport.php

Owen, M. P., Panken, A., Moss, R., Alvarez, L., & Leeper, C. (2019, Sept. 2019). ACAS Xu: Integrated Collision Avoidance and Detect and Avoid Capability for UAS. 2019 IEEE/AIAA 38th Digital Avionics Systems Conference (DASC),

Pedregosa, F., Varoquaux, G., Gramfort, A., Michel, V., Thirion, B., Grisel, O., Blondel, M., Prettenhofer, P., Weiss, R., Dubourg, V., Vanderplas, J., Passos, A., Cournapeau, D., Brucher, M., Perrot, M., & Duchesnay, E. (2011). Scikit-learn: Machine Learning in Python. *Journal of Machine Learning Research*, *12*, 2825-2830.

RTCA. (2005). *Safety Analysis of Proposed Change to TCAS RA Reversal Logic*. (DO-298).

RTCA. (2021). *Terms of Reference*. https://www.rtca.org/sc-147/

SC-147. (2022a). *Minimum Operational Performance Standards for Airborne Collision Avoidance System sXu (ACAS sXu)* (RTCA Paper No: 079-22/SC147-830). (Volume I - Draft, Issue 0.05).

SC-147. (2022b). *Minimum Operational Performance Standards for Airborne Collision Avoidance System sXu (ACAS sXu)* (DO-396).

SC-228. (2021). *Minimum Operational Performance Standards (MOPS) for Detect and Avoid (DAA) Systems* (DO-365B).

Schäfer, M., Strohmeier, M., Lenders, V., Martinovic, I., & Wilhelm, M. (2014, 15-17 April 2014). Bringing up OpenSky: A large-scale ADS-B sensor network for research. IPSN-14 Proceedings of the 13th International Symposium on Information Processing in Sensor Networks,

Serres, C., Gill, B., Reheis, P., & Edwards, M. (2021). *RTCA Detect and Avoid Phase 2 Safety Risk Management Modeling and Simulation Final Report*. MIT Lincoln Laboratory.

Serres, C., Gill, B., Reheis, P., Edwards, M., Guendel, R., Weinert, A., Williams, R., & Klaus, R. (2020). *mit-ll/degas-core: Initial Release (v1.0)*. Zenodo. https://doi.org/10.5281/zenodo.4323620

The MathWorks Inc (2021). *Matlab R2021b* In Natick, Massachussetts.

Underhill, N., & Weinert, A. (2021). Applicability and Surrogacy of Uncorrelated Airspace Encounter Models at Low Altitudes. *Journal of Air Transportation*, 1-5. https://doi.org/10.2514/1.D0254

Weinert, A. (2020). *Airspace-Encounter-Models/em-pairing-geospatial: SPDX and bug fixes (v1.1)*. Zenodo. https://doi.org/10.5281/zenodo.3978267

Weinert, A. (2021). *Airspace-Encounter-Models/em-pairing-geospatial: October 2021 - Version 2.0.0 (v2.0.0)*. Zenodo. https://doi.org/10.5281/zenodo.3978267

Weinert, A., Alvarez, L., Owen, M., & Zintak, B. (2022). Near Midair Collision Analog for Drones Based on Unmitigated Collision Risk. *Journal of Air Transportation*, *30*(2), 37-48. https://doi.org/10.2514/1.D0260

Weinert, A., Campbell, S., Vela, A., Schuldt, D., & Kurucar, J. (2018). Well-Clear Recommendation for Small Unmanned Aircraft Systems Based on Unmitigated Collision Risk. *Journal of Air Transportation*, *26*(3), 113-122. https://doi.org/10.2514/1.D0091

Weinert, A., Kochenderfer, M., Edwards, M. W. M., Gill, B., Guendel, R., Serres, C., & Underhill, N. (2021). *Airspace-Encounter-Models/em-model-manned-bayes: October 2021 (v2.1.0)*. Zenodo. https://doi.org/10.5281/zenodo.5544340

Weinert, A., & Underhill, N. (2018). *Generating Representative Small UAS Trajectories using Open Source Data* (2155-7209). 2018 IEEE/AIAA 37th Digital Avionics Systems Conference (DASC). https://doi.org/10.1109/DASC.2018.8569745

Weinert, A., Underhill, N., & Wicks, A. (2019). *Developing a Low Altitude Manned Encounter Model Using ADS-B Observations* (1095-323X). 2019 IEEE Aerospace Conference. https://doi.org/10.1109/AERO.2019.8741848

Weinert, A. J., Brittain, M., & Guendel, R. (2020). Frequency of ADS-B Equipped Manned Aircraft Observed by the OpenSky Network. *Proceedings*, *59*(1), 15. https://doi.org/10.3390/proceedings2020059015

Weinert, A. J., Edwards, M., Alvarez, L., & Michelle Katz, S. (2020). *Representative Small UAS Trajectories for Encounter Modeling* (AIAA 2020-0741). AIAA Scitech 2020 Forum. https://doi.org/10.2514/6.2020-0741

Weinert, A. J., Harkleroad, E. P., Griffith, J. D., Edwards, M. W., & Kochenderfer, M. J. (2013). *Uncorrelated Encounter Model of the National Airspace System, Version 2.0*. MIT Lincoln Laboratory.

Young, T. (2021). *Integration Guidance for ACAS sXu Version 3 (V3R0)*. Traffic Alert & Collision Avoidance System (TCAS), Program Office (PO), & Federal Aviation Administration.